CARDIFF UNIVERSITY
PRIFYSGOL CAERDYDD

# The Selective Oxidation Of Methanol Over Iron Molybdate Catalysts

Matthew Peter House

School of Chemistry, Cardiff University





ProQuest LLC
789 East Eisenhower Parkway
P.O. Box 1346
Ann Arbor, MI 48106-1346

# DECLARATION

This work has not previously been accepted in substance for any degree and is not concurrently submitted in candidature for any degree.

Signed ..... (candidate) Date 14/6/07

**STATEMENT 1**

This thesis is being submitted in partial fulfilment of the requirements for the degree of PhD.

Signed ..... (candidate) Date 14/6/07

**STATEMENT 2**

This thesis is the result of my own independent work/investigation, except where otherwise stated.
Other sources are acknowledged by footnotes giving explicit references.

Signed ..... (candidate) Date 14/6/07

**STATEMENT 3**

I hereby give consent for my thesis, if accepted, to be available for photocopying and for inter-library loan, and for the title and summary to be made available to outside organisations.

Signed ..... (candidate) Date 14/6/07

# Abstract

The selective oxidation of methanol to formaldehyde over iron molybdate catalysts has been investigated. It has been shown that when $Fe_2O_3$ is present at the surface $CO_2$ and $H_2$ are observed from surface formates, while neighbouring pairs of molybdena sites leads to the production of formaldehyde and water from surface methoxys. When molybdenum sites are isolated then the surface methoxy is stabilised and a direct pathway to CO and $H_2$ is created. On molybdena rich surfaces the production of CO is observed, but as a secondary oxidation product following the linear pathway: $CH_3OH \rightarrow CH_2O \rightarrow CO \rightarrow CO_2$, established by varying bed lengths. Catalysts with addition of small amounts of molybdena added to the surface of $Fe_2O_3$, are similar to those with a low bulk ratio of Mo:Fe showing increased activity over $Fe_2O_3$. Selectivity is dictated by the presence of isolated or pairs of molybdena sites, which guide the reaction to the primary products of CO and formaldehyde respectively.

Structural analysis showed the phases of $\alpha$-$Fe_2O_3$, $\alpha$-$MoO_3$ and $\alpha$-$Fe_2(MoO_4)_3$, depending on the ratio of the cations present. Molybdenum has been shown to concentrate at the surface of iron molybdates by reactor results from low ratio catalysts, Raman spectroscopy, XP spectroscopy and STEM/EEL spectroscopy.

The normal reaction of iron molybdates is via the Mars-van Krevelen mechanism, so tests were made without the presence of gaseous oxygen. The reduction of the surface layer can occur at temperatures as low as 200 °C. At temperatures above 250 °C diffusion of lattice oxygen to replace the lost surface oxygen can occur, leading to the production of further oxidised products. If the oxidation state of surface molybdenum drops below +6 then formaldehyde selectivity drops markedly, with direct production of CO and secondary production of $CO_2$ observed.

# Acknowledgements

This thesis has only proved possible due to the help and support of many people. Firstly, thanks must go to Prof. Mike Bowker for offering me the opportunity to study in Cardiff for three years on this project and all his help within this period. My gratitude must also be expressed to my co-supervisor Dr. Albert Carley whose knowledge has proved extremely useful.

As with any project of this nature funding must be provided, and to this end I am grateful to both the EPSRC and Perstorp AB in Sweden. I would also like to show my appreciation to all those at Perstorp who have provided input throughout the course of the three years and made my visits so memorable, most notably Philippe, Andreas, Ola and Neil.

Thanks must be given to Prof. Mervyn Shannon and Dr. Andrew Bleloch at Daresbury for help during my brief stay at the Super STEM facility.

I would also like to express my gratitude to the fellow group members who have provided support and help with work. There have been some real characters amongst you and you have given me many anecdotes to dine out on.

Thanks to friends and family who have supported me through the three (and a bit) years of the PhD. Mum and dad, you have always been there to maintain my focus and ensure that I finished, with out you this thesis would not be what it is. I am also indebted to Suz for proof reading (maybe you even finally learnt what I have been up to). Cheers also to the footy lads and Pete and Jon who have generally helped make Cardiff a better place, and who have always been there to share a beer or two with.

# Glossary

| | |
|---|---|
| AFM | Atomic Force Microscopy |
| AMU | Atomic Mass Units |
| BET | Brunauer, Emmett and Teller |
| DMFC | Direct Methanol Fuel Cell |
| DRIFTS | Diffuse Reflectance Infrared Spectroscopy |
| DSC | Differential Scanning Calorimetry |
| DME | Dimethyl Ether |
| EELS | Electron Energy Loss Spectroscopy |
| FEG | Field Emission Gun |
| FTIR | Fourier Transform Infrared |
| FWHM | Full Width Half Maximum |
| HADDF | High Angle Annular Dark Field |
| HREELS | High Resolution Electron Energy Loss Spectroscopy |
| HTF | Heat Transfer Fluid |
| IPFR | Isothermal Pulsed Flow Reaction |
| IR | Infrared |
| KIE | Kinetic Isotope Effect |
| ML | Monolayer |
| PEELS | Parallel Electron Energy Loss Spectroscopy |
| PFR | Pulsed Flow Reactor/Reaction |
| PPM | Parts Per Million |
| SEELS | Serial Electron Energy Loss Spectroscopy |
| SEM | Scanning Electron Microscopy/Microscope |
| SMR | Steam Methanol Reforming |
| STEM | Scanning transmission Electron Microscopy/Microscope |
| TCD | Thermal Conductivity Detector |
| TEM | Tunnelling Electron Microscopy/Microscope |
| TOF | Turn Over Frequency |
| TPD | Temperature Programmed Desorption |
| TPPFR | Temperature Programmed Pulse Flow Reaction |
| TPR | Temperature Programmed Reduction |

| | |
|---|---|
| UHV | Ultra High Vacuum |
| XAFS | X-Ray Absorption Fine Structure |
| XRD | X-Ray Diffraction |
| XPS | X-Ray Photoelectron Spectroscopy |

# Contents

# 1 Introduction and Literature Review

## 1.1 Catalysis

A catalyst is a substance that accelerates the rate of a reaction but undergoes no net chemical change itself. A catalyst works by lowering the activation energy of the reaction by providing an alternative reaction pathway that avoids the rate determining step of the uncatalysed reaction, leading to an increased reaction rate at the same temperature. A catalyst does not effect the final equilibrium composition of a system, only the rate at which it is approached.

The first time humans used catalysis is lost in prehistoric history when they first started to produce alcohol by fermentation, with the first known reference to the use of an inorganic catalyst occurring in 1552, when Valerius Cordus used sulphuric acid to catalyse the conversion of alcohol to ether[1]. The principle features of catalysis were first presented by Fulhame in 1794, when she suggested that small quantities of water were required for the oxidation of carbon monoxide and that the water was unaffected by the chemical reaction. The first person to use the word catalysis was Berzelius in 1835, when after studying the effect of sulphuric acid on ethanol to the decomposition of hydrogen peroxide and drawing analogies with the conversion of starch into sugar stated:

*"It is then shown that several simple and compound bodies, soluble and insoluble, have the property of exercising on other bodies and action very different from chemical affinity. The body effecting the changes does not take part in the reaction and remains unaltered through the reaction. This unknown body acts by means of an internal force, whose nature is unknown to us. This new force, up till now unknown, is common to organic and inorganic nature. I do not believe that this force is independent of the electrochemical affinities of matter; I believe on the contrary, that it is a new manifestation of the same, but, since we cannot see their connection and independence, it will be more convenient to designate the force by a new name. I will therefore call it the "Catalytic Force" and I will call "Catalysis" the decomposition of bodies by this force, in the same was we call "Analysis" the decomposition of bodies by chemical affinity."*

A major advance was made in the understanding of catalysis when in 1877 Lemoine showed that a catalyst could change the rate at which a chemical equilibrium was reached, but the position of the equilibrium was unaltered. In 1915 Langmuir presented his theories on adsorption based on the early work done by Haber[2]. The most significant step in catalysis modelling was made in 1927, when Hinshelwood presented a kinetic theory based on the earlier findings of Langmuir. This lead to Hinshelwood being awarded the Nobel prize in 1932, with these theories still being applied to catalysis modelling today.

Heterogeneous catalysis occurs when the catalyst and the reagents are in different phases, most typically a solid catalyst with the reagents in the gaseous phase. In the case of solid/gas catalysis, the gas is adsorbed onto the surface of the catalyst before reaction and product desorption. Heterogeneous catalysis has the major advantage over homogeneous catalysis (where the catalyst and reagents are in the same phase) of separation, however, due to a lower contact area, the rate of catalysis is often much lower. The exhaust gas catalyst system (the most common catalytic reactor in the world) is an example of heterogeneous catalysis[1].

## *1.2 Background*

### 1.2.1 Iron - Uses and Properties

Iron is a first row transition metal above ruthenium and osmium, with the atomic number 26 and in the metallic state has the electron configuration [Ar] $3d^6$ $4s^2$. Iron is the most abundant metal on earth (34.6 % by mass) and is believed to be the tenth most abundant element in the universe. 95 % of all the metal tonnage produced worldwide is iron, its low cost and high strength making it indispensable in the production of steel and use in applications such as automobiles, large ship hulls, and

structural components for buildings. As well as its use in steel, iron is used in the form of iron (III) oxide in the production of magnetic storage media for computers.

Industrially, iron is extracted from its ores, principally hematite (nominally $Fe_2O_3$) and magnetite ($Fe_3O_4$) by reduction with carbon in a blast furnace at temperatures of around 2000 °C. Production of approximately 1100 Mt (Million tonnes) of iron ore was produced in 2000. Iron ore prices have recently increased considerably, from US$ 23.87 $ton^{-1}$ in 2001 to an estimated US$ 44.00 in 2005[3].

Excess iron is toxic to the human body as the excess ferrous ion reacts with peroxides in the body to form free radicals. This excess iron can damage the gastrointestinal tract, damaging the cells that would otherwise regulate iron uptake. Once in the bloodstream, excess iron causes damage primarily to the cells of the heart and liver.

### 1.2.2 Molybdenum - Uses and Properties

Molybdenum exists in the second row of the transition metals, below chromium and above tungsten, with the atomic number 42 and in the metallic state has the electron configuration [Kr] $4d^5\ 5s^1$. The word molybdenum comes from the Greek *molybdos*, meaning lead like, and until the late 18th century molybdenum compounds were confused with those of carbon or lead. Molybdenum is found in minerals such as wulfenite ($PbMoO_4$) or powellite ($CaMoO_4$), but the main commercial source is from molybdenite ($MoS_2$). Molybdenum is both mined directly and recovered as a by-product from copper mining. The greatest use for molybdenum is as an alloying agent due to its hardening properties, with around three quarters of molybdenum produced being used in the production of steel, cast and wrought alloy, and superalloy. Molybdenum is a component within the catalyst used in the petroleum industry for removing organic sulfurs.

Amongst other factors, the continuing growth of the Chinese economy and its demand for steel has lead to a high demand for molybdenum and a greater than 10 fold price increase in 5 years (Figure 1-1).

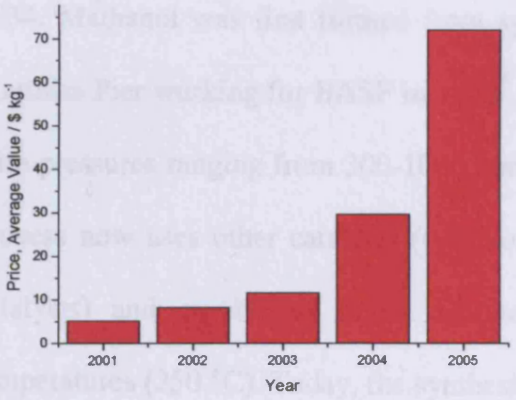


**Figure 1-1 - Time-averaged price per kilogram of molybdenum contained in technical grade molybdic oxide[3].**

Insoluble molybdenum compounds have a low toxicity, with no reports to date of harm due to exposure to either molybdenum or molybdenum trioxide dust, while water-soluble molybdenum compounds can have toxicity. Molybdenum toxicity can occur in animals if they graze soil rich in molybdenum, and deficient in copper as the molybdenum causes excretion of copper reserves, leading to copper depletion. A reported case study of this occurred near Uppsala, Sweden, after farmers heavily limed fields due to acid rain, leading to an increase in heavy and trace metals in the soil. The moose who ate the crops grown in the field suffered a disturbance in the molybdenum to copper ratio in their livers leading to emaciation, hair discoloration, ulcers, diarrhoea, convulsions, blindness, osteoporosis and finally heart failure.

### 1.2.3 Methanol - Uses and Properties

Methanol ($CH_3OH$, also known as wood alcohol and methyl alcohol) is a naturally occurring substance produced by many bacteria in anaerobic metabolism. It is colourless, tasteless, volatile, flammable, poisonous liquid with a density of 0.7914

g $cm^{-3}$, boiling point of 65.0 °C and a melting point of -93.9 °C[4]. Pure methanol was first isolated by Robert Boyle in 1661 by the distillation of boxwood, well before its elemental composition was determined by Jean-Baptiste Dumas and Eugene Peligot in 1834. Methanol was first formed from synthesis gas (a mixture of CO and $H_2$) by Matthias Pier working for BASF in 1923[5]. This process used a zinc chromate catalyst with pressures ranging from 300-1000 atm and a temperature of around 400 °C. This process now uses other catalysts (commonly mixed copper, zinc oxide and alumina catalysts) and capable of being operated at lower pressures (50-100 atm) and temperatures (250 °C). Today, the synthesis gas used in the process is most commonly produced from methane in natural gas rather than from coal. At moderate pressures (10-20 atm) and high temperatures (850 °C) methane is reacted with steam on a nickel catalyst:

$$CH_4 + H_2O \rightarrow CO + 3H_2 \qquad (1\text{-}1)$$

This process, called Steam Methane Reforming (SMR) is endothermic and heat transfer limitations constrict the size of reactor that can be used. Methane can also undergo partial oxidation with molecular oxygen:

$$CH_4 + \tfrac{1}{2} O_2 \rightarrow CO + 2H_2 \qquad (1\text{-}2)$$

This reaction is exothermic and the heat given off can be used to drive the SMR process *in-situ*. Combining the two processes is known as autothermal reforming, with the water gas shift reaction (1-3) being used to adjust the ratio of CO and $H_2$ for the appropriate stoichiometry for methanol synthesis.

$$CO + H_2O \rightarrow CO_2 + H_2 \qquad (1\text{-}3)$$

Reaction to form methanol then occurs by equations 1-4 and 1-5, leaving the overall equation as shown in 1-6:

$$CO_2 + 2\,H_2 \rightarrow CH_3OH + O_a \qquad (1\text{-}4)$$

$O_a + CO \rightarrow CO_2$ (1-5)

$CO + 2\,H_2 \rightarrow CH_3OH$ (1-6)

An important consideration when working with methanol is the flammability limits (Figure 1-2). For obvious reasons it is preferable to work outside these regions and as shown in the diagram, as temperature increases the explosion limits become more spread.

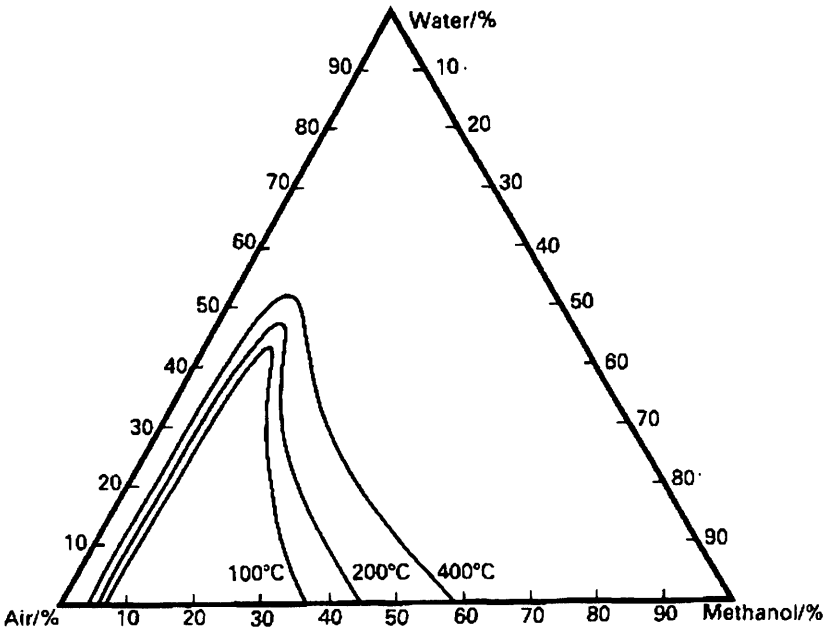


**Figure 1-2 - Flammability limits for air/methanol water vapour mixtures at different temperatures and atmospheric pressure[6].**

Methanol is used in a wide number of applications. It can be blended with petrol or used unmixed in certain internal combustion engines such as those used to power American Indy cars and Drag cars. Methanol has been suggested as a renewable alternative to petroleum based hydrocarbons, as methanol can be produced from wood or other organic materials (bioalcohol). However, current petrol engines would require modification before they were able to run on pure bioalcohol.

Methanol can be used in direct methanol fuel cells which can operate at low temperatures and low pressures, which has lead to miniaturisation and the hope that

they may be used in consumer electronics. In 2005 Toshiba released the smallest commercially available fuel cell measuring 22 x 56 x 4.6 mm using Direct Methanol Fuel Cell (DMFC) technology.

Methanol is used as a solvent, and is added to ethanol as a denaturant because of its poisonous properties and is used as anti-freeze in pipelines. However, the single biggest use of methanol is the production of other chemicals, most notably formaldehyde, which accounts for 40 % of methanol usage. Methanol can also be converted to dimethyl ether, which in some cases has been used to replace the now banned chlorofluorocarbons (CFCs) as a propellant in aerosols.

### 1.2.4 Formaldehyde - Uses and Properties

Formaldehyde is rarely found in the monomeric form ($H_2CO$), but instead is more commonly encountered in the forms of aqueous solutions and solid polymers. Dry monomeric formaldehyde is a colourless gas at room temperature with a boiling point of -21 °C and a melting point of -92 °C[4]. Gaseous formaldehyde presents a pungent odour and is irritating to the eyes and the mucous of the nose and throat even when present in concentrations of 20 ppm.

Polymerisation of the formaldehyde molecules is very well known and usually takes the form of polymethylenes (Figure 1-3)[7]. These polymers form reversibly and react chemically as solid forms of formaldehyde.

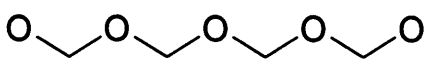

**Figure 1-3 – Polymethylene type polymer from formaldehyde.**

Another form of formaldehyde polymer is polyhydroxyaldehdyes (Figure 1-4), which are substantially irreversible and are usually formed by aldol type condensations.

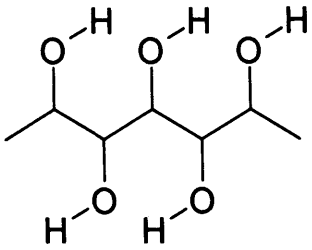

**Figure 1-4 - Polyhydroxyaldehdye type polymer from formaldehdye.**

Formaldehyde has been produced on a commercial basis for over 100 years, with its initial uses being as disinfectant and embalming agent[7]. Formaldehyde was first prepared by Alexander M. Butlerov in 1859[8] and was first produced from methanol in 1868 when August W. von Hofmann passed methanol vapours and air over a heated platinum spiral[9].

The commercial demand for formaldehyde first began increasing significantly after the discoveries of Leo Baekeland in 1909 which lead to the formation of the synthetic resin industry[10]. The formation of bakelite from the reaction under heat and pressure of formaldehyde and phenol with wood flour was the first plastic from synthetic components and because of this, was designated an American Chemical Society national historic chemical landmark in 1993.

These first industrial catalysts involved dehydrogenation over a copper gauze, which were later replaced by silver catalysts due to their higher yields and greater resistance to poisoning. In the 1950's an alternative process was commercialised, involving selective oxidation of the methanol over an Fe-Mo oxide catalyst, which was first discovered as a selective oxidation catalyst by Adkins in 1931[11]. At present the silver and oxide processes each count for approximately 50 % of the total production of formalin (an aqueous solution of formaldehyde), which amounts to around 20 Mton per annum (when measured as a 37 w/t % formaldehyde in water). However, the majority of the new capacity taken on within the last ten years has been

with the oxide process. The main advantages of the oxide catalyst can be summarised as[12]:

a) higher yield, which allows production of solutions with a low methanol concentration;
b) higher resistance to poisoning, so no special air purification methods are required;
c) longer life of the catalyst;
d) lower fire and explosion hazards due to the low methanol concentration.

Improvements are still sought after however, with the industry expected to grow by around 10 Mton per annum within the next ten years.

Today within the wood industry, formaldehyde is used to create resins for wood binding in products such as plywood, chipboard, medium density fibreboard (MDF), and condensed hardboard. Within the chemical industry, formaldehyde is used in the production of traditional plastics (e.g. urea-formaldehyde) and also new, high growth products such as acetals and polyurethanes. Along with these uses formaldehyde is also used as an important starting point for some herbicides and pharmaceuticals.

## *1.3 Industrial Process*

The following short section provides details of a current formaldehyde production plant, using methanol as a feedstock over an iron molybdate catalyst.

### 1.3.1 Industrial Plant

Shown in Figure 1-5, is a schematic of the industrial formaldehyde production plant.

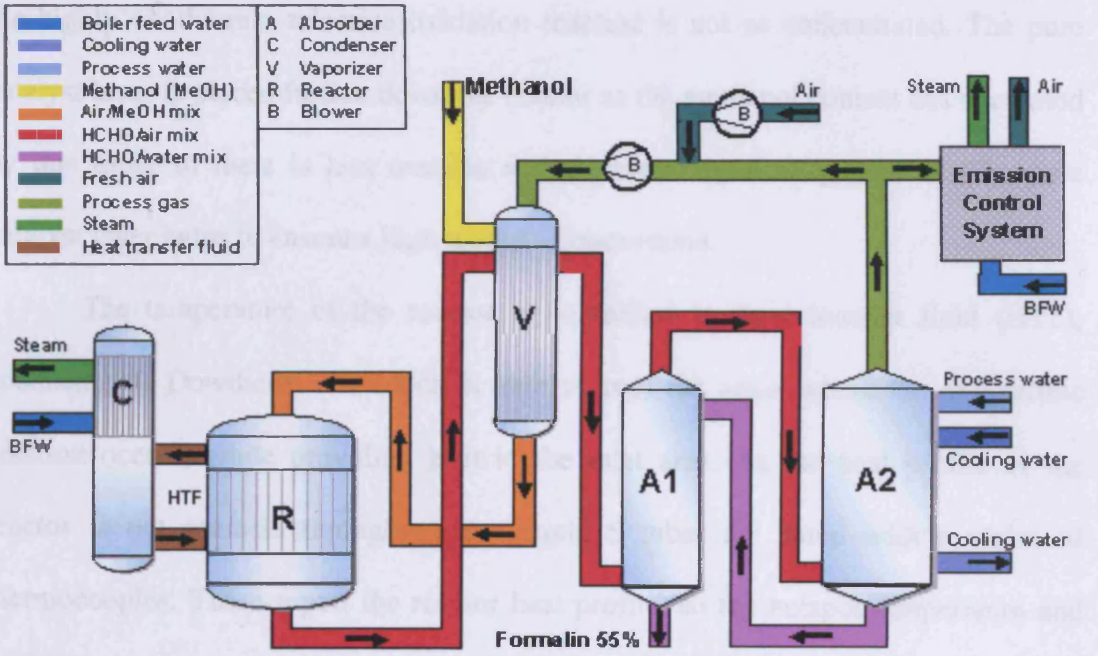


**Figure 1-5 - Schematic of a formaldehyde production plant.**

Air is drawn into the system by blowers before being mixed with recycled process gas to create a gas mixture with 11 mol % $O_2$. The gas mixture passes into the vaporiser (V) where methanol is sprayed in and vaporised. In some industrial plants a pre-vaporiser is added, when this is done two thirds of the methanol is injected and vaporised in the pre-vaporiser, while the balance of the methanol feed is sprayed into the vaporiser. The methanol/gas mixture then passes into and through the reactor (R) at a pressure of around 1.4 bar. Each reactor holds 8,000 to 16,000 reactor tubes, which can vary in length from 12,000 mm to 14,000 mm. The tubes contain a layer of inert ceramic rings to allow further heating of the gases, a layer of inert and catalyst, a pure layer of catalyst and a final layer of inert to allow some cooling of the product before leaving the reactor. A mixed layer of inert and catalyst is used before the pure catalyst layer to avoid an overly high 'hotspot' temperature within this region, as a high hotspot temperature can lead to faster deactivation of the catalyst. The inert ceramic rings work by spreading the catalyst pellets out and so the heat generated by

the highly exothermic selective oxidation reaction is not so concentrated. The pure catalyst layer is placed further down the reactor as the methanol content has decreased by this time, so there is less reaction and therefore less heat generated. The pure catalyst layer helps to ensure a high methanol conversion.

The temperature of the reactor is controlled by heat transfer fluid (HTF), consisting of Dowtherm oil, which is able to cool the areas where the exothermic reaction occurs, while providing heat to the inlet area. As the heat profile of the reactor is not uniform throughout its length, 8 tubes are fitted with a series of thermocouples. These report the reactor heat profile, so the hotspot temperature and position, and the inlet and outlet gas temperatures can be monitored. The HTF is used at its boiling point and to adjust the temperature at which it operates, adjustments to the pressure of the HTF must be made. The HTF temperature is raised throughout the course of a catalysts life from 257 °C to around 320 °C to keep the yield high, as the activity of the catalyst decreases. The vapours from the HFT flow to the condenser (C), where the heat is recovered by generating steam, before the condensed fluid is returned to the reactor. The steam generated can then be used for either producing electricity through a steam generator or for heating purposes. At the Perstorp complex in Sweden, the steam generator is used for a remote heat programme, which provides a nearby village with heating for their central heating, hot water and local swimming baths.

The process gas then passes through the outside of the vaporiser where excess energy is used to evaporate the incoming methanol. The formaldehyde is absorbed into process water, in the absorbers (A1 and A2). The tubing between the reactor and the absorbers are heated to prevent the polymerisation of the formaldehyde. The flow of the process water is adjusted so that the desired concentration of formalin solution

is obtained. The solutions obtainable are up to around 55 w/t % formaldehyde. When quoting the production from a plant however, production is always quoted for arbitrary reasons as 37 w/t % formaldehyde in water. A very small amount of caustic NaOH is added to the process water as this promotes the absorption of formaldehyde, however, care is taken that no process water is flushed back through the system as the Na is a strong poison to the catalyst. Cooling water is used to remove the heat of absorption, which promotes further absorption. By controlling the absorber top temperature it is possible to control the level of water and formaldehyde leaving in the exit gas. Some of the process gas is then recycled, whilst the remainder is sent to an integrated emissions system, which consists of a heat exchanger and platinum based catalyst. In this system all the volatile organic compounds are oxidised to $CO_2$ and $H_2O$.

The process has a yield of around 93 % formaldehyde and the minor products observed are CO, unconverted methanol, dimethyl ether, a limited amount of $CO_2$ and formic acid.

To produce a metric ton of formalin (37 % w/t %) around 421-426 kg of methanol, 55-65 kWh of electricity, 400 kg of process water and 0.03 – 0.05 kg of catalyst are used while 450-700 kg of steam is produced. The overall cost of producing 1 ton of formalin is currently estimated at £57.25. Buying 1 ton of formalin 37 w/t % from Avocado would cost £5,600.

### 1.3.2 Current Industrial Catalyst

At present the industrial iron-molybdate catalysts are made by a coprecipitation method. This process involves the mixing together of iron chloride solution, $FeCl_3$ and ammonium heptamolybdate $(NH_4)_6Mo_7O_{24}$ and adjusting the pH of the solution until both components coprecipitate. The precipitate is then filtered and

dried to remove 60-70 % of the water present, with care taken to avoid the pores collapsing. The dried mixture is combined with a binding agent before being pelletised and calcined. Industrial catalysts have a composition of Mo:Fe above that required to form stoichiometric $Fe_2(MoO_4)_3$. The reasons behind this are discussed further in the sections on the reactivity of $Fe_2(MoO_4)_3$ and catalyst deactivation (Sections 1.7.3 and 1.12).

Catalysts unloaded after use in an industrial reactor have been studied and showed the surface area of catalysts decreased along the reactor tube[13]. The minimum activity catalyst was that present at the 'hot-spot', while above and below this point the activities were similar, but lower than for the fresh catalyst. Selectivity was found to be higher for samples taken from below the 'hot-spot'. Above and below this point, the selectivity decreases slightly, but is still well above that of the initial catalyst.

A more recent study by Andersson *et al.* on the industrial catalyst showed catalyst from the inlet area with increased specific area, increased pore volume and decreased activity[14]. From this inlet area molybdenum was sublimed and condensed as needle like $MoO_3$ crystals on the surface of other catalyst rings nearer the exit.

## 1.4 Thermodynamics of Methanol Oxidation

The main reactions to be considered when methanol is oxidised to formaldehyde are shown below, with the thermodynamics for the reactions shown in Table 1-1 for 250 °C.

**Dehydrogenation Reactions:**

$$CH_3OH \rightarrow H_2CO + H_2 \qquad \Delta G = 145 \text{ kJ mol}^{-1} \qquad (1\text{-}7)$$

$$CH_3OH \rightarrow CO + 2\,H_2 \qquad \Delta G = 218 \text{ kJ mol}^{-1} \qquad (1\text{-}8)$$

**Oxidative Dehydrogenation Reaction:**

$$CH_3OH + \tfrac{1}{2}\,O_2 \rightarrow H_2CO + H_2O \qquad \Delta G = -123 \text{ kJ mol}^{-1} \qquad (1\text{-}9)$$

**Combustion Reactions:**

$CH_3OH + 1½\ O_2 \rightarrow CO_2 + 2\ H_2O \quad \Delta G = -678\ kJ\ mol^{-1}$ (1-10)

$CH_3OH + O_2 \rightarrow CO + 2\ H_2O \quad \Delta G = -324\ kJ\ mol^{-1}$ (1-11)

**Other Reactions:**

$CH_3OH \rightarrow CH_4 + ½\ O_2 \quad \Delta G = 153\ kJ\ mol^{-1}$ (1-12)

$2\ CH_3OH \rightarrow CH_3OCH_3 + H_2O \quad \Delta G = -34\ kJ\ mol^{-1}$ (1-13)

| Equation | $\Delta H$ / kJ mol$^{-1}$ | $\Delta S$ J K$^{-1}$ mol$^{-1}$ | $\Delta G$ / kJ mol$^{-1}$ |
|---|---|---|---|
| 1-7 | 80 | -122 | 145 |
| 1-8 | 88 | -245 | 216 |
| 1-9 | -164 | -72 | -123 |
| 1-10 | -707 | -55 | -678 |
| 1-11 | -400 | -145 | -324 |
| 1-12 | 124 | -53 | 153 |
| 1-13 | -27 | 15 | -34 |

**Table 1-1 – Thermodynamic data for reactions at 250 °C.**

The silver process is most efficient under lean air mixtures (1-7 and 1-9) with a net reducing gas mixture. In contrast, a net oxidising gas mixture is present in the oxide process with a lean fuel (methanol) mixture where the reaction progresses mainly through (1-9). By looking at the thermodynamic data above it can be seen that both combustion reactions (1-10 and 1-11) are more favourable than the oxidative dehydrogenation (1-9). This has an inhibiting effect on the oxidative dehydrogenation reaction, where $CO_2$ and $H_2O$ are more thermodynamically favoured products when compared to formaldehyde. The catalysts used therefore direct this reaction pathway either *via* both the selective reactions (1-7 and 1-9) in the silver process or purely by the oxidative dehydrogenation reaction (1-9) in the oxide process.

## 1.5 Alternative Catalysts

The production of formaldehyde from methanol is not a reaction that is unique to iron molybdate catalysts. As has already been mentioned, silver is also used in

industrial conditions, and previously copper was used. This short section deals with some of the details of these alternative catalysts, as many use different reaction pathways.

### 1.5.1 Silver

The silver process takes place under methanol rich conditions, with values above the upper explosion limit. The claimed advantages of the silver process include relatively low investment cost, high yield and stable production.

There are two major variations of the silver process used industrially. The first process (described as the *methanol ballast process*) uses only air and pure methanol as a feed and is utilised by a number of companies (e.g. ICI and Degussa). The notable features of this process are the incomplete methanol conversion followed by its recovery by distillation. The alternative silver process (described as the *water ballast process*) is used by BASF and involves feeding water over the catalyst along with the reaction mixture, to achieve complete conversion of the methanol. The addition of water is limited by the strength of the formalin product required and the extra water required for tail gas scrubbing. The commercial process is usually carried out with a water/methanol ratio of 0.67[15]. The excess water helps to remove a great deal of the reaction heat, helping to prevent detrimental overheating and sintering of the catalyst. More importantly, the lifetime of the catalyst in the water ballast process is increased as the water vapour is able to aid the process of burning away coke deposits on the catalyst surface.

The process now carried out on silver was originally carried out on copper, with a recent patent utilising both technologies, using a reactor containing a silver catalyst before a copper catalyst[16].

On the silver catalyst it is believed it is a prerequisite to understand the interaction of oxygen with silver before the total reaction route can be explained. Studies have shown that there appears to be three different oxygen species $O_\alpha$, $O_\beta$ and $O_\gamma$ in the course of the reaction. Molecular oxygen dissociates on the silver and forms the weakly bound atomic oxygen species $O_\alpha$ which benefits especially the formation of HCOOH and the complete oxidation products $H_2O$ and $CO_2$. It has been suggested that molecularly adsorbed oxygen acts as a precursor and transforms to atomic oxygen in this process[17]. Oxygen has similar atomic dimensions to silver ($\phi_{Ag+}$ = 129 pm, $\phi_{O2-}$ = 126 pm), so may dissolve into the silver lattice to form $O_\beta$. This $O_\beta$ cannot participate directly in the reaction. The strongly bound $O_\gamma$ is formed from $O_\beta$, when the latter segregates from the bulk to the surface. $O_\gamma$ exists predominately in the upper layer of the silver catalyst and tends to only catalyse the dehydrogenation of methanol. The adsorption of methanol is also believed to be influenced by the silver-oxygen chemistry as it hardly occurs at all on an oxygen-free silver surface. Under the reaction conditions, the silver catalyst is constantly exposed to oxygen, some of which will be adsorbed and form the species $O_\alpha$, $O_\beta$, and $O_\gamma$, which are depleted by the corresponding reactions, this shows a dynamic equilibrium. The population of the different oxygen species is strongly dependent on the parameters and pre-treatment. The three species for example have stability regions at different temperatures. The silver is also dynamically restructured: SEM images have shown that the morphology of silver changes dramatically throughout the course of the reaction. Firstly "pinholes" appear in the vicinity of initial surface defects and spread gradually from the region of the defects to the entire silver surface. The reaction-induced morphological restructuring reinforces the formation of grain boundary defects over the catalyst,

which enables more oxygen to penetrate into the silver lattice and, in turn, to intensify the reaction.

### 1.5.2 Sodium Catalysts

In recent years, new processes have come through but these are yet to be commercialised. One of the new processes uses an evaporated sodium catalyst to produce anhydrous formaldehyde which is used in the production of polyoxymethylenes. At present anhydrous formaldehyde is made by a two step process, the first involves the production of hydrous formaldehyde and the second, rather expensive step is to dry the formaldehyde[18].

This system relies on the fact it is possible to convert methanol into anhydrous formaldehyde without catalysts at high temperatures. In a reactor tube, with residence times of less than 1 second at 900 °C the maximum formaldehyde yield is reached when no catalyst is present, with a methanol conversion of approximately 45 % and 43 % formaldehyde selectivity. The low selectivity is explained by the fact that hydrogen atoms act as chain carriers. Hydrogen atoms can react with both methanol (to give formaldehyde) and formaldehyde (to give the main by-product CO). There is an inverse relationship between the methanol conversion with increasing temperature and the formaldehyde selectivity. By homogeneous catalysis with evaporated sodium, total methanol conversion and 70 % formaldehyde selectivity can be reached at 700 °C[19].

In a more recent development of this process a micro structured reactor system was designed and built for use with an evaporated sodium catalyst[20]. The optimised setup of this reactor was able to achieve formaldehyde selectivity of 80.3 % at a methanol conversion of higher than 97 %.

### 1.5.3 Ag-$SiO_2$-MgO-$Al_2O_3$ Catalysts

Another method in development to produce anhydrous formaldehyde is the production of a Ag-$SiO_2$-MgO-$Al_2O_3$ catalyst by a sol-gel method[21]. Continuous flow tests showed extremely high activity and selectivity (close to 100 %). Unfortunately these catalysts suffered a drop in methanol conversion, so that after 10 hours on stream the conversion was just 10 % due to an accumulation of silver at the catalyst surface. Despite the activity drop, the selectivity to formaldehyde remained unaltered. The optimum reaction conditions used had a 20 w/t % loading of silver and a reaction temperature of 650 °C to give a formaldehyde selectivity of 76 %[22].

### 1.5.4 Vanadium Containing Catalysts

Catalysts containing $V_2O_5$-NiO, $V_2O_5$-$Fe_2O_3$, and $V_2O_5$-$Co_3O_4$ show selectivity towards formaldehyde that is higher than the respective single metal oxides, even when only a small amount (a few percent) of the $V_2O_5$ is added[23]. The mixed metal oxides however, have a much lower conversion than the single metal oxides. The highest formaldehyde yields were obtained by catalysts with an atomic ratio of V/M = 1 (where M = Ni, Fe or Co). Isothermal pulses of methanol were made across the catalysts with a V/M ratio of 1; these showed that the most selective catalyst (that containing nickel) showed no hydrogen production, while the iron containing catalyst produced $H_2$ throughout and the cobalt catalyst had an increasing $H_2$ production throughout. These differences were explained as showing that the cobalt catalyst was unable to regenerate the active oxygen centres as quickly as the nickel catalyst. The iron catalyst passed by a different mechanism with the dehydrogenation of methanol being exerted by oxygen atoms which were not abstracted from the catalyst surface. It is suggested that the lack of oxygen defects is the reason for the selective oxidation of methanol to formaldehyde and that the oxides which have the ability for selective

oxidation are those in which no dissociative oxygen chemisorption occurs. They also show that the M=O is more stable in mixed metal oxides than the M-O bond system.

When monolayer vanadium oxide supported on $CeO_2$ catalysts are studied it is seen that the activation energy for the production of formaldehyde is dependent on the oxidation state of the vanadium[24]. While there is no difference in the heat of adsorption of methanol, for the reaction there is an activation energy of 147 kJ $mol^{-1}$ on $V^{+5}$, while on $V^{+3}$ the activation energy is 158 kJ $mol^{-1}$. When combined these results demonstrate that a lower oxidation state for vanadium destabilises the transition state for the dehydrogenation reaction.

A recent study using a V-Mg-O catalyst has shown a yield of formaldehyde of 94 % at a selectivity of 97 % methanol conversion at optimised reactor conditions in the temperature range of 450 °C[25]. This catalyst showed no change in performance (methanol conversion, formaldehyde selectivity and yield) over 60 hours of operation. Characterisation suggested the formation of a pyrovanadate ($Mg_2V_2O_7$) with an irregular surface structure, which is efficient for methanol oxidative dehydrogenation.

### 1.5.5 Supported Ruthenium Oxide Clusters

Domains of $RuO_2$ can be used on common metal oxide supports ($SnO_2$, $ZrO_2$, $TiO_2$, $Al_2O_3$, $SiO_2$) to selectively oxidise methanol to formaldehyde (<25 % selectivity), methyl formate (<83 % selectivity), and dimethoxy methane (<67 % selectivity) at temperatures in the range 27-127 °C[26]. The support choice influenced the turnover rate and the ability of the $RuO_2$ domain to undergo redox cycles. Formation of formaldehyde required lattice oxygen and in anaerobic transient experiments, selectivities were not affected.

## 1.6 The Structure of Oxides Relevant to Iron Molybdate Catalysis

### 1.6.1 $MoO_3$

The structure of α-$MoO_3$ was first described by Kihlborg in 1963 as having a space group of $P_{nma}$, an orthorhombic crystal structure with lattice parameters of a = 3.962 Å, b = 13.858 Å and c = 3.607 Å[27] (Figure 1-6). The layer structure is built up of distorted $MoO_6$ octahedra at two levels connected along one direction by common corners, and in another direction by common corners and edges. This structure involves three different types of oxygen atom, connected to one, two and three molybdenum atoms respectively.

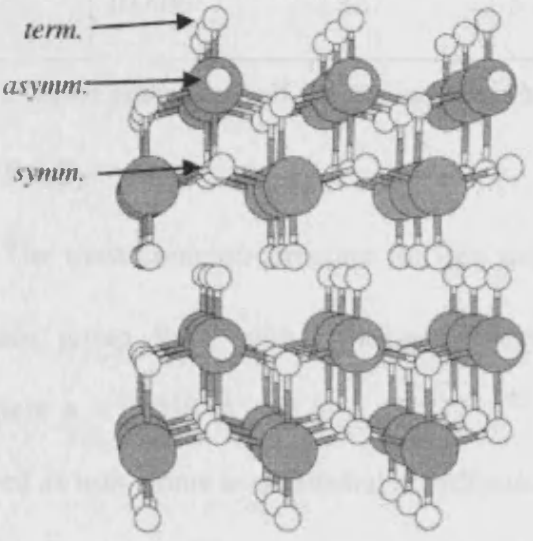


**Figure 1-6 - Structure of bulk α-$MoO_3$[28]. Mo atoms are shown as larger grey spheres, O atoms as white spheres. The three types of oxygen (terminal, asymmetric and symmetrical bridging) are shown.**

A monoclinic form of β-$MoO_3$ is also known, for which the space group is $P2_1/c$ with lattice parameters of a = 7.122 Å, b = 5.374 Å and c = 5.565 Å[29]. The monoclinic form of $MoO_3$ is isostructural with $ReO_3$ and involves corner sharing, distorted octahedra.

Hydrates of molybdena $MoO_3.xH_2O$ are known for x = 2, 1, ½, and ⅓, with two forms for x =1. The structural features presented by the hydrates generally occur from the presence of $MoO_5(OH_2)$ octahedra sharing either corner equatorial oxygens or edges. The space groups, and unit cell parameters of the various $MoO_3$ hydrates are given in Table 1-2[30-34].

| | $MoO_3.2H_2O$ | $MoO_3.H_2O$ | $MoO_3.H_2O$ | $MoO_3.\frac{1}{2}H_2O$ | $MoO_3.\frac{1}{3}H_2O$ |
|---|---|---|---|---|---|
| Cell | Monoclinic | Monoclinic | Triclinic | Monoclinic | Orthorhombic |
| Space Group | $P2_1/n$ | $P2_1/c$ | $P\bar{1}$ | $P2_1/m$ | C*/* |
| a Å | 10.476 | 7.548 | 7.372 | 9.679 | 12.647 |
| b Å | 13.822 | 10.712 | 6.553 | 3.708 | 7.697 |
| c Å | 10.606 | 7.327 | 3.707 | 7.104 | 7.338 |

**Table 1-2 - Space groups and unit cell parameters for $MoO_3$ hydrates.**

### 1.6.2 $Fe_2O_3$

The most common structure for iron oxide is α-$Fe_2O_3$ (hematite), which has the space group $R\bar{3}c$, with a hexagonal crystal structure and with the lattice parameters a = 5.038 Å and c = 13.772 Å[35] (Figure 1-7). The structure can be described as iron atoms in octahedral coordination with oxygens in a hexagonal close-packed arrangement. The structure can also be described as sheets of octahedrally coordinated $Fe^{3+}$ ions stacked between two close-packed layers of oxygens. Since Fe is in a trivalent state, each of the oxygens is bonded to only two Fe ions, and therefore, only two out of three available oxygen octahedrons are occupied.

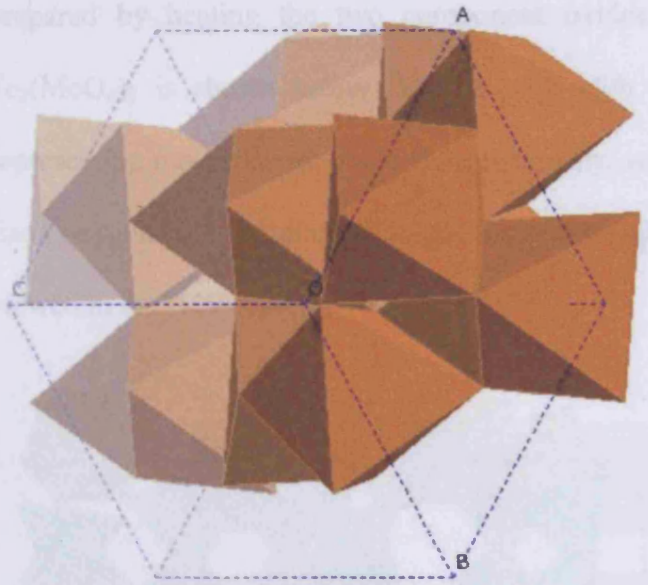


**Figure 1-7 - Structure of bulk α-$Fe_2O_3$ viewed along the (111) direction, with Fe at the centre of the polyhedra.**

γ-$Fe_2O_3$ has cubic symmetry and is in the space group Fd3m with a lattice constant of 8.35 Å[36]. The structure is spinel like and has the Fe atoms occupying the eight tetrahedral sites and in addition 13⅓ Fe atoms occupying the sixteen octahedral sites. All of the thirty two oxygen sites are occupied.

### 1.6.3 $Fe_2(MoO_4)_3$

Single crystals of $Fe_2(MoO_4)_3$ exist in the space group $P2_1$ in a monoclinic structure with lattice parameters of a = 15.693 Å, b = 9.235 Å, c = 18.218 Å and β = 125.21 °[37]. The eight crystallographically unique iron atoms are essentially octahedrally coordinated by six oxygen atoms at an average distance of 1.992 Å. The twelve molybdenum atoms are in a rather distorted oxygen tetrahedral with an average Mo-O distance of 1.756 Å. Each oxygen atom links an $FeO_6$ octahedron with one $MoO_4$ tetrahedron leading to a rather open structure with the nearest Fe-Fe distance of 5.03 Å. Measurements on non stoichiometric ferric molybdates excluded the possibility of excess $MoO_3$ being soluble within the $Fe_2(MoO_4)_3$ when the sample is

prepared by heating the two component oxides together[38]. The structure of α-$Fe_2(MoO_4)_3$ is shown below (Figure 1-8), with the green and orange polyhedra representing molybdenum and iron, respectively, with oxygen in the corner positions. Each oxygen is 2-coordinated, being shared between two polyhedra. The structure is viewed in the [100].

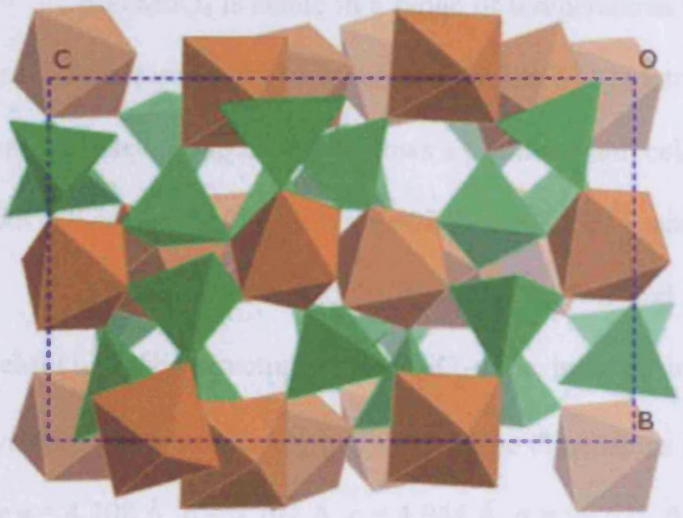


**Figure 1-8 – Structure of α-$Fe_2(MoO_4)_3$ viewed along the (100) plane, with Mo at the centre of the green tetrahedra and Fe in the orange octahedra.**

There is a non-destructive reversible phase transition to β-$Fe_2(MoO_4)_3$ from the monoclinic form at 513 °C, with the β-$Fe_2(MoO_4)_3$ crystallising in the orthorhombic scandium tungstate [$Sc_2(WO_4)_3$] structure[39]. The orthorhombic $Fe_2(MoO_4)_3$ has the space group Pnca lattice parameters of a = 9.236 Å, b = 12.821 Å, and c = 9.108 Å[40].

It has been reported the unit cell of α-$Fe_2(MoO_4)_3$ is larger along some crystallographic planes when excess $MoO_3$ is present when compared to the stoichiometric molybdate[41]. The explanation of this was that the structure is $Fe^{3+}$ defective, *i.e.* $Mo^{6+}$ atoms replace some of the $Fe^{3+}$, with the presence of extra $O^{2-}$ to maintain neutrality. The evidence suggests that the lattice disorder in $MoO_3$-$Fe_2(MoO_4)_3$ is due to this extra $O^{2-}$.

### 1.6.4 $FeMoO_4$

The low temperature, low pressure form α-$FeMoO_4$ can be found as a stable compound at room temperature[40]. This compound has a monoclinic unit cell in the space group $C\frac{2}{m}$ with the following lattice parameters a = 9.807 Å, b = 8.950 Å, c = 7.659 Å and β = 114.02 °.

β-$FeMoO_4$ is stable in a range of temperatures from 25-800 °C in which Fe is in an almost octahedral environment, while Mo is tetracoordinated[42]. The compound has the space group $C\frac{2}{m}$ and shows a primitive unit cell with lattice parameters for the unit cell are a = 10.301 Å, b = 9.402 Å, c = 7.053 Å, and β = 106.28 °.

A third form $FeMoO_4$-II is also known and is the high pressure form of $FeMoO_4$[43]. The structure of $FeMoO_4$-II is isostructural with $NiWO_4$, with triclinic symmetry and the space group of $P\bar{1}$. The dimensions of the units cell are reported to be a = 4.708 Å, b = 5.701 Å, c = 4.944 Å, α = 90.67°, β = 90.27°, and γ = 87.68°.

### 1.6.5 $MoO_2$

Molybdenum dioxide exists in a monoclinic structure with the space group $P2_{1/n}$ with the lattice parameters for the unit cell being a = 5.607 Å, b = 4.860 Å, c = 5.537 Å, and β = 119.37 °[44] (Figure 1-9).

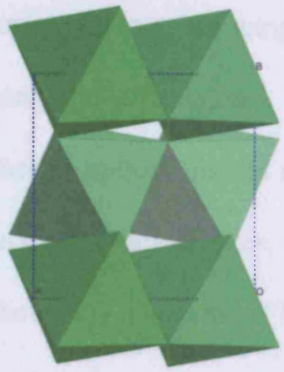

**Figure 1-9 - Structure of bulk $MoO_2$ viewed along the (001) direction, with Mo at the centre of the octahedra.**

## 1.7 Reactivity

As this study is primarily concerned with the selective oxidation of methanol, it is important to establish the knowledge of this reaction on the phases of $MoO_3$, $Fe_2O_3$, and $Fe_2(MoO_4)_3$. The reaction has been shown to produce formaldehyde and water off the molybdenum containing species, while pure $Fe_2O_3$ is selective instead to $CO_2$ and $H_2$[45]. The following section discusses this in more detail, relating to the surface species observed and rate limiting steps to these reactions.

### 1.7.1 Molybdena

The reaction of methanol to formaldehyde on molybdena is highly selective in both reactor and TPD studies[45]. The adsorbed methanol at room temperature is seen in two separate forms, both bound as a methoxy and as undissociated methanol[46]. A methoxy coverage of 3-4 % can be estimated. The undissociated methanol is observed to be weakly chemisorbed through a hydrogen bond to lattice oxygen. Chemisorption is very inefficient on $MoO_3$ (sticking coefficients of approximately $10^{-8}$ at $10^{7}$ Langmuir to $10^{-11}$ at $10^{11}$ Langmuir), and the efficiency of methanol oxidation during UHV TPD experiments is around 40 %[47]. The adsorbed intermediates are not produced in a single elementary step as methanol adsorption at 100 °C, when compared to room temperature leads, to a reduction in uptake by a factor of two for comparable exposures. The suggestion followed that the (010) face is not involved in chemisorption, instead chemisorption at room temperature is localised on other crystal faces and defect sites, where the coordination of Mo is less than 6. This was also shown by a recent AFM study of the (010) face of $MoO_3$ which showed anaerobic methanol reaction at undercoordinated molybdenum sites, although in this case the abstracted H was being used to form a bronze $H_xMoO_3$, and not being released from

the surface[48]. An early study had shown that while methanol is adsorbed onto the (010) face, it does so molecularly and therefore no reactive methoxy is formed[49]. This speculation came about as methoxy groups bound to the surface of $MoO_3$ and $Mo_2O_5(OCH_3)_2$ are very similar when observed by IR and the apparent necessity for coordinatively unsaturated molybdenum atoms for the reaction to occur. However, *ab initio* calculations show that a single-site, single-step proposal is not favourable, leading to the conclusion that two adjacent surface *dioxo units* (Figure 1-10) are required, each extracting one H in a sequence of steps[50]. These required dual dioxo sites are present on the $MoO_3$ (010) surface, but not on other low index faces. During TPD oxygen is removed from the surface, but oxygen movement also occurs through the lattice as, after prolonged exposure to methanol the number of oxygen atoms lost can be calculated to be greater than the number of Mo atoms at the surface. So, the Mo atoms at the surface of $MoO_3$ can be reduced, reoxidised from the bulk and then reduced again.

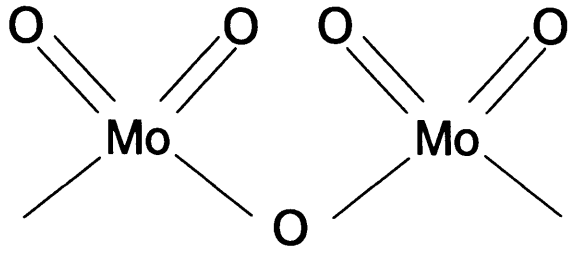


**Figure 1-10 - A dual surface dioxo unit[50].**

These face sensitivity studies contrast with earlier work into the structure sensitivity of methanol oxidation on pure $MoO_3$[51]. Approximately 10 % of the surfaces of a powdered sample of $MoO_3$ were estimated not to be (010) surfaces and this compared well with experimental data which suggested that only 12 % of the surface sites of molybdenum are catalytically active. This demonstrated that the (010) face carried the active centres for dehydrogenation (*i.e.* formaldehyde production),

while the (100) faces had the correct groups and Lewis acid centres active for dehydration (*i.e.* dimethylether formation).

A theoretical study has shown that both molecular and dissociative adsorption on α-$MoO_3$ always involves the interaction of methanol with an unsaturated molebdenum[52]. The molecular chemisorption complex has increasing stability from the (100) face to the (001) and (010), if the (010) presents an oxygen vacancy before methanol adsorption. In the dissociative process, the hydrogen of the methanol OH has to interact with unsaturated surface oxygen ((100) and (001) faces). The dissociative chemisorption then leads to states of greater stability than molecular chemisorption, though this is reversed if the superficial oxygen involved is saturated.

Calculations on an α-$MoO_3$ (010) surface, showed that the bonding of oxygen to the molybdenum is a combination of ionic and covalent for all oxygen species[53]. The covalent nature of the terminal oxygen is stronger than either of the two bridging oxygens. When hydrogen is absorbed onto the surface, the most stable site for hydrogen binding is the terminal oxygen, with a lengthening from 1.66 to 1.89 Å for the M-O bond.

Formaldehyde and CO (a minor by-product, usually detected) have been shown to be formed mainly from a methoxy on the vacancy of a terminal bonded Mo-O[54]. Reduced oxygen vacancy sites in $MoO_3$ weaken the C-H bond, but strengthen the C-O bond in the chemisorbed methoxy, resulting in the formation of more hydrogen-abstracted products. Once formed, formaldehyde can be further oxidised to CO or $CO_2$. Competitive adsorption experiments have shown that on a $MoO_3$ surface the presence of undissociated methanol and water help to retard the further oxidation of the formaldehyde product by blocking the adsorption sites[55].

A study of methane oxidation on $MoO_3$, suggested that the Mo=O sites are responsible for the production of formaldehyde and subsequent oxidation to CO, while Mo-O-Mo bridging sites are responsible for the direct production of CO and $CO_2$[56]. TPR data presented showed the easier reduction of the bridging sites compared to the terminal double bonded oxygen. The Mo-O-Mo sites are also reoxidised more easily by gaseous oxygen, while the Mo=O sites are more easily oxidised by lattice oxygen. methanol onto a thin film of preoxidised $MoO_3$ at 200 °C leads to new IR bands which are associated with the methoxy intermediate and Mo(V)=O[47]. These observed bands are metastable, *i.e.* they are reliant on the presence of gas phase molecules.

Studied model synthetic equivalents, showing formation, decomposition and reoxidation of $Mo_2O_5(OCH_3)_2$ correspond well with the three elementary steps of the catalytic cycle shown (Figure 1-11), with the model yielding formaldehyde with C-H bond breaking in the methoxy being rate limiting[49,57]. $Mo_2O_5(OCH_3)_2$ is formed from the reaction of $MoO_3.2H_2O$ and methanol at 30-60 °C, while this reaction at 0 °C leads to the formation of $MoO_3.CH_3OH$[58].

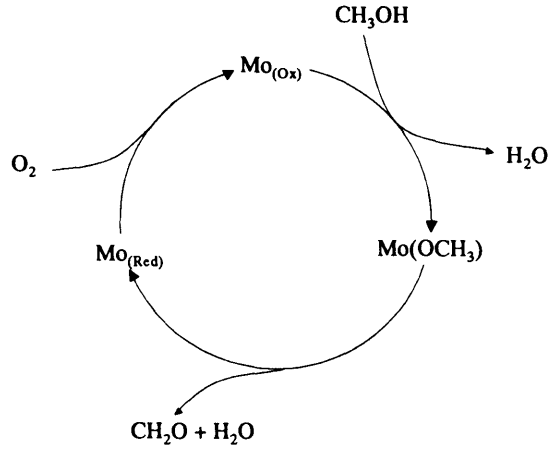


**Figure 1-11-Schematic diagram for the selective oxidation of methanol on a molybdena catalyst.**

Reaction of methanol with gas phase molybdates to formaldehyde has been achieved[59]. The reaction requires a binuclear ion $[Mo_2O_6(OH)]^-$ for the catalytic cycle,

instead of a mononuclear $[MoO_3(OH)]^-$ which was found to be uncreative to the methanol. The rate limiting step was found to be the elimination of the aldehyde, with the reaction not proceeding at room temperature, and instead requiring the use of collision activation.

$MoO_3$ has been found to be an extremely slow oxygen exchanger, as it is a vacancy conductor, with an essential role for defects in the exchange process[60]. The rate of oxygen exchange was not significantly changed by the presence of $H_2O$ in the gas phase. Isotopic exchange of gaseous oxygen with $MoO_3$ has a reaction order of 0.4 with respect to oxygen pressure and the activation energy for the exchange is 172 kJ $mol^{-1}$ [61].

### 1.7.2 Iron Oxide

The interactions between methanol and formic acid on iron oxide (a catalyst selective towards combustion products) surfaces have been studied using XPS and Fourier Transform Infrared (FTIR)[62,63]. These studies show that the mechanism of methanol adsorption can be either dissociative to produce hydroxy and methoxy groups, or molecular, by the interaction of methanol with the Lewis acid and Lewis base sites present on the oxide surface. After chemisorption of methanol at room temperature a marked decrease was observed in the O/Fe atomic ratio, from around 1.5 before chemisorption to around 1.3 after. This indicates a partial reduction of the catalyst surface as a result of the simultaneous partial oxidation of the adsorbate. When adsorbed methanol is heated to temperatures in excess of 127 °C, a surface formate species is formed. The formate is believed to be formed by the combination of methoxy groups and lattice oxygen, as it occurs, even in the absence of external oxygen sources. Oxidation of formaldehyde, as well as methanol can occur on a $Fe_2O_3$ surface, even with an absence of oxygen[64]. Heating to higher than 227 °C has been

shown to cause the decomposition of the surface formate species with the formation of carbon monoxide, carbon dioxide, hydrogen and water.

The formation of formate species is seen with both adsorbed methanol and formic acid on $Fe_2O_3$, but these are not observed with adsorbed formaldehyde[65]. Following a similar mechanism, adsorption of ethanol leads to the formation of acetate groups on the $Fe_2O_3$ surface[66].

Methanol adsorbs onto the Fe (110) surface as a methoxy at -163 °C and dehydrogenates at ~127 °C, to yield $H_2$ and CO[67]. The hydroxyl hydrogens leave the surface as $H_2$ at the slightly lower temperature of 102 °C. The presence of surface oxygen on Fe (110) inhibits O-H and C-O bond dissociation in methanol, which leads to a decrease in the total amount of reaction and an increase in the amount of methanol desorbed from the surface. Methanol adsorbs onto a clean $\alpha$-$Fe_2O_3$ (0001) surface in an intact molecular state, with monolayer methanol desorbing between - 133 and - 93 °C[68].

### 1.7.3 Iron Molybdates

The reactivity of iron molybdates for methanol oxidation has been the focus of a steady production of literature since the late 1960's due to its importance as an industrial reaction. Industrial catalysts always have an excess of molybdenum present (in the form of $MoO_3$) compared to that required for the stoichiometric $Fe_2(MoO_4)_3$. The active phase is considered by some authors to be $Fe_2(MoO_4)_3$, while others consider the active phase to be the mixed oxides with molybdenum excess.

$Fe_2(MoO_4)_3$, $MoO_3$ and binary mixtures of the single oxides were tested for methanol oxidation with all catalysts showing selectivity towards formaldehyde, and those that contained $Fe_2O_3$ also showed selectivity towards CO[69]. This study showed the reaction to be first order with respect to $O_2$ on iron molybdates, with an activation

energy of 45.2 kJ $mol^{-1}$. A defective mass balance was observed during pulsed microreactor studies of methanol oxidation to formaldehyde over $MoO_3$-$Fe_2(MoO_4)_3$ catalysts[70]. Pure $Fe_2(MoO_4)_3$ was shown to be active in pulsed flow experiments, however it was virtually inactive in continuous flow experiments. This was explained as being due to fast acting centres participating in the reaction for the pulsed flow work, but because of the difficulty in reoxidising or poisoning by products/intermediates only limited activity was observed in continuous flow. The formaldehyde yield was independent of flow rate, while the methanol conversion is not, so the incorrect suggestion was made that formaldehyde desorption was rate limiting. A later study suggested that it was in fact the $Fe_2(MoO_4)_3$ phase that was active as little difference was found in steady state catalytic behaviour between catalysts with Mo/Fe atomic ratios of 1.5 and 3[71].

An article by Trifiro *et al.* discusses the need for excess Mo and concludes that it is necessary for three reasons[72]: i) to increase the mechanical properties of the catalyst, ii) to dope the $Fe_2(MoO_4)_3$ in order to reach a Mo/Fe ratio greater than 1.5 in the active phase, and iii) to allow the re-oxidation process of β-$FeMoO_4$ to $Fe_2(MoO_4)_3$ by supplying *in-situ* the $MoO_3$ involved in the reaction. In reviewing ammoxidation catalysts Grasselli stated that a small molybdenum excess was required for the best catalytic performance in all molybdate based catalysts[73]. The excess $MoO_3$ was considered to be a spectator phase which is able to provide mobile mononuclear $MoO_3$ or $MoO(OH)_2$ to the reduced phase. The mobile Mo species were said to have the ability to regenerate the damaged catalyst. A recent review article on iron molybdates for methanol oxidation also concludes that it is the $Fe_2(MoO_4)_3$ phase that is active in the reaction, with the $MoO_3$ required to replace volatilised molybdenum (for details on catalyst deactivation, see Section 1.12)[74].

When catalysts with different iron to molybdenum ratios were prepared by precipitation it was found that an amount of molybdenum above that expect for $Fe_2(MoO_4)_3$ was always found[75]. From this a proposal was made that a correlation exists between Mo at the surface and selectivity instead of a correlation between Mo-excess in the bulk and activity. This excess molybdenum also had the beneficial effects of increasing the surface area and mechanical strength of the catalyst. This work also showed that argon sputtering of a catalyst prepared to have an Mo/Fe ratio of 1.6 ± 0.1 lead to a change in the surface composition from a Mo/Fe ratio of 1.95 to 1.35 as monitored by XPS.

The effect of calcination temperature has been investigated and it was found the most active catalyst was produced when a stoichiometric mixture was calcined at 673 K, as opposed to the other temperatures of 573, 773, and 973 K tested[76]. This peak in activity and selectivity with calcination temperature was found as at lower temperatures the catalyst showed an amorphous structure, while at 673 K the crystallisation was complete. Those calcined to higher temperatures also had high activities and selectivities, but not as high as those for the catalyst calcined at 673 K.

When an iron molybdate is subjected to mechanical treatment an amorphous inactive phase is formed, however after the catalytic oxidation of methanol the amorphous samples transform back to crystalline forms as observed before mechanical treatment[77]. Stoichiometric Fe-Mo oxide presents an ordered plate lamella whereas Mo rich oxides present an amorphous sponge like pattern when studied by SEM[78]. Studies by del Arco *et al.* showed two types of crystallite, stick like crystals corresponding to $MoO_3$ and sponge like crystals corresponding to $Fe_2(MoO_4)_3$[79,80]. When a stoichiometric catalyst was compared to a Mo rich catalyst, after 72 hours on stream, the Mo excess seemed to decrease the amount of reduced iron species seen at

the surface. (*i.e.* the $Fe^{2+}$:$Fe^{3+}$ ratio increased more for the stoichiometric catalyst). XPS measurements discovered no $Mo^{4+}$ or $Mo^{5+}$ at the surface of the fresh or used catalysts.

Detailed investigation into the active sites for both supported and bulk oxide catalysts using methanol chemisorption was carried out by Burcham *et al.*[81,82]. On supported $MoO_3$ it was found that about 0.3 methoxylated surface species existed per active metal oxide atom across the surface, due to steric limitation. On Lewis acid sites, methanol tends to adsorb as $CH_3OH_{ads}$, while on less Lewis acid or Lewis base sites methanol tends to adsorb as $OCH_{3ads}$. Molybdenum cations are the adsorption sites on iron molybdates and have a tendency to adsorb methanol as $CH_3OH_{ads}$, due to the acidity associated with $MoO_3$. Bulk metal molybdates have similar intrinsic turn-over frequencies (TOFs) to those observed for supported model catalysts (e.g. $MoO_3$/NiO) *vs.* $NiMoO_4$)[82]. The suggestion by the authors is that this is possibly due to the formation of a "monolayer" of molybdenum oxide species on the surface of bulk metal oxides. In both supported and bulk metal oxides the same electronic ligand effect appears to control the methanol oxidation TOF, in that with increasing ligand cation electronegativity there is a decrease in the TOF. By analogy to previous work into structure reactivity relationships[81], it was concluded that electronic variations in localised Mo-O-ligand bonds were mainly responsible for differences in TOF in bulk metal oxides. The idea of a Mo monolayer is in contrast to conclusions drawn from work ongoing at a similar time in which it is suggested that the $Fe_2(MoO_4)_3$ is the active phase, as an excess of $MoO_3$ in the catalysts leads to an increase in the surface area of the catalyst, but does not cause a significant change in the activity of methanol oxidation per unit area[83].

Isotopic exchange of molecular oxygen with the oxygen of iron molybdates shows that at high temperatures (above 500 °C), the rate of oxygen diffusion within the bulk is much faster than the rate of exchange, so it can be assumed there is no substantial difference between surface and bulk oxygen[84]. The activation of the exchange on a sample with a Mo/Fe ratio of 1.5 was found to be 210 ± 13 kJ $mol^{-1}$, while with a ratio of 1.75 the activation energy was found to be 200 ± 13 kJ $mol^{-1}$. While on an unreduced sample no low temperature isotopic exchange was observed, the removal of two monolayers of oxygen leads to the formation of centres active for low temperature exchange. The exchange proceeds *via* heteroexchange with the participation of oxygen from the catalyst surface, which despite a high rate shows unstable activity.

While the reaction of methanol over iron molybdates is highly selective, some by-product formation does occur. In a review on methanol oxidation Tatibouët proposed a reaction scheme (Figure 1-12) showing all reactions, except formation of dimethyl ether being reliant on at least one oxidation step[85]. The same author proposed that the methanol oxidation was structure sensitive, with the formation of the different products dependant on the acid-base strength of the catalyst. The selectivity towards formaldehyde of the iron molybdates increases with conversion, until high methanol conversion, when the formation of CO, often considered the major by-product, starts to become important[74]. The selectivity of formaldehyde from iron molybdates has been shown not to differ significantly from $MoO_3$ under similar reaction conditions[55]. Edwards *et al.*, related the formation of by-products of dimethyl ether, methyl formate, and methylal at low temperatures to the increased residence time of the intermediates[86]. The formation of CO is usually from the oxidation of formaldehyde,

but at high temperature has been observed to also be formed directly from methanol oxidation[87].

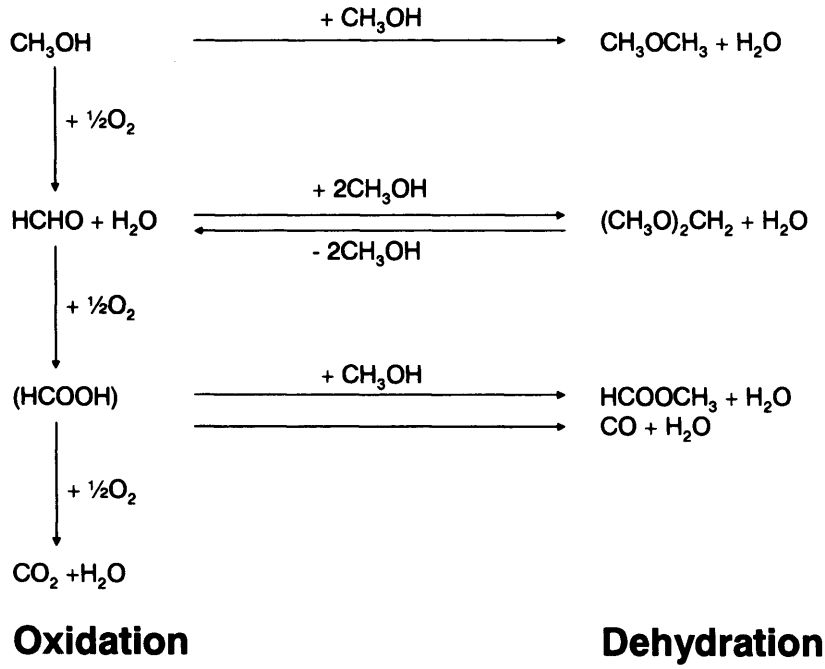


**Figure 1-12 - Schemes of reaction for the oxidation and dehydration of methanol[85].**

The rate limiting step of the selective oxidation of methanol to formaldehyde on iron molybdates has been suggested to be numerous steps, but a kinetic isotope study by Machiels and Sleight revealed that (similar to $MoO_3$) hydrogen abstraction from the methoxy group is rate limiting[88]. Further study of the rate limiting C-H bond breaking in the oxidation of methanol on supported $MoO_3$ was recently reported with an activation energy of 98 kJ $mol^{-1}$ [89,90]. The presence of water in the gas stream acts as a product inhibitor, as water vapour chemisorbs dissociatively to form hydroxyl groups, which serve to reduce the steady state concretion of surface methoxy groups, by reacting with them to form methanol[90].

A recent kinetic study concluded that methanol selective oxidation to formaldehyde could be well described with Langmuir-Hinshelwood kinetics[91], assuming two different metal oxide sites, one containing absorbed oxygenoates and

the other containing lattice oxygen. This same study discovered that the rate of CO production is first order with respect to formaldehyde with the same oxygen dependency as the formaldehyde formation from methanol. Previously it had been shown that the production of CO was from the further oxidation of formaldehyde by varying the residence times[71].

The high activity and selectivity of iron molybdates for methanol to formaldehyde have recently seen the system used for a novel atmospheric monitoring system[92]. The range of methanol measured by this system was in the ppb range.

Computational work has discovered that an improved formaldehyde yield could be obtained with a distributed heat flux, while an oxygen flux had no effect[93]. This study found the most important variables in the catalytic process were the surface area of the catalyst and the rate of formaldehyde desorption. Unfortunately, despite the novel approach used in this work the value of the results obtained is questionable as the calculations for modelling used formaldehyde desorption as the rate limiting step. The abstraction of hydrogen from the methoxy is rated at a factor of 10 faster, when in fact work published in 1982 showed hydrogen abstraction from the methoxy to yield formaldehyde to be rate limiting[88].

From the published literature the main conclusions that are drawn are that the active phase is $Fe_2(MoO_4)_3$, which oxidises methanol through the same method as $MoO_3$. This method involves molecular adsorption as methanol, transformation to methoxy, before the rate limiting step of hydrogen abstraction and formaldehyde release, before hydroxyl recombination and water release. The reduced surface is then re-oxidised from oxygen in the gas flow.

## 1.8 Preparations of Iron Molybdates

While the industrially used iron molybdates are prepared by coprecipitation of a ferric salt ($FeCl_3$ or $Fe(NO_3)_3$) and an alkali molybdate ($(NH_4)_6Mo_7O_{24}$)[94,95], different methods have been tested within the literature.

In 1994, Ivanov reported that he believed the maximum selectivity and activity of iron molybdate catalysts were yet to be reached[96]. He demonstrated how higher selectivity could be retained at high activity, CO could be reduced in the exhaust gas and less bulk density of catalyst could be generated by recycling waste catalyst. His recycling process involved grinding the waste catalyst, chemical treatment (though no mention is made of details), followed by drying and shaping, before calcinations at 500 °C.

New preparation methods for iron molybdate catalysts have been tried in the last few years[97,98]. A method of buffer precipitation by Belhekar *et al.* was compared to an industrial coprecipitation catalyst and a laboratory scale coprecipitation catalyst. The buffer catalyst was found to be more similar to the industrial catalyst, with a more homogeneous surface morphology than the laboratory coprecipitation catalyst. It is suggested that the reason for this is that on heat treatment the buffer and industrial catalysts are better able to form Mo-O-Mo bonds. The buffer prepared and industrial catalysts showed a more intimate mixture of $MoO_3$ and $Fe_2(MoO_4)_3$ and demonstrated a higher temperature stability which is in turn related to the activity-stability of the catalyst in the selective oxidation reaction. Another novel preparation technique was presented by Soares *et al.* and involved a sol-gel preparation. These catalysts were able to operate at lower temperatures than a current industrial catalyst and they reduced the amount of formaldehyde further oxidised to CO. The excess Mo in this case formed an amorphous phase that provided a large contribution to the surface area,

which was increased compared to the industrial catalyst, so increasing the number of methanol adsorption sites.

Wet and dry mixing of iron (III) nitrate and ammonium heptamolybdate, followed by calcination have shown both techniques can produce iron molybdates for formaldehyde production from methanol[99]. The catalyst produced by wet mixing were found to be more reproducible than those from the dry mixing, though both catalysts showed phases of $Fe_2(MoO_4)_3$ and $MoO_3$ after calcination. Solid phase synthesis is possible using iron-oxide-hydroxide (FeO(OH)) and ammonium heptamolybdate, with heating to 400 °C after centrifugal milling of the two reagents[100]. Without the milling, a temperature 200 °C higher is required to form the $Fe_2(MoO_4)_3$ phase.

A novel method of preparation with a yield of up to 92 % was recently reported[101]. The method involves the reaction of iron powder and molybdena in a Mo:Fe ratio equal to or above that required for $Fe_2(MoO_4)_3$ in an aqueous solution before oxidising the mixture with hydrogen peroxide to form $Fe^{3+}$ and $Mo^{6+}$.

Wachs and Braind have prepared iron molybdates *in-situ* for selective methanol oxidation[102]. To do this they placed the single oxides in a physical mix within the reactor and passed methanol/oxygen mixtures over the catalyst and this lead to the formation of $Fe_2(MoO_4)_3$ in the methanol conversion zones as observed by Raman spectroscopy.

## 1.9 Supported Catalysts

While the current iron molybdate industrial catalyst is an unsupported catalyst, a high level of research has been carried out with respect to supported molybdena and iron molybdates. Typical supports used in catalysis, usually have significantly higher surface areas than the ~8 $m^2$ $g^{-1}$ recorded for the industrial catalyst, and in fluidised beds, unsupported iron molybdates are weak to mechanical abrasion[74,103].

When iron molybdates supported on $SiO_2$ and $Al_2O_3$ were studied by Raman spectroscopy, no bands associated with $Fe_2(MoO_4)_3$ or $MoO_3$ were observed until the iron molybdate made up at least 10 w/t %[104]. This was result was described in terms of significant catalyst-support interactions, which were noted to be stronger for the alumina support than the silica support. At 10 w/t %, bands associated with $Fe_2(MoO_4)_3$ were observed, while those associated with $MoO_3$ were not observed until 33 w/t %. The appearance of the bands were independent of the Mo:Fe ratio within the supported catalyst, although a ratio above that required to form $Fe_2(MoO_4)_3$ was always maintained. With a loading of less than 33 w/t %, the samples presented a colour with a red/orange tint. The authors suggest that this may show the presence of $Fe_2O_3$, which is a very weak Raman scatterer, and so may not have been detected.

The choice of support can severely affect the molybdenum structure formed for supported molybdena catalysts[105]. Tetrahedral Mo sites with $MoO_3$ crystallites were observed on the one type (Cabosil, L-90) of silica, while a second type (Cabosil, EH-5) showed a mixture of dioxo (Mo=O) tetrahedral and distorted octahedral sites. On $Al_2O_3$ the sites were likely adsorbed $MoO_4$ units, while on $TiO_2$ the catalyst was comprised of distorted octahedral sites. TPR studies showed that the reducibility of these samples in TPR were as follows: $MoO_3/TiO_2$ < $MoO_3/SiO_2$ (L-90) < $MoO_3/Al2O_3$ < $MoO_3/SiO_2$ (EH-5)[89]. The increasing ease of accommodation of charge by the metal centres in supported molybdena can be shown to explain the positive relationships between catalytic activity and decreasing electronegativity of the support ion, the increasing reducibility of dispersed molybdenum centres, and the increasing size of the molybdenum ensemble.

On $TiO_2$ supported $MoO_3$, dispersed phases of molybdenum oxide, were found to be more easily reduced than crystalline $MoO_3$ on the surface, which in turn is more

easily reduced than bulk $MoO_3$[106]. The dispersed species were bonded to Ti cations through bridging oxygens, with the overall coordination dependent on the level of surface hydration. Surface species observed with adsorbed methanol are similar for dispersed and crystalline $MoO_3$ on $TiO_2$ and include the presence of formate groups at 200 °C, with high levels of methyl formate observed in reactor conditions[107].

Adsorption of methanol onto a $SiO_2$ supported $MoO_3$ catalyst, occurs on the $MoO_3$, with the methoxy groups able to spillover and migrate onto the $SiO_2$[108]. The spillover of the methoxy groups leads to a consumption of all of the surface Si-OH groups. Two types of methoxy were distinguished, noted spectators and intermediates, with only the intermediates able to be oxidised below 300 °C on the molybdena surface[109]. The $SiO_2$ was not involved in the reaction, but the surface held six times as many methoxy species as the number of molybdenum species, showing the $SiO_2$ to be inert to reaction, but able to hold a substantial population of the reactive intermediates. The reaction rate of methanol over $MoO_3$ on $SiO_2$ catalysts, is dependent on the molybdena coverage, and *in-situ* Raman spectroscopy has shown that during this reaction the molybdenum oxide species aggregate to form β-$MoO_3$[110]. The extent of aggregation increases with increasing surface molybdenum coverage, and this was used to account for the decrease in activity for methanol oxidation with increasing surface molybdenum coverage.

When methane is oxidised on a finely divided $MoO_3$ on $SiO_2$ catalyst, the addition of water helps to prevent the over oxidation of the initially formed methanol to formaldehyde[111]. The same effect was not observed with a less finely divided catalyst made by the impregnation method (as opposed to the high division, sol-gel method), leading the authors to ascribe the feature to the formation of silicomolybdic acid on the surface when the molybdena was finely divided. The presence of calcium

impurities within a silica support can lead to the formation of calcium molybdate on the surface, rather than pure molybdena[110].

With molybdena supported on $\gamma$-$Al_2O_3$, it has been shown that $Mo^{5+}$ leads to a deactivation towards oxidation products (formaldehyde), with an increase in non oxidative products (dimethyl ether) in comparison to $Mo^{6+}$ [112]. This work showed the importance of the polymolybdate phase in supported molybdates. Molybdates supported on $Al_2O_3$ can also be used to oxidise dimethyl ether to formaldehyde, with some methanol also obsereved[113-115].

At low surface coverages of $MoO_3$ on $Al_2O_3$ and $TiO_2$, $MoO_x$ are isolated and tetrahedrally coordinated[116]. At higher coverages, a difference appears, with the primary species on $TiO_2$ being polymerised and octahedrally coordinated, while on $Al_2O_3$, there is a mixture of octahedrally and tetrahedrally coordinated species. The molecular structure of the molybdena does not effect the reaction selectivity, for methanol oxidation, but does have a slight influence over TOF[117]. The TOF, is controlled to a much greater extent however by the reducibility of the support, suggesting a strong influence of the Mo-O-support bond. Studies of supported vanadia showed the same support effect for methanol oxidation with changes noted in the methoxy decomposition rate constant and, to a lesser extent, the adsorption equilibrium constant[118]. The effect was correlated to the electronegativity of the support cation, with this effecting the hydrogen abstraction from the methoxy and the steady state adsorption of methanol to methoxy through the basicity of the V-O-support bond.

Molybdenum supported on tantalum oxide (prepared by an impregnation method) forms a structure similar to $Mo_8O_{24}^{4-}$ (the ionic species present in acidic solution) in ambient hydrated conditions, while calcination to 450 °C led to the

formation of $MoO_3$ in isolated and/or polymerised species[119]. Of the supported metal oxides ($Re_2O_7$, $CrO_3$, $MoO_3$, $WoO_3$, $V_2O_5$, and $Nb_2O_5$ on tantalum oxide), only the molybdena showed both acidic and redox properties required for formaldehyde production.

When $MoO_3$ is added to the surface of $\alpha$-$Fe_2O_3$, a calcination temperature of 420 °C leads to the dispersal of $MoO_3$ on the surface, with the formation of surface "Mo-O" species, while a calcination temperature of 500 °C leads to the formation of $Fe_2(MoO_4)_3$[120]. A catalyst active for the selective oxidation of methanol to formaldehyde was made by the dry mixing of molybdic acid and $Fe_2O_3$[121]. The mixture was wetted to form a paste before calcination to temperatures in excess of 550 °C. The molybdena monolayer was found to be active, with two neighbouring molybdenum sites playing the role of the active site; one for the adsorption of the methanol and the second for the abstraction of hydrogen. The structure of the monolayer was found to be similar to that of iron defective $Fe_2(MoO_4)_3$ with $MoO_3$.

$MoO_3$ has been shown to be spread onto the surface of oxide supports during alcohol oxidation[122]. This spreading has been shown to be much greater for methanol than for other primary alcohols and water. This higher reaction induced spreading is related to the high volatility and stability of the methanol molybdenum complex.

While supported catalysts have proved useful for research processes, they are not used commercially because reaction of the support with formaldehyde leads to a lowering of the selectivity, with further oxidation to CO and $CO_2$.

## *1.10 Promoted Iron Molybdates*

It is reported that incorporation of chromium as a promoting agent in iron molybdates can lead to catalysts with a higher selectivity to formaldehyde, and at lower temperatures[123]. The chromium containing catalysts had smaller molybdena

crystals, with a different topology with plates forming instead of sticks. It is claimed the chromium acts to increase the mobility of the oxygen ions bound to molybdenum through a change in coordination number, stereochemistry, or oxidation state of molybdenum. These catalysts have also been shown to have a greater stability when used over a long period of time, when compared to iron molydates[124].

Modifications of the catalyst by incorporating tungsten so that solid solutions of $Fe_2(Mo_xW_{1-x}O_4)_3$ and $Mo_xW_{1-x}O_3$ are formed by coprecipitation have been studied[125]. When tested at 250 and 350 °C the catalysts with $WoO_3$ up to 15.9 w/t % showed high selectivity and activity. The catalysts with up to 5 w/t % $WoO_3$ showed improvement over the pure iron-molybdate with selectivities up to 93.4 % formaldehyde with a total methanol conversion of 97 % reported.

Incorporation of cerium, in the form of cerium molybdate to the precipitated catalyst, before calcination, has been shown to lower the hot spot temperature[126]. The cerium molybdate was prepared separately, typically by precipitation and was mixed with the iron molybdate before calcination to over 450 °C. The formaldehyde yield achieved with this catalyst was 92 %.

Addition of a cobalt salt and further ammonium heptamolybdate to a ground precipitate prior to calcination have been suggested to lower side product formation[127]. The cobalt added was in low concentration (<0.2 w/t %), and formed a phase of $CoMoO_4$ near the surface of the catalyst.

Iron phosphate catalysts have been tested for the selective oxidation of methanol, and have been shown to be highly selective towards formaldehyde[128]. The high selectivity of the catalyst is attributed to the similarity of the $Mo^{6+}$ and $P^{5+}$ ions in terms of electronegativities and high covalency of the M-O bond. The catalysts show a

lower activity than corresponding iron molybdate catalysts with conversion of methanol of around 50 % at 427 °C.

When iron is replaced by manganese, it is found that the most selective catalyst contains a slight excess of $MoO_3$ as well as $MnMoO_4$[129]. These catalysts (prepared by the impregnation of $MnMoO_4$ with ammonia paramolybdate) have an activity and selectivity close to that of industrial iron molybdates with conversion of 95.4 % of the methanol and 94.4 % selectivity to formaldehyde at 350 °C.

An investigation into tin molybdate catalysts suggested that the active species for methanol oxidation to formaldehyde was $Mo^{5+}$, which was present even after calcination to 500 °C[130]. The mechanism proposed for the reaction of methanol involved the reaction of the $Mo^{5+}$ species with water to form a hydroxide (1-14), before reaction with methanol to yield a surface methoxy.

$$Mo^{5+} + H_2O \rightarrow (Mo^{5+}\text{-}OH)^- + H^+ \qquad (1\text{-}14)$$

A multi component oxide catalyst containing Co, Ni, Fe and Bi molybdate, has a high selectivity to formaldehyde over a temperature range of 350-390 °C[131]. These catalysts suffer a decrease in formaldehyde yield of about 30 % after a period of 80 hours on stream. However, when phosphorus and thallium were added as promoters, the selectivity remained high, with the major kinetic parameters reduced by 5-10 % over a period of 60 days on stream. The promoters effect the structure of the catalyst and the electronic properties of their surfaces.

## *1.11 Reactor Designs*

There has been increasing interest in recent years for a move away from the traditional fixed bed reactor, as used in the partial oxidation of methanol to other reactor designs.

Iron molybdates have been used in fluidised bed reactors with yields up to 87 %[132]. The iron molybdate was prepared by co-precipitation but was stabilised with the impregnation of $Bi_2O_3$ onto the surface. The fluidised bed reactor was less efficient for methanol conversion with the same weight of catalyst, at the same temperature. A small laboratory scale membrane-assisted fluidised bed reactor has also been tested and this allowed for safe operation of the reaction with increased methanol inlets[133]. Inlets up to 18 % methanol were used, which still showed greater than 90 % methanol conversion. Total formaldehyde yields observed from this reactor were at best ~85 %.

A packed-bed membrane reactor using iron molybdate catalyst has shown an improved selectivity of formaldehyde and methanol conversion compared to a fixed bed reactor when oxygen is the permeating component[134,135]. However, when methanol was used as the permeating component, the performance observed was worse than that for the fixed bed reactor.

The normal industrial reactor contains a mix of inert and iron molybdate catalysts near the inlet to control the 'hot-spot' temperature before a layer of pure iron molybdate to complete the methanol conversion[14]. A recent patent by Wachs and Bourne however, suggests that good performance can be achieved with the first part of bed containing a vanadia-titania catalyst[136]. The claimed advantage of this system is that in the initial region the catalyst is free of molybdena, the volatilisation of which is known to be a major cause of deactivation (see Section 1.12). A previous patent by Hoene suggested the combination of the two major current technologies, with an initial reactor with a silver catalyst, before the reaction mixture is passed over an iron molybdate catalyst[137].

## 1.12 Deactivation of the Catalyst

While the typical description of a catalyst is that it undergoes no net chemical change, in practice over long periods of time this is often not the case. Iron molybdate catalyst loads used industrially usually require changing at least yearly, as the catalyst activity drops and formation of undesired products increases[14].

Research by Popov *et al.* concluded that a major reason for deactivation of iron molybdate catalysts during the selective oxidation of methanol was the volatilisation of molybdenum from the surface[138]. They found the partial pressure of the volatile molybdenum species to be dependant on methanol concentration and increased with temperature. The presence of water also formed volatile species, but at three orders of magnitude lower than that for methanol. The molybdenum volatile species increased with the molybdenum content of the catalyst and when oxygen partial pressure decreased.

Pernicone ascribes the deactivation as being caused by the accumulation of $Fe_2O_3$ on the surface of the catalyst pellet, as well as the volatilisation of molybdenum from the hot spot region[139]. He proposed accelerated tests for the iron molybdate catalysts, but it is stressed that these tests merely allow for the comparison of catalysts in terms of deactivation behaviour, as in industrially conditions, other factors may influence the deactivation procedure.

A recent study of an iron molybdate catalyst under industrial conditions, showed movement of molybdenum from the upper layer of mixed iron molybdate and inert to a lower layer of pure iron molybdate[14]. The volatilisation of the molybdenum led to an increase in surface area of the mixed phase layer, with a build up of $Fe_2O_3$ on the surface of the catalyst pellets. The loss of molybdenum also leads to a lowering of the activity of the catalyst, with the hot spot moving further down the reactor. The

volatilised molybdenum species condensed in the lower part of the reactor in the form of needle like crystals of $MoO_3$, this led to a surface area decrease and an increase in pressure drop across the bed. A patent by Wachs *et al.* has shown the ability to regenerate a spent iron molybdate catalyst by moving the $MoO_3$ formed around with methanol in a nitrogen stream flowing in the opposite direction to that normally used within industrial conditions[140]. Investigations into the loss of Mo from supported Fe-Mo/$SiO_2$ catalysts showed that when heating in $N_2$, a catalyst composed of $Fe_2(MoO_4)_3$ with excess $MoO_3$, the crystalline $MoO_3$ would be lost first[141].

Heat treatment leads to the deactivation of the catalyst, which was associated by Ma and Knimotek with the decomposition of the catalytically active ferric molybdate $Fe_2(MoO_4)_3$ to the catalytically inactive ferrous molybdate $FeMoO_4$[142]. The rate of volatilisation of molybdena was associated with the deactivation of the ferric molybdate reaction sites, as the deactivation observed occurred mainly at the surface.

The mechanism of the deactivation process of the iron molybdate catalysts was recently restudied and showed an increase in surface reduction as there is an increase in the $Fe^{2+}$:$Fe^{3+}$ ratio and surface loss of Mo[78,143,144]. Mo loss occurred from the surface by $MoO_3$ sublimation, Mo-methanol compounds and Mo-water volatile compounds, while migration of Mo from the bulk to compensate for the surface Mo loss was also seen. These studies demonstrated that the loss of molybdenum was not negligible as previously described[138], and may be similar to work reported by Zhang *et al.* for bismuth molybdate catalysts, which refer to the formation of $MoO_2(OH)_2$ compounds[145]. With water present in the reactor feed, an enhanced deactivation of the catalyst was noted, and was ascribed to water retarding the reoxidation of the catalyst[143].

The loss of molybdenum from a supported Fe-Mo/$SiO_2$ in water vapour atmospheres was fitted to the equation[146]:

$$-dC_s/dt = kVC_s \quad (1\text{-}15)$$

Where $C_s$ is the $MoO_3$ content of the catalyst after reaction (kg/kg support), t is the reaction time (hours), k is the loss-rate constant ($kg/m^3$), and V is the flow rate of gas ($m^3$/(kg support x h).

$$\ln k = 11.065 - 10633.7/T \quad (1\text{-}16)$$

Where k is the same as (1-15) and T is temperature (K). This mechanism of this loss was proposed to be:

$$MoO_4^{2-} + 2H_2O = MoO_2(OH)_2 + 2\,OH^- \quad (1\text{-}17)$$

$$MoO_2(OH)_2 = MoO_3 + H_2O \quad (1\text{-}18)$$

An industrial iron molybdate catalyst was found to be considerably more stable than the supported catalyst with a loss constant rate constant, k, of 0.00197 compared to 0.40. In this study the added stability was attributed to the formation of other molybdate compounds on reduction of the catalyst that helped prevent the formation of $MoO_2$ and therefore the volatile compound.

The increased volatility of $MoO_3$ in the presence of water has been known for a considerable time. In 1949, Millner and Neugenbauer observed an increase of seventeen times in the amount of $MoO_3$ lost at 600 °C when water was present, as opposed to moisture free air[147]. The increased volatility of $MoO_3$ in $H_2O$ containing atmospheres has been used to disperse $MoO_3$ onto supports of $SnO_2$, $Al_2O_3$ and $SiO_2$ to make active catalysts[148-150]. Typical conditions employed involved in creating the $SiO_2$ supported catalysts involved passing air, with a partial pressure of 107 Torr $H_2O$ over a bed of $MoO_3$ at 540 °C, before a bed of the support held at 700 °C. After a period of 24 hours 5.7 w/t % $MoO_3$ was observed on the $SiO_2$[150]. A band of $MoO_3$

could be observed spreading down the $SiO_2$, showing a strong interaction between the $MoO_3$ and the support.

The ideal (010) surface of molybdena has been studied by AFM, with an atomically resolved image showing array with 0.40 and 0.37 nm along the [100] and [001] respectively, corresponding to the topmost double bonded oxygen atoms[151]. The $MoO_3$ (010) surface suffers changes in morphology with the volatilisation of molybdenum when methanol is partially oxidised at 250 °C and above[152]. Deep pits in 7 Å integers (the distance between the van der Waals gaps which separate the adjacent layers of the α-$MoO_3$ structure) are formed and grow so that evaporation occurs in an almost layer by layer fashion. An interesting point to note is that chemical etching of the $MoO_3$ (010) surface with NaOH also produces steps of ~7 Å[153]. The pit depth and the sites exposed along the edges when exposed to methanol are dependant on oxygen concentration, with high partial pressures only the first one or two layers are exposed, with the steps generally orientated along 001, while with lower ratios more than five layers may be simultaneously exposed, with edge orientations closer to 100[152]. Oxidation of methanol on the (010) face of molybdena in the absence of oxygen however leads to the formation of a $H_xMoO_3$ bronze and no molybdenum loss[154]. When the molybdenum (010) surface, has pits formed on it in advance, it is capable of intercalating more H into the bronze, with the bronze observed growing from the edge of the pits[48]. The volatilisation was increased by the presence of atmospheric water impurities, with the condensation of crystalline $Mo_2O_5(OCH_3)_2$ at the reactor exhaust when the reaction mixture was passed over a powdered $MoO_3$ sample[152]. The observance of $Mo_2O_5(OCH_3)_2$, fits with previous data on this compound which was used a synthetic equivalent in studying the methanol oxidation reaction over molybdena, and decomposed to yield formaldehyde[49,57,58]. It is suggested that pit

nucleation occurs at oxygen vacancies on the (010) surface, which have previously been shown to be sites of methanol chemisorption[155]. Once pit nucleation has occurred, the pit is then free to grow outwards as the edges provide more under-coordinated molybdenum sites.

## 1.13 Other Uses of Iron Molybdate Catalysts

As well as catalysing the reaction of methanol to formaldehyde, iron molybdates can be used to produce hydrogen cyanide from the ammoxidation reaction of methanol, ammonia, and oxygen[156].

Depending on the Mo:Fe ratio, 2-propanol is decomposed over iron molybdates in different ways[157]. With an increase in iron concentration, greater numbers of Brönsted base sites are present and these direct the product towards acetone production. Conversely an increase in molybdenum leads to an increase in Brönsted acid sites and so the product distribution is shifted towards propene formation.

The reaction of methane partial oxidation over iron molybdate catalysts has been studied[158]. A maximum of methanol formation (5.6 % methane conversion, 43.5 % methanol selectivity) was found at 470 °C and 34 bar. Two reaction mechanisms were found; below 430 °C the initial products were methanol and formaldehyde, while above this temperature, carbon monoxide was the initial product observed.

In a similar reaction to that of methanol to formaldehyde iron molybdate catalysts can be used to produce acetaldehyde from ethanol, and butanone from sec-butanol, although in the later case, minor amounts of butane were also produced[159,160].

## 1.14 Previous work within the Bowker Group

Over a period of several years research has been carried out within the Bowker group into iron-molybdate catalysts for the selective of oxidation of methanol to

formaldehyde. This work has generally been centred on comparisons between the oxides of both iron and molybdenum. The major techniques used have been TPD and pulsed flow reaction (PFR), although other techniques such as XPS have been used to characterise and investigate other aspects.

Some of the early work carried out were TPD investigations into $MoO_3$, $Fe_2O_3$ and fresh Perstorp FA catalyst[161,162]. The work by C. Entwistle, also investigated catalysts that had been at the 'hot-spot' and at the end of the bed in an industrial reactor. These TPD experiments discovered that while $MoO_3$ is selective towards formaldehyde, its activity is low. $Fe_2O_3$ was shown to have only a very small selectivity towards formaldehyde, although the temperature of formaldehyde desorption was lower for $Fe_2O_3$. They showed that the Perstorp FA catalyst showed combined and modified properties of the two oxides (*i.e.* it is showing the higher activity to methanol conversion of $Fe_2O_3$, with the higher selectivity of $MoO_3$). Of the two used industrial catalysts investigated, the end of bed catalyst appeared similar to the fresh FA catalyst whist the catalyst from the 'hot-spot' behaved similarly to the fresh FA catalyst except small yields of $CO_2$ were observed and the peak in formaldehyde desorption occurred at a higher temperature.

TPD data for formaldehyde adsorbed onto the surface of the Perstorp FA catalyst showed formaldehyde desorption at a lower temperature than when methanol was dosed. This showed formaldehyde desorption was not the rate limiting step. When formic acid TPD data was obtained this showed $CO_2$ desorption at very low temperature (57 °C), showing that a surface formate group is not an intermediate in the selective oxidation of methanol to formaldehyde. Instead it was shown that the formate is part of the combustion process on the catalyst surface.

Catalysts from the 'hot-spot' and the end of the bed from an industrial reactor after use were tested and were compared to fresh reference catalyst[163]. The fresh catalyst showed high activity and selectivity towards formaldehyde in oxygen rich conditions (1:0.75 helium to oxygen ratio). Concentrations of oxygen closer to those used in industry (1:0.13 and 1:0.05 helium to oxygen mixtures) lead to significant hydrogen production, an increased formaldehyde selectivity at higher temperatures and surprisingly the $CO_2$ to CO ratio appeared to increase. The fresh catalyst began converting the methanol at increased temperatures when the gas flow contained no oxygen. The lack of oxygen also lead to formaldehyde selectivity dropping more sharply as the temperature was increased, with a subsequent increase in levels of $CO_2$ observed. A catalyst from the 'hot-spot' of an industrial reactor showed higher formaldehyde selectivity at higher temperatures in the high oxygen flow, while in the lower oxygen concentration showed higher oxygen conversion, mainly due to the higher levels of $CO_2$ observed. Studies of the surface of the catalysts showed the 'hot-spot' catalyst had a higher surface iron concentration when compared to the fresh catalyst. The catalyst from the end of the bed, behaves similarly to the 'hot-spot' catalyst in most conditions producing higher levels of formaldehyde than the fresh catalyst, but less than the 'hot-spot'.

The minority products from the industrial reaction were passed over the fresh catalyst in oxygen rich conditions. Formic acid showed decomposition at 175 °C with dehydration products (CO and $H_2$) observed. At temperatures in excess of 350 °C dehydrogenation to $CO_2$ and $H_2$ becomes dominant although it is suggested these may have come from the water-gas shift reaction of CO and $H_2O$. Dimethyl ether was observed to be more stable than either methanol or formic acid, with conversion not observed until temperatures were in excess of 300 °C. The stability of dimethyl ether

was presumed to be caused by its lack of an acidic proton. When conversion did occur, the major products observed were CO, $CO_2$, $H_2$ and $H_2O$. Methyl formate was also more stable than methanol, with reaction beginning at around 230 °C. At low conversion temperatures the major products seen are CO and formaldehyde and increasing the temperature until 350 °C leads to an increase in formaldehyde production. Above this temperature the formaldehyde production is lowered and an increase in $CO_2$ is observed, while the observed CO levels remain approximately constant.

A study into composition and calcination temperature concluded that a higher calcination temperature lead to structural change and led to a catalyst more like the current industrial catalyst[164]. Molybdenum in excess of that required to form stoichiometric $Fe_2(MoO_4)_3$ was found to have little effect on the catalytic properties, although it did add mechanical strength and increase the surface area of the catalyst. A calcination temperature of 500 °C instead of 300 °C caused a structural change that was observed by XRD and lead to a more active catalyst. Catalysts with ratios of Mo:Fe of 1.5:1 (stoichiometric iron molybdate), 1.9:1, and 2.2:1 were created and those with greater molybdenum showed improved activity, although this was most noticeable in the catalysts calcined at the lower temperature. The catalysts calcined at the higher temperature showed greater formaldehyde selectivity in the absence of oxygen whereas the low temperature calcination led to catalysts where the selectivity is highest in the presence of oxygen. A mechanical mixture catalyst made from $Fe_2O_3$ and $MoO_3$ with a Mo:Fe of 2.2:1 was calcined at 600 °C. This showed good activity and higher formaldehyde selectivity in the presence of oxygen.

A paper published in 2002 from the Bowker research group reported on the selective oxidation of methanol to formaldehyde on $Fe_2O_3$, $MoO_3$, and a Perstorp

industrial iron molybdate catalyst[45]. In TPD, the molybdenum containing compounds showed formaldehyde as the only carbon containing compound, from the decomposition of a surface methoxy species. In contrast to this $Fe_2O_3$ was a combustor of methanol, yielding only $CO_2$ and $H_2$, indicating the presence of a formate species on the surface. It was shown by pulsed flow reactor work that the activity of the industrial catalyst was in excess of 90 % by 240 °C where formaldehyde selectivity was still above 80 %. The iron molybdate catalyst was more active than the molybdena, with conversion beginning at 150 °C for the former and 270 °C for the latter. This work lead to the production of a proposed energy profile for the reaction showing an energy barrier of 132 kJ $mol^{-1}$ to the rate-determining step of hydrogen abstraction.

Two previous studies have been carried out into catalysts with low loadings of Mo onto the surface of iron oxide[165,166]. This work demonstrated that with coverages of 1 monolayer or over highly selective (>95 %) catalysts for formaldehyde could be created. With catalysts of less than a monolayer Mo coverage it was observed that the Mo was able to affect not only the sites it occupied, but other surface sites as well, as a catalyst with 0.1 ML Mo coverage gave greater than 80 % formaldehyde selectivity, while the 0.02 ML catalyst gave greater than 60 % formaldehyde selectivity. The simulation of formate groups on the surface through formic acid dosing showed the catalysts with monolayer or greater coverage decomposed the formate to CO, whereas those with less than monolayer coverage showed a more mixed behaviour with both CO and $CO_2$ desorbed.

## *1.15 Research Objectives*

One of the greatest challenges facing this project is to identify the role of the individual phases within the catalyst. It is known that both $MoO_3$ and $Fe_2(MoO_4)_3$ are

necessary for effective an efficient catalyst, but the roles are still debated. Various suggestions have been made as to the role of the phases as a greater understanding has been reached, current thoughts of possible roles are that a monolayer of one or other species is formed to cover the bulk structures, another thought is that a spillover process maybe occurring and a third possibility is that there is a phase boundary or intergrowth phenomenon. To investigate the various phases, catalysts containing the single oxides ($Fe_2O_3$ and $MoO_3$) will be compared to a single phase $Fe_2(MoO_4)_3$ and catalysts with mixed phases with a range of Mo:Fe ratios. These will be characterised and tested for their catalytic activity by TPD and pulsed flow experiments. The characterisation will use the techniques of XRD to determine the bulk structure, and XPS and Raman spectroscopy to discover surface composition.

The first chapter of results deals with the more general properties of methanol oxidation, with investigation into the method of methanol introduction (continuous *vs.* pulsed flow), the pH of catalyst preparation and the order of product formation.

The second chapter of results investigates the reaction in the absence of oxygen. While the reaction normally proceeds *via* the Mars and van Krevelen, with the role of gaseous oxygen to replace the lost lattice oxygen, experiments have been conducted anaerobically to observe the effect on catalytic performance and structural effects at a range of temperatures. The changes in both bulk and surface structure are investigated using XRD and XPS. The performance of these reduced catalysts are compared to the reduced phases of $MoO_2$ and $FeMoO_4$, which were sourced commercially.

The third results chapter will concentrate on the effects of varying the Mo:Fe ratio within the bulk of the catalyst. The work presents results of catalytic performance and structures of catalysts with ratios across the range, both above and

below that required to form the stoichiometric $Fe_2(MoO_4)_3$. The results of this are discussed with regards to the surface structure of the catalyst and are compared to results for catalysts with $MoO_3$ impregnated onto the surface of $Fe_2O_3$.

A final concluding chapter will then bring together the data discussed, relating this to the aims of the research. A short section will be included on how the work could be developed further.

## 1.16 References


(1) Lindstroem, B.; Pettersson, L. J. *Cattech* **2003**, *7*, 130.
(2) Langmuir, I. *Physical Review* **1915**, *6*, 79.
(3) *Mineral Commodity Summaries*; U.S. Department of the Interior U.S. Geological Society, **2006**.
(4) Weast, R. C.; Editor *Handbook of Chemistry and Physics*, 55th ed.; CRC Press, **1974**.
(5) Mittasch, A.; Pier, M.; Muller, C., DE 544665, **1923**
(6) Twigg, M. V. *Catalyst Handbook*, 2nd ed.; Wolfe Publishing, **1989**.
(7) Walker, J. F. *Formaldehyde*, 3rd ed.; Reinhold, **1964**.
(8) Butlerov, A. *Ann.* **1859**, *111*, 242.
(9) von Hofmann, A. W. *Ann.* **1868**, *145*, 357.
(10) Baekeland, L. H. *Journal of Industrial and Engineering Chemistry* **1909**, *1*, 545.
(11) Adkins, H.; Peterson, W. R. *Journal of the American Chemical Society* **1931**, *53*, 1512.
(12) Pernicone, N. *Journal of the Less-Common Metals* **1974**, *36*, 289.
(13) Popov, B. I.; Skomorokhova, N. G. *Reaction Kinetics and Catalysis Letters* **1981**, *18*, 101.
(14) Andersson, A.; Hernelind, M.; Augustsson, O. *Catalysis Today* **2006**, *112*, 40.
(15) Qian, M.; Liauw, M. A.; Emig, G. *Applied Catalysis, A: General* **2003**, *238*, 211.
(16) Wachs, I. E.; Wang, C. B., WO 9955655, **1999**
(17) Deng, J.; Xu, X.; Wang, J.; Liao, Y.; Hong, B. *Catalysis Letters* **1995**, *32*, 159.
(18) Ruf, S.; May, A.; Emig, G. *Applied Catalysis, A: General* **2001**, *213*, 203.
(19) Ruf, S.; Emig, G. *Journal of Molecular Catalysis A: Chemical* **1999**, *146*, 271.
(20) Maurer, R.; Renken, A. *Chemical Engineering Research and Design* **2003**, *81*, 730.
(21) Ren, L. P.; Dai, W. L.; Cao, Y.; Li, H.; Fan, K. *Chemical Communications* **2003**, 3030.
(22) Ren, L. P.; Dai, W. L.; Cao, Y.; Fan, K. N. *Catalysis Letters* **2003**, *85*, 81.
(23) Malinski, R.; Akimoto, M.; Echigoya, E. *Journal of Catalysis* **1976**, *44*, 101.
(24) Feng, T.; Vohs, J. M. *Journal of Catalysis* **2004**, *221*, 619.
(25) Isaguliants, G. V.; Belomestnykh, I. P. *Catalysis Today* **2005**, *100*, 441.
(26) Liu, H.; Iglesia, E. *Journal of Physical Chemistry B* **2005**, *109*, 2155.
(27) Kihlborg, L. *Arkiv foer Kemi* **1963**, *21*, 357.

(28) Remediakis, I. N.; Kaxaris, E.; Chen, M.; Friend, C. M. *Journal of Chemical Physics* **2003**, *118*, 6046.
(29) Parise, J. B.; McCarron, E. M., III; Von Dreele, R.; Goldstone, J. A. *Journal of Solid State Chemistry* **1991**, *93*, 193.
(30) Svensson, G.; Kihlborg, L. *Reactivity of Solids* **1987**, *3*, 33.
(31) Boudjada, N.; Rodriguez-Carvajal, J.; Anne, M.; Figlarz, M. *Journal of Solid State Chemistry* **1993**, *105*, 211.
(32) Oswald, H. R.; Guenter, J. R.; Dubler, E. *Journal of Solid State Chemistry* **1975**, *13*, 330.
(33) Fellows, R. L.; Lloyd, M. H.; Knight, J. F.; Yakel, H. L. *Inorganic Chemistry* **1983**, *22*, 2468.
(34) Seguin, L.; Figlarz, M.; Cavagnat, R.; Lassegues, J. C. *Spectrochimica Acta, Part A: Molecular and Biomolecular Spectroscopy* **1995**, *51A*, 1323.
(35) Blake, R. L.; Hessevick, R. E.; Zoltai, T.; Finger, L. W. *American Mineralogist* **1966**, *51*, 123.
(36) Cornell, R. M.; Schwertmann, U.; Editors *The Iron Oxides: Structure, Properties, Reactions, Occurrence and Uses*, **1996**.
(37) Rapposch, M. H.; Anderson, J. B.; Kostiner, E. *Inorganic Chemistry* **1980**, *19*, 3531.
(38) Massarotti, V.; Flor, G.; Marini, A. *Journal of Applied Crystallography* **1981**, *14*, 64.
(39) Harrison, W. T. A. *Materials Research Bulletin* **1995**, *30*, 1325.
(40) Koenig, U.; Morgenstern, T.; Foersterling, G. *Materials Science Forum* **1993**, *133-136*, 687.
(41) Fagherazzi, G.; Pernicone, N. *Journal of Catalysis* **1970**, *16*, 321.
(42) Rodriguez, J. A.; Hanson, J. C.; Chaturvedi, S.; Maiti, A.; Brito, J. L. *Journal of Physical Chemistry B* **2000**, *104*, 8145.
(43) Sleight, A. W.; Chamberland, B. L.; Weiher, J. F. *Inorganic Chemistry* **1968**, *7*, 1093.
(44) JCPDS Card Number 32-671.
(45) Bowker, M.; Holroyd, R.; Elliott, A.; Morrall, P.; Alouche, A.; Entwistle, C.; Toerncrona, A. *Catalysis Letters* **2002**, *83*, 165.
(46) Groff, R. P. *Journal of Catalysis* **1984**, *86*, 215.
(47) Wadayama, T.; Saito, T.; Suetaka, W. *Applications of Surface Science* **1984**, *20*, 199.
(48) Smith, R. L.; Rohrer, G. S. *Journal of Catalysis* **1999**, *184*, 49.
(49) McCarron, E. M., III; Sleight, A. W. *Polyhedron* **1986**, *5*, 129.
(50) Allison, J. N.; Goddard, W. A., III. *Journal of Catalysis* **1985**, *92*, 127.
(51) Tatibouet, J. M.; Germain, J. E. *Journal of Catalysis* **1981**, *72*, 375.
(52) Rahmouni, A.; Barbier, C. *Theochem* **1995**, *330*, 359.
(53) Chen, M.; Waghmare, U. V.; Friend, C. M.; Kaxiras, E. *Journal of Chemical Physics* **1998**, *109*, 6854.
(54) Chung, J. S.; Miranda, R.; Bennett, C. O. *Journal of Catalysis* **1988**, *114*, 398.
(55) Cheng, W. H. *Journal of Catalysis* **1996**, *158*, 477.
(56) Smith, M. R.; Ozkan, U. S. *Journal of Catalysis* **1993**, *141*, 124.
(57) McCarron, E. M., III; Staley, R. H.; Sleight, A. W. *Inorganic Chemistry* **1984**, *23*, 1043.
(58) McCarron, E. M., III; Harlow, R. L. I.; Li, Z. G.; Suto, C.; Yuen, Y. *Journal of Solid State Chemistry* **1998**, *136*, 247.

(59) Waters, T.; O'Hair, R. A. J.; Wedd, A. G. *Journal of the American Chemical Society* **2003**, *125*, 3384.
(60) Mestl, G.; Ruiz, P.; Delmon, B.; Knozinger, H. *Journal of Physical Chemistry* **1994**, *98*, 11269.
(61) Novakova, J.; Jiru, P. *Collection of Czechoslovak Chemical Communications* **1964**, *29*, 1114.
(62) Glisenti, A.; Favero, G.; Granozzi, G. *Journal of the Chemical Society, Faraday Transactions* **1998**, *94*, 173.
(63) Glisenti, A. *Journal of the Chemical Society, Faraday Transactions* **1998**, *94*, 3671.
(64) Novakova, J.; Jiru, P.; Zavadil, V. *Journal of Catalysis* **1971**, *21*, 143.
(65) Busca, G.; Lorenzelli, V. *Journal of Catalysis* **1980**, *66*, 155.
(66) Lorenzelli, V.; Busca, G.; Sheppard, N. *Journal of Catalysis* **1980**, *66*, 28.
(67) Rufael, T. S.; Batteas, J. D.; Friend, C. M. *Surface Science* **1997**, *384*, 156.
(68) Guo, Q.; McBreen, P. H.; Moller, P. J. *Surface Science* **1999**, *423*, 19.
(69) Habersberger, K.; Jiru, P. *Collection of Czechoslovak Chemical Communications* **1972**, *37*, 535.
(70) Liberti, G.; Pernicone, N.; Soattini, S. *Journal of Catalysis* **1972**, *27*, 52.
(71) Kim, T. H.; Ramachandra, B.; Choi, J. S.; Saidutta, M. B.; Choo, K. Y.; Song, S. D.; Rhee, Y. W. *Catalysis Letters* **2004**, *98*, 161.
(72) Trifiro, F.; Carbucicchio, M.; Villa, P. L. *Hyperfine Interactions* **1997**, *111*, 17.
(73) Grasselli, R. K. In *Handbook of Heterogeneous Catalysis*; Ertl, G., Knozinger, H., Weitkamp, J., Eds.; VCH, **1997**; Vol. 5; 2302.
(74) Soares, A. P. V.; Portela, M. F.; Kiennemann, A. *Catalysis Reviews - Science and Engineering* **2004**, *47*, 125.
(75) Nguyen Van, T.; Tittarelli, P.; Villa, P. L. *Chem. Uses Molybdenum, Proc. Int. Conf., 3rd* **1979**, 161.
(76) Popov, B. I.; Skomorokhova, N. G. *Reaction Kinetics and Catalysis Letters* **1981**, *18*, 107.
(77) Popov, B. I.; Shkuratova, L. N.; Kuznetsov, V. I.; Pavlyukin, Y. T. *Reaction Kinetics and Catalysis Letters* **1984**, *25*, 255.
(78) Soares, A. P. V.; Portela, M. F.; Kiennemann, A. *Catalysis Communications* **2001**, *2*, 159.
(79) del Arco, M.; Martin, C.; Rives, V.; Estevez, A. M.; Marquez, M. C.; Tena, A. F. *Journal of Materials Science* **1989**, *24*, 3750.
(80) Del Arco, M.; Martin, C.; Rives, V.; Estevez, A. M.; Marquez, M. C.; Tena, A. F. *Materials Chemistry and Physics* **1989**, *23*, 517.
(81) Burcham, L. J.; Briand, L. E.; Wachs, I. E. *Langmuir* **2001**, *17*, 6164.
(82) Burcham, L. J.; Briand, L. E.; Wachs, I. E. *Langmuir* **2001**, *17*, 6175.
(83) Soares, A. P. V.; Farinha Portela, M.; Kiennemann, A.; Hilaire, L.; Millet, J. M. M. *Applied Catalysis, A: General* **2001**, *206*, 221.
(84) Klissurski, D.; Kancheva, M. *Journal of the Chemical Society, Faraday Transactions 1: Physical Chemistry in Condensed Phases* **1981**, *77*, 1795.
(85) Tatibouet, J. M. *Applied Catalysis, A: General* **1997**, *148*, 213.
(86) Edwards, J.; Nicolaidis, J.; Cutlip, M. B.; Bennett, C. O. *Journal of Catalysis* **1977**, *50*, 24.
(87) Soares, A. P. V.; Portela, M. F.; Kiennemann, A. *Studies in Surface Science and Catalysis* **2001**, *133*, 489.
(88) Machiels, C. J.; Sleight, A. W. *Journal of Catalysis* **1982**, *76*, 238.

(89) Oyama, S. T.; Radhakrishnan, R.; Seman, M.; Kondo, J. N.; Domen, K.; Asakura, K. *Journal of Physical Chemistry B* **2003**, *107*, 1845.
(90) Holstein, W. L.; Machiels, C. J. *Journal of Catalysis* **1996**, *162*, 118.
(91) Deshmukh, S. A. R. K.; van Sint Annaland, M.; Kuipers, J. A. M. *Applied Catalysis, A: General* **2005**, *289*, 240.
(92) Solomon, S. J.; Custer, T.; Schade, G.; Dias, A. P. S.; Burrows, J. *Atmospheric Chemistry and Physics* **2005**, *5*, 2787.
(93) Faliks, A.; Yetter, R. A.; Floudas, C. A.; Bernasek, S. L.; Fransson, M.; Rabitz, H. *Journal of Physical Chemistry A* **2001**, *105*, 2099.
(94) Allyn, C. L.; Barrentine, E. M.; Hodgins, T. S.; Shelton, F. J.; Rawson, R. L., US 2849492, **1958**
(95) GB 1080508, **1971**
(96) Ivanov, K. *Applied Catalysis, A: General* **1994**, *116*, L1.
(97) Belhekar, A. A.; Ayyappan, S.; Ramaswamy, A. V. *Journal of Chemical Technology and Biotechnology* **1994**, *59*, 395.
(98) Soares, A. P. V.; Portela, M. F.; Kiennemann, A. *Studies in Surface Science and Catalysis* **1997**, *110*, 807.
(99) Li, J. L.; Zhang, Y. X.; Liu, C. W.; Zhu, Q. M. *Catalysis Today* **1999**, *51*, 195.
(100) Radev, D. D.; Blaskov, V.; Klissurski, D.; Mitov, I.; Toneva, A. *Journal of Alloys and Compounds* **1997**, *256*, 108.
(101) Conca, E.; Rubini, C.; Marchi, M., EP 1674156, **2006**
(102) Wachs, I. E.; Briand, L. E., WO 9952629, **1999**
(103) Cairati, L.; Di Fiore, L.; Forzatti, P.; Pasquon, I.; Trifiro, F. *Industrial & Engineering Chemistry Process Design and Development* **1980**, *19*, 561.
(104) Hill, C. G., Jr.; Wilson, J. H., III. *Journal of Molecular Catalysis* **1991**, *67*, 57.
(105) Radhakrishnan, R.; Reed, C.; Oyama, S. T.; Seman, M.; Kondo, J. N.; Domen, K.; Ohminami, Y.; Asakura, K. *Journal of Physical Chemistry B* **2001**, *105*, 8519.
(106) del Arco, M.; Martin, C.; Rives, V.; Sanchez-Escribano, V.; Ramis, G.; Busca, G.; Lorenzelli, V.; Malet, P. *Journal of the Chemical Society, Faraday Transactions* **1993**, *89*, 1071.
(107) Liu, Y. C.; Griffin, G. L.; Chan, S. S.; Wachs, I. E. *Journal of Catalysis* **1985**, *94*, 108.
(108) Seman, M.; Kondo, J. N.; Domen, K.; Oyama, S. T. *Chemistry Letters* **2002**, 1082.
(109) Seman, M.; Kondo, J. N.; Domen, K.; Radhakrishnan, R.; Oyama, S. T. *Journal of Physical Chemistry B* **2002**, *106*, 12965.
(110) Banares, M. A.; Hu, H.; Wachs, I. E. *Journal of Catalysis* **1994**, *150*, 407.
(111) Aoki, K.; Ohmae, M.; Nanba, T.; Takeishi, K.; Azuma, N.; Ueno, A.; Ohfune, H.; Hayashi, H.; Udagawa, Y. *Catalysis Today* **1998**, *45*, 29.
(112) Branhorst, M.; Cristol, S.; Capron, M.; Dujardin, C.; Vezin, H.; Le bourdon, G.; Payen, E. *Catalysis Today* **2006**, *113*, 34.
(113) Liu, H.; Iglesia, E., US 2004044252, **2004**
(114) Liu, H.; Cheung, P.; Iglesia, E. *Physical Chemistry Chemical Physics* **2003**, *5*, 3795.
(115) Cheung, P.; Liu, H.; Iglesia, E. *Journal of Physical Chemistry B* **2004**, *108*, 18650.
(116) Hu, H.; Wachs, I. E.; Bare, S. R. *Journal of Physical Chemistry* **1995**, *99*, 10897.
(117) Hu, H.; Wachs, I. E. *Journal of Physical Chemistry* **1995**, *99*, 10911.
(118) Burcham, L. J.; Wachs, I. E. *Catalysis Today* **1999**, *49*, 467.

(119) Chen, Y.; Wachs, I. E. *Journal of Catalysis* **2003**, *217*, 468.
(120) Xu, F.; Hu, Y.; Dong, L.; Chen, Y. *Chinese Science Bulletin* **2000**, *45*, 214.
(121) Danilova, I. G.; Demidov, A. V.; Balashov, V. A.; Osipova, N. A., SU 1796244, **1993**
(122) Wang, C. B.; Cai, Y.; Wachs, I. E. *Langmuir* **1999**, *15*, 1223.
(123) Estevez, A. M.; Marquez, M. C.; Tena, A. F.; Del Arco, M.; Martin, C.; Rives, V. *Chemical and Biochemical Engineering Quarterly* **1990**, *4*, 61.
(124) Klissurski, D.; Rives, V.; Pesheva, Y.; Mitov, I.; Abadzhjieva, N. *Catalysis Letters* **1993**, *18*, 265.
(125) Ivanov, K.; Mitov, I.; Krustev, S. *Journal of Alloys and Compounds* **2000**, *309*, 57.
(126) Conca, E.; Rubini, C.; Marchi, M., US 2006135821, **2006**
(127) Chang, G. M., US 3855153, **1974**
(128) Klissurski, D.; Rives, V.; Abadzhjivea, N.; Pesheva, Y.; Pomonis, P.; Sdoudkos, T.; Petrakis, D. *Journal of the Chemical Society, Chemical Communications* **1993**, 1606.
(129) Ivanov, K.; Litcheva, P.; Klissurski, D. *Collection of Czechoslovak Chemical Communications* **1992**, *57*, 2529.
(130) Niwa, M.; Mizutani, M.; Takahashi, M.; Murakami, Y. *Journal of Catalysis* **1981**, *70*, 14.
(131) Klisurski, D.; Pesheva, I.; Abadzhieva, N.; Mitov, I.; Filkova, D.; Petrov, L. *Applied Catalysis* **1991**, *77*, 55.
(132) Sohrabi, M.; Aghdasinia, H. *Chemical Engineering & Technology* **2003**, *26*, 69.
(133) Deshmukh, S. A. R. K.; Laverman, J. A.; van Sint Annaland, M.; Kuipers, J. A. M. *Industrial & Engineering Chemistry Research* **2005**, *44*, 5966.
(134) Diakov, V.; Lafarga, D.; Varma, A. *Catalysis Today* **2001**, *67*, 159.
(135) Diakov, V.; Blackwell, B.; Varma, A. *Chemical Engineering Science* **2002**, *57*, 1563.
(136) Wachs, I. E.; Bourne, R., Wo 2002022541, **2002**
(137) Hoene, D. J., US 4343954, **1982**
(138) Popov, B. I.; Bibin, V. N.; Boreskov, G. K. *Kinetika i Kataliz* **1976**, *17*, 371.
(139) Pernicone, N. *Catalysis Today* **1991**, *11*, 85.
(140) Wachs, I. E.; Briand, L. E., WO 9952630, **1999**
(141) Dazhuang, L.; Jianhong, Z.; Huimin, T.; Dongxia, H. *Reaction Kinetics and Catalysis Letters* **1997**, *62*, 347.
(142) Ma, Y. H.; Kmiotek, S. J. *Journal of Catalysis* **1988**, *109*, 132.
(143) Soares, A. P. V.; Portela, M. F.; Kiennemann, A.; Millet, J. M. M. *Reaction Kinetics and Catalysis Letters* **2002**, *75*, 13.
(144) Vieira Soares, A. P.; Farinha Portela, M.; Kiennemann, A.; Hilaire, L. *Chemical Engineering Science* **2003**, *58*, 1315.
(145) Zhang, L.; Liu, D.; Yang, B.; Zhao, J. *Applied Catalysis, A: General* **1994**, *117*, 163.
(146) Zhao, J.; Tian, H.; Liu, D.; Wang, L. *Fenzi Cuihua* **1995**, *9*, 471.
(147) Millner, T.; Neugebauer, J. *Nature* **1949**, *163*, 601.
(148) Buiten, J. *Journal of Catalysis* **1968**, *10*, 188.
(149) Sonnemans, J.; Mars, P. *Journal of Catalysis* **1973**, *31*, 209.
(150) Patterson, W. R.; Taylor, S. D. *Journal of Catalysis* **1988**, *114*, 460.
(151) Suzuki, S.; Ohminami, Y.; Tsutsumi, T.; Shoaib, M. M.; Ichikawa, M.; Asakura, K. *Chemistry Letters* **2003**, *32*, 1098.

(152) Smith, R. L.; Rohrer, G. S. *Journal of Catalysis* **1998**, *180*, 270.
(153) Hsu, Z. Y.; Zeng, H. C. *Journal of Physical Chemistry B* **2000**, *104*, 11891.
(154) Smith, R. L.; Rohrer, G. S. *Journal of Catalysis* **1998**, *173*, 219.
(155) Farneth, W. E.; McCarron, E. M., III; Sleight, A. W.; Staley, R. H. *Langmuir* **1987**, *3*, 217.
(156) Ebner, J. R., US 4425260, **1984**
(157) Al-Shihry, S. S.; Halawy, S. A. *Journal of Molecular Catalysis A: Chemical* **1996**, *113*, 479.
(158) Chellappa, A. S.; Viswanath, D. S. *Industrial & Engineering Chemistry Research* **1995**, *34*, 1933.
(159) Appel, L. G.; Pereira, S. E. d. C.; Medeiros, P. R. d. S., BR 9002392, **1991**
(160) Halawy, S. A. *Oxidation Communications* **1998**, *21*, 486.
(161) Bentley, J. "The adsorption and decomposition of methanol on Metal-Oxide surfaces," Project Report, The University of Reading, **1997**.
(162) Bowker, M. "A TPD Investigation of Formaldehyde Synthesis Catalysts," The University of Reading, **1997**.
(163) Holroyd, R.; York, I.; Bowker, M. "A pulsed flow reactor and XPS study of formaldehyde synthesis catalyst," The University of Reading.
(164) White, E. "A study of Iron Molybdate, the catalyst for the partial oxidation of methanol to formaldehdye," Project Reort, The University of Reading, **2001**.
(165) Ingham, E. "An investigation into the selective oxidation of methanol to formaldehdye in iron molybdate catalysts," Project Report, The University of Reading, **2002**.
(166) House, M. P. "Novel catalysts for the selective oxidation of methanol to formaldehyde," Project Report, The University of Reading, **2003**.

# 2 Experimental

## 2.1 Introduction

This chapter is concerned with the materials and methods used within this research. The first section is dedicated to the preparation of the catalytic materials that were tested for activity and selectivity in the pulsed flow reactor. Characterisation of the materials was performed by X-Ray diffraction (XRD), Raman spectroscopy, X-Ray photoelectron spectroscopy (XPS) and BET surface area analysis. Scanning transmission electron microscopy (Super-STEM) and electron energy loss spectroscopy (EELS) were collected on a limited number of samples.

## 2.2 Catalyst Preparation

The catalysts used in this research were prepared by a variety of methods, as described below. Following preparation, all catalysts were pressed at a pressure of 10 tonnes within a pellet die, crushed and sieved to produce granules of between 850-600 μm diameter before catalytic testing.

### 2.2.1 Single oxides

Commercially sourced single metal oxides of molybdena ($MoO_3$, BDH, ≥99.5 %) and haematite ($Fe_2O_3$, Aldrich, ≥99 %) were tested for comparison with the more complex systems prepared in this research.

A second sample of $Fe_2O_3$ was created in house by the dropwise addition of 50 ml iron nitrate ($Fe(NO_3)_3.9H_2O$, BDH, ≥98 %) solution, to a dilute solution of 100 ml nitric acid (~pH 2, $HNO_3$, Fisher, Laboratory Grade) with stirring at 60 °C. Water was then evaporated from the sample at 90 °C, before overnight drying at 120 °C and calcination at 500 °C for 48 hours.

### 2.2.2 Iron Molybdates

The iron molybdate catalysts were made by co-precipitation. The catalysts were single phase $Fe_2(MoO_4)_3$, and mixed phase $Fe_2(MoO_4)_3.xMoO_3$. The molybdenum rich catalyst was made to contain 25.9 w/t % $MoO_3$. The atomic ratio and labels used hereafter for these two catalysts are Mo:Fe 1.5:1 and 2.2:1 respectively.

The desired amount of ammonium heptamolybdate ($(NH_4)_6Mo_7O_{24}.4H_2O$, BDH, ≥99 %) was dissolved in 100 ml deionised water before being acidified to ~pH 2 using nitric acid ($HNO_3$, Fisher, Laboratory Grade). To this a solution of iron nitrate ($Fe(NO_3)_3.9H_2O$, BDH, ≥98 %, 6.83 g in 50 ml) was added dropwise with stirring at 60 °C. A canary yellow precipitate was formed, which was evaporated to near dryness at 90 °C. The resulting solids were dried at 120 °C overnight before being calcined to 500 °C for 48 hours.

Also tested was a commercial catalyst provided by Perstorp, with the designation KH 26. This catalyst was prepared by coprecipitation of iron chloride with ammonium molybdate, followed by washing, drying, pelletisation and calcination. The ratio of Mo:Fe in this catalyst was 2.2:1.

## *2.3 The Pulsed Flow Reactor*

### 2.3.1 Overview

The pulsed flow microreactor was designed and built in-house and has been used in the past by other group members to study CO catalysis on gold nanoparticles, propene oxidation/ammoxiation and $NO_x$ storage and reduction catalysts[1-3]. The microreactor allows for the examination of industrially important catalytic reactions on a small scale and can provide kinetic and mechanistic data. A diagram of the

reactor is shown below in Figure 2-1, with a labelled photograph in Figure 2-2, and the mass spectrometer vacuum system shown in Figure 2-3.

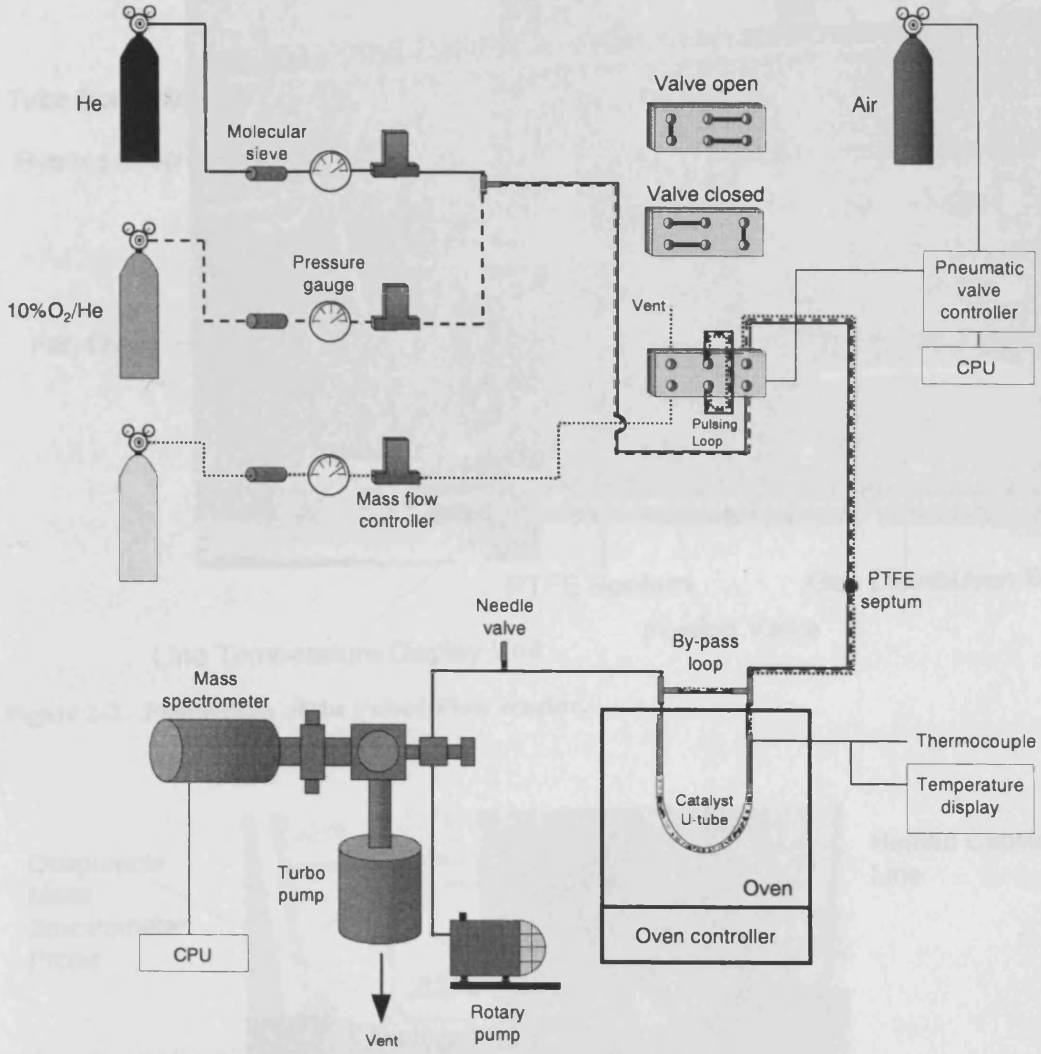


**Figure 2-1 - Schematic of the pulsed flow microreactor.**

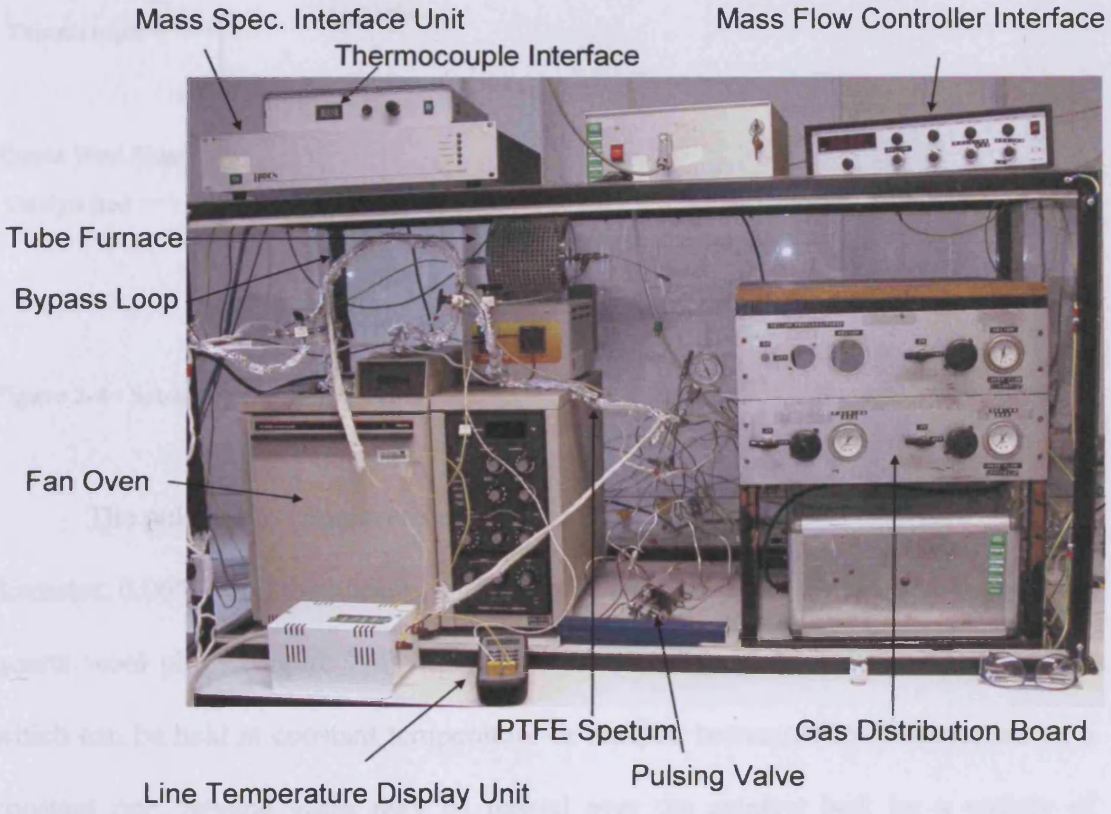


**Figure 2-2 - Photograph of the Pulsed Flow reactor.**

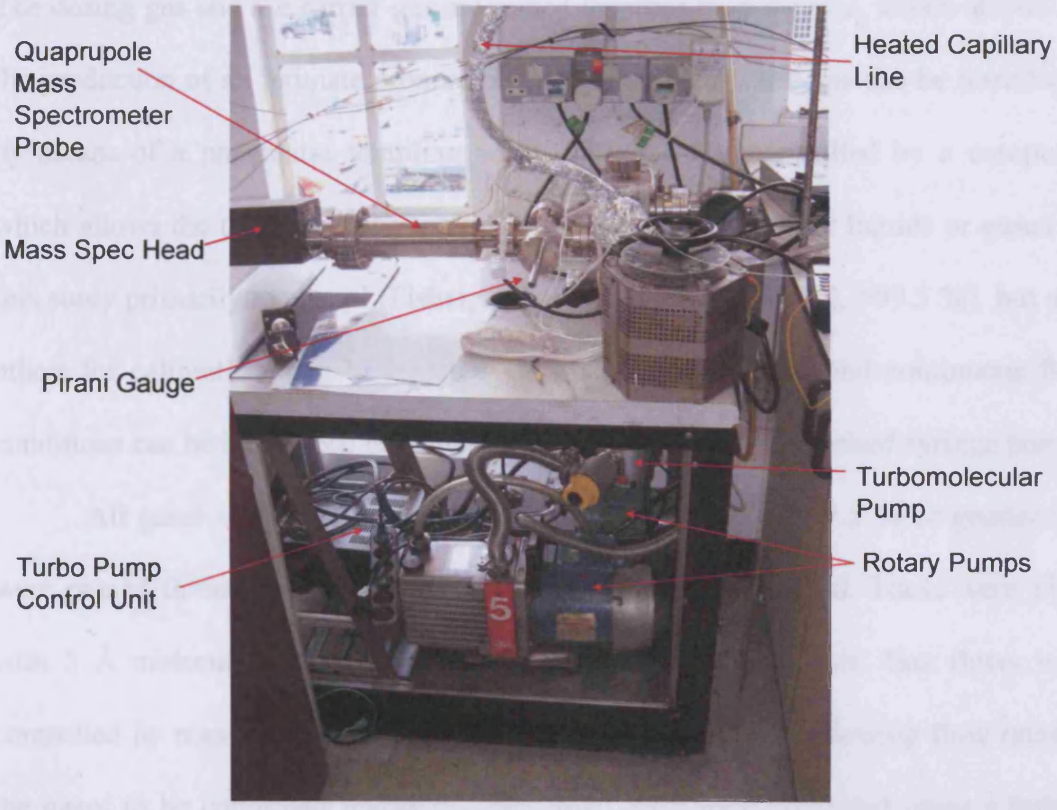


**Figure 2-3 - Photograph of the mass spectrometer trolley of the pulsed flow reactor.**

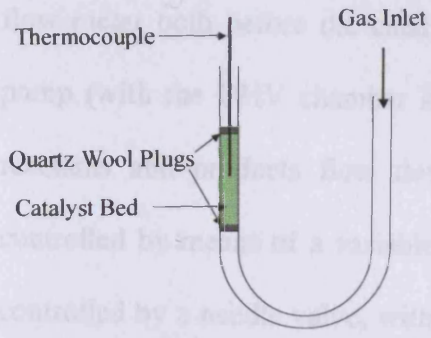


**Figure 2-4 - Set-up of a loaded U-tube.**

The pulsed flow microreactor consists of a stainless steel U-tube (1/4'' outside diameter, 0.065'' wall thickness) containing the catalyst (typically 0.5 g) between two quartz wool plugs (Figure 2-4) mounted vertically in a Phillips PU 4500 GC oven which can be held at constant temperature or ramped between two temperatures at a constant rate. Several gases may be passed over the catalyst bed, by a variety of methods. Two gases can flow continuously; a carrier gas (helium) and a dosing gas. The dosing gas and the carrier gas are joined together by a T-piece, which allows for the production of an intimate mixture of the two gases. A third gas can be introduced by means of a pneumatic sampling valve. The valve is controlled by a computer, which allows the user to set the timing of the gas pulses. Further liquids or gases (in this study primarily methanol (Fisher, Laboratory grade methanol, >99.5 %), but also others for calibration) can be injected *via* a septum assembly, and continuous flow conditions can be introduced here by means of a Razel A-99 motorised syringe pump.

All gases were supplied by BOC Ltd with a purity of 99.5 % or greater and were passed through Puritubes supplied by Phase Separation Ltd. These were filled with 5 Å molecular sieves to remove carbon dioxide and water. Gas flows were controlled by mass flow controllers (Brookes 5850TR series), allowing flow rates of the gases to be controlled within 0.1 $cm^3$ $min^{-1}$, and were calibrated using a bubble

flow meter both before the catalyst bed and on the exit of the capillary line rotary pump (with the UHV chamber kept shut). After flowing over the catalyst bed, the reactants and products flow down a heated capillary line, with the temperature controlled by means of a variable resistor. The flow of gas to the capillary line was controlled by a needle valve, with most of the gas then vented by a Leybold Heraeus Trivac rotary pump, allowing a small fraction to be bled into the UHV chamber containing the mass spectrometer. The mass spectrometer assembly consists of a high vacuum chamber, pumped by a Leybold 151 turbo molecular pump and backed by an Edwards 5 rotary pump. The mass spectrometer was a Hiden Analytical quadrupole Hal 201, which is computer controlled and allows for the displaying of results in real time. The mass spectrometer was used with an emission of 1000 μA, a cage potential of 3 V, and a multiplier potential of 850 V. To account for sensitivity drift within the mass spectrometer pulses of methanol were passed through the bypass before each run.

To accurately measure the temperature a thermocouple was inserted into the catalyst bed (Figure 2-4), the output was also recorded by the controlling computer.

### 2.3.2 Modes of Operation

Three different modes of operation were utilised on the pulsed flow reactor. The first mode is *Temperature Programmed Pulsed Flow Reaction* (TPPFR) and can accurately show the light off point of a reaction and the variation of products as a function of temperature. This technique involves introducing known volumes of liquid/gas (normally 1 μl liquid, 0.53 ml gas) at periodic intervals (typically every 2 minutes) to the gas flow while the temperature of the catalysts is linearly ramped (typically 8 °C $min^{-1}$). From the resulting data, conversions and selectivities can then be calculated. An example of the raw data obtained from this mode of operation is

shown in Figure 2-5. In this figure the data has been separated vertically by the addition of constants to the baseline signal for presentation purposes. The time zero value for all masses is effectively zero, apart from mass 32, some oxygen is present in the continuous gas flow in this case, and the constant added to this mass is $2.6 \times 10^{-8}$. The first five pulses, up to 10 minutes run time are generated by pulses of methanol through the bypass, these are completed so that daily drift in the sensitivity of the mass spectrometer may be accounted for. From these peaks, it can be seen that some reaction occurs on the mass spectrometer filament itself. For example, there is a large 44 peak, which would not normally be expected in the cracking pattern of methanol (Section 2.3.8.3), however, it is present here due to the oxidation of the methanol on the hot thoriated tungsten filament. The next point of note is the drop in mass 32 at approximately 12 minutes, this occurs as there is disturbance in gas flow during a switch in flow from the bypass to the catalyst bed. There is then a series of injections of methanol at 2 minute intervals beginning at 14 minutes and continuing until the end of the run. The first of the peaks (mass 31) is lower in height and area than those following, due to adsorption of some of the methanol within that pulse on the catalyst. At 18 minutes the heating region begins and the mass 31 peak begins to fall at ~35 minutes, due to the start of methanol conversion. By careful measurement of the area under the peak it is possible to calculate the methanol conversion. In the example data it is possible to see that conversion of methanol is near complete by 50 minutes.

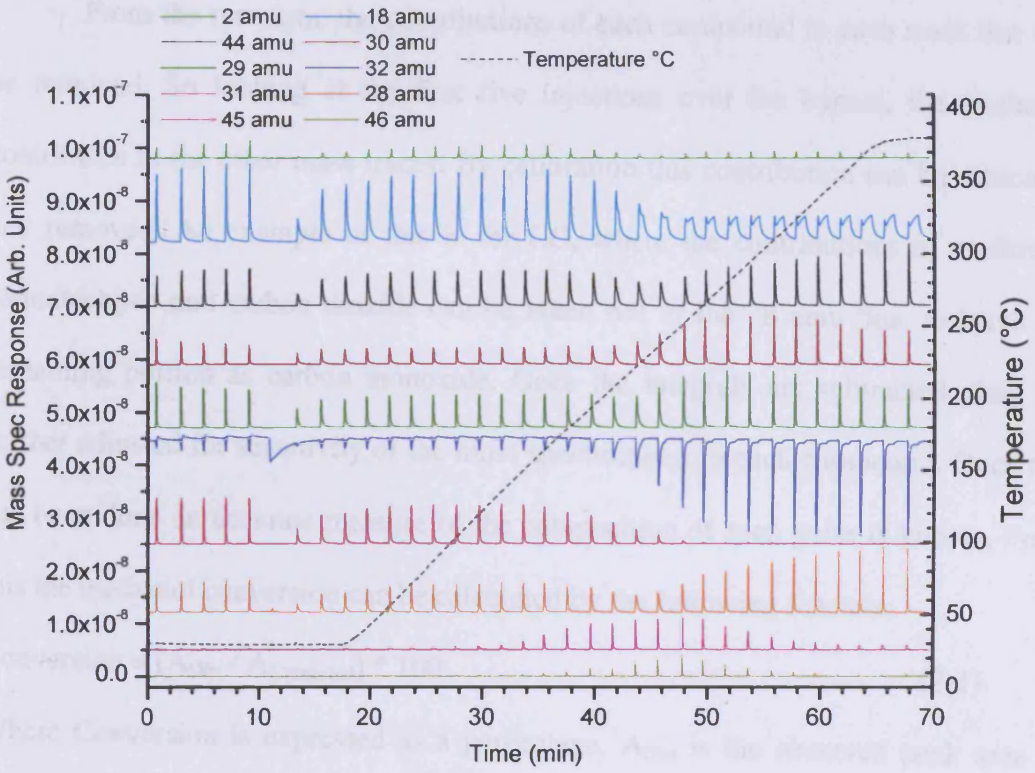


**Figure 2-5 - Raw data of a TPPFR of methanol over 2.2:1 Mo:Fe catalyst.**

The next step after collecting the raw data is to obtain the raw peak integrals, and these are shown in Figure 2-6. From the raw peak integrals, the reaction profile begins to take shape in a more obvious way as features such as the methanol decline (mass 31) begin to be quantified.

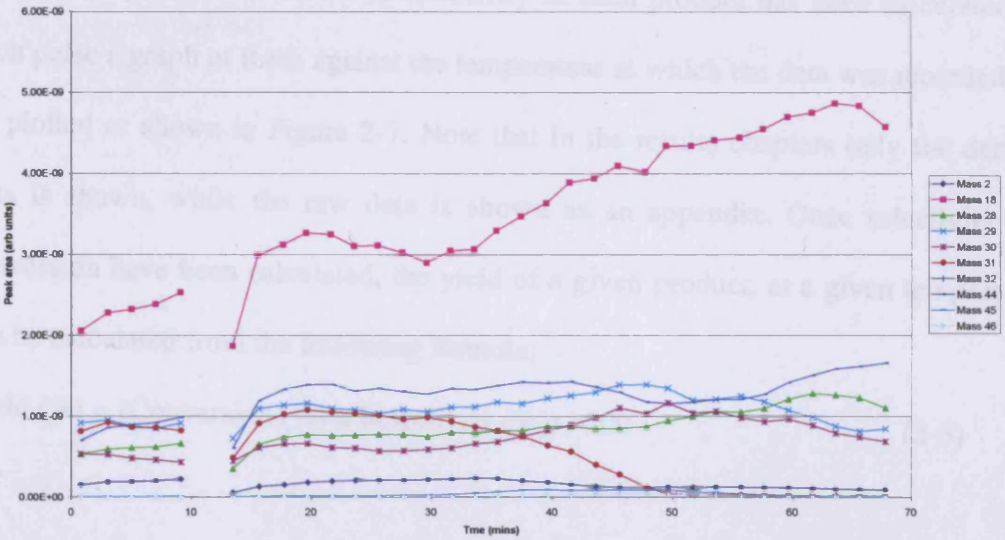


**Figure 2-6 - Raw peak integrals from methanol TPPFR over 2.2:1 Mo:Fe catalyst.**

From the raw data, the contributions of each compound to each mass line can be removed. So looking at the first five injections over the bypass, the methanol contributes to the other mass traces. By calibration this contribution can be estimated and removed. An example of this is for CO, where the contributions of methanol, formaldehyde and carbon dioxide can be taken out of the 28 amu line, to leave the remaining portion as carbon monoxide. Once the integrals are subtracted, they are further adjusted for sensitivity of the mass spectrometer to each compound. Once this has been done an accurate measure of the composition of each pulse is known. From this the methanol conversion can be calculated by the following formula:

$$\text{Conversion} = (A_{Obs} / A_{Unreacted}) * 100 \qquad (2\text{-}1)$$

Where Conversion is expressed as a percentage, $A_{Obs}$ is the observed peak area of methanol, and $A_{Unreacted}$ is the average area of a methanol pulse with no conversion over the catalyst bed.

The selectivity of the catalyst to each compound can be calculated using the following formula:

$$\text{Selectivity}_i = \left[\frac{\text{Product}_i}{\Sigma\,\text{Products}}\right] x100 \qquad (2\text{-}2)$$

When the conversion and selectivity of each product has been calculated for each pulse a graph of these against the temperature at which the data was recorded can be plotted as shown in Figure 2-7. Note that in the results chapters only the derived data is shown, while the raw data is shown as an appendix. Once selectivity and conversion have been calculated, the yield of a given product, at a given temperature can be calculated from the following formula:

$$\text{Yield (\%)} = (\text{Conversion (\%)} \times \text{Selectivity (\%)}) / 100 \qquad (2\text{-}3)$$

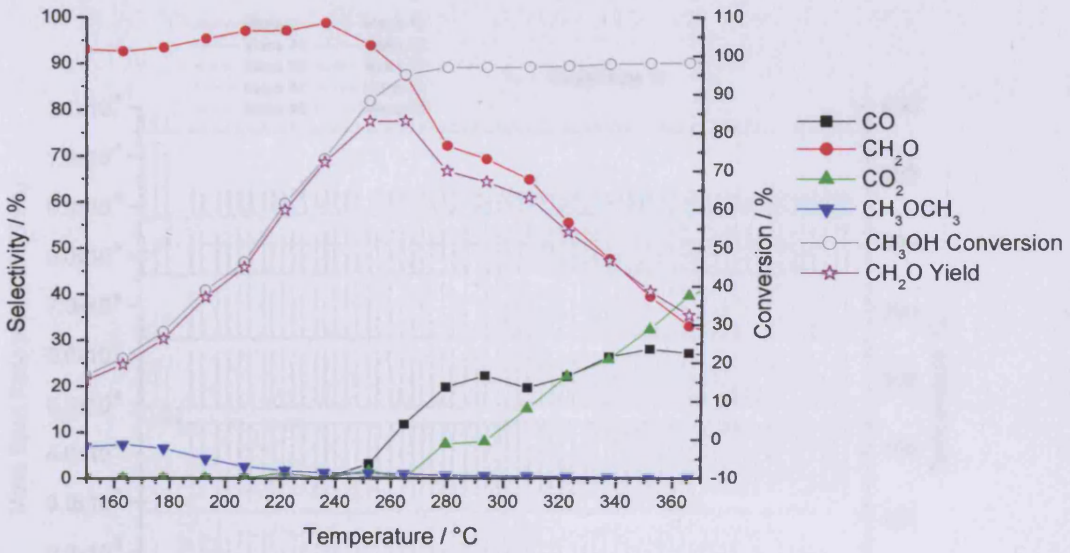


**Figure 2-7 – Conversion and selectivity against temperature for methanol injections over 2.2:1 Mo:Fe catalyst.**

The second mode of operation is *Isothermal Pulsed Flow Reaction* (IPFR) and this can give information on the rates of surface reactions, the sequence of product formation and product distribution change with time. Practically, this mode is very similar to TPPFR except that instead of having a temperature ramp in operation as the pulses are made, the catalyst is held at one temperature. This technique has the advantage that changes in conversion, selectivity, and line shape with time can be monitored and also it has good reproducibility. An example of the raw data produced is shown in Figure 2-8.

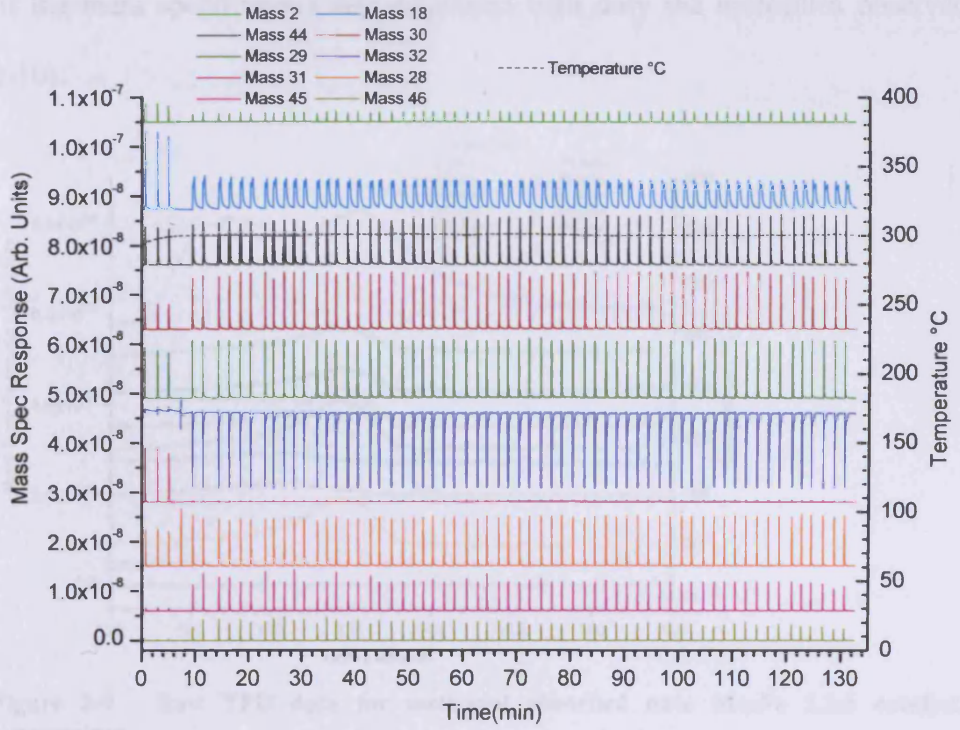


**Figure 2-8 - Raw data of a IPFR of methanol over 2.2:1 Mo:Fe catalyst.**

The derivation of the data to produce selectivity and conversion plots is then carried out in the same way as for TPPFR, but as the temperature remains constant, the total methanol injected can instead be used on the x-axis.

The third mode of operation is *Temperature Programmed Desorption* (TPD), which can provide information on surface coverage, adsorption probabilities, reaction kinetics and the separate steps in a reaction profile. Further details on this technique are provided later (Section 2.3.3), but the basic premise is after dosing a liquid or gas the temperature of the catalyst can be increased linearly. The adsorbate and any reaction products gain enough energy ($E_d$) to desorb from the surface and move into the gas phase, from where they are detected by the mass spectrometer. The raw data from this kind of experiment (Figure 2-9), is then processed to remove the cracking patterns of the molecules from each other, the effect of the filament and the sensitivity

of the mass spectrometer and displayed with only the molecules observed (Figure 2-10).

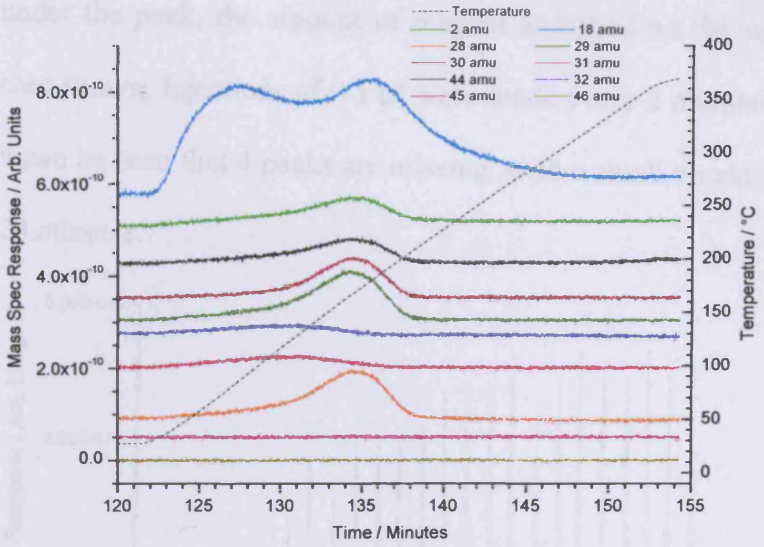


**Figure 2-9 - Raw TPD data for methanol absorbed onto Mo:Fe 2.2:1 catalyst at room temperature.**

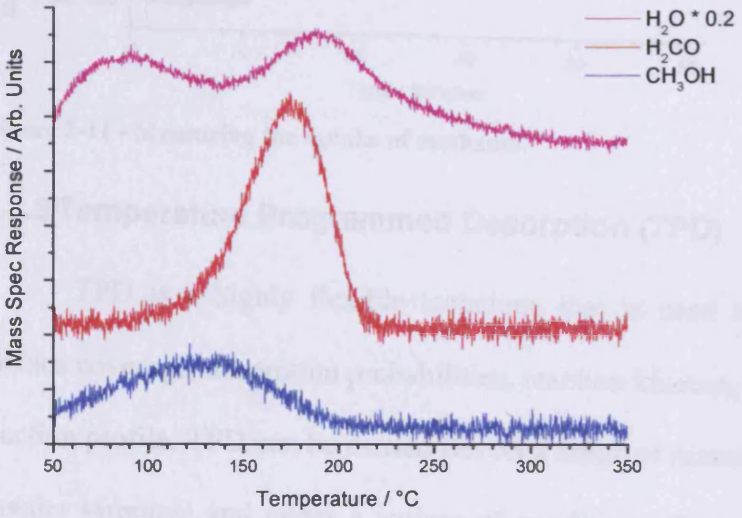


**Figure 2-10 - Processed TPD data for methanol absorbed onto Mo:Fe 2.2:1 catalyst at room temperature.**

Uptake of the adsorbate onto the surface can be measured by determining where the saturation breakthrough occurs (Figure 2-11). Small injections can be used (often 0.1 µl of liquid), so that breakthrough is not observed for 5 or more pulses. Initially the pulses are completely adsorbed on the catalyst surface, then breakthrough

of methanol is observed, eventually reaching an integral corresponding with the input injection. By calculating the methanol area expected and that observed by integration under the peak, the amount of reagent absorbed on the surface is calculated. In the case shown, injections of 0.1 μl were made every 2 minutes starting at 12 minutes, so it can be seen that 4 peaks are missing, with a small breakthrough on the fifth pulse at 20 minutes.

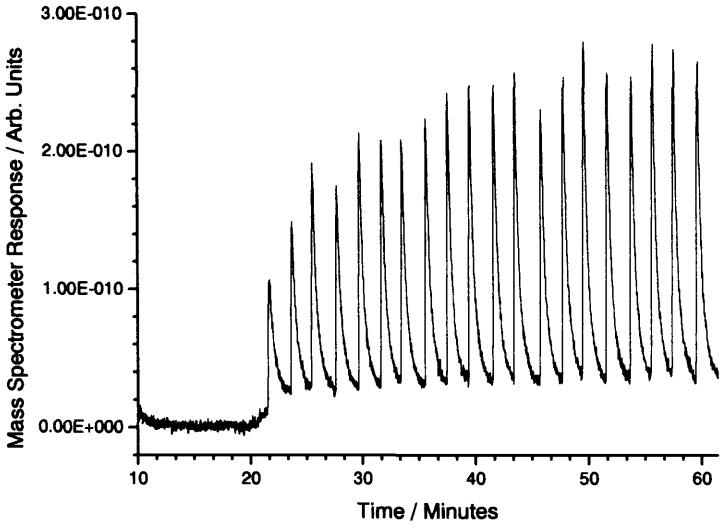


**Figure 2-11 - Measuring the uptake of methanol.**

### 2.3.3 Temperature Programmed Desorption (TPD)

TPD is a highly flexible technique that is used to provide information on surface coverage, adsorption probabilities, reaction kinetics, and the separate steps in a reaction profile. TPD can be carried out on a range of materials (e.g. single crystals or powder samples) and under a variety of conditions (from UHV (*i.e.* $<10^{-9}$ Torr) to high pressure).

A plot of the change in levels of desorption by various species with increasing temperature can then be produced.

For a first order process the rate of desorption can be described as:

$$Rate = k_d.\theta \quad (2\text{-}4)$$

Where $k_d$ is the rate constant for desorption and $\theta$ is the coverage. The rate constant, $k_d$ given by the Arrhenius equation:

$$k_d = A.\exp(-E_d/RT) \quad (2\text{-}5)$$

Where R is the gas constant and T is the temperature. At low temperatures, the coverage remains approximately constant so an Arrhenius plot of ln Rate *vs.* 1/T can yield a value for $E_d$ from the slope and hence the pre-exponential factor (A) can be derived. However, in most cases the processes are more complicated due to the change in $\theta$, so an alternative equation can be used to identify the desorption energies for a particular species, by simply using the temperature of maximum desorption rate ($T_p$). For a first order process this is:

$$E_d/(RT_p^2) = \frac{A}{\beta}.\exp(-E_d/RT_p) \quad (2\text{-}6)$$

Where $T_p$ is the temperature at which peak desorption occurs for a specific adsorbate, $\beta$ is the heating rate and A is usually assumed to be $10^{13}$ $s^{-1}$.

### 2.3.4 Methanol Peak Area

A test of the linearity of the peak areas produced with different size injections was carried out. The results produced for different reagents in different flow gases were similar, so the data is shown here only for methanol (31 amu), by means of a series of 5 injections ranging in size from 0.1 µl to 5 µl. A plot of the area under these peaks was made against the size of the injection, and linear plot fitted, shown in Figure 2-12 for aerobic conditions. When a linear fit is made of the points and passing through the origin, a gradient of $y = 8.33 * 10^{-10}$ is obtained with an $R^2$ value of 0.997.

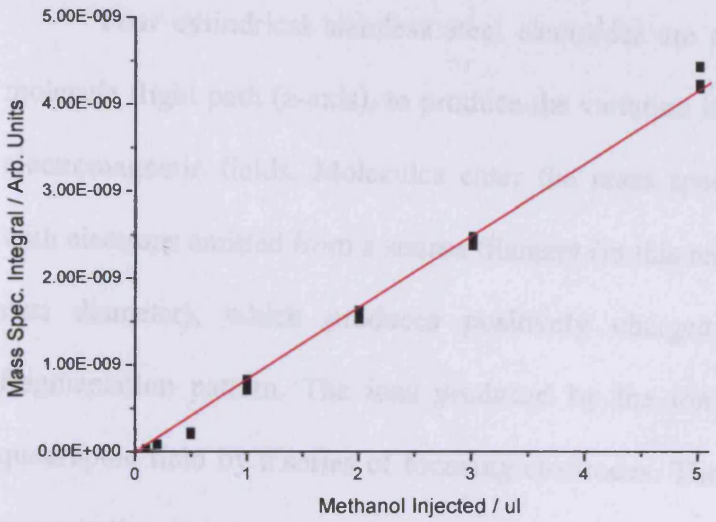


**Figure 2-12 – 31 amu Integral against methanol injection size in 30 ml/min He flow.**

### 2.3.5 Quadrupole Mass Spectrometry

All mass spectrometers cause the separation of ions with different mass charge ratios (m/e) to follow different special trajectories by the application of a three dimensional magnetic field. Magnetic fields can be used to deflect the ions by amounts proportional to their momentum, however, in quadrupole mass spectrometers it is alternating electric fields that are used to selectively separate the masses. Shown below in Figure 2-13, is a schematic representation of the basic make up of a quadrupole mass spectrometer.

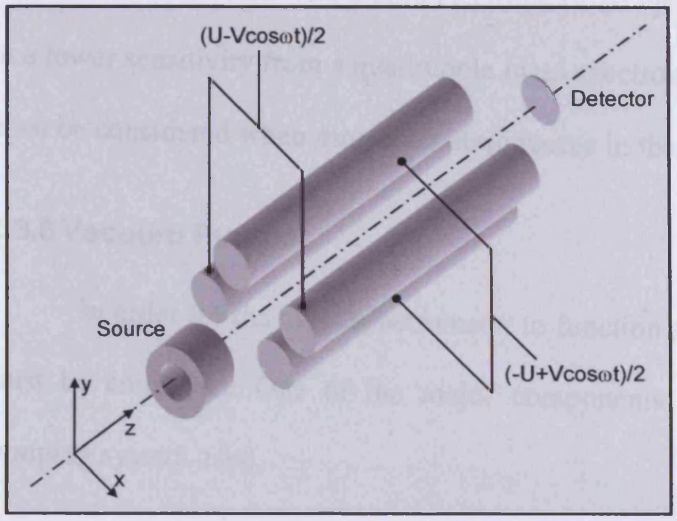


**Figure 2-13 - Schematic representation of the basic components of a quadrupole mass spectrometer.**

Four cylindrical stainless steel electrodes are arranged symmetrically to the molecule flight path (z-axis), to produce the variation in potential required to give the electromagnetic fields. Molecules enter the mass spectrometer and are bombarded with electrons emitted from a source filament (in this research thoriated tungsten, 0.15 mm diameter), which produces positively charged ions with a characteristic fragmentation pattern. The ions produced by the ion source are focused into the quadrupole field by a series of focusing electrodes. The electric field is alternated to generate the necessary potential to select the desired mass. To obtain a mass spectrum, an alternating voltage applied to one pair of opposing poles (V) is scanned, with a direct voltage is applied to the other pair of opposing poles (U), so that V and U follow a linearly increasing or decreasing modulation. The transmitted ion current can be monitored while V and U are scanned so that a mass spectrum is produced with a linear mass scale related to V. Depending on the voltage, only certain masses will execute a stable trajectory and travel down the quadrupole arrangement to reach the detector, allowing the quadrupole to act as a mass filter. The oscillation amplitude of the applied field is greatest at highest masses, so there is an increased probability that these ions will collide with a pole electrode or be ejected from the filter. This results in a lower sensitivity from a quadrupole mass spectrometer for higher masses, and this must be considered when molecular abundances in the spectra are obtained.

### 2.3.6 Vacuum Pumps

In order for the mass spectrometer to function properly, a good vacuum system must be employed. One of the major components of this vacuum system is the pumping system used.

### 2.3.6.1 Turbo Molecular Pumps

A turbo molecular pump (shown in Figure 2-14) can used to generate a vacuum down to $10^{-9}$ mbar and is a form of kinetic pump in which gas molecules have energy imparted into them by collision with the surface of a high speed rotor, causing them to move towards the pump outlet[4]. The rotor is fitted with blades rotating between corresponding discs in the stator Figure 2-15. The linear velocity of a peripheral point of the rotor is of the same order of magnitude as the velocity of the gas molecules. A backing pump is used to exhaust the turbo pump to atmosphere, usually a two vane rotary pump.

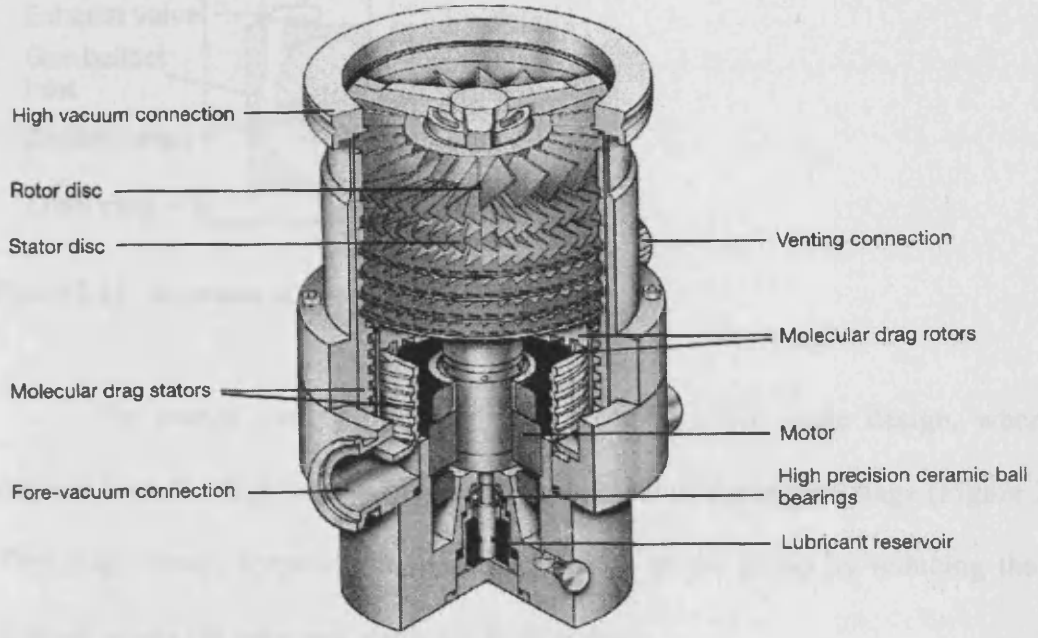


**Figure 2-14 - Cross section of a turbo molecular pump[4].**

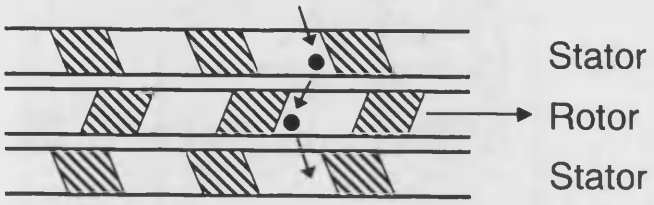


**Figure 2-15 - Path of gas molecule within a turbo pump[4].**

### 2.3.6.2 Rotary Vane Pumps

The rotary vane pump consists of an eccentrically placed slotted rotor that turns in a cylindrical stator (Figure 2-16) driven by a directly coupled electric motor. The slots contain, two (or three) sliding vanes which are in continuous contact with the walls of the stator. Gas is drawn in, compressed and expelled through a spring loaded exhaust valve. The vanes and rotor are sealed in a fluid film, with the stator immersed in the fluid to provide heat transfer to the pump casing.

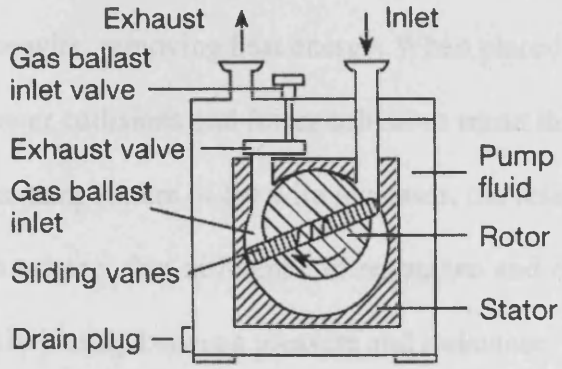


**Figure 2-16 - Schematic of a sliding vane rotary pump[4].**

The pumps used within this work were of a two stage design, where the exhaust from the first stage is connected to the inlet of the second stage (Figure 2-17). Two stage pumps improve the ultimate pressure of the pump by reducing the back leakage where the rotor and stator are fluid sealed.

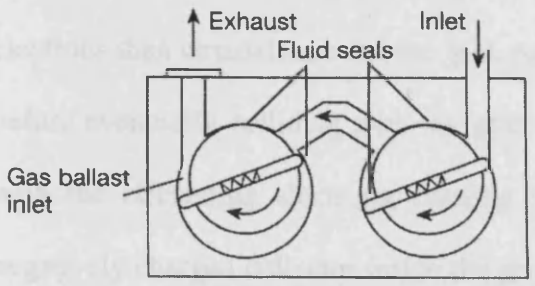


**Figure 2-17 - Schematic of a two stage rotary vane pump[4].**

### 2.3.7 Pressure Measurement

Two different types of pressure gauge are present on the vacuum system of the pulsed flow reactor: a pirani gauge and an ionisation gauge.

#### 2.3.7.1 Pirani Gauges

Pirani gauges are used to measure pressures in the low vacuum range (30 mbar-$10^{-3}$ mbar) and work on the principle of measuring the resistance of a heated wire placed within the vacuum system. At atmospheric pressure, gas molecules collide with the wire, removing heat energy. When placed in vacuum there are fewer molecules, so fewer collisions and fewer collisions mean that less heat is removed from the wire. As the temperature of the wire increases, the resistance increases meaning a simple circuit can detect this difference in resistance and once calibrated can directly correlate the relationship between pressure and resistance.

#### 2.3.7.2 Ionisation Gauges

Ionisation gauges are used for measuring pressures below those covered by a Pirani gauge ($10^{-3}$ - $10^{-11}$ mbar). The ionisation gauge consists of three main parts (shown in schematic form in Figure 2-18), these are the filament, the grid and the detector. The filament is used for the production of electrons by thermonic emission. The grid has a positive charge that attracts the electrons away from the filament. The electrons then circulate around the grid, passing through the fine structure many times before eventually colliding with the grid. Gas molecules within the grid may collide with the circulating electrons, causing the gas molecule to become ionised. The negatively charged collector inside the grid attracts these now positively charged ions, while they are simultaneously repelled from the negatively charged grid. The number of ions to collide with the collector is directly proportional to the number of molecules

within the vacuum system, so measuring the ion current gives a direct reading of the pressure.

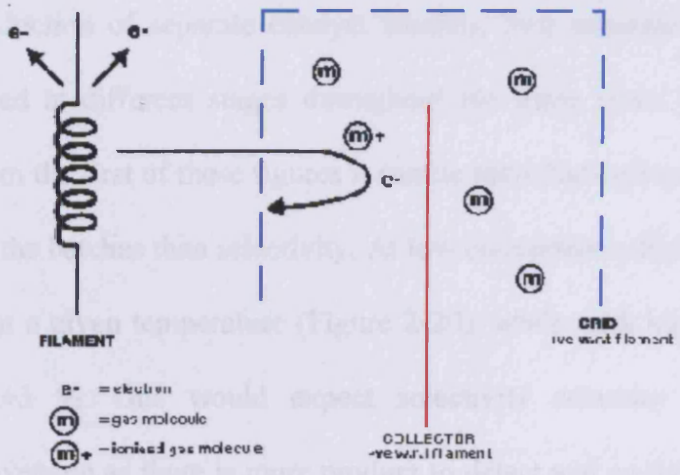


**Figure 2-18 - Schematic of construction of an ionisation gauge[5].**

### 2.3.8 Quantification

For any scientific experiment to prove meaningful, the equipment used to record the measurements must first be calibrated so that quantifiable and reliable results can be obtained. After this, the reproducibility of the machine also needs to be measured so that results obtained on the machine at different times may be compared with a level of certainty.

#### 2.3.8.1 Blank Tube Reactivity

The reactivity of a blank U-tube, with the same amount of quartz wool usually used to hold the catalyst in place was tested in a flow of 10 % $O_2$/He so that the influence of these always present components could be established and removed from any data observed with a tube loaded with catalyst. The tube is mainly unreactive to the methanol at the temperatures tested, showing no reactivity to 300 °C, with conversion reaching less than 4 % by 390 °C. The products formed from the reaction of the methanol and oxygen on the stainless steel tube were $CO_2$ and $H_2O$.

### 2.3.8.2 Reproducibility

To establish the reliability of both the pulsed flow reactor and of the production of separate catalyst batches, four separate batches of Mo:Fe 2.2:1 were tested at different stages throughout the three years of experiments (Figure 2-19). From the first of these figures it can be seen that conversion is replicated more closely for the batches than selectivity. At low conversions, the measurement is accurate to ±5 % at a given temperature (Figure 2-20), while with higher conversions this improves to ±3 %. One would expect selectivity accuracy to improve with increasing conversion as there is more product to detect and so the data is further from the limits of detection for the machine. From the data shown, selectivity is accurate to around ±8 % at 40 % methanol conversion or greater.

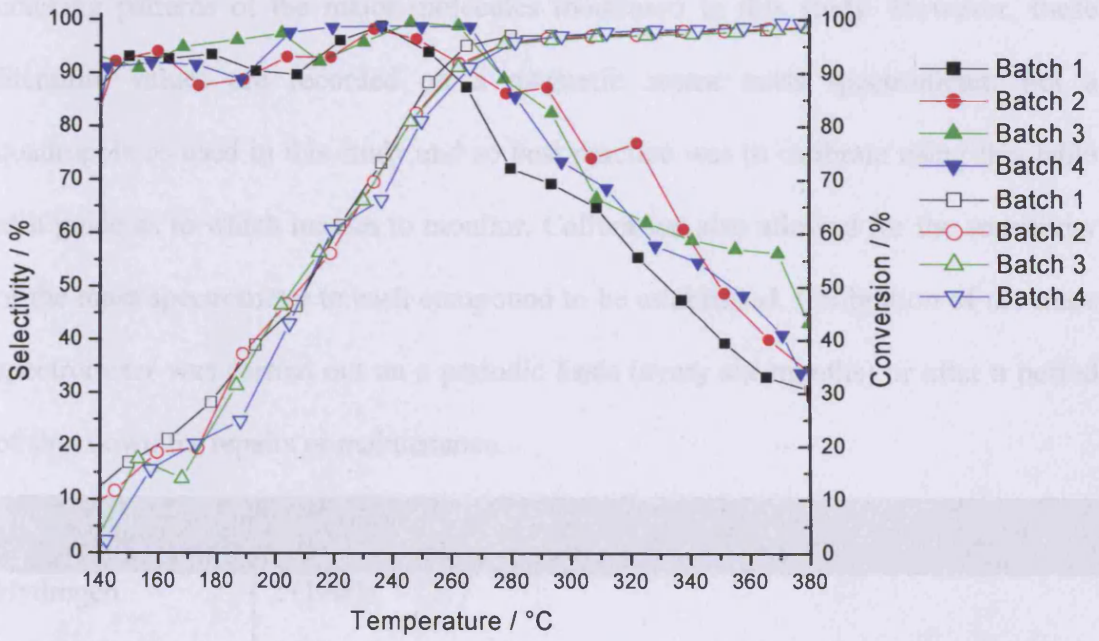


**Figure 2-19 - Comparison of four batches of Mo:Fe 2.2:1 catalyst for conversion and selectivity.**

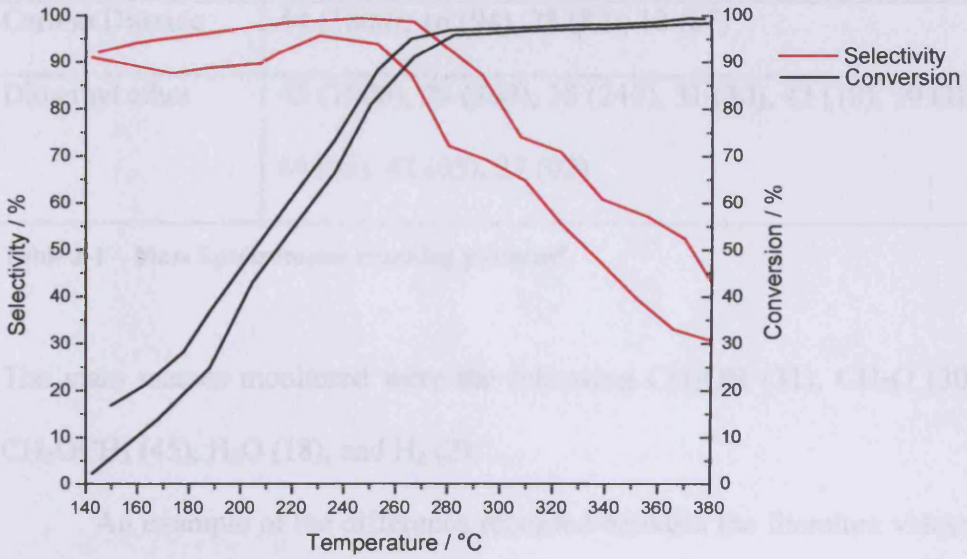


**Figure 2-20 - Limits of error for different batches of Mo:Fe 2.2:1**

### 2.3.8.3 Cracking Patterns

Shown in Table 2-1 are the literature values for the mass spectrometer cracking patterns of the major molecules monitored in this study. However, these literature values are recorded on a magnetic sector mass spectrometer, not a quadrupole as used in this study and so best practice was to calibrate using this table as a guide as to which masses to monitor. Calibration also allowed for the sensitivity of the mass spectrometer to each compound to be established. Calibration of the mass spectrometer was carried out on a periodic basis (every six months) or after a period of shut down for repairs or maintenance.

| Compound | Cracking Fractions |
|---|---|
| Hydrogen | 2 (1000), 1 (21) |
| Water | 18 (1000) 17 (211), 16 (09), 19 (05) 20 (03) |
| Carbon Monoxide | 28 (1000) 12 (47), 16 (17), 29 (12), 14 (08), 30 (02), 13 (01) |
| Formaldehyde | 29 (1000), 30 (660), 28 (330), 31 (30), 15 (06), 27 (03) |
| Methanol | 31 (1000), 32 (717), 29 (421), 28 (90), 30 (78), 33 (11), 27 (05) |
| Oxygen | 32 (1000), 16 (36) |

| | |
|---|---|
| Carbon Dioxide | 44 (1000), 16 (94), 28 (82), 12 (67) |
| Dimethyl ether | 45 (1000), 29 (390), 15 (240), 31 (30), 43 (10), 30 (10), 28 (09), 44 (06), 42 (03), 27 (02) |

**Table 2-1 – Mass Spectrometer cracking patterns[6].**

The main masses monitored were the following $CH_3OH$ (31), $CH_2O$ (30), $O_2$ (32), $CH_3OCH_3$ (45), $H_2O$ (18), and $H_2$ (2).

An example of the difference recorded between the literature values and those recorded in this study, are the cracking patterns observed for methanol, in the presence (Figure 2-21) and absence of oxygen (Figure 2-22). A major reason for this difference is that the filament used within the quadrupole mass spectrometer itself acts as a catalyst. It works to combust the methanol, as can be seen by the presence of 44 amu ($CO_2$) and 18 amu ($H_2O$) (Figure 2-21). These are also present, but to a lower extent in anaerobic conditions (Figure 2-22), but both are reduced in intensity as there is no gas phase $O_2$ present.

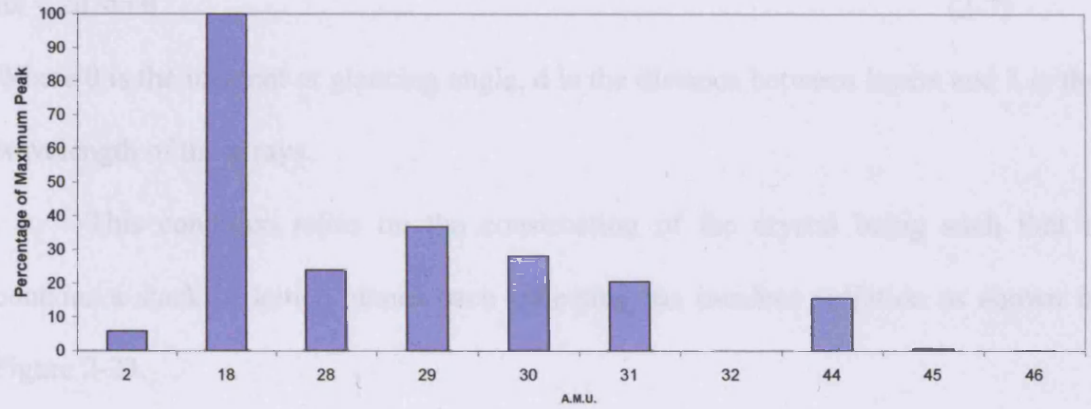


**Figure 2-21 - Methanol cracking pattern in aerobic conditions.**

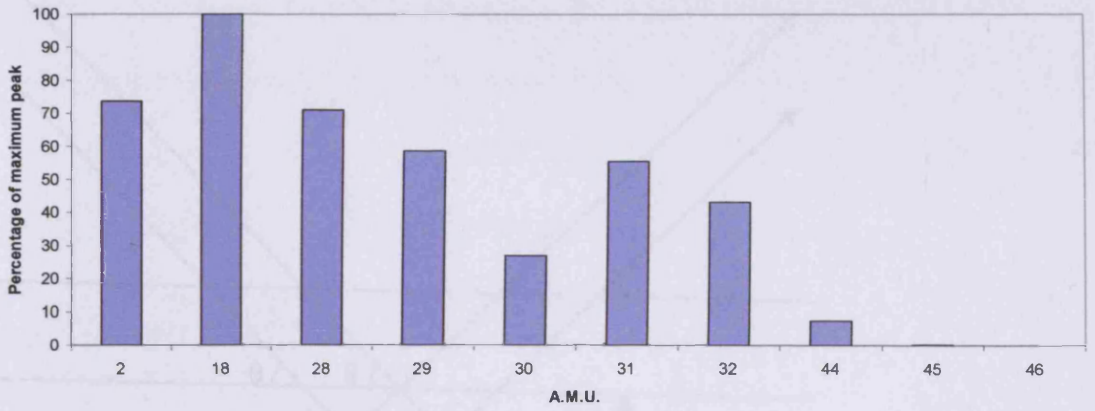


**Figure 2-22 - Methanol cracking pattern in anaerobic conditions.**

## 2.4 X-Ray Diffraction

### 2.4.1 Theory

X-ray diffraction is an important technique for identifying bulk structure. It is capable of giving detailed information on the internal structure of a crystal. The technique was developed by the Braggs, William and his son Lawrence, who were later jointly awarded the Nobel Prize for physics in 1915. The fundamental equation applied in XRD is the Bragg equation:

$$n\lambda = 2d \sin\theta \qquad (2\text{-}7)$$

Where $\theta$ is the incident or glancing angle, d is the distance between layers and $\lambda$ is the wavelength of the x-rays.

This condition relies on the construction of the crystal being such that it contains a stack of lattice planes each reflecting the incident radiation as shown in Figure 2-23.

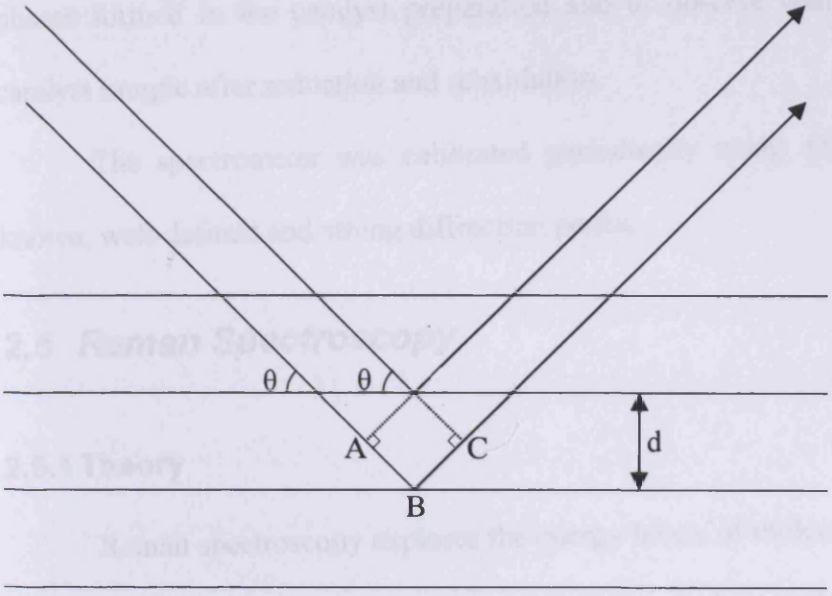


**Figure 2-23 - An illustration of the Bragg equation.**

The net path length difference of the two incident rays is AB + BC, which is equal to $2d\sin\theta$. The path length is dependent on the incident angle of the x-rays. If AB + BC is not an integral number of wavelengths, then the waves will interfere largely destructively, whereas if AB + BC = $n\lambda$, the waves will be in phase and will interfere constructively. From the θ value of the observed reflection it is then possible to calculate the layer spacing (d) from the Bragg equation.

In this research the materials used were powder samples and so a powder diffractometer was used to measure bulk composition. Powders consist of a collection of randomly orientated crystals so that several of them will satisfy the Bragg equation. Powder diffraction involves analysing a powdered sample using monochromatic x-rays, and can give qualitative analysis of powdered samples.

### 2.4.2 Experimental

The XRD spectra were obtained using a Enraf Nonus FR590 fitted with a hemispherical analyser. The conditions employed were Cu Kα radiation (λ=1.540598 Å), with a voltage of 40 kV and a current of 30 mA. XRD was used to detect the

phases formed in the catalyst preparation and to observe changes within the bulk catalyst sample after reduction and reoxidation.

The spectrometer was calibrated periodically using silicon which has well known, well-defined and strong diffraction peaks.

## 2.5 Raman Spectroscopy

### 2.5.1 Theory

Raman spectroscopy explores the energy levels of molecules by examining the frequencies present in the radiation scattered by molecules. Typically, a monochromated incident beam is passed through the sample and the radiation scattered perpendicular to the beam is monitored. The set up of a typical Raman spectrometer is shown below in Figure 2-24.

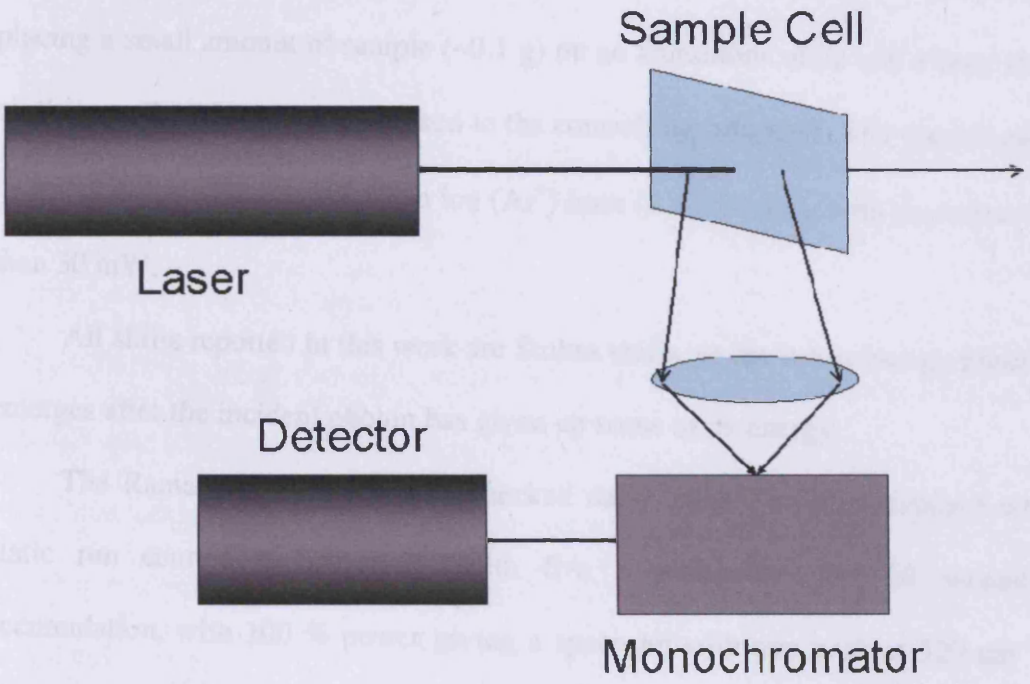


**Figure 2-24 - Arrangement of a Raman Spectrometer.**

About 1 in $10^7$ of the incident photons collide with the molecules, give up some of their energy, and emerge with lower energy, which is known as Stokes

radiation. Other incident photons may collect energy from the molecules (if they are already excited), and emerge as higher frequency anti-Stokes radiation. Radiation scattered in the forward direction without change in frequency is known as Rayleigh radiation. Lasers are used as they are highly monochromated and so the small shifts in frequency from the incident radiation can be observed. They also provide an intense incident beam which is required, due to the low intensity of scattered radiation.

The general selection rule for Raman activity is: 'In order to be Raman active, a molecular rotation or vibration must cause some change in a component of the molecular polarizability. A change in polarizability is reflected by a change in either the *magnitude* or the *direction* of the polarizability ellipsoid.'[7]

### 2.5.2 Experimental

The Raman microscope used was a Renishaw Ramascope, which is operated by placing a small amount of sample (~0.1 g) on an aluminium slide and a laser to focus on the sample using a camera linked to the controlling computer. The spectra can then be recorded using the green argon ion ($Ar^+$) laser ($\lambda$ = 514 nm), with an output of less than 30 mW.

All shifts reported in this work are Stokes shifts, so the lower energy photon that emerges after the incident photon has given up some of its energy.

The Raman spectrometer was checked daily using a silicon standard where a static run centred at 520 $cm^{-1}$, with five accumulations for 10 seconds per accumulation, with 100 % power giving a spectrum with one peak at 520 $cm^{-1}$ with counts in the region of 50000.

Spectra were recorded in different areas of the sample to ensure they were representative of the whole composition, with no differences observed.

Raman spectra were obtained by Andrew Watts at Cardiff University.

## 2.6 X-Ray Photoelectron Spectroscopy

### 2.6.1 Theory

XPS is a surface sensitive technique first reported by Siegbahn in 1967[8]. XPS analyses surfaces by irradiating them with monoenergetic soft x-rays (from either a Mg or Al source) under UHV and analysing the emitted electrons by energy. The photons have limited penetrating power in a solid of the order of 1 - 10 μm, causing atoms in this region to emit photoelectrons by the photoelectric effect. XPS is a surface sensitive technique as photoelectrons have a very small inelastic mean free pathway, meaning only those photoelectrons produced in the near surface region escape and are detected. The emitted electrons have a kinetic energy which is dependent on the energy of the photon they are irradiated by and the orbital they have been ejected from. The kinetic energy of the emitted electrons is given by:

$$KE = h\nu - BE - \Phi_s \qquad (2\text{-}8)$$

Where hν is the energy of the photon, BE is the binding energy of the atomic orbital from which the electron originates, and $\Phi_s$ is the spectrometer work function and can be calibrated for each instrument used.

The energies of the emitted photoelectrons are analysed through a lens system, which focuses the electrons into a hemispherical analyser. This consists of two curved plates that act as a condenser and have a potential applied. The electrons entering the analyser feel this electric field, which forces them to travel in direction that is dictated by the equation:

$$F = q/E = m(V^2/R) \qquad (2\text{-}9)$$

Where F is force, q is the charge (of the electron), E is the electric field, m is the mass (of the electron), V is the voltage on the analyser and R is the radius of the hemisphere.

The electron analyser detects the number of electrons emitted with a given kinetic energy, and the binding energy of the detected electrons is calculated (from equation 2-8). A plot of the number of electrons released with a given energy against binding energy is then produced, called a photoelectron spectrum.

As each element has a unique set of binding energies, XPS can be used to identify the elements at the surface. The chemical states of the elements being analysed can also be determined, as the binding energy is dependent on the chemical potential and polarizability of the compound. Changes in the chemical potential and polarizabilitlty (e.g. by a change in oxidation state) lead to a change in the binding energy, known as a chemical shift. From the area under a peak it is possible to measure how much of an element, in a given oxidation state, is present. However, it is necessary to allow for sensitivity factors as some elements and oxidation states give much stronger signals than others.

Auger electrons may also be emitted, as once an electron is removed from an inner orbital, the available space will be occupied by an electron from an outer orbital with a release of energy. This energy can be removed from the atom in two ways: the emission of a photon of appropriate energy (X-ray fluorescence), or it may be transferred to a third electron, which will be excited and escape with a certain energy. The kinetic energy of this third electron is independent of the irradiating photon energy used in the first place, and so Auger electron peaks do not appear at the same apparent binding energy for Mg Kα and Al Kα experiments.

### 2.6.2 Generation of X-rays

X-ray sources make use of the characteristic emission lines from a target (anode) when it is bombarded with high energy electrons. The choice of source for XPS work is based upon the width of the emission line (>1.0 eV) and the x-ray energy, which determines the deepest core energy level from which an electron can be emitted. The discrete X-ray lines produced are superimposed on a continuum which is termed Bremsstrahlung. The continuum is formed when the high speed electrons are slowed rapidly by multiple collisions within the anode material. This continuum is removed in the case of XPS by the use of a thin aluminium foil.

Shown in Figure 2-25 is a typical layout for a double anode X-ray source. It features two filaments for electron bombardment, and two water cooled anode surfaces, one made of magnesium and the other of aluminium. The thin aluminium film separates the sample from the x-ray source and is present to prevent the sample being exposed to stray electrons and from contamination in the source region.

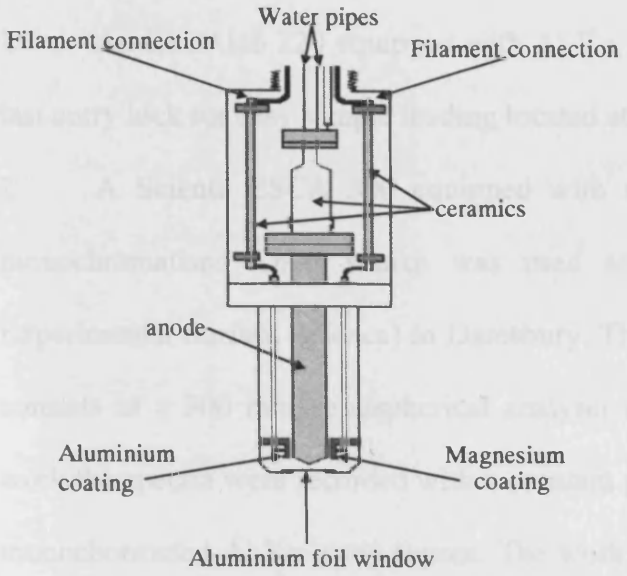


**Figure 2-25 - Schematic of a typical double anode X-ray source.**

The filament and anode are not in a direct sight line so that filament material is not evaporated onto the surface of the anode, which would cause an attenuation in the x-ray flux and introduce impurity lines in the spectra. A positive potential of up to 15 kV is applied to the anode, while the filament is kept as close to ground potential as possible. This positive potential ensures scattered electrons do not strike the aluminium window, but are instead drawn back towards the anode. This avoids the window being melted at high power, and also prevents the generation of Al Kα and secondary electrons from the window that can irradiate the sample.

The x-ray source has a separate pumping system for two reasons. Firstly it stops the sample being studied becoming exposed to degassing products from the filaments in the x-ray source and secondly it keeps the anode surface clean, whilst volatile species are being studied.

### 2.6.3 Experimental

Three different machines were used to obtain XPS spectra:

1. An ESCAlab 220 equipped with Al Kα and Mg Kα sources and fitted with a fast entry lock for easy sample loading located at Cardiff University.

2. A Scienta ESCA 300 equipped with a high power rotating anode and a monochromatised Cr/Al source was used at the NCESS (National Centre for Experimental Surface Science) in Daresbury. The detection system of this instrument consists of a 300 mm hemispherical analyser and a multi-channel detector. In this work the spectra were recorded with a constant pass energy of 150 eV, using the non-monochormated Al Kα x-ray source. The work on the ESCA 300 was performed by Matthew Hall (University of Cardiff).

3. A Kratos *AXIS (DLD)* fitted with a monochromated Al Kα radiation source and a refocusing lens to give high resolution XPS. The survey scans were acquired

with a pass energy of 160 eV in a single sweep with a step of 0.5 eV. Region scans were acquired with a pass energy of 40 eV, in 5 to 10 sweeps in steps of 0.1 eV. This machine is also located at Cardiff University.

## 2.7 BET Surface area measurement

### 2.7.1 Theory

A free gas and that adsorbed are in dynamic equilibrium, with the fractional coverage of the surface dependent on the pressure of the overlying gas. The variation of the coverage with pressure at a constant temperature is called the adsorption isotherm.

In 1938 Brunauer, Emmett and Teller derived an adsorption isotherm that considers multilayer adsorption[9]. Multilayer adsorption differs from monolayer adsorption as monolayer adsorption is controlled by the adsorbate-surface interactions, whereas multilayer adsorption is controlled by adsorbate-adsorbate interactions.

Gases can adsorb onto a surface either through the formation of a chemical bond, chemisorption, or by a weak physical interaction, physisorption. Physisorption is reasonably sample independent for the adsorption of molecules such as $N_2$, which at low temperatures generally form a monolayer that is controlled by the size of the $N_2$ molecule (a known standard of 0.16 $nm^2$). The $N_2$ molecules pack as close together regardless of the atomic structure of the substrate. The BET isotherm acknowledges that while the monolayer of a physical adsorbate is being filled, monolayers can form and is written:

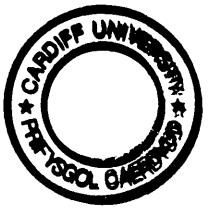

$$\frac{V}{V_{Mon}} = \frac{cz}{(1-z)(1-(1-c)z)} \qquad z = \frac{p}{p^*} \qquad (2\text{-}10)$$

Where V is the total volume of the adsorbed material in $cm^{-3}$, $V_{mon}$ is the volume corresponding to monolayer coverage in $cm^{-3}$, p is the equilibrium pressure for a particular surface coverage, p* is the vapour pressure above a layer of adsorbate that is more than one molecule thick and which resembles a pure bulk liquid, and c is a constant which is large when the enthalpy of desorption from a monolayer is large when compared with the enthalpy of vaporization of the liquid adsorbate.

The form of c is expressed as:

$$c = e^{(\Delta_{ads}H^{\Theta} - \Delta_{liq}H^{\Theta})/RT} \qquad (2\text{-}11)$$

Where $\Delta_{ads}H^{\Theta}$ is the enthalpy of adsorption , $\Delta_{liq}H^{\Theta}$ is the enthalpy of liquefaction, R is the gas constant and T is the temperature.

The BET isotherm can be used to calculate the surface area associated with a monolayer of gas adsorbed onto the surface, and therefore determine the surface area of the sample. When nitrogen is adsorbed onto the surface at 77 K, the technique can be used to provide highly accurate surface areas. Only a small number of points are required to give surface areas, so in this work five or six points of the isotherm were taken. If a whole isotherm is measured, the total surface area can be divided into subgroups, each being associated with a particular pore size, allowing pore density distribution information to be gathered.

### 2.7.2 Experimental

The BET surface areas were obtained on two separate machines:

1. A Micromeretics Gemini 2360 was used in a static volumetric method, in which between 0.5 and 2.5 g of catalyst was weighed and placed in a sample tube holder, before being heated to 150 °C under vacuum for 1 hour to remove water from

the surface. The sample tube and a blank reference were then connected to the machine. The sample and reference were cooled using liquid nitrogen and the pressure to achieve equilibrium measured. The analyser collected five points at different pressures from the isotherm, before calculating the surface area in $m^2 g^{-1}$.

2. A CE instruments QSurf M1 was used in a flow method with up to 2 g of sample being weighed and added to a pre-weighed sample holder. The sample holder was then connected to one of the degas stations on the machine where a nitrogen helium mix was passed over the catalyst whilst heating to 150 °C for 1 hour to remove surface water. The sample was then moved to the measuring bay of the machine, where six points, with $N_2$/He fractional mixtures of 0.09, 0.14, 0.18, 0.22, 0.26, and 0.30 were used. Before each $N_2$/He mixture the thermal conductivity detector (TCD) was calibrated by sampling a known amount of $N_2$ gas. The sample was then immersed into a liquid nitrogen bath where $N_2$ in the $N_2$/He flow was absorbed onto the surface. Upon removal from the bath the sample began to be heated and the $N_2$ was desorbed from the surface. The amount of $N_2$ desorbed was measured by the TCD comparing the $N_2$ in the exit flow to that entering the sample loop. This was repeated for each of the six $N_2$/He mixtures. The new weight was entered into the controlling computer and the surface area was calculated in meters squared per gram of sample.

Both BET machines used were calibrated using a carbon black sample of known surface area (22.4 $m^2 g^{-1}$).

## *2.8 Super-STEM*

### 2.8.1 Theory

STEM is a technique in which a fine electron probe is scanned across a thin specimen and the intensity of the transmitted electron signal is measured using one or

more electron detectors (Figure 2-26)[10]. In this way an image can be built up pixel by pixel, in the same way as a conventional scanning electron microscope (SEM). Chemical microanalysis is also possible in a point by point method if other detectors, such as an electron energy loss (for details see Section 2.8.3) spectrometer or an X-ray detector.

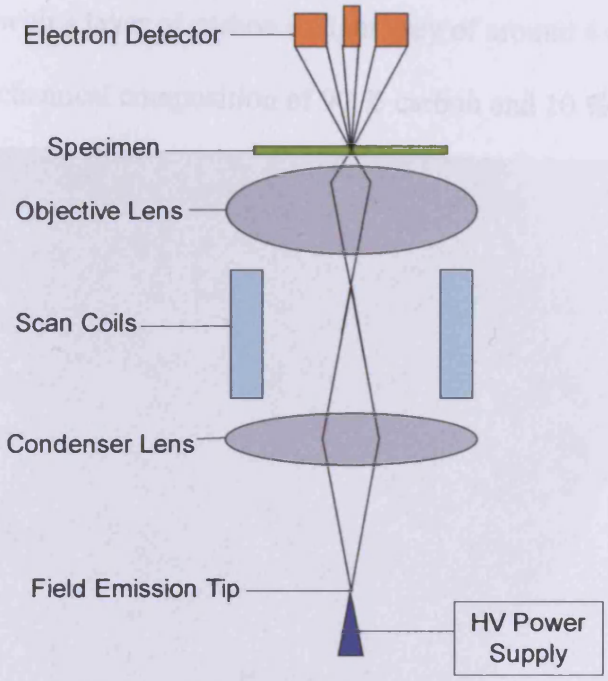


**Figure 2-26 - Typical layout of STEM with the electron beam going from top to bottom[10].**

The advantage of STEM over techniques such as conventional SEM or a conventional TEM in which the beam can be scanned, lies in the small size of the probing electron beam (~1 Å) and the beam current density (electrons per unit time per unit area) that is delivered to the sample.

If the fine probing beam is to be held for several seconds for chemical microanalysis or diffraction on a sample, then a clean sample and clean high vacuum system are required otherwise contamination will rapidly occur. A machine is commonly referred to as a 'dedicated' STEM when the field emission source is connected to a UHV column. The problem of contamination is one of the most

common faced by microscope users and occurs as mobile hydrocarbons diffuse across the sample surface to the point of analysis, where the electron beam cracks them into there constituent atoms. Carbon deposits as amorphous contamination spots above and below the sample and is deposited quicker than any removal due to electron beam sputtering. An example of a bright field image (Figure 2-27) shows the dark particle with a layer of carbon in light grey of around 4 nm. A typical contamination film has a chemical composition of 90 % carbon and 10 % oxygen.

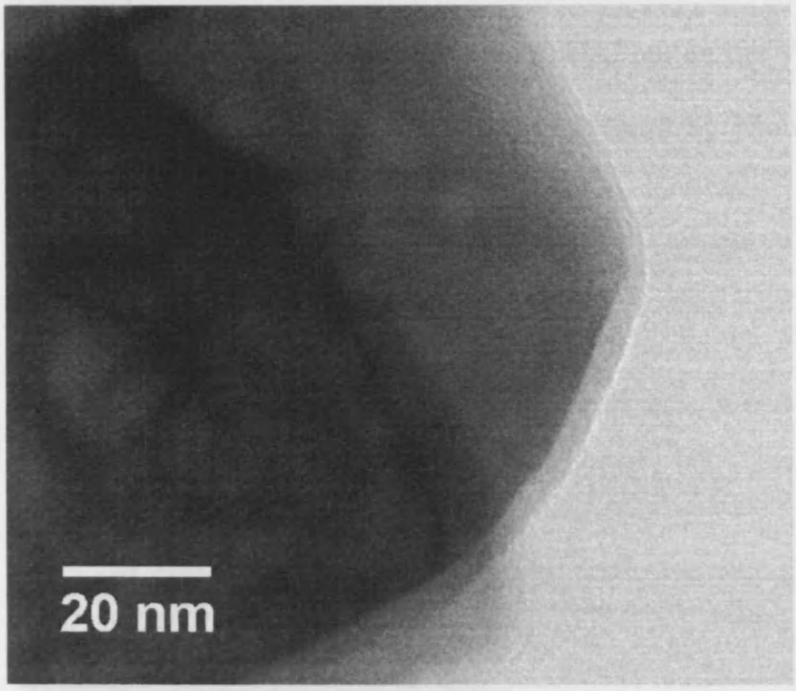


**Figure 2-27 - STEM image showing an amorphous layer of surface carbon.**

The electron beam used in STEM can cause damage to the sample in one of two ways, direct displacement of atoms by electrons (momentum transfer) and ionization damage (bond breaking). Ionization damage is most often a problem within oxide samples, where oxygen atoms can be released from their bonds and if mobile within the structure of the specimen, collect together as bubbles. The bubbles can be seen growing under the beam and burst out through the surface leaving a hole (termed hole drilling). The rate of damage is a function of the electron density within the beam

so use of a field emission gun (FEG) system can cause most damage as it has a very high electron density.

STEM has the advantage over TEM that only the parts of the sample that are scanned are irradiated, meaning there is no hidden beam damage happening outside the field of view. Another advantage is that when focused at higher magnification, an image will remain in focus at lower magnification.

### 2.8.2 Experimental

Super-STEM experiments were carried out on the VG Microscopes 501 FEG CTEM, fitted with an aberration corrector fitted by Nion at Daresbury, shown in Figure 2-28.

**Figure 2-28 – Super-STEM system at Daresbury.**

The parameters of the microscope are an electron energy of 100 keV ± 0.3 eV, a gun brightness of $10^8$ A $cm^{-2}$ $sr^{-1}$, and a current density at the specimen of 0.1 mA in 1.0 Å beam which is approximately 1 x $10^6$ A $cm^2$. The vacuum system of the

microscope allows for a typical pressure of below 5 x $10^{-8}$ mbar within the column and less than 3 x $10^{-11}$ mbar within the field emission gun.

Before mounting the samples, they were crushed in an agate pestle and mortar where they were mounted onto a lacy carbon sample disc, which was placed into the top entry sample cartridge.

The experiments were carried out with the help of Prof. Mervyn Shannon and Dr. Andrew Bleloch.

### 2.8.3 Electron Energy Loss Spectroscopy

#### 2.8.3.1 Theory

EELS measures the spectral distribution of energy transferred from a monochromatic electron beam in to a specimen[11]. Two types of geometry are used for EELS, firstly low energy primary electron beams are reflected by solid surfaces, giving a spectrum covering the millielectron volt to the electron volt range (equivalent to the infra red domain of the electromagnetic spectrum) and is largely a vibrational spectroscopy. The second case (and that utilised in this thesis) uses high energy primary beams transmitted through thin foils or at glancing incidence along surfaces. The inelastic scattering events involved encompass a wide range of excitations from the electron volt to the kiloelectron volt (equivalent to the visible to the soft X-ray domain), making it a spectroscopy of electron states related to the valence and conduction electrons in the low energy loss range (*i.e.* 1-50 eV), and atomic core electrons in the high energy loss domain (50 eV-1000's eV).

The technique of EELS is now widely combined with electron microscopy due to the elementally specific signal obtained, and is used to obtain special resolution on the sub-nanometer level.

The history of electron energy loss as a micro-analytical technique can be traced back to the early work of Hillier and Baker in the 1940's[12]. The technique became practically used in the 1960's as a result of the progress in realising and coupling analysers and filters to electron microscope columns.

A typical EELS spectra exhibits the following characteristic features: a zero energy loss peak; a major contribution (the low loss region) extending from around 5 to 50 eV and corresponding to the excitation of electrons in the valence band and low-lying levels; and superimposed on a continuously decreasing background, a succession of element specific edges at increasing energy losses. The low loss structures reflect a mixture of collective (plasmon) and interband processes (*i.e.* a kind of average electron properties). The core-loss features that appear between 100-1000 eV are chemically representative, with not all visible edges displaying similar shapes due to the their general behaviour being imposed by atomic considerations.

### 2.8.3.2 Experimental

The EELS experiments were carried out in tandem with the STEM imaging in the super-STEM machine at Daresbury, which is described in Section 2.8.2.

## 2.9 References

(1) Soares, J. M. C.; Morrall, P.; Crossley, A.; Harris, P.; Bowker, M. *Journal of Catalysis* **2003**, *219*, 17.
(2) James, D. Selective Propene Oxidation on Mixed Metal Oxide Catalysts. PhD, University of Reading, **2002**.
(3) James, D.; Fourre, E.; Ishii, M.; Bowker, M. *Applied Catalysis, B: Environmental* **2003**, *45*, 147.
(4) Chambers, A.; Fitch, R. K.; Halliday, B. S. *Basic Vacuum Technology*, 2nd ed.; Institute of Physics, **1998**.
(5) http://www.vacgen.com/asp/catalogue.asp?url=http%3A//www.vacgen.com/catalogue/section-8/page08_06.htm&frame=1, **07/04/2006**.
(6) Cornu, A.; Massot, R. *Compilation of Mass Spectroscopic Data*; Methen, London and Presses Universitaires: France, **1966**.
(7) Banwell, C. N. *Fundamentals of Molecular Spectroscopy*, 3rd ed.; McGraw-Hill Book Company, **1983**.

(8) Siegbahn, K.; et al. *Nova Acta Regiae Societatis Scientiarum Upsaliensis* **1967**, *20*, 282.
(9) Brunauer, S.; Emmett, P. H.; Teller, E. *Journal of the American Chemical Society* **1938**, *60*, 309.
(10) Keyse, R. J.; Garratt-Reed, A. J.; Goodhew, P. J.; Lorimer, G. W. *Introduction to Scanning Transmission Electron Microscopy*; BIOS Scientific Publishers, **1998**.
(11) Amelinckx, S.; van Dyck, D.; van Landuyt, J.; van Tendeloo, G. *Handbook of Microscopy. Applicatiosn in Materials Science, Solid-State Physics and Chemistry. Methods I*; VCH, **1997**.
(12) Hillier, J.; Baker, R. F. *Journal of Applied Physics* **1944**, *15*, 663.

# 3 Methanol Oxidation on Iron Molybdate Catalysts

## 3.1 Introduction

This chapter investigates the properties of methanol oxidation over iron molybdate catalysts. To do this, the single oxides of haematite ($Fe_2O_3$) and molybdena ($MoO_3$) are tested and compared to $Fe_2(MoO_4)_3$ and a mixed oxide of $Fe_2(MoO_4)_3.xMoO_3$, with a typical industrial composition of Mo:Fe 2.2:1.

Effects of flow conditions (continuous or pulsed methanol introduction), preparation method, and space velocity are all tested to gain insight into what is required for a good formaldehyde production catalyst. The mechanism of the reaction is also probed by studying the peak shapes from pulsed methanol reaction and through the use of deuterated methanol.

Liberti *et al.* previously claimed that pure $Fe_2(MoO_4)_3$, prepared by calcination of a mixed phase ($Fe_2(MoO_4)_3$ and $MoO_3$ to sublime excess $MoO_3$) catalyst at 700 °C for one week, was active to methanol oxidation in pulsed conditions, but not in continuous flow[1]. This was ascribed by the authors at the time as showing fast acting centres in pulsed flow conditions, that are either difficult to reoxidise or poisoned by products in the continuous flow conditions. No other authors have reported a lack of conversion over single phase $Fe_2(MoO_4)_3$.

The method and variables within the preparation of the iron molybdates is investigated in this chapter as previously it has been shown that this can effect the catalyst performance, as described in a recent review[2]. The primary method of catalyst manufacture used in this research involved evaporating the precipitate to dryness, before calcination. This procedure was followed as the catalyst prepared by this method has the same Mo:Fe in the final catalyst as that in the precursor solutions, whereas varying other preparation parameters and washing of the catalyst can lead to changes in the ratio[3].

A review by Trifirò of molybdate based catalysts described some important aspects of preparation of molybdate mixed oxide catalysts[4]:

- Species of molybdenum ions within the aqueous solution.
- Formation of heteropolyanions.
- The transformation of the amorphous precipitate to crystalline structure.
- Solid-state reaction with oxide impurities during calcination.

In the same review it is stated that the type of molybdenum species in solution can depend on certain variables (Table 3-1), and the ratio of an iron molybdate catalyst is determined by the pH of precipitation, the concentration of parent solutions and the volume of solutions during precipitation.

| | Mo Species | | | | | | |
|---|---|---|---|---|---|---|---|
| | *Cis*-$Mo_2^{+}$ | $HMo_2O_6^{+}$ | $Mo_2O_7^{2-}$ | $Mo_4O_{13}^{2-}$ | $Mo_8O_{24}^{4-}$ | $Mo_7O_{24}^{6-}$ | $MoO_4^{2-}$ |
| pH | From 1 to 6 | | | | | | |
| Temperature | Room Temperature to 110 °C | | | | | | |
| [Mo] | Decreasing → | | | | | | |

**Table 3-1 – Evolution of soluble molybdenum species with the variation of pH, temperature and molybdenum concentration[4].**

Most laboratory scale production of iron molybdates uses iron nitrate and ammonium heptamolybdate, so as to avoid contamination that may occur using iron chloride or sodium molybdate[2,5-12].

The evolution of phases within the calcination stage of iron molybdates has been studied. Under vacuum conditions at 120 °C no crystal phases are seen, at 250 °C the $Fe_2(MoO_4)_3$ phase is observed, while not until 400 °C is the $MoO_3$ also seen, although, no measurements were taken between these temperatures[9]. The sample is completely dehydrated by 300 °C as there is no subsequent weight change and an exotherm is seen in Differential Scanning Calorimetry (DSC) measurements at 373 °C, suggesting that it is at this temperature that the polymolybdate ions form in the

precipitation separate to $MoO_3$. When prepared from ferric nitrate, a calcination temperature of 230 °C is required to remove the nitrate, as evidenced by the disappearance of the Raman band at 1045 $cm^{-1}$ (a typical band seen for nitrate species)[3]. The Raman spectra of catalysts are affected by temperature, with the bands associated with $Fe_2(MoO_4)_3$ and $MoO_3$ seen at 70 and 250 °C respectively, with an increase in the ratio to $Fe_2(MoO_4)_3$ bands by raising the calcination temperature from 250 to 350 °C. Catalysts calcined at 500 °C were not affected by the length of calcination.

## *3.2 Experimental*

### 3.2.1 Catalyst Preparation

In addition to the catalysts mentioned in the experimental section, further preparations of Mo:Fe 2.2:1 were made with parameters in the preparation altered.

A high pH catalyst was prepared, by adding a solution of iron nitrate dropwise to a solution of ammonium molybdate. This lead to the formation of a yellow precipitate with pH 1.5, which turned chocolate brown as the pH was raised to 10 by addition of ammonium hydroxide ($NH_4OH$, Acros 28-30 w/t % $NH_3$). The treatments that followed such as evaporation to dryness, drying and calcination used the procedures set out in the experimental section (Chapter 2).

The industrial preparation of iron molybdates involves filtering and washing the catalyst after precipitation, not evaporation of the solvent. To investigate the effect of this a 2.2:1 Mo:Fe catalyst was prepared by filtering and washing with 3 x 50 ml $H_2O$ the precipitate formed after the usual addition of iron nitrate to ammonium heptamolybdate. This was dried and calcinined in the same manner.

A further catalyst was prepared with a Mo:Fe ratio of 2.2:1 by using the iron chloride salt ($FeCl_3.6H_2O$, Alfa Aesar, 98 %). The procedure followed was the same as that for the filtered and washed catalyst prepared with iron nitrate.

### 3.2.2 Deuterated Methanol

To gain further understanding into the mechanism of reaction, deuterated methanol was used in some experiments. The sample used was $d_4$ methanol (Cambridge Isotope Laboratories, >99.8 % d enrichment).

### 3.2.3 Flow Conditions

#### 3.2.3.1 Isothermal Pulsed Reaction

To ensure that the product distribution is stable at a given temperature, an IPR experiment was conducted. This involved holding the catalyst at a steady temperature, while a number of methanol injections of 1 μl methanol were passed over the bed.

#### 3.2.3.2 Continuous Flow Conditions

The difference between pulsed flow and continuous flow conditions was investigated. For the purpose of continuous flow conditions the methanol was introduced by means of a syringe pump. This method was chosen to minimise the pulsations of flow that are usually observed when using piston-based pumps. The flow of carrier gas was unchanged from pulsed flow conditions at 30 ml $min^{-1}$. The methanol was introduced so as to be 10 % of the total flow, as this mixture matches well that used in industrial reactors. The experiments were performed in an isothermal mode, and the production at a given temperature was allowed to stabilise before activity and selectivity measurements were made.

### 3.2.3.3 Calibration

Care was taken to achieve the correct flow rate of methanol so as to give 3.3 ml $min^{-1}$ gaseous methanol (3.73 µl $min^{-1}$ liquid). To do this the pump was calibrated using a 100 µl syringe by monitoring the methanol dispensed in a five minute period. This was then converted in µl $min^{-1}$ and after a number of measurements a linear plot was made (Figure 3-1). The setting used was therefore 57, which gave a flow rate of 3.70 µl $min^{-1}$ liquid methanol.

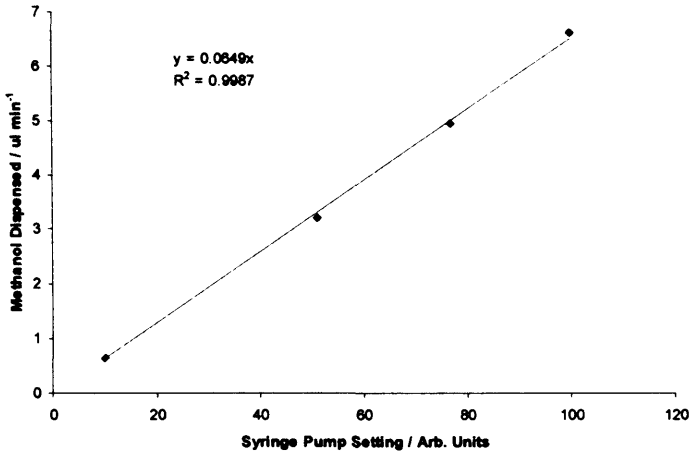


**Figure 3-1 - Methanol dispensed against syringe pump setting for 100 µl syringe.**

## 3.2.4 Varying space velocity

Different size injections were passed over the catalyst. To do this the catalyst was held isothermally at a given temperature while three pulses of the smallest injection size were passed over the catalyst at 2 minute intervals. This was repeated at the given temperature for all the injection sizes, approximately doubling the pulse size each time. The catalyst was then raised to the next temperature and the process of injecting the increasing pulse sizes was repeated.

Work was also carried out on an extended bed of $MoO_3$, which consisted of 2 g of pelletised material, rather than the usual 0.5 g due to the low reactivity and low surface area of $MoO_3$.

### 3.2.5 Introduction of other gases over catalyst

The reaction of $H_2$ and CO over the 1.5:1 Mo:Fe and $MoO_3$ catalysts were also performed to test the reducibility of the catalyst. These were introduced automatically using the pulsing valve, with a spacing of 1 minute and a volume of 0.53 $cm^3$. This volume corresponds to 2.21 x $10^{-5}$ moles of gas at room temperature and pressure, which is comparable to the 2.47 x $10^{-5}$ moles of methanol that are introduced with an injection size of 1 µl.

## 3.3 Results and Discussion

### 3.3.1 BET

Before testing a catalyst for its reactivity under given conditions it is important to know the surface area, so this can be accounted for. As an example of this, two catalysts may produce the same conversion at the same temperature, but one has half the surface area of the second catalyst. In this case the lower surface area catalyst would have a reactivity per unit area of twice that of the higher surface area catalyst. The surface areas of the catalysts tested in this chapter are shown below (Table 3-2).

| Catalyst | Surface Area ($m^2 g^{-1}$) |
|---|---|
| $MoO_3$ | 1.0 |
| $Fe_2O_3$ (Aldrich) | 2.8 |
| $Fe_2O_3$ (Synthesised) | 16.8 |
| Mo:Fe 1.5:1 | 6.5 |
| Perstorp (KH 26) | 7.8 |
| Mo:Fe 2.2:1 (Low pH) | 6.7 |
| Mo:Fe 2.2:1 (High pH) | 6.5 |
| Mo:Fe 2.2:1 (Low pH and Washed) | 7.5 |
| Mo:Fe 2.2:1 (Made with $FeCl_3$) | 1.6 |

**Table 3-2 - Surface areas of the catalysts tested.**

The data shows that the $MoO_3$ catalyst has a very low surface area, with the Aldrich $Fe_2O_3$ also being low. The measured area of the industrial catalysts and the

different preparations of Mo:Fe 2.2:1 are similar except for that made using $FeCl_3$ which presents a considerably lower surface area.

### 3.3.2 Temperature Programmed Pulsed Flow Reaction

This section contains details on methanol TPPFR for the single oxides and iron molybdenum oxide catalysts.

The commercially available $Fe_2O_3$ (Aldrich) catalyst shows itself to be a combustor of methanol (Figure 3-2, Appendix A-1) with the conversion reaching 50 % at 290 °C and nearly 100 % by 330 °C. The selectivity of the catalyst is mainly towards $CO_2$, with a small amount of CO at low temperatures and a minor amount (<6 %) of formaldehyde that peaks at 330 °C.

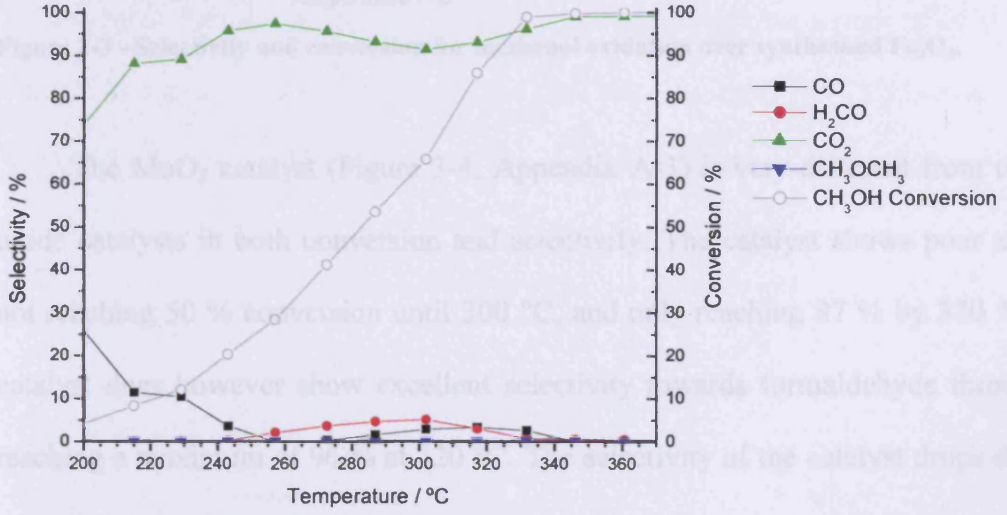


**Figure 3-2 - Selectivity and conversion for methanol oxidation over Aldrich $Fe_2O_3$.**

The synthesised iron oxide (Figure 3-3, Appendix A-2) shows much higher conversion than the Aldrich $Fe_2O_3$, reaching 50 % conversion by 240 °C and 90 % at 260 °C. The selectivity of the catalyst is again dominated by $CO_2$, with only a small amount (<10 % selectivity) of CO being produced at low conversion (<10 %).

The increased activity observed from the synthesised $Fe_2O_3$ in comparison to the Aldrich sample can be seen to be due to a large increase in surface area (Table 3-2), leading to more sites for methanol conversion.

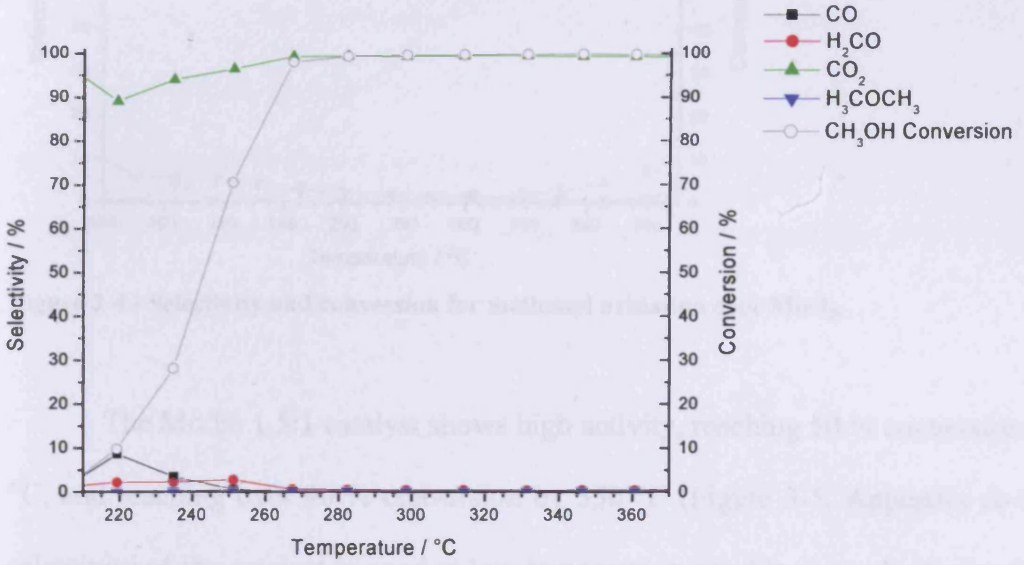


**Figure 3-3 - Selectivity and conversion for methanol oxidation over synthesised $Fe_2O_3$.**

The $MoO_3$ catalyst (Figure 3-4, Appendix A-3) is very different from the iron oxide catalysts in both conversion and selectivity. The catalyst shows poor activity, not reaching 50 % conversion until 300 °C, and only reaching 87 % by 370 °C. The catalyst does however show excellent selectivity towards formaldehyde throughout, reaching a maximum of 96 % at 320 °C. The selectivity of the catalyst drops down to around 90 % by 370 °C.

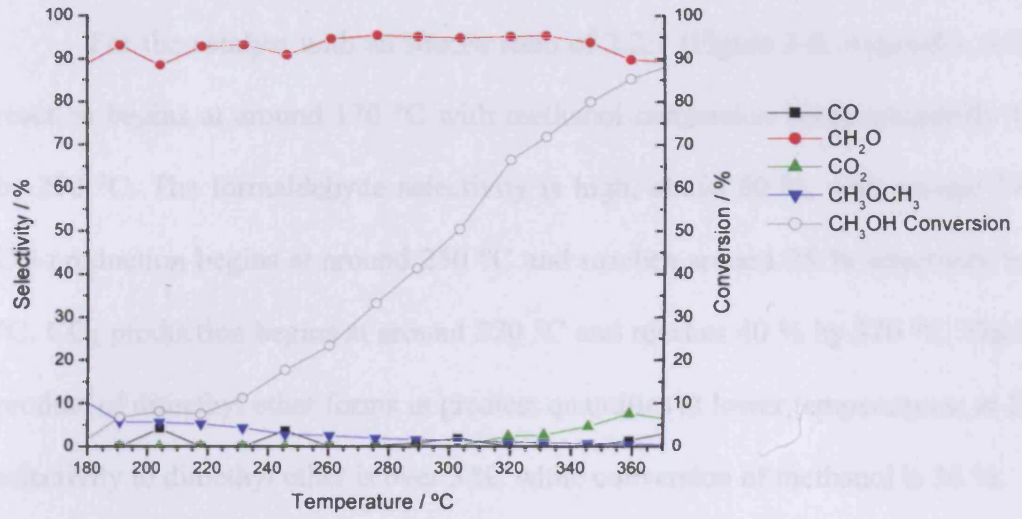


**Figure 3-4 - Selectivity and conversion for methanol oxidation over $MoO_3$.**

The Mo:Fe 1.5:1 catalyst shows high activity, reaching 50 % conversion at 200 °C, and reaching over 90 % conversion by 350 °C (Figure 3-5, Appendix A-4). The selectivity of the catalyst is good at low temperature, reaching a peak of over 90 % at 230 °C, but drops after this so that by the final temperature (370 °C) it is around 35 %. With this drop in formaldehyde selectivity comes an increase in CO, with a maximum of 25 % at 290 °C. $CO_2$ begins to be produced at 260 °C, reaching over 50 % selectivity by 370 °C.

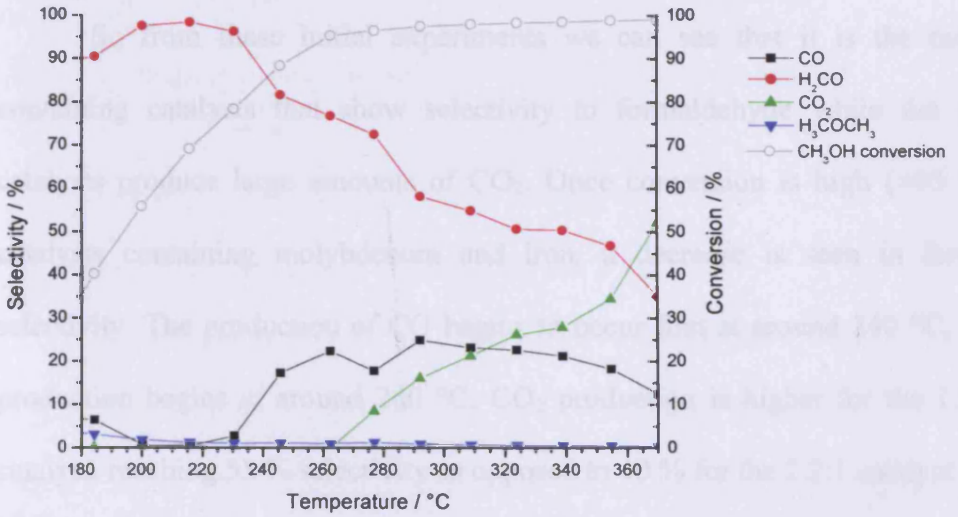


**Figure 3-5 - Selectivity and conversion for methanol oxidation over $Fe_2(MoO_4)_3$ (Mo:Fe 1.5:1) catalyst.**

For the catalyst with an Mo:Fe ratio of 2.2:1 (Figure 3-6, Appendix A-5), the reaction begins at around 170 °C with methanol conversion being essentially 100 % by 270 °C. The formaldehyde selectivity is high, above 80 %, until around 270 °C. CO production begins at around 250 °C and reaches around 25 % selectivity by 370 °C. $CO_2$ production begins at around 270 °C and reaches 40 % by 370 °C. The minor product of dimethyl ether forms in greatest quantities at lower temperatures; at 180 °C selectivity to dimethyl ether is over 5 %, while conversion of methanol is 30 %.

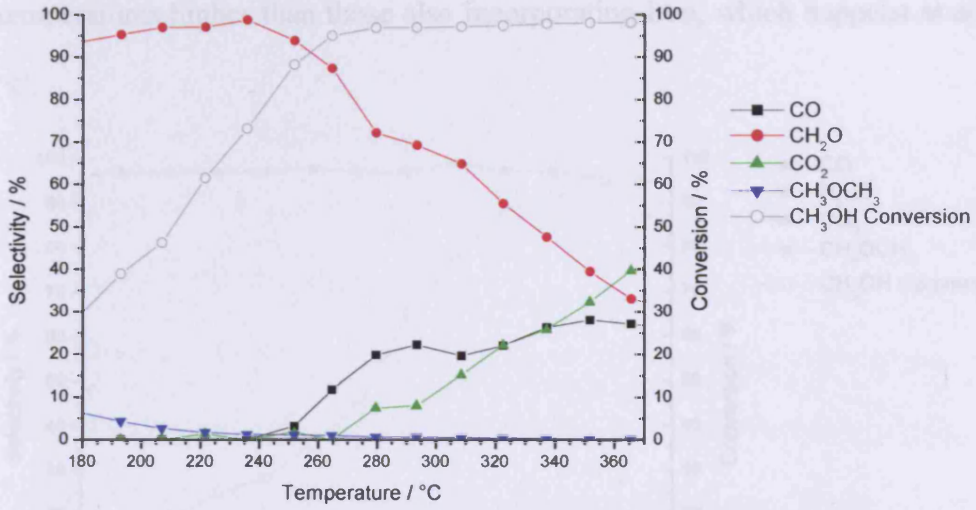


**Figure 3-6 - Selectivity and conversion for methanol oxidation over Mo:Fe 2.2:1 catalyst.**

So from these initial experiments we can see that it is the molybdenum containing catalysts that show selectivity to formaldehyde while the iron oxide catalysts produce large amounts of $CO_2$. Once conversion is high (>90 %) for the catalysts containing molybdenum and iron, a decrease is seen in formaldehyde selectivity. The production of CO begins to occur first at around 240 °C, while $CO_2$ production begins at around 260 °C. $CO_2$ production is higher for the 1.5:1 Mo:Fe catalyst, reaching 55 % selectivity as opposed to 40 % for the 2.2:1 catalyst.

Due to the low surface area of $MoO_3$ (for details see Section 3.3.1) conversion is low, never reaching more than 90 % conversion, so secondary formaldehyde

oxidation is less likely and selectivity never drops significantly. Therefore, a larger loading (2 g) of catalyst was tested (Figure 3-7, Appendix A-6) and this shows that, as would be expected, a given conversion was reached at a lower temperature than the smaller loading (50 % conversion at 280 °C as opposed to 300 °C). The selectivity of the catalyst to formaldehyde remained high (>95 % for >95 % conversion), but when it does drop CO is mainly produced (10 % at 370 °C), with some $CO_2$ (~5 % at 370 °C). The production of these non-selective products only begins to occur at temperatures higher than those also incorporating iron, which happens at around 240 °C.

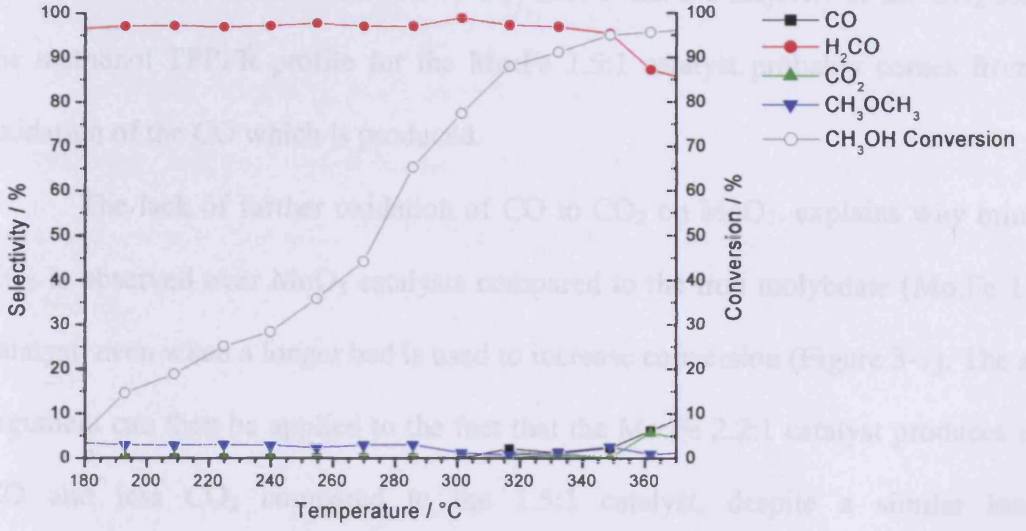


**Figure 3-7 - Selectivity and conversion for methanol oxidation over 2g $MoO_3$.**

The activity of the large $MoO_3$ loading and Mo:Fe 1.5:1 to CO oxidation to $CO_2$ was also probed through TPPFR with CO pulses.

The oxidation of CO over the Mo:Fe 1.5:1 shows conversion beginning at around 170 °C (Figure 3-8, Appendix A-7), rising steadily from here to be 50 % by 370 °C and by 390 °C reaches around 70 %. This differs to the reaction profile over $MoO_3$ considerably, which when tested, showed that no reaction of the CO is observed, even up to 390 °C, over 2 g of catalyst.

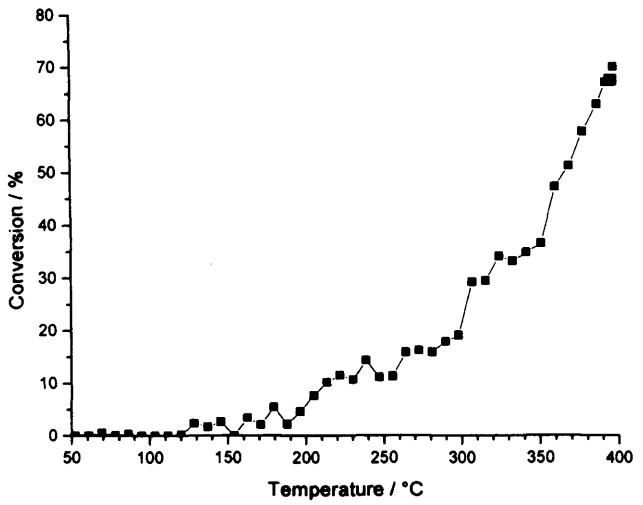


**Figure 3-8 - Conversion of CO pulses over Mo:Fe 1.5:1 catalyst.**

The result of this oxidation of CO, shows that the majority of the $CO_2$ seen in the methanol TPPFR profile for the Mo:Fe 1.5:1 catalyst probably comes from the oxidation of the CO which is produced.

The lack of further oxidation of CO to $CO_2$ on $MoO_3$, explains why minimal $CO_2$ is observed over $MoO_3$ catalysts compared to the iron molybdate (Mo:Fe 1.5:1) catalyst, even when a longer bed is used to increase conversion (Figure 3-7). The same argument can then be applied to the fact that the Mo:Fe 2.2:1 catalyst produces more CO and less $CO_2$ compared to the 1.5:1 catalyst, despite a similar loss in formaldehyde selectivity, because the former contains an extra phase of $MoO_3$ (Section 3.3.8.1) and less $Fe_2(MoO_4)_3$.

The Mo:Fe 1.5:1 catalyst is reducible with hydrogen even at very low temperatures (Figure 3-9, Appendix A-8), with conversion being 15 % by 50 °C, and 50 % conversion being reached by 125 °C. Over 90 % of the hydrogen pulse is being used by 230 °C, with the only product observed from the reduction being water. The data shows that oxygen removal from the surface layer of catalyst is relatively easy, with this being replaced with oxygen from the gas flow (10% $O_2$/He) between hydrogen pulses.

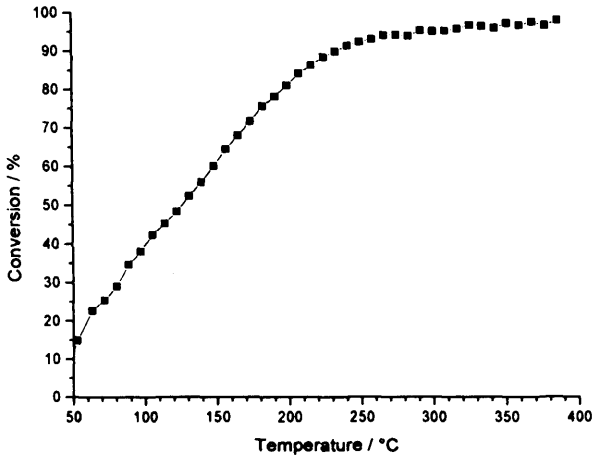


**Figure 3-9 - Conversion of $H_2$ pulses over Mo:Fe 1.5:1 catalyst.**

The reduction of $MoO_3$ with $H_2$, is much more difficult than reducing the Mo:Fe 1.5:1 catalyst in the same way, with conversion only reaching 10 % at around 300 °C, and only reaching 24 % even by 390 °C (Figure 3-10, Appendix A-9) not withstanding the quadrupled loading. It must be noted that this graph has been smoothed using a nine point FFT filter due to the noise in the collected data for low conversion.

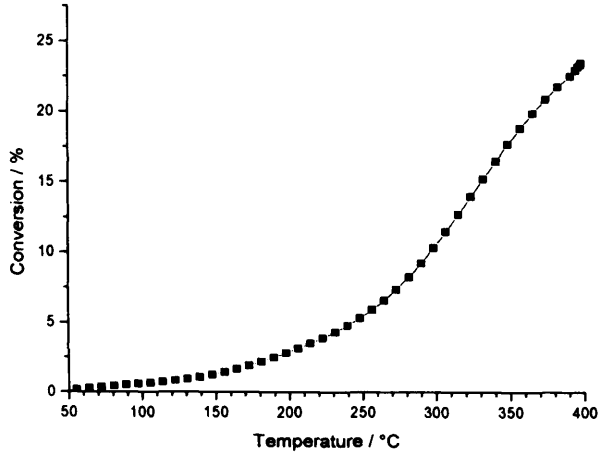


**Figure 3-10 - Conversion of $H_2$ pulses over 2g $MoO_3$.**

The difficulty of reducing $MoO_3$, in comparison to the Mo:Fe 1.5:1 catalyst may be due to two reasons. The first of these is that the ease of dissociation of the

hydrogen may be different on the two materials and the second is a difference in the surface M-O strength of the two materials.

A TPR study of $MoO_3$, has shown that the reduction by $H_2$ to $MoO_2$ can be limited by two different variables[13]. Firstly, the rate determining step can be $H_2$ dissociation when the formation of catalytic sites is limited, or Mo-O bond breaking when excess sites are present. As it was found that low valent molybdenum sites are important for the dissociation of $H_2$, the limitation in the reduction of the $MoO_3$ in this study would be the formation of these sites. While these sites would form during each pulse, the gaseous phase $O_2$, would reoxidise these before the next pulse. The activation energy needed to form these sites is high and was calculated to be 190-250 kJ $mol^{-1}$ which is lowered to 80-155 kJ $mol^{-1}$ when there is an excess of autocatalytic sites and Mo-O bond breaking is rate limiting. Autocatalysis occurs when the reaction itself produces the catalyst for the reaction, in this case, this means the initial reduction of the sites produces sites with a lower activation energy, so the reduction can then occur more easily. The calculated activation energy for the reduction of $Fe_2(MoO_4)_3$ (Equation 3-1) is 75 kJ $mol^{-1}$ [14].

$$Fe_2(MoO_4)_3 + H_2 \rightarrow 2\ FeMoO_4 + MoO_3 + H_2O \qquad (3\text{-}1)$$

This easier reduction of $Fe_2(MoO_4)_3$, in terms of lower activation energy and the dependence of $MoO_3$ on autocatalytic low valence Mo sites helps to explain why the Mo:Fe 1.5:1 catalyst is the more active of the two in both $H_2$ and CO oxidation.

The reduction of $MoO_3$ with CO, as attempted here, can be likened to that for propene, which does not occur until ~350 °C[15]. Reduction of the $MoO_3$ occurs at this temperature as it is appears to be when molybdenum-oxygen bonds in the lattice have sufficient energy and the oxygen in the lattice is able to participate in the oxidation reactions occurring at the surface. The reduction of hydrogen and methanol can occur

at temperatures lower than this as H is incorporated into the lattice to form a $H_xMoO_3$ bronze[16,17], but this is not possible for propene oxidation as no hydrogen bronze is formed in the reduction of $MoO_3$ with propene[18].

### 3.3.2.1 Details of Individual Pulses

As the pulsed flow reactor is capable of recording data points quickly, it is possible to see and compare the differing shapes for the different mass ions within an overall methanol injection peak. It may be expected that when pure methanol is injected all of the relevant masses give the same shape, with the heights determined by the cracking pattern of the molecule, but this is found not to be case (Figure 3-11). All the peaks except 18 amu have the same full width half maximum (fwhm) of around 6 seconds, with the 18 amu having a fwhm of 8 seconds. There is a large tailing effect on the mass 18, this is because the mass 18 observed is from the reaction of the methanol to form water on the mass spectrometer filament (as described in more detail in the experimental section), with the water taking time to pump away. The 29 and 30 amu show different shapes to the other masses, showing an early peak before dropping slightly and rising to a second peak. This is again as a consequence of the mass spectrometer filament, this time acting to crack and also to react the methanol. The early peak is due to formaldehyde produced off the filament while the second peak is from the methanol cracking. Thus the mass spectrometer filament itself is a catalyst, enabling some dehydrogenation, combustion and selective oxidation to take place.

Studying the 32 amu line, shows a dip when the methanol is injected. The 32 amu line has contributions from both methanol and oxygen, so the drop is caused by a disturbance in the flow from the methanol injection.

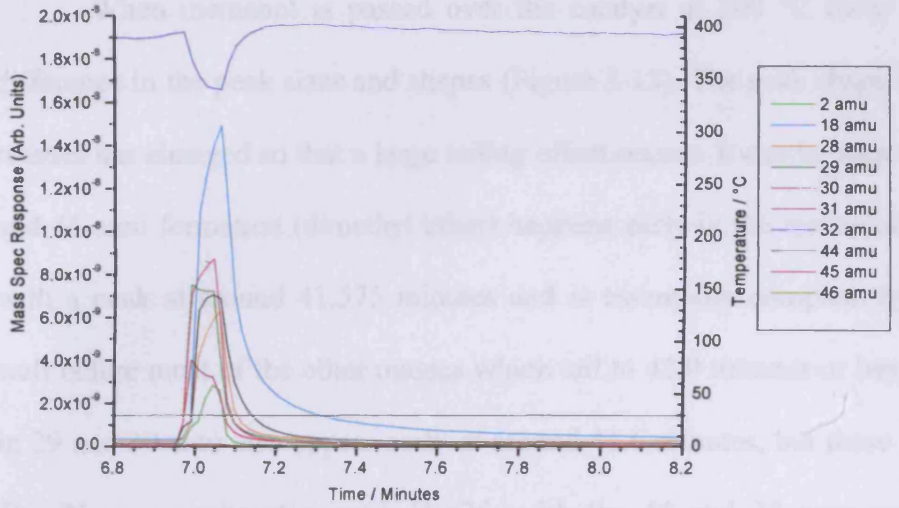


**Figure 3-11 - Raw data for injection of 1µl methanol over the catalyst bypass.**

Passing of methanol over the catalyst at around 120 °C leads to no reaction of the methanol, however the peak shapes are changed slightly (Figure 3-12). The maximum heights are reduced slightly with 31 amu now peaking at ~7.5 x $10^{-8}$ a.u. as opposed to ~9 x $10^{-8}$ a.u. when the pulse is over the bypass (Figure 3-11). The width of these peaks is increased slightly however, as integration of the peaks leads to similar sizes. As there is no reaction over the catalyst, the responses of the different masses remains in the same ratio to 31 amu, as these reactions continue to occur on the mass spectrometer filament.

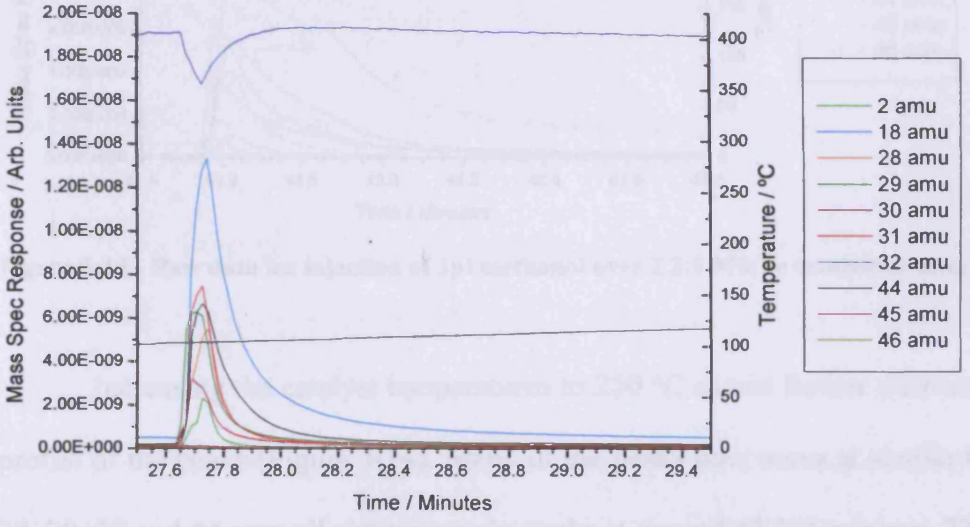


**Figure 3-12 - Raw data for injection of 1µl methanol over the over 2.2:1 Mo:Fe catalyst at around 120 °C.**

When methanol is passed over the catalyst at 200 °C there is a noticeable difference in the peak sizes and shapes (Figure 3-13). The peak shape for many of the masses has changed so that a large tailing effect occurs. It can be seen that the 45 amu and 46 amu formation (dimethyl ether) happens early in the methanol injection cycle with a peak at around 41.575 minutes and is essentially complete by 41.7 minutes, well before most of the other masses which tail to 42.0 minutes or beyond. The peaks in 29 and 30 amu also appear early at around 41.6 minutes, but these have long tails. The 31 amu peaks at around 41.625, with the 44 and 28 amu peaks reaching a maximum at 41.65 minutes. There is a double maximum in the 18 amu line, corresponding with water formed on the mass spectrometer filament at 41.95 minutes and a smaller shoulder feature of reaction water at 41.875 minutes. The negative peak of the 32 amu line shows a broad minimum at around 41.65 and a second small shoulder feature corresponding with the product water maximum at 41.875 minutes.

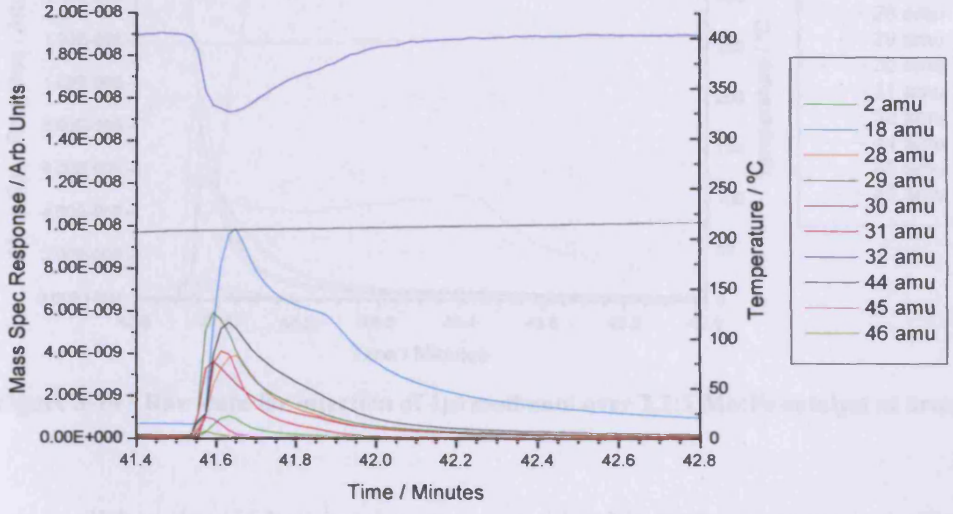


**Figure 3-13 - Raw data for injection of 1µl methanol over 2.2:1 Mo:Fe catalyst at around 200 °C.**

Increasing the catalyst temperatures to 250 °C shows further differences in the profile of the peaks (Figure 3-14). Many of the peaks now occur at similar times with 28, 29, 30 and 44 amu all showing early peaks at around 47.775 minutes. The 44 amu

line has a more prominent tailing effect however. The 18 amu line again shows a double maximum, however, this time both peaks are approximately the same height and are further spread to 47.85 and 48.45 minutes. The negative peak in the 32 amu line shows a major minimum at 47.8, with a small shoulder feature on the tail, again coincident with the second water peak at 48.45 minutes. The now small 31 amu line shows that methanol conversion is high as little methanol is in the exit gas. In fact, the derived data (Figure 3-6) shows that at this temperature conversion is up to 88 %. The large presence of 29 and 30 amu peaks shows that there is a large amount of formaldehyde present. Selectivity to formaldehyde selectivity is over 90 % with the 28 amu signal present due both cracking and oxidation of the formaldehyde molecule on the mass spectrometer filament.

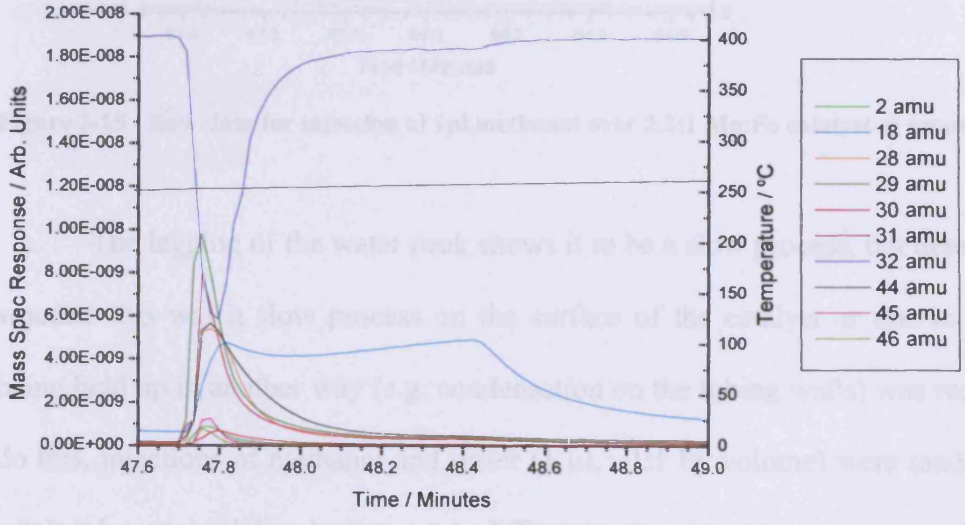


**Figure 3-14 - Raw data for injection of 1µl methanol over 2.2:1 Mo:Fe catalyst at around 250 °C.**

When the catalyst is taken to a considerably higher temperature of around 375 °C, the peaks have changed further (Figure 3-15). Again ignoring the change in height of the peaks caused by the different selectivity of the catalyst, the 2, 28, 29, 30, and 44 amu peaks are all in approximately the same position at 63.5 minutes. The spacing between the 2 peaks in the 18 amu spectra is now at its largest at around 1 minute with

the two peaks at 63.525 and 64.425 minutes respectively. The 32 amu line, again follows a similar pattern with a large minima at around 65.55 caused by there being no 32 fragment from methanol (no 31 amu signal is observed), the displacement of gas mentioned earlier and the use to rexodise the catalyst after the reaction of methanol to oxidised products ($CO_2$, $H_2O$ etc).

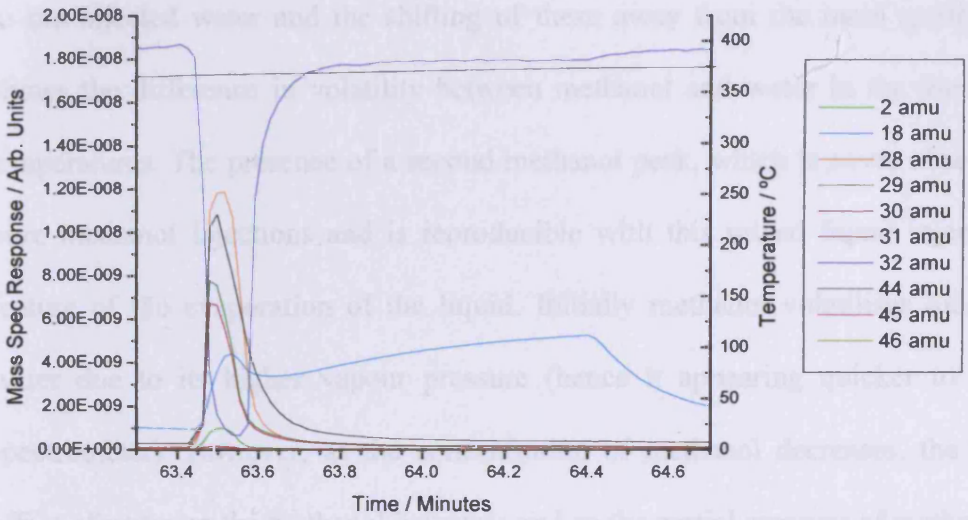


**Figure 3-15 - Raw data for injection of 1µl methanol over 2.2:1 Mo:Fe catalyst at around 375 °C.**

The lagging of the water peak shows it to be a slow process, but determination whether this was a slow process on the surface of the catalyst or due to the water being held up in another way (e.g. condensation on the tubing walls) was required. To do this, injections of methanol and water (1 µl, ~1:1 by volume) were made over the catalyst bypass with line heaters set to different temperatures.

At the lowest temperature of 25 °C, there is a noticeable separation between the peaks observed for methanol (31 amu) and water (18 amu) (Figure 3-16). The methanol peaks at around 19.65 minutes, before declining, with a smaller, second peak at 19.925 minutes. The methanol peak shows considerable tailing and is not essentially complete until 20.1 minutes, a total width of 30 seconds. The mass 18 line shows two peaks at the same times as methanol (19.65 and 19.925), but the height

order for these two peaks is reversed. There is an extra mass 18 peak at 20.1 seconds and the tailing of the peak is not complete even 1 minute after injection.

The early peak in the mass 18 spectra (19.65 minutes) is not the injected water, but instead is the product of the reaction of methanol on the mass spectrometer filament as explained in the experimental section (Chapter 2). The later peaks are due to the injected water and the shifting of these away from the main methanol peak shows the difference in volatility between methanol and water in the lines at these temperatures. The presence of a second methanol peak, which is never observed with pure methanol injections and is reproducible with this mixed liquid injection, is a feature of the evaporation of the liquid. Initially methanol volatilises quicker than water due to its higher vapour pressure (hence it appearing quicker to the mass spectrometer). However, as the concentration of methanol decreases, the solvation effect of water on the methanol increases and so the partial pressure of methanol in the gas phase decreases.

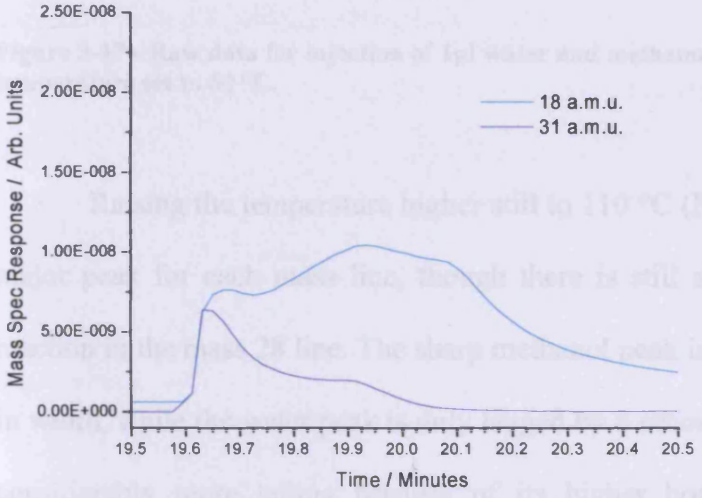


**Figure 3-16 - Raw data for injection of 1µl water and methanol over catalyst bypass with the line temperature set to 25 °C.**

When the temperature of the gas lines (from before the PTFE septa to the mass spectrometer system) is raised to 60 °C (Figure 3-17), both the 31 and 18 amu peaks

become more sharply focused. The methanol peak rises rapidly to a peak at 1.26 minutes with a second feature on the tail at 1.4 minutes and is essentially complete by 1.6 minutes, meaning the width of the peak is 22.5 seconds. The 18 amu line rises rapidly, again due to methanol reaction on the filament but produces a peak due to the water injected at 1.4 minutes, approximately 8 seconds after the peak for methanol. The peaks are now closer due to the faster evaporation of the water with the increased temperature.

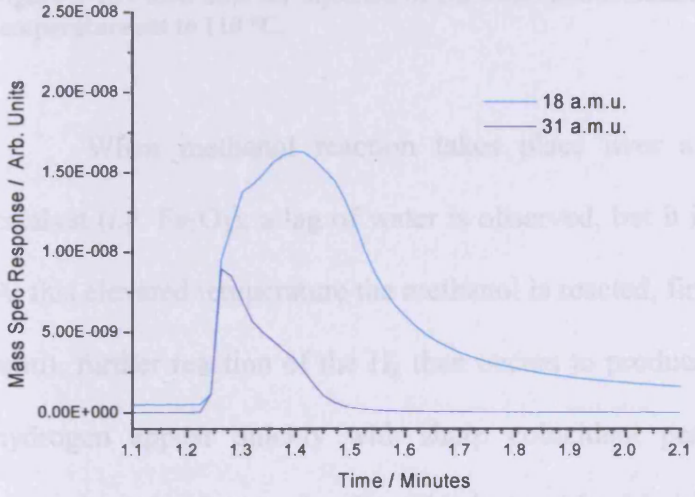


**Figure 3-17 - Raw data for injection of 1µl water and methanol over catalyst bypass with the line temperature set to 60 °C.**

Raising the temperature higher still to 110 °C (Figure 3-18) produces only one major peak for each mass line, though there is still a feature of methanol filament reaction in the mass 28 line. The sharp methanol peak is now approximately 8 seconds in width, while the water peak is only lagged by 6 seconds. The water peak still shows considerably more tailing because of its higher boiling point and lower vapour pressure.

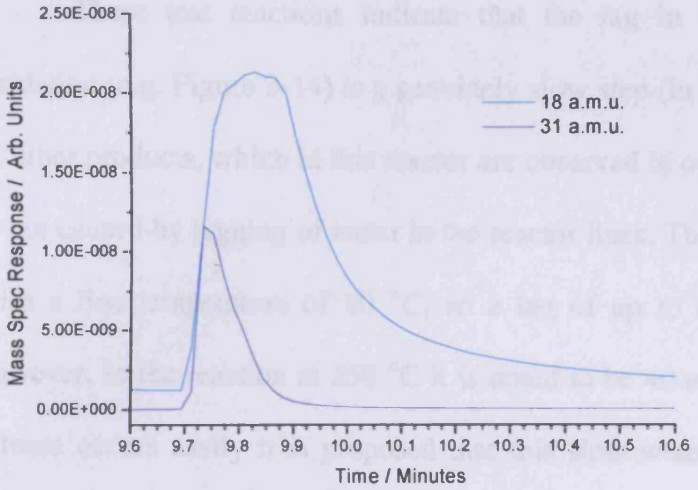


**Figure 3-18 - Raw data for injection of 1µl water and methanol over catalyst bypass with the line temperature set to 110 °C.**

When methanol reaction takes place over a non-molybdenum containing catalyst (*i.e.* $Fe_2O_3$), a lag of water is observed, but it is much reduced (Figure 3-19). At this elevated temperature the methanol is reacted, firstly to $CO_2$ (44 amu) and $H_2$ (2 amu), further reaction of the $H_2$ then occurs to produce $H_2O$ (18 amu). The $CO_2$ and hydrogen appear quickly with sharp coincident peaks, while the water appears approximately 12 seconds after. This is considerably less than the near minute it takes for the water maximum for methanol oxidation over the Mo:Fe 2.2:1 catalyst (Figure 3-15).

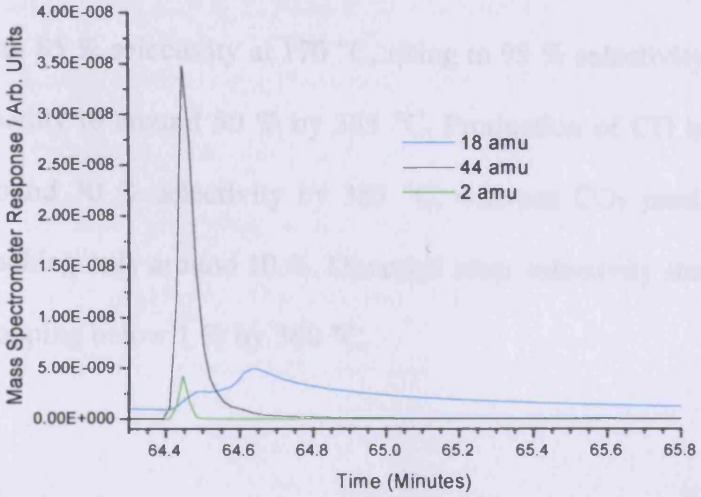


**Figure 3-19 - Raw data for injection of 1µl methanol over $Fe_2O_3$ catalyst at around 385 °C.**

These test reactions indicate that the lag in water seen in the methanol oxidation (e.g. Figure 3-14) is a genuinely slow step (in comparison to the production of other products, which in this reactor are observed to occur near simultaneously) and is not caused by lagging of water in the reactor lines. The reactions were typically run with a line temperature of 80 °C, so a lag of up to 8 seconds may be expected, however, in the reaction at 250 °C it is noted to be 40 seconds. As the formaldehyde release occurs easily it is proposed that this slow water evolution is caused by the difficulty of surface hydroxyl combination on the surface to yield water to the gas phase.

### 3.3.2.2 Deuterated Methanol

The activity of the 2.2:1 Mo:Fe catalyst can be seen to be reduced for $d_4$-methanol conversion, with 50 and 90 % conversion reached at 220 and 280 °C respectively (Figure 3-20, Appendix A-10), compared to the 210 and 250 °C seen when non deuterated methanol is used (Figure 3-6). This decrease in conversion observed with the $d_4$-methanol is caused by the Kinetic Isotope Effect (KIE) increasing the activation energy to methanol conversion. When the products of the $d_4$-methanol are examined, it can be seen that formaldehyde is the dominant product, with 85 % selectivity at 170 °C, rising to 95 % selectivity by 280 °C, before dropping steadily to around 50 % by 385 °C. Production of CO begins at 280 °C and rises to around 30 % selectivity by 385 °C, whereas $CO_2$ production starts around 300 °C reaching only around 10 %. Dimethyl ether selectivity starts at around 15 % at 170 °C, dropping below 1 % by 360 °C.

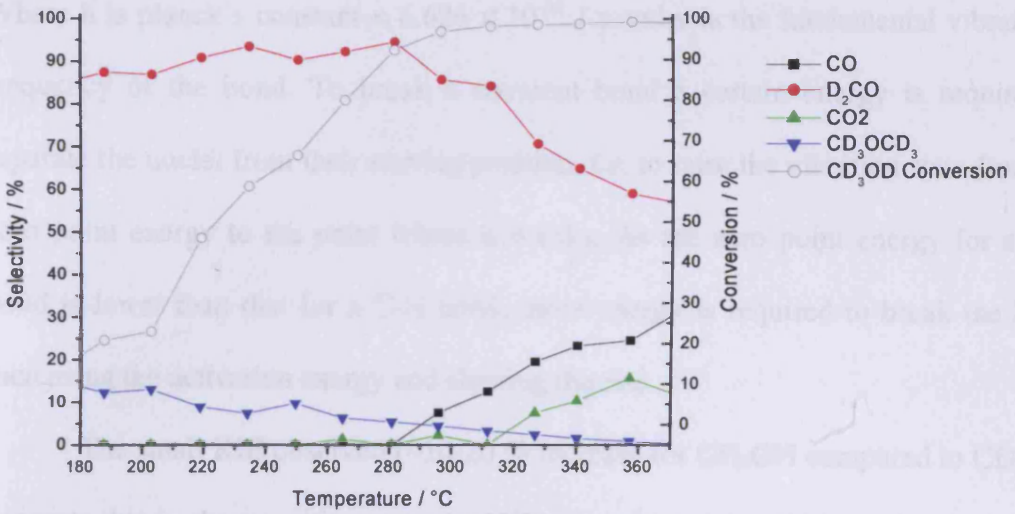


**Figure 3-20 - Conversion and selectivity for aerobic TPPFR of $d_4$-methanol over Mo:Fe catalyst.**

The formaldehyde selectivity can be seen to drop at higher temperature with $CD_3OD$, compared with $CH_3OH$, with this is most likely caused by the lower methanol conversion. Data on different bed lengths of Mo:Fe 2.2:1 demonstrates that product ratios are primarily based on conversion of $CH_3OH$, rather than temperature of reaction (Section 3.3.5.1). Therefore the lower productions of CO and $CO_2$ are also partially caused by this, but are probably also lowered by a KIE on the dehydrogenation of formaldehyde to CO, slowing the rate of CO formation.

The KIE applies if bonds involving hydrogen are broken in the rate-determining step of a reaction and is monitored as a reduction in rate when a hydrogen atom is replaced by a deuterium. The KIE comes about as even in its ground state a molecule is still vibrating, because otherwise it would violate the Heisenberg uncertainty principle, since a non-vibrating pair of atoms would have zero momentum at fixed locations. The minimum energy a bond can have is called the zero point energy and is given by the expression:

$$E_0 = h\nu \qquad (3\text{-}2)$$

Where h is planck's constant = 6.626 x $10^{-34}$ J s and ν is the fundamental vibrational frequency of the bond. To break a covalent bond a certain energy is required to separate the nuclei from their starting position, *i.e.* to raise the vibration state from the zero point energy to the point where it breaks. As the zero point energy for a C-D bond is lower than that for a C-H bond, more energy is required to break the bond, increasing the activation energy and slowing the rate.

The small KIE observed (~10-20 % increase for $CH_3OH$ compared to $CD_3OD$) suggests that in the transition state the H(D) atom is mainly still bound to the methyl carbon. A small kinetic isotope effect is observed when the difference in zero point energy at the transition state is at its maximum, which occurs when the H(D) is nearly completely transferred, or hardly transferred at all. If the atom is half transferred at the transition state then it will be equally bonded on both sides, lowering the force constant and reducing the vibrational frequency. This causes the zero point difference to be small at the transition state and leads to a higher KIE. The reaction here can be shown to have an early transition state (similar to the reactants), as the reaction is highly exothermic, and in this case the Hammond postulate states that in this case the transition state will most resemble the reactants (as the reactants and transition state are similar in energy).

The dimethyl ether selectivity is considerably higher using $CD_3OD$ than that observed using $CH_3OH$, and is this reflected in the yield graph (Figure 3-21). As can easily be seen, not only is the dimethyl ether production higher, but the peak in yield is shifted to a higher temperature by ~70 °C from ~180 to ~250 °C. This is another function of the KIE. Information in the literature suggests that the abstraction of H from the surface methoxy is the rate limiting step in formaldehyde production[19]. If this is the case then the methoxy will require more energy to decompose to formaldehyde

(with the method of formation proposed by Machiels and Sleight *et al.* shown in Figure 3-22), due to a primary KIE, whereas this is not the case for methoxys converting to dimethyl ether through the mechanism suggested for this reaction on $MoO_3$ as breaking of a C-H bond is not involved in the rate limiting step (Figure 3-23)[20]. The production of dimethyl ether will also be aided by longer residence times of methoxys on the surface, as this will increase the chances of two methoxys being on adjacent sites and thus being able to couple.

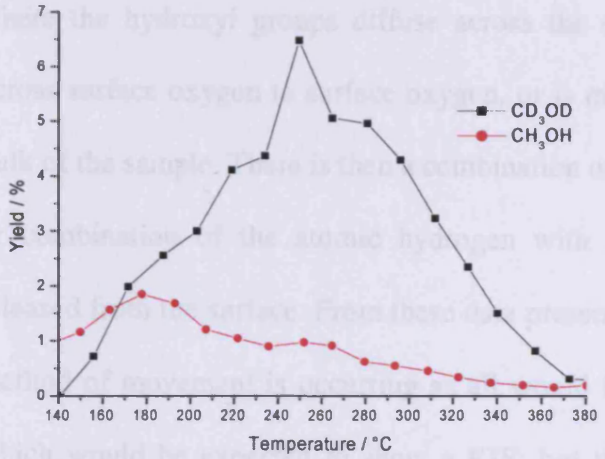


**Figure 3-21 – Dimethyl ether yield using deuterated and non-deutearted methanol.**

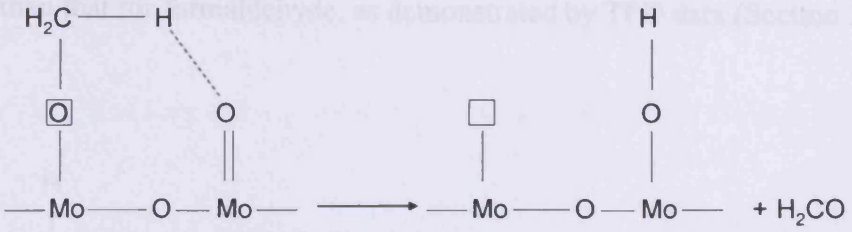


**Figure 3-22 - Suggested mechanism for the formation of formaldehyde on the surface of $MoO_3$[20].**

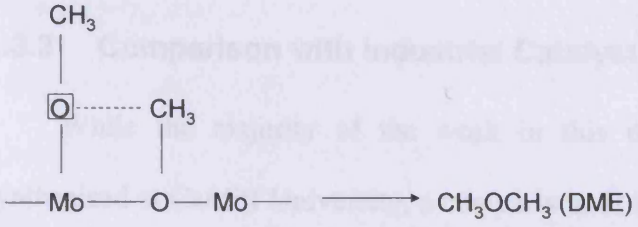


**Figure 3-23 - Suggested mechanism for the formation of DME on the surface of $MoO_3$[20]. Where $V_t$ is a terminal oxygen vacancy in Mo=O, $V_b$ is a bridged oxygen vacancy in Mo-O-Mo.**

When the lag times of $D_2O$ production from the oxidation of $CD_3OD$ are compared to those for $H_2O$ from $CH_3OH$, the two are very similar suggesting that there is no KIE, *i.e.* there is no H(D) bond breaking in the rate limiting step to water production. The hydroxyl recombination proposed by Chung *et al.* on $MoO_3$ (Figure 3-24) seems not to be fully satisfactory as it does not consider all steps. Firstly the hydroxyls are formed at some distance from each other as methoxy groups drop a hydrogen atom to form formaldehyde (Figure 3-22). There is then a movement phase where the hydroxyl groups diffuse across the surface, a hydrogen atom is passed across surface oxygen to surface oxygen, or is moved from anion to anion within the bulk of the sample. There is then a combination of hydroxyls with a hydrogen transfer, or combination of the atomic hydrogen with a hydroxyl group with water then released from the surface. From these data presented here it is difficult to know which method of movement is occurring as all would involve the breaking of a O-D bond which would be expected to show a KIE, but the energy of production of water is higher than that for formaldehyde, as demonstrated by TPD data (Section 3.3.7).

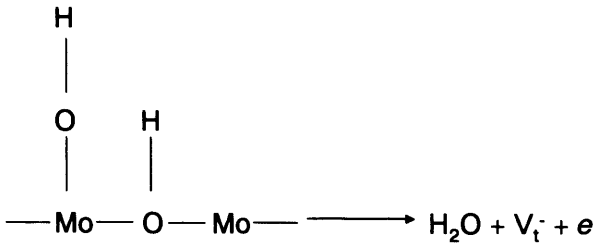


**Figure 3-24 - Suggested mechanism for the formation of $H_2O$ on the surface of $MoO_3$[20].**

### 3.3.3 Comparison with Industrial Catalyst

While the majority of the work in this thesis is concerned with catalysts synthesised at Cardiff University, a comparison of these to a current industrial catalyst was performed.

The conversion profile for the industrial Perstorp KH 26 catalyst (Figure 3-25, Appendix A-11) shows good methanol conversion reaching 50 % conversion at around 195 °C and 90 % at 240 °C. Formaldehyde selectivity is excellent at over 90 % until above 250 °C where it drops steadily to around 30 % by 370 °C. CO production begins at 220 °C and rises to 50 % by 370 °C, while $CO_2$ production starts 290 °C and reaches 20 % by 370 °C. Dimethyl ether selectivity is highest at low conversions/temperatures at around 10 % at 160 °C, dropping to less than 1 % by 220 °C.

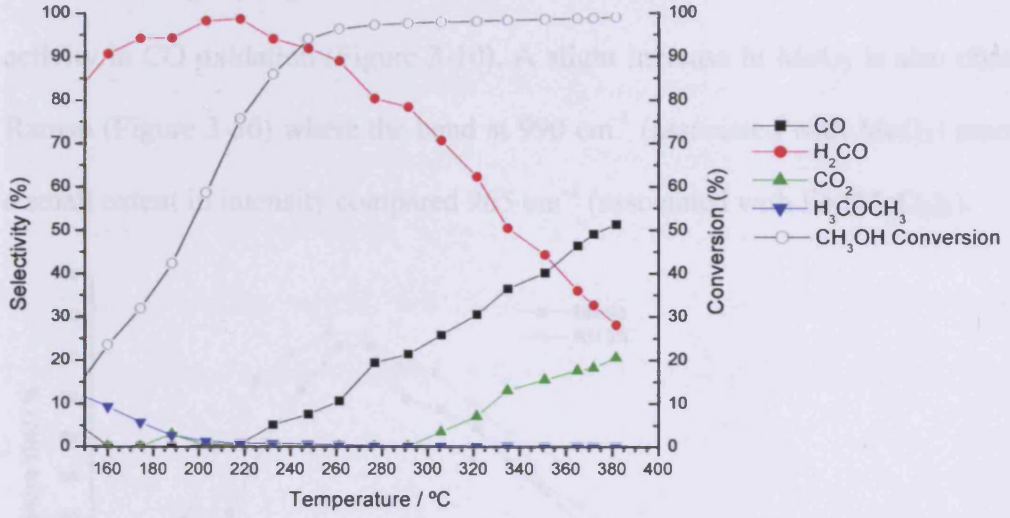


**Figure 3-25 - Selectivity and conversion for methanol oxidation over Perstorp KH 26 catalyst.**

Comparing the yield of the two catalysts (Industrial Perstorp KH 26, and the mimic Mo:Fe 2.2:1, Figure 3-26) shows the profiles to be very similar with the Perstorp catalyst slightly better throughout. The maximum for the Perstorp catalyst is 86 % at ~250 °C and for the mimic the maximum yield is 83 % at 265 °C (note the maximum yield are within error the same, see Section 2.3.8.3). The improved yield of the industrial catalyst at moderate temperatures (200 °C) is due to the industrial catalyst being more active (50 % conversion as opposed to 40 %), when compared to

the Cardiff prepared mimic. This added activity is most likely the result of a higher surface area for the industrial catalyst (7.8 $m^2 g^{-1}$ opposed to 6.7 $m^2 g^{-1}$, Table 3-2)

Another difference between the catalysts comes when studying the by-products. The mimic catalyst shows 40 % $CO_2$ selectivity and 28 % CO selectivity at 370 °C, while at the same temperature, these values are 18 and 50 % for the industrial catalyst. This is somewhat surprising because the industrial catalyst shows higher activity to formaldehyde production from methanol, with CO, and $CO_2$ being products from further oxidation steps. A possible reason for this is that the industrial catalyst may have a slightly higher surface level of $MoO_3$, as this has been shown to have poor activity in CO oxidation (Figure 3-10). A slight increase in $MoO_3$ is also observed in Raman (Figure 3-56) where the band at 990 $cm^{-1}$ (associated with $MoO_3$) increases to a small extent in intensity compared 965 $cm^{-1}$ (associated with $Fe_2(MoO_4)_3$).

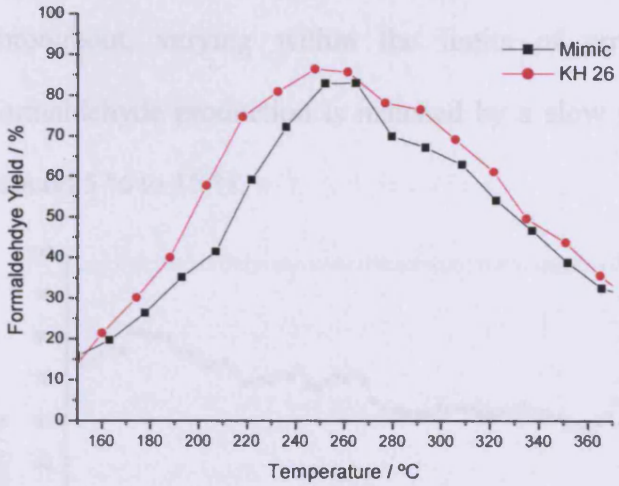


**Figure 3-26 - Formaldehyde yield as a function of temperature for pulsed reaction over Perstorp and Perstorp mimic (2.2:1 Mo:Fe) catalysts.**

### 3.3.4 Flow Conditions

Another important variable to investigate was the method of methanol introduction. While most of the work in this thesis has made use of the temperature programmed pulsed technique for its simplicity and quick data gathering, in industrial conditions the methanol feed is continuous whilst the catalyst is held isothermally.

The catalyst was therefore tested with isothermal pulses to ensure time stability of the products and also in isothermal continuous flow conditions. The continuous flow conditions utilised in this experiment used an approximation to the industrial conditions, by using a feed containing 10 % methanol vapour, 10 % $O_2$ and the rest inert (a significant increase in $O_2$ or $CH_3OH$ would mean conditions were within the explosion limits).

The IPR reaction of the catalyst at 300 °C shows that the activity and product distribution of the catalyst are affected only to a limited extent by the number of pulses that have been made over the sample (Figure 3-27, Appendix A-12). The sample records very high conversion throughout the course of the two hour long experiment (>95 %) with formaldehyde selectivity dropping slightly from around 75 % selectivity at the start to 65 % by the 60$^{th}$ pulse. CO selectivity is fairly constant throughout, varying within the limits of error from 15-20 %. The drop in formaldehyde production is matched by a slow rise in the production of $CO_2$, from around 5 % to 15 %.

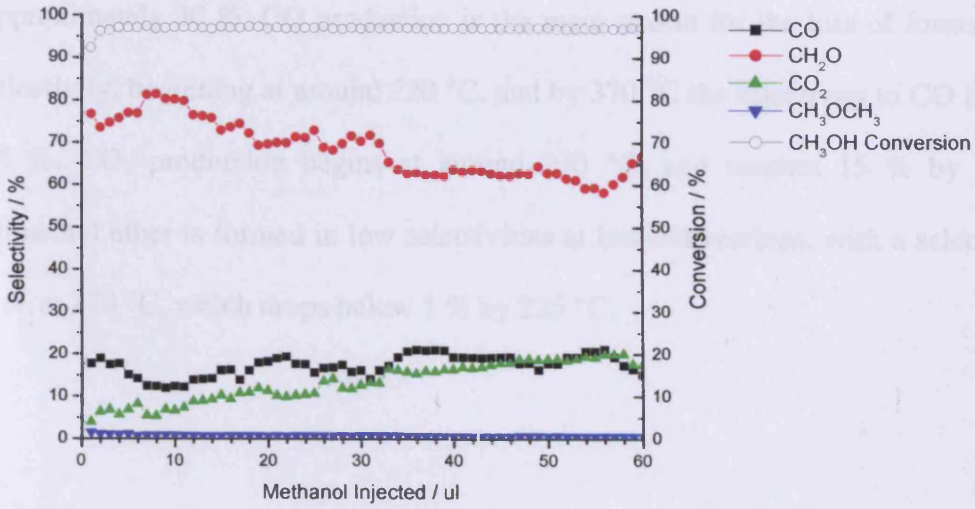


**Figure 3-27 - Conversion and selectivity for aerobic IPR of methanol over Mo:Fe catalyst at 300 °C.**

When the data from the IPR experiment on the Mo:Fe 2.2:1 catalyst are compared to those for TPPFR reaction on the same catalyst, it can be seen that at 300 °C, the conversion is 97 % with a selectivity of 67 % to formaldehyde. These are both within the error limits the same as those for the initial values recorded over the catalyst in isothermal conditions. The small drop in formaldehyde production was unexpected as catalysts of this type are used industrially without change for periods of months. It may be that the catalyst is just normalising out, but the data is also somewhat more confused as the IPR plot (Figure 3-27) is a figure which has been smoothed to remove the noise. Overall the catalyst seems to be reasonably stable, with a number of pulses of methanol, and this is further enhanced as a conclusion as repeated TPPFR, produced results that were equal within the limits of machine error.

Using the continuous flow conditions (Figure 3-28, Appendix A-13), the catalyst shows good methanol conversion, rising to 50 % by 190 °C and over 90 % by 225 °C. The catalyst also shows good formaldehyde selectivity of over 95 % until 225 °C, where it drops at a roughly linear rate until by 370 °C the selectivity is approximately 30 %. CO production is the main reason for the loss of formaldehyde selectivity, beginning at around 220 °C, and by 370 °C the selectivity to CO is around 55 %. $CO_2$ production begins at around 270 °C, and reaches 15 % by 370 °C. Dimethyl ether is formed in low selectivities at low conversions, with a selectivity of 3 % at 170 °C, which drops below 1 % by 225 °C.

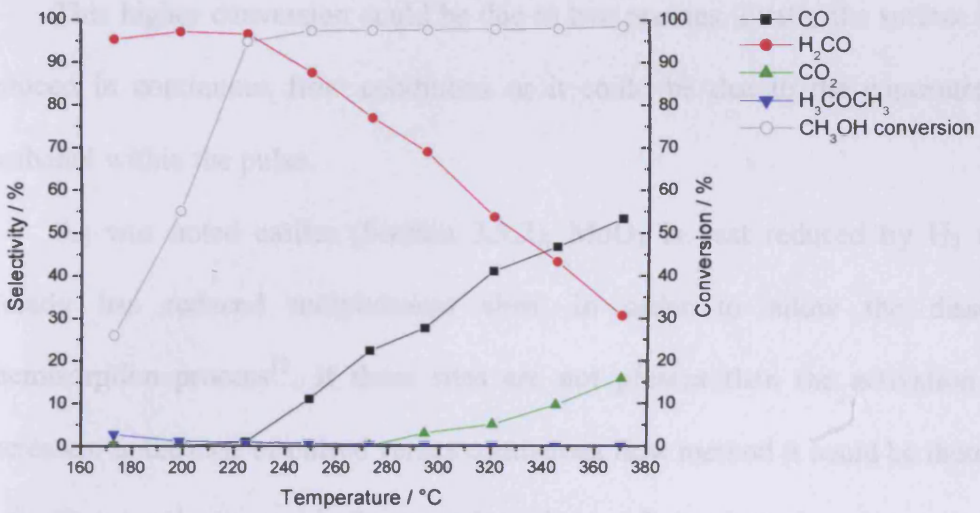


**Figure 3-28 - Conversion and selectivity for continuous flow reaction over Mo:Fe 2.2:1 catalyst.**

The formaldehyde yield in continuous flow conditions (Figure 3-29) shows a sharp rise from around 25 % at 170 °C to a maximum of 92 % at 225 °C. This declines away so that by 370 °C the yield of formaldehyde is 30 %. The yields from pulsed and continuous flow of methanol are very similar throughout, with only two points at around 195 and 225 °C showing noticeably higher yield in continuous flow conditions. The main reason for this higher formaldehyde yield below 240 °C in the continuous conditions is due to higher conversion in these conditions.

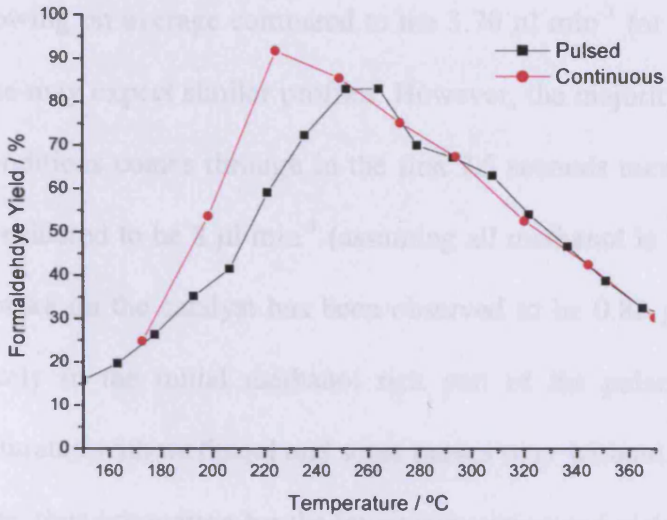


**Figure 3-29 - Formaldehyde yield as a function of temperature for pulsed and continuous flow conditions.**

This higher conversion could be due to two reasons. Firstly the surface is more reduced in continuous flow conditions or it could be due to the concentration of methanol within the pulse.

As was noted earlier (Section 3.3.2), $MoO_3$ is best reduced by $H_2$ when it already has reduced molybdenum sites, in order to allow the dissociative chemisorption process[13]. If these sites are not present then the activation energy increases. In the case of pulsed versus continuous flow method it could be thought that these sites may be present in the case of continuous flow where there is a constant flux of methanol over the catalyst to keep these sites reduced. In contrast, these sites will only be formed temporarily during the pulse as they will be reoxidised in between pulses. The reactivity of the catalyst is likely to be lower while these low valency molybdenum sites are formed in the early part of the pulse.

To consider the methanol concentration in the pulse we need to study the peak profiles. The average pulse width for a 1μl injection is seen to be 15 seconds (Figure 3-11), which means over this period, the equivalent of 4 μl $min^{-1}$ of methanol is flowing on average compared to the 3.70 μl $min^{-1}$ for continuous flow conditions, so one may expect similar profiles. However, the majority of the methanol in the pulsed conditions comes through in the first 7.5 seconds meaning the methanol flow can be considered to be 8 μl $min^{-1}$ (assuming all methanol is through in this time). Methanol uptake on the catalyst has been observed to be 0.82 μl at room temperature, so it is likely in the initial methanol rich part of the pulse the catalyst surface becomes saturated with methanol and some passes over without reaction, due to a low turn over rate, thus accounting for the lower conversion and yield.

The concentration of methanol in the pulse would seem to be the most likely answer to the difference when the TPD data (Section 3.3.7) is taken into account. This

shows that methanol is readily adsorbed onto the catalyst surface at room temperature, with the ability to be converted to formaldehyde through a methoxy species with a peak desorption at 175 °C.

The drop in yield in the different conditions match each other very well and suggests that steps in the production of CO, the main reason for the drop in selectivity are not affected too much by the conditions. CO is the product from further oxidation of the formaldehyde (Section 3.3.5), so it can be seen that, once full methanol conversion is reached, the production of CO from the formaldehyde is independent of the methanol introduction method (*i.e.* pulsed or continuous flow).

From the data gathered, it can therefore be concluded that the temperature programmed pulsed flow conditions employed in this study show comparable results in terms of catalytic performance to the continuous flow conditions the catalyst is subjected to in industry. It is therefore satisfactory to use pulsed conditions for the further experimentation.

### 3.3.5 Effect of space velocity

To gain understanding of primary and secondary products formed over the catalyst, the effects of catalyst loading size and different methanol injection sizes were investigated.

#### 3.3.5.1 Varying Catalyst Loadings

By studying different catalyst loadings, it can be understood what is happening over each section of a catalyst bed at a given temperature. From this it is possible to deduce which of the products are formed in the early part of the bed and where they are further oxidised.

Testing 1 g of catalyst in pulsed conditions shows a high level of conversion at low temperatures (Figure 3-30, Appendix A-14), with 50 % methanol conversion being reached by 175 °C, and 90 % at 220 °C. Formaldehyde selectivity is excellent, even with increasing conversions, being around 90 % selectivity until 90 % conversion is reached. Formaldehyde selectivity then drops so that by 370 °C it is less than 20 %. CO begins to be produced at around 250 °C, and rises steadily, reaching 55 % by 370 °C. $CO_2$ begins at around 280 °C and rises to 25 % by 370 °C. There is a small production of the minor product of dimethyl ether at low temperatures, with a maximum selectivity of around 3 % at 160 °C which drops to near zero by 260 °C.

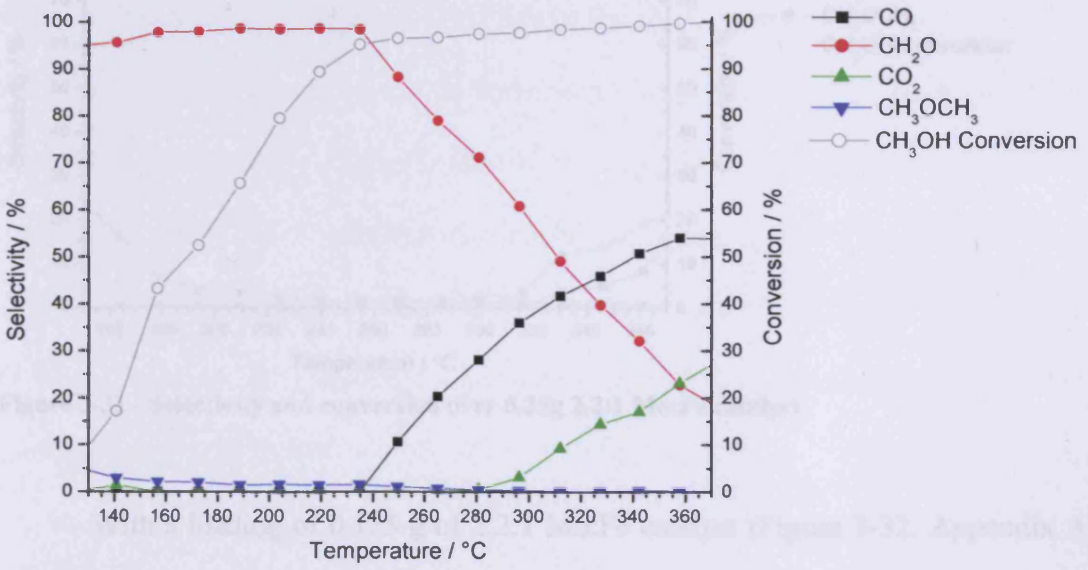


**Figure 3-30 - Selectivity and conversion over 1g 2.2:1 Mo:Fe catalyst.**

A plot for 0.5 g 2.2:1 Mo:Fe catalyst was used as a standard reaction and is shown earlier in the chapter (Section 3.3.2).

With a loading of 0.25 g of 2.2:1 Mo:Fe catalyst (Figure 3-31, Appendix A-15) 50 % conversion is reached only at 235 °C, with 90 % conversion reached at 290 °C. Formaldehyde selectivity rises from around 75 % at 150 °C to over 90 % by 180 °C, where it remains at this excellent value until 315 °C, where conversion is 95 %, when

it drops to around 60 % by 370 °C. CO production is low, and only begins above 310 °C, reaching 15 % by 370 °C. $CO_2$ production begins at above 280 °C, but only reaches 20 % by 370 °C. There is a large level of dimethyl ether production at low temperatures, with a selectivity of 25 % at 150 °C however, yield of this product is still very low as conversion is less than 5 % at this temperature. As temperature/conversion increases the dimethyl ether selectivity drops so that by 240 °C it is only around 1 %.

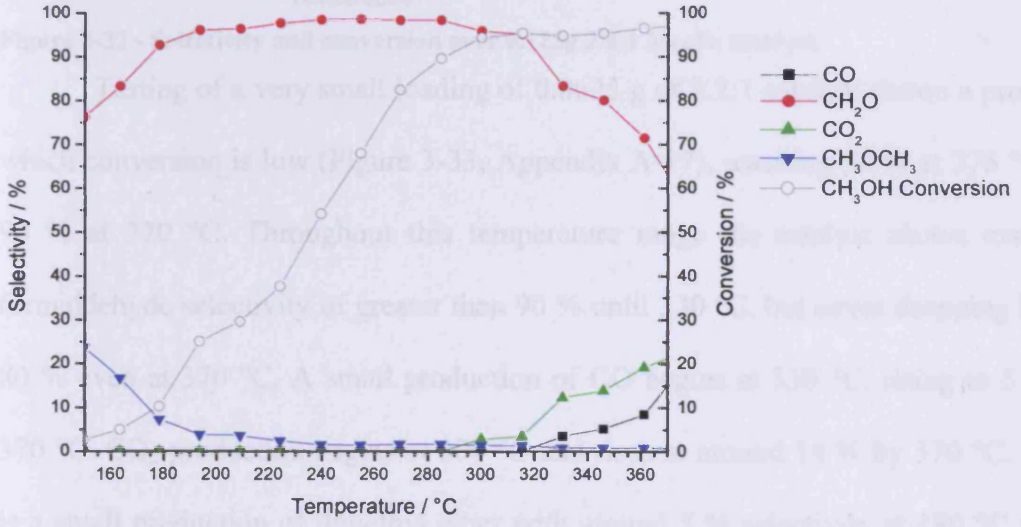


**Figure 3-31 - Selectivity and conversion over 0.25g 2.2:1 Mo:Fe catalyst.**

With a loading of 0.125 g of 2.2:1 Mo:Fe catalyst (Figure 3-32, Appendix A-16) 50 % conversion is reached at around 265 °C, with 90 % conversion at 340 °C. Formaldehyde selectivity is high throughout the profile, being over 90 % until 340 °C, but even by 370 °C, selectivity is still above 80 %. CO and $CO_2$ selectivities are low, never rising above 10 % for either product. These by-products do not appear until 335 °C. Moderate dimethyl ether selectivity is observed at low conversions, with selectivity of around 10 % observed at 195 °C. This declines to around 1 % by 260 °C and continues to fall after this.

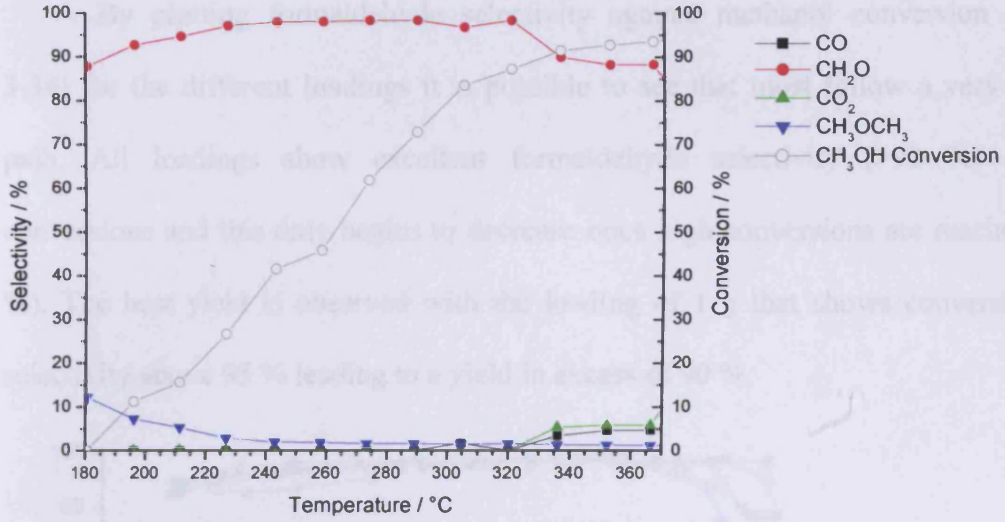


**Figure 3-32 - Selectivity and conversion over 0.125g 2.2:1 Mo:Fe catalyst.**

Testing of a very small loading of 0.0625 g of 2.2:1 catalyst shows a profile in which conversion is low (Figure 3-33, Appendix A-17), reaching 50 % at 275 °C and 90 % at 370 °C. Throughout this temperature range the catalyst shows excellent formaldehyde selectivity of greater than 90 % until 330 °C, but never dropping below 80 % even at 370 °C. A small production of CO begins at 330 °C, rising to 5 % by 370 °C. $CO_2$ production begins at 300 °C and rises to around 14 % by 370 °C. There is a small production of dimethyl ether with around 5 % selectivity at 180 °C which drops below 1 % by 260 °C.

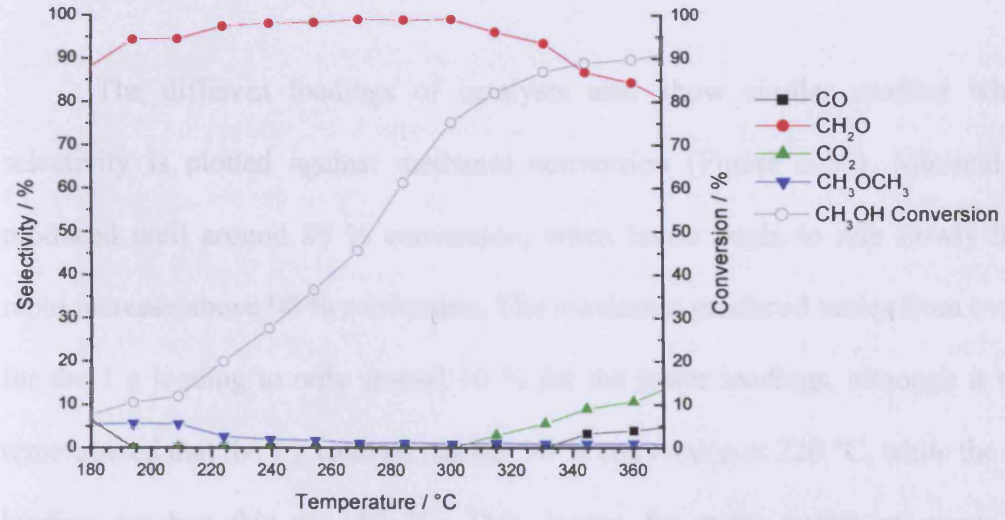


**Figure 3-33 - Selectivity and conversion over 0.0625g 2.2:1 Mo:Fe catalyst.**

By plotting formaldehyde selectivity against methanol conversion (Figure 3-34) for the different loadings it is possible to see that most follow a very similar path. All loadings show excellent formaldehyde selectivity (>90 %) at low conversions and this only begins to decrease once high conversions are reached (~90 %). The best yield is observed with the loading of 1 g that shows conversion and selectivity above 95 % leading to a yield in excess of 90 %.

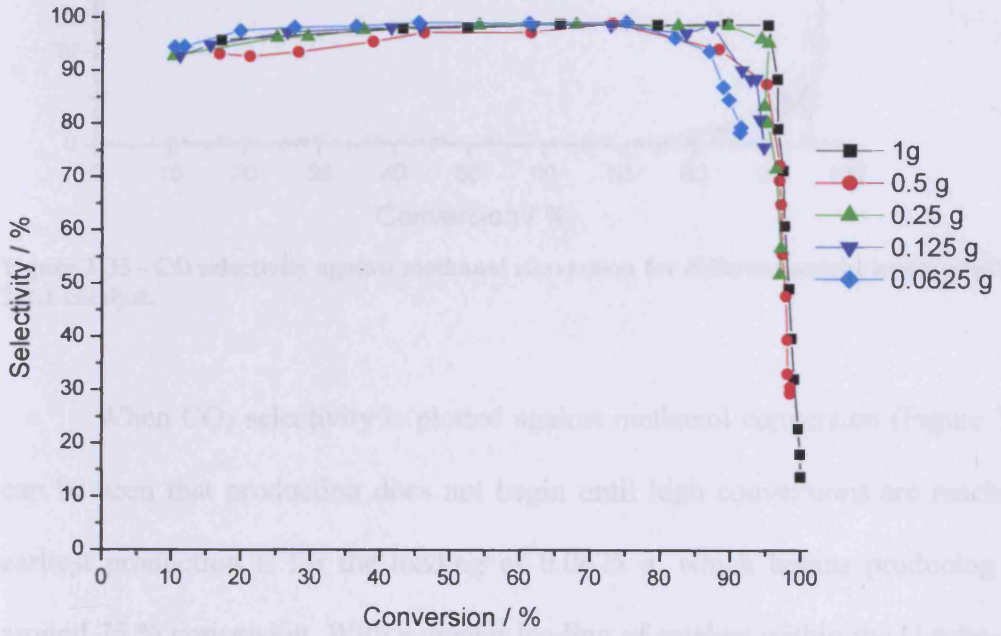


**Figure 3-34 - Formaldehyde selectivity against methanol conversion for different weight loadings of Mo:Fe 2.2:1 catalyst.**

The different loadings of catalysts also show similar profiles when CO selectivity is plotted against methanol conversion (Figure 3-35). Minimal CO is produced until around 85 % conversion, when levels begin to rise slowly before a rapid increase above 90 % conversion. The maximum produced varies from over 55 % for the 1 g loading to only around 10 % for the lower loadings, although it must be remembered that the 1 g catalyst reaches 90 % conversion at 220 °C, while the 0.125 g loading reaches this at 340 °C. This means far more points at much greater conversions are recorded for the larger loadings.

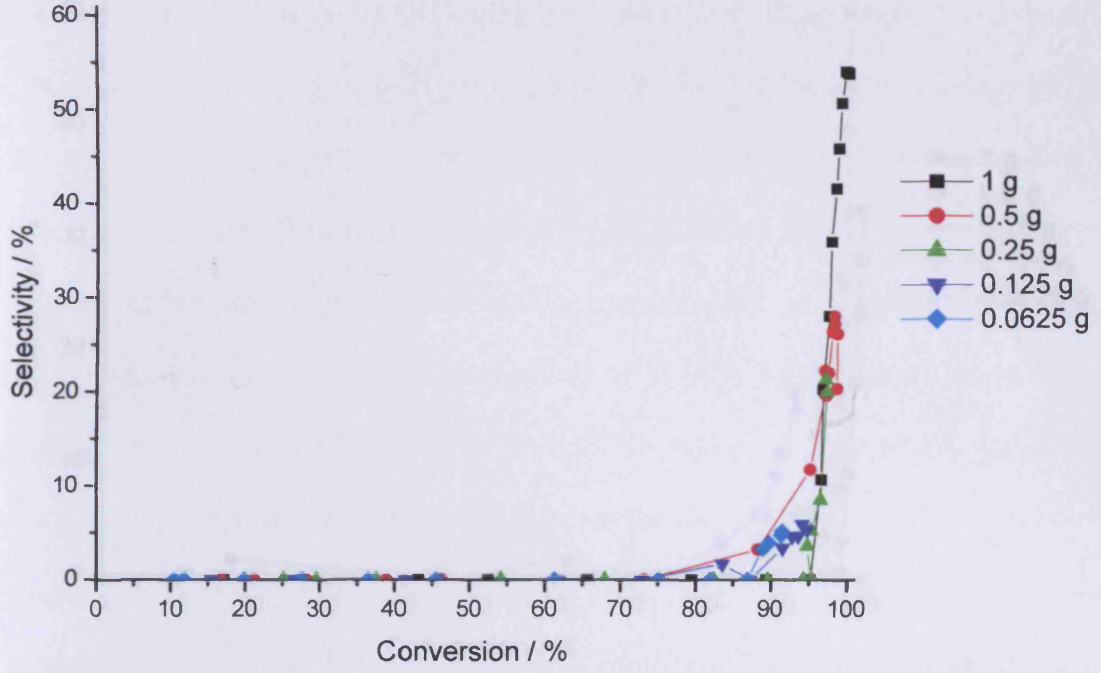


**Figure 3-35 - CO selectivity against methanol conversion for different weight loadings of Mo:Fe 2.2:1 catalyst.**

When $CO_2$ selectivity is plotted against methanol conversion (Figure 3-36), it can be seen that production does not begin until high conversions are reached. The earliest production is for the loading of 0.0625 g, which begins producing $CO_2$ at around 75 % conversion. With a greater loading of catalyst within the U-tube a higher conversion is required to produce significant amounts of $CO_2$. However, it must be remembered that 75 % methanol conversion for the 0.0625 g loading occurs at 300 °C (Figure 3-37), which is the temperature where the other loadings also begin to produce $CO_2$. These are off set in the graph however as this temperature also leads to higher conversions. Except for the smallest loading all catalysts show a greater than 90 % conversion, with less than 5 % $CO_2$ selectivity, in the case of the 1 g loading 97 % conversion is reached with less than 3 % $CO_2$ selectivity.

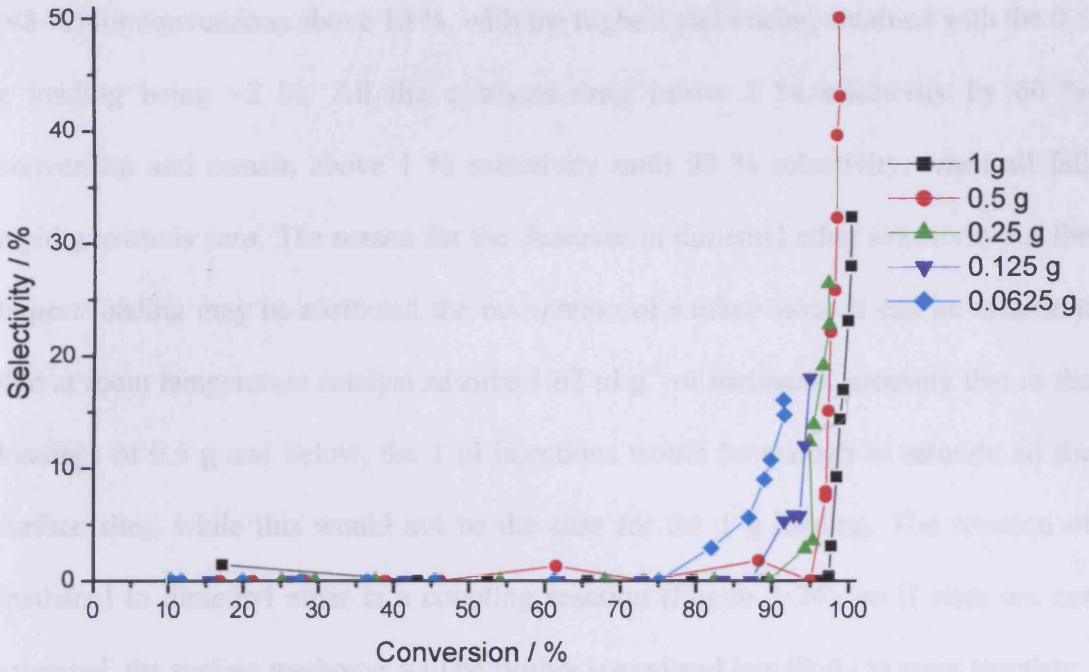


**Figure 3-36 - $CO_2$ selectivity against methanol conversion for different weight loadings of Mo:Fe 2.2:1 catalyst.**

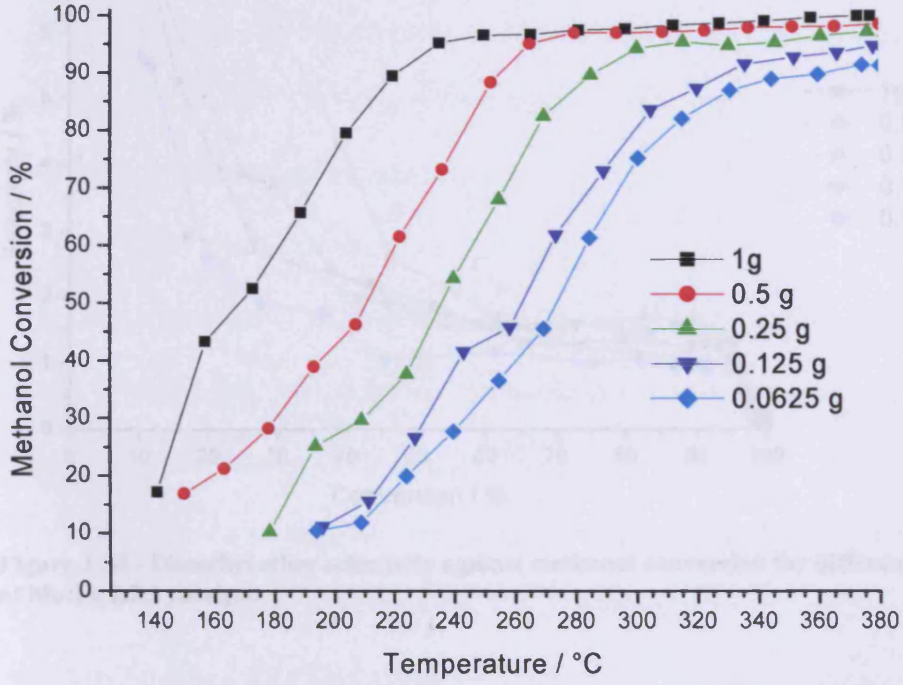


**Figure 3-37 - Methanol conversion against temperature for different weight loadings of Mo:Fe 2.2:1 catalyst.**

There is a decrease in dimethyl ether selectivity with decreasing loading except for the large loading of 1 g (Figure 3-38). The selectivity for all catalysts is low

(<8 %) for conversions above 10 %, with the highest yield being obtained with the 0.5 g loading being ~2 %. All the catalysts drop below 2 % selectivity by 60 % conversion and remain above 1 % selectivity until 90 % selectivity, when all fall rapidly towards zero. The reason for the decrease in dimethyl ether selectivity for the largest loading may be attributed the occupation of surface sites. It can be measured that at room temperature catalyst adsorbs 1.62 μl $g^{-1}$ of methanol, meaning that in the loadings of 0.5 g and below, the 1 μl injections would be enough to saturate all the surface sites, while this would not be the case for the 1 g loading. The reaction of methanol to dimethyl ether is a coupling reaction (Figure 3-24), so if sites are not saturated, the surface methoxys will be further spread and less likely to react together.

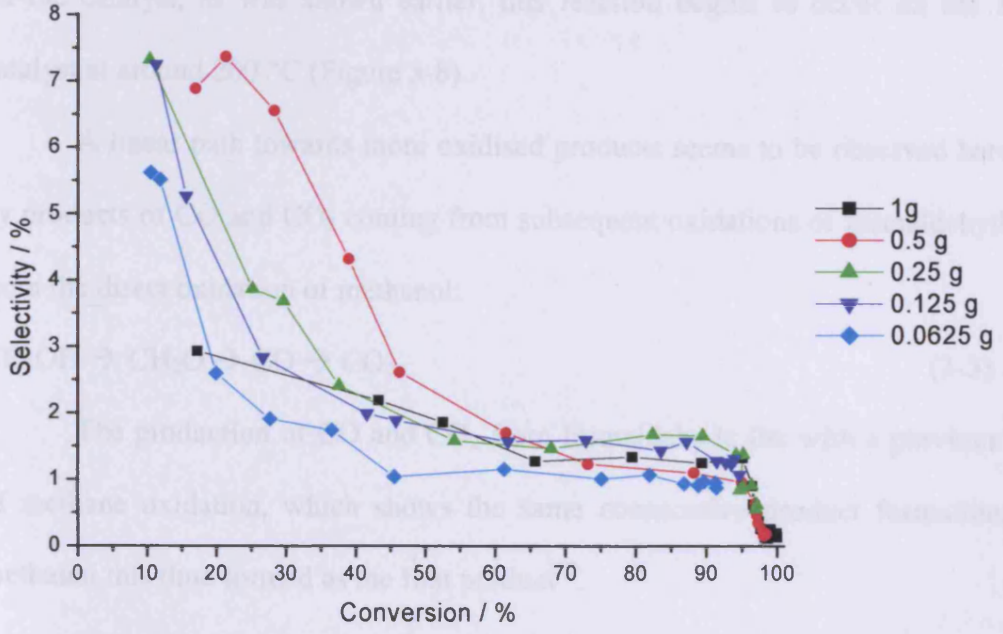


**Figure 3-38 - Dimethyl ether selectivity against methanol conversion for different weight loadings of Mo:Fe 2.2:1 catalyst.**

Comparing the conversion and selectivities of the catalyst at 310 °C gives an interesting insight into what happens down the bed. In the first 0.0625 g of the bed, 80 % methanol conversion occurs, with nearly all (>95 %) of this being converted to formaldehyde, while by the time it has passed through 0.125 g of catalyst 85 % of the

methanol is converted, still with very high (>95 %) methanol conversion. By the time the methanol has passed over 0.25 g of catalyst, conversion is up to 95 %, with 95 % formaldehyde selectivity. When passed over a further 0.25 g of catalyst (0.5 g total), formaldehyde selectivity has dropped to 65 %, with 20 % CO selectivity and 15 % $CO_2$ selectivity. By the time the methanol has passed the full length of a 1 g bed, formaldehyde and CO selectivity are 45 %, with 10 % $CO_2$ selectivity. When errors are accounted for it can be seen that at 310 °C a high conversion, highly selectivity bed can be created with 0.25 g of catalyst. Adding more catalyst beyond this creates secondary reactions with the formaldehyde being further oxidised to CO and $CO_2$.

The production of the $CO_2$ is likely to come from the further oxidation of CO on the catalyst, as was shown earlier, this reaction begins to occur on the Mo:Fe catalyst at around 200 °C (Figure 3-8).

A linear path towards more oxidised products seems to be observed here with by products of CO and $CO_2$ coming from subsequent oxidations of formaldehyde, not from the direct oxidation of methanol:

$$CH_3OH \rightarrow CH_2O \rightarrow CO \rightarrow CO_2 \qquad (3\text{-}3)$$

The production of CO and $CO_2$ from formaldehyde fits with a previous study of methane oxidation, which shows the same consecutive product formation, with methanol this time formed as the first product[12].

From this work, varying the loading of catalyst, it has been demonstrated that in pulsed flow conditions a high production of formaldehyde is possible, independent of the loading size (>90 % selectivity at >90 % conversion). It has also been shown that a surface with neighbouring methoxys is required for the formation of the coupled product of dimethyl ether. A linear pathway of oxidation has been observed (Equation

3-3), where formaldehyde is the primary product of methanol oxidation, with formaldehyde oxidised on to CO, and then CO can oxidised to $CO_2$.

### 3.3.5.2 Varying Pulse Size

In addition to testing the effect of bed length, the effect of methanol pulse size was also examined at a series of temperatures. In these experiments the catalyst was held isothermally at a given temperature while the different sizes of methanol injection were passed across at two minute intervals (Appendix A-18 to A-22).

By placing trend lines through the plots it is possible to work out the pulse size required to give 90 % methanol conversion at a given temperature and to calculate the selectivity of the catalyst under these conditions (Figure 3-39). From this data it can be seen that when the 90 % conversion is reached at a higher temperature (*i.e.* with a larger pulse) the catalyst is more selective to formaldehyde and dimethyl ether, with lower CO generation.

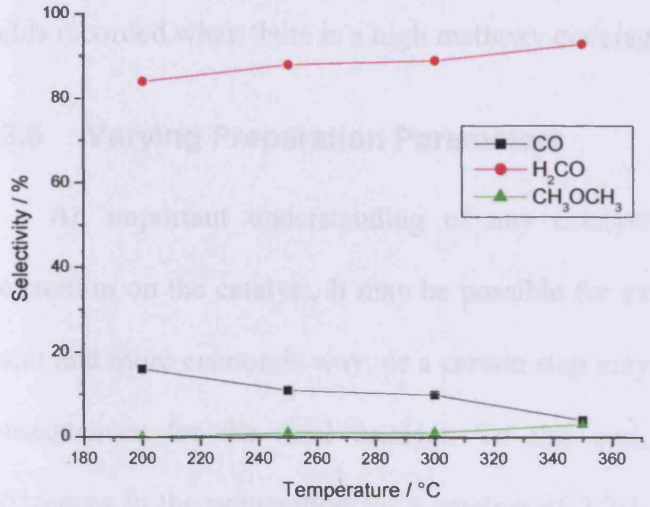


**Figure 3-39 - Selectivity of the 0.5 g 2.2:1 Mo:Fe catalyst at 90 % conversion for different temperatures, note that injection size of methanol differ.**

By having the temperature set higher, and so requiring more methanol to obtain 90 % conversion it can be seen that selectivity of both formaldehyde and

dimethyl ether is increased, with CO selectivity decreased. The increase in dimethyl ether can be explained by the increased number of methanol molecules being passed across the catalyst. To achieve 90 % conversion at 200 °C, 0.25 μl of methanol is injected compared to 3 μl at 350 °C. This higher number of methanol molecules will mean there is a higher coverage of methoxys on the surface, meaning a greater chance of the coupling reaction of two of these methoxys to form dimethyl ether occurring. Remembering 0.5 g of 2.2:1 Mo:Fe catalyst is saturated at room temperature with 0.81 μl methanol. The increased methanol injection size is also likely to account for the improvement in the formaldehyde selectivity for two reasons. Firstly as it is a larger injection, if the same absolute amount of CO is formed, this will be less in terms of a percentage. Secondly, it is likely the formaldehyde secondary reaction occurs on the same sites as the methanol oxidation, so the extra methanol will lead to a competitive adsorption process. These data reinforce the conclusions made previously (Section 3.3.5.1), with a linear production of CO observed and the highest dimethyl ether yields recorded when there is a high methoxy coverage.

### 3.3.6 Varying Preparation Parameters

An important understanding of any catalyst to establish is the effects of preparation on the catalyst. It may be possible for example to make the catalyst in an easier and more economic way, or a certain step may be essential or lead to beneficial consequences for the final catalyst. To this end, this short section investigates differences in the preparation for a catalyst of 2.2:1 Mo:Fe and the reasons for these differences.

The first point that should be noted about these catalysts is that after calcination, all looked very similar with a yellow green colour, this despite the fact that the precipitate which was raised to pH 10, changed colour to a chocolate brown before

calcination, whereas the other preparations all presented a canary yellow colour at this stage.

### 3.3.6.1 Co-precipitation with Washing

The usual 2.2:1 Mo:Fe catalyst preparation involved co-precipitation before evaporation to dryness. When the precipitate is washed and filtered instead, a catalyst is produced (Figure 3-40, Appendix A-23) with good activity, reaching 50 % methanol conversion at 190 °C, and 90 % by 250 °C. The activity of the catalyst is better than the catalyst produced without washing and filtering (Figure 3-6), and is more similar to the Perstorp catalyst (Figure 3-25). This follows the surface area data (Table 3-2), which shows the filtered and washed catalyst to be similar in area to the Perstorp catalyst. At high temperatures the catalyst shows less $CO_2$ and more CO, when compared to the 2.2:1 Mo:Fe catalyst, again like the Perstorp sample.

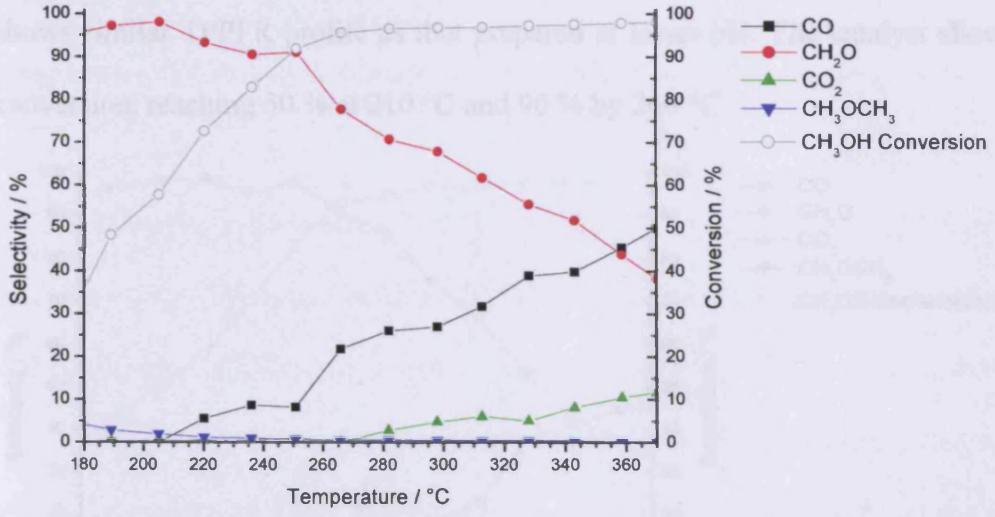


**Figure 3-40 - Selectivity and conversion for methanol oxidation over 2.2:1 Mo:Fe catalyst prepared at low pH, with filtering and washing.**

### 3.3.6.2 Use of Different Iron Precursor

The industrial catalyst is currently produced using iron (III) chloride, so a comparative catalyst was made using this salt with ammonium heptamolybdate and filtering and washing steps. This lead to a less active catalyst (Figure 3-41, Appendix

A-24) compared with that evaporated to dryness, with 50 % conversion being reached at 225 °C and 90 % conversion at 270 °C.

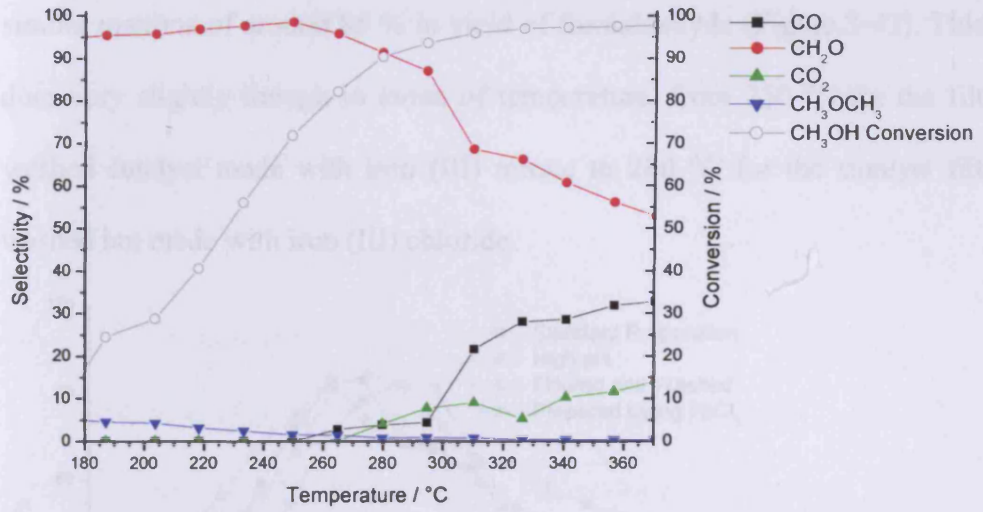


**Figure 3-41 - Selectivity and conversion for methanol oxidation over 2.2:1 Mo:Fe catalyst prepared using $FeCl_3$.**

### 3.3.6.3 Preparation at High pH

The Mo:Fe 2.2:1 catalyst prepared at high pH (Figure 3-42, Appendix A-25) shows similar TPPFR profile as that prepared at lower pH. The catalyst shows good conversion, reaching 50 % at 210 °C and 90 % by 260 °C.

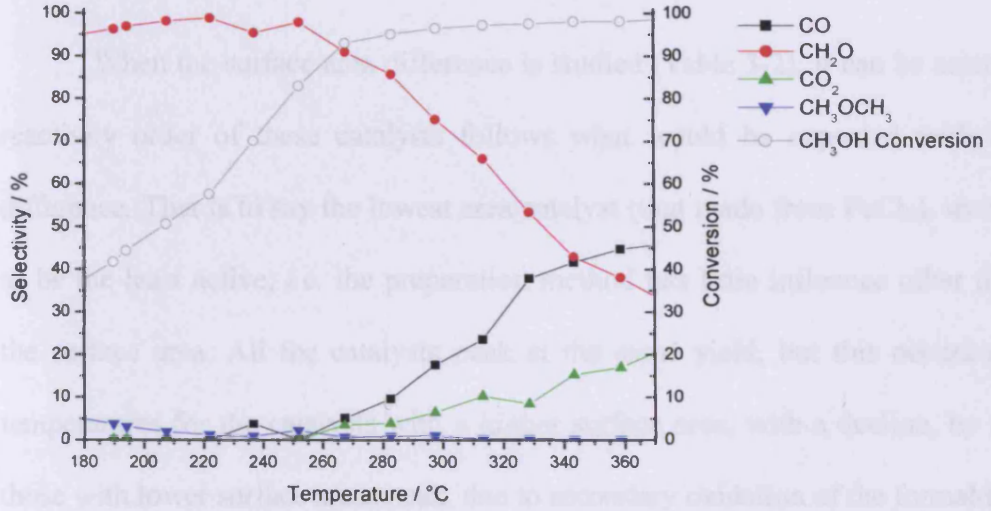


**Figure 3-42 - Selectivity and conversion for methanol oxidation over 2.2:1 Mo:Fe catalyst prepared at high pH.**

### 3.3.6.4 Comparison

Despite differing preparation methods, the four tested catalysts show very similar maxima of around 85 % in yield of formaldehyde (Figure 3-43). This maxima does vary slightly though in terms of temperature, from 250 °C for the filtered and washed catalyst made with iron (III) nitrate to 280 °C for the catalyst filtered and washed but made with iron (III) chloride.

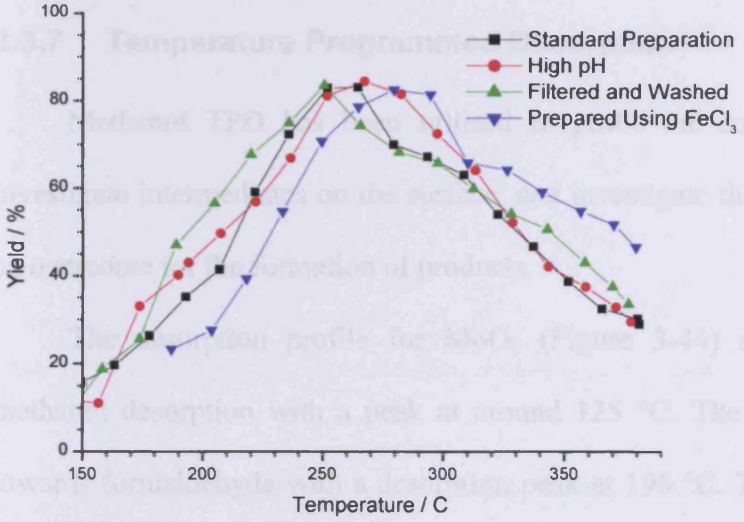


**Figure 3-43 - Comparison of formaldehyde yield with temperature for catalysts with a Mo:Fe ratio of 2.2:1 prepared by different methods.**

When the surface area difference is studied (Table 3-2), it can be seen that the reactivity order of these catalysts follows what would be expected with the area difference. That is to say the lowest area catalyst (that made from $FeCl_3$), shows itself to be the least active, *i.e.* the preparation method has little influence other than over the surface area. All the catalysts peak at the same yield, but this occurs at lower temperatures for the catalysts with a higher surface area, with a decline, by the time those with lower surface areas peak, due to secondary oxidation of the formaldehyde.

At high temperatures the catalysts prepared by alternative methods produced less CO than that prepared by evaporation to dryness. This is most likely due to the higher levels of $MoO_3$ within the catalysts (Figure 3-55 and Figure 3-57), which has

been shown to be a poor oxidiser of CO (Section 3.3.2). The loss of iron from the catalysts produced with filtering and washing steps has previously been noted by Hill and Wilson[3]. The catalyst produced at high pH has no filtering or washing steps so it is assumed the Mo:Fe ratio in the catalyst is the same as in the preparation, in which case an extra iron phase must be present that is not detected by the characterisation techniques used (Section 3.3.8).

### 3.3.7 Temperature Programmed Desorption

Methanol TPD has been utilised to probe the surface of the catalysts, to investigate intermediates on the surface, and investigate the energy barriers that must be overcome for the formation of products.

The desorption profile for $MoO_3$ (Figure 3-44) shows a small but broad methanol desorption with a peak at around 125 °C. The catalyst shows selectivity towards formaldehyde with a desorption peak at 190 °C. There are two water peaks, first a much larger peak at around 90 °C, with a second smaller peak at around 200 °C.

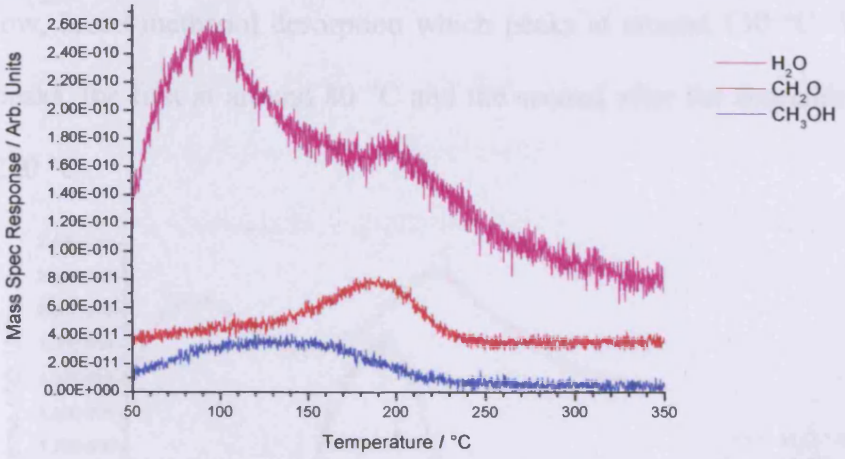


**Figure 3-44 - TPD of $MoO_3$ saturated with methanol at room temperature.**

The TPD profile for $Fe_2O_3$ (Figure 3-45) shows no selectivity towards formaldehyde with a peak of $H_2$ at 290 °C and a large $CO_2$ peak at 300 °C. The water signal shows a low temperature peak at around 100 °C and there is also a small

methanol desorption centred at around 80 °C. The TPD shown is for the Aldrich $Fe_2O_3$, the synthesised sample is not shown, as the desorption profile is the same as that for the Aldrich sample except with larger desorption peaks due to a larger surface area (Table 3-2).

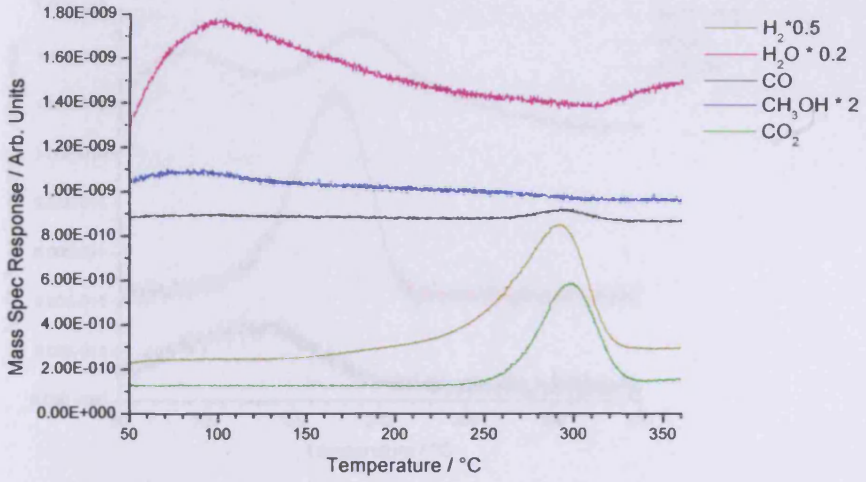


**Figure 3-45 - TPD of $Fe_2O_3$ saturated with methanol at room temperature.**

The TPD profile of Mo:Fe 1.5:1, shows a high level of selectivity towards formaldehyde (Figure 3-46) with a large desorption centred at 190 °C. Before this is a low, broad methanol desorption which peaks at around 150 °C. Water presents two peaks, the first at around 80 °C and the second after the formaldehyde desorption at 220 °C.

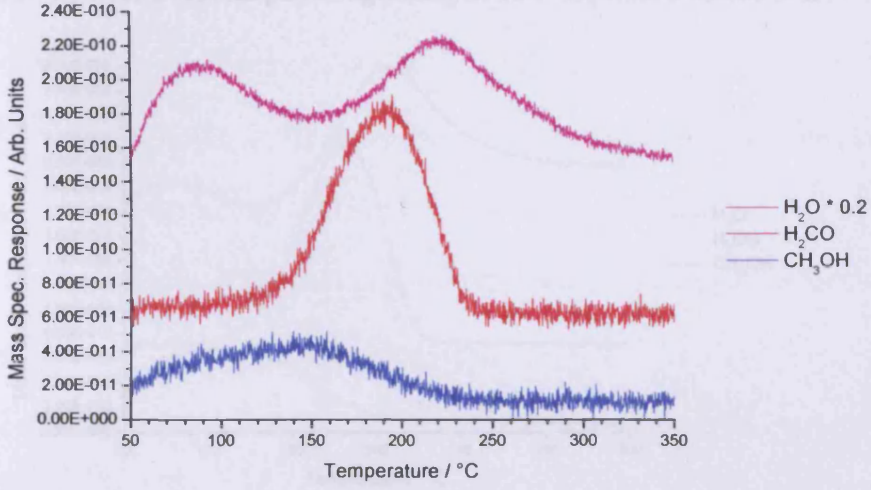


**Figure 3-46 - TPD of Mo:Fe 1.5:1 saturated with methanol at room temperature.**

The TPD of the fresh 2.2:1 Mo:Fe catalyst (Figure 3-47) shows a broad low temperature methanol desorption centred at 130 °C, followed by a large formaldehyde desorption centred at 175 °C. There is a double peak in the water desorption at 90 and 190 °C.

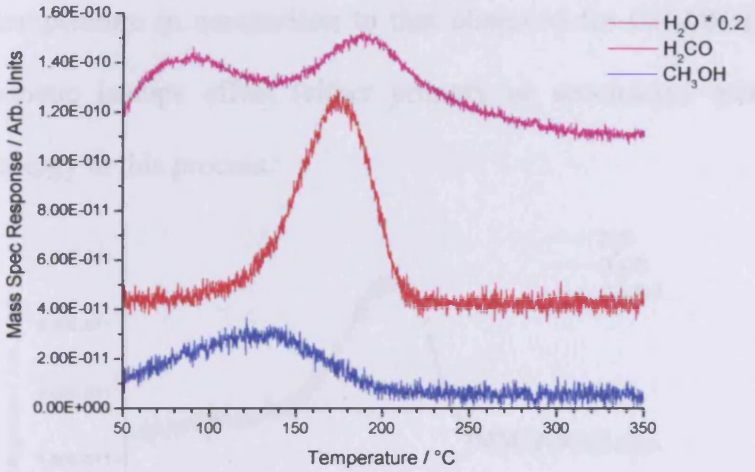


**Figure 3-47 - TPD of Mo:Fe 2.2:1 saturated with methanol at room temperature.**

The TPD plot for the commercial Perstorp KH 26 catalyst again shows 100 % selectivity to formaldehyde (Figure 3-48), which begins at around 100 °C, and is centred with a large peak at 180 °C and is complete by 230 °C. There is a broad methanol desorption, centred at around 100 °C, which is essentially complete by 200 °C. There are two water peaks observed, the first, smaller peak is centred around 75 °C, with a second peak beginning at 130 °C, with a centre at 210 °C.

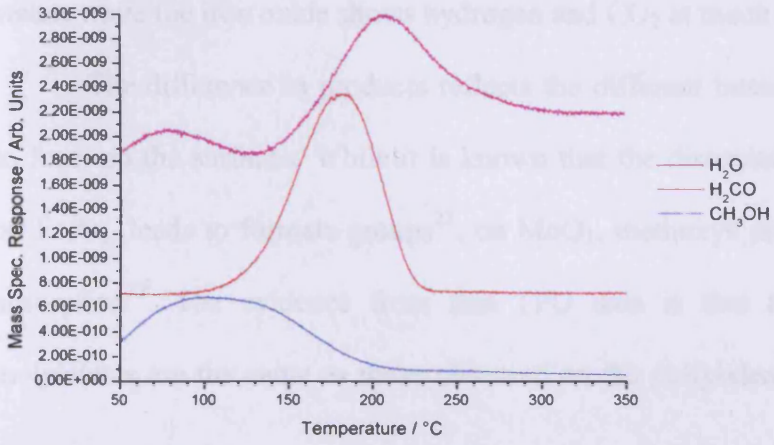


**Figure 3-48 - TPD of Perstorp KH26 catalyst saturated with methanol at room temperature.**

TPD of $d_4$-methanol adsorbed onto the 2.2:1 Mo:Fe catalyst (Figure 3-49) shows a low, broad methanol desorption with a maxima at around 160 °C, followed by a large formaldehyde desorption at 200 °C and a small water desorption at 210 °C. The temperature of the formaldehyde desorption is shifted to ~30 °C higher in temperature in comparison to that observed for $CH_3OH$ (Figure 3-47), indicating a kinetic isotope effect (either primary or secondary) meaning a higher activation energy to this process.

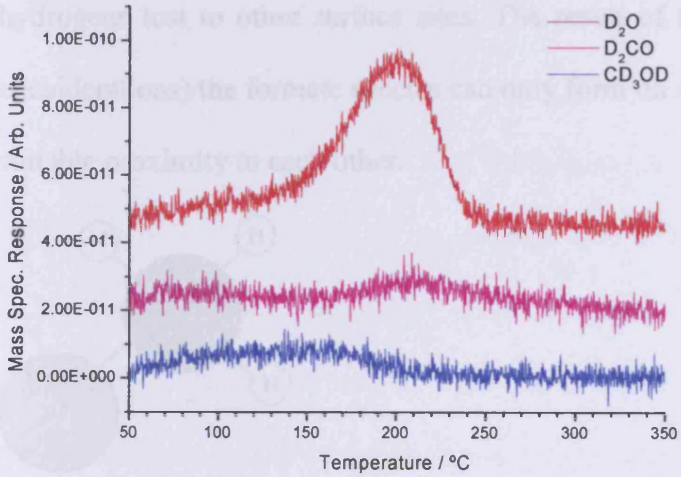


**Figure 3-49 - TPD of Mo:Fe 2.2:1 saturated with $d_4$-methanol at room temperature.**

The first and most obvious difference between the various TPDs is that between the $Fe_2O_3$ and all the molybdenum containing catalysts. In the case of molybdenum containing catalysts, the major products seen are formaldehyde and water, while the iron oxide shows hydrogen and $CO_2$ at much higher temperatures.

The difference in products reflects the different intermediates that are known to form on the surfaces. While it is known that the dissociative methanol adsorption on $Fe_2O_3$ leads to formate groups[21], on $MoO_3$, methoxys are formed from methanol adsorption[22]. The evidence from this TPD data is that the species on the iron molybdates are the same as those observed on the molybdena, *i.e.* methoxys[22]. From

these surface species formed, methoxys can have one hydrogen abstracted to yield formaldehyde, while formates are completely dehydrogenated and lead to $CO_2$.

A major reason for this difference in adsorbed species can be seen when the structures of the oxides are studied. A methoxy group (Figure 3-50) is absorbed in a monodentate manner onto a singular site, with the acidic proton of the hydrogen absorbed onto a separate neighbouring site. In contrast to this the formate group (Figure 3-51) is absorbed in a bidentate manner to two adjacent sites, with two methyl hydrogens lost to other surface sites. The result of this is that (in addition to other considerations) the formate species can only form on surfaces with two surface sites in suitable proximity to each other.

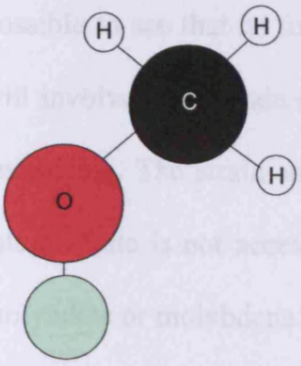


**Figure 3-50 - Schematic of an adsorbed methoxy.**

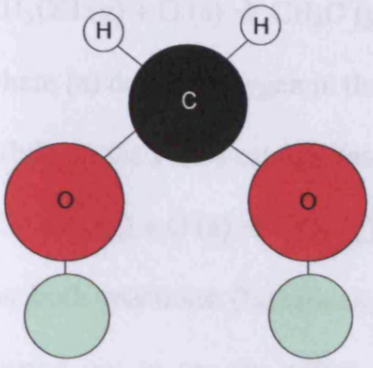


**Figure 3-51 - Schematic of an adsorbed formate group.**

If the case of $\alpha$-$Fe_2O_3$ is examined, the closest Fe-Fe bond in the bulk material is ~3.0 Å, while the carbon atom of the formate group can be considered to be $sp^3$ hybridised, meaning an angle between bonds of 109°. If the M-O bonds are considered to be perpendicular to the surface, then these constraints would mean a C-O bond length of ~1.8 Å. As a comparison, the average length of a C-O covalent bond in a standard hydrocarbon can be considered as 1.43 Å[23]. If similar calculations to these are carried out for $\alpha$-$MoO_3$ with the smallest Mo-Mo distance of 3.48 Å[24] and $\alpha$-$Fe_2(MoO_4)_3$ with a Mo-Mo distance of 4.24 Å and Mo-Fe distance of 3.6 Å, the C-O bonds would need to be 2.1, 2.6 and 2.2 Å respectively.

So by considering the adsorbed formate species with simple calculations, it is possible to see that its formation on molybdenum oxide and iron molybdate surfaces will involve more strain (in comparison to iron oxide) on the molecule and so be less favourable. The strain and energy of formation are so unfavourable that the formate intermediate is not accessed by the room temperature methanol adsorption on ferric molybdate or molybdena.

The catalyst surface is left reduced after this work as the stoichiometry of the reaction on molybdena and Mo:Fe 2.2:1 and 1.5:1 catalysts is:

$$CH_3OH\ (g) + O\ (a) \rightarrow CH_2O\ (g) + H_2O\ (g) \qquad (3\text{-}4)$$

where (a) denotes oxygen in the surface layer of the catalyst.

While on the $Fe_2O_3$ catalyst (as seen by TPD) the reaction is:

$$CH_3OH\ (g) + O\ (a) \rightarrow CO_2\ (g) + 2H_2\ (g) \qquad (3\text{-}5)$$

As both reactions (Equations 3-4 and 3-5) use surface oxygen, repeat TPD were carried out to see the affect on products produced. However, the surface oxygen vacancies appear to be filled from the bulk at the temperatures used here (up to ~400 °C) as the repeat experiments show the same results.

All the molybdenum catalysts show the formaldehyde peak in approximately the same positions, meaning the energy barrier to desorption (Table 3-3) is also similar. The energy to the decomposition of the formate group on $Fe_2O_3$ is much higher however.

| Catalyst | Product Formed | Peak Temperature / °C | Energy (kJ $mol^{-1}$) |
|---|---|---|---|
| $Fe_2O_3$ | $CO_2$ | 300 | 155 |
| Mo:Fe 1.5:1 | $H_2CO$ | 190 | 125 |
| Mo:Fe 2.2:1 | $H_2CO$ | 175 | 121 |
| Mo:Fe 2.2:1 | $D_2CO$ | 200 | 128 |
| $MoO_3$ | $H_2CO$ | 190 | 122 |

**Table 3-3 - Desorption energies from methanol TPD.**

The origin of the first water peak which is typically centred at around 90 °C was investigated to discover if this was a real desorption that was present on all catalysts or, was due to another reason. Use of anhydrous methanol (methanol anhydrous, Sigma-Aldrich, >99.8 %, <0.002 % $H_2O$), produced the same result as that previously reported. A blank TPD was then run to check if the water was being introduced with the gas flow. The same procedure of pre-heating cooling, and an allowance of time where the dosing would usually occur were followed. The resulting TPD is shown below (Figure 3-52). As can be seen, this early water peak is still present so it can be deduced that this will also be present in the other TPDs recorded, thus meaning water peaks centred at around 90 °C can be attributed to this and not a surface process. Also present in the blank TPD is a much smaller, second peak in the water trace recorded, which is centred around 270 °C, this may be the recombination of hydroxyl groups formed on the surface by dissociative adsorption of the water.

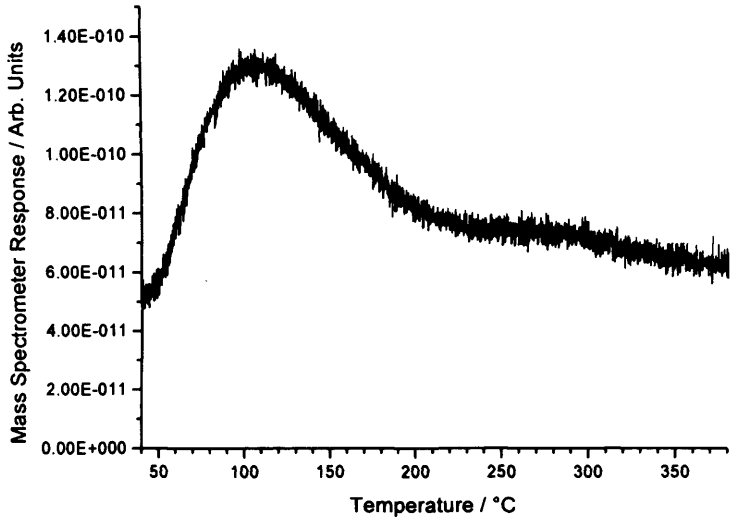


**Figure 3-52 – 18 amu trace, relating to water for a blank TPD of Mo:Fe 2.2:1 catalyst.**

In the TPDs for the iron molybdate catalysts (Mo:Fe 2.2:1 and 1.5:1), it is noticeable that there is no CO or $CO_2$ production, which helps to support the argument presented earlier (Section 3.3.5), that the production of CO and $CO_2$ off these catalysts at high temperature are secondary oxidation products, from the further reaction of formaldehyde.

A further TPD on the Mo:Fe 1.5:1 catalyst with dosing of methanol at a higher temperature (115 °C) was carried out (Figure 3-53). A temperature of 120 °C was used as this was above the temperature of the maximum water desorption and also a temperature where some molecular methanol desorption also occurs, but is lower than the temperature at which formaldehyde production begins. Monitoring of methanol uptake, showed this now to be 0.49 μl, as opposed to the 0.73 μl when the uptake is carried out at room temperature. This difference is best explained as being due the molecularly adsorbed methanol that is seen to be a more major feature in the TPD when the methanol is absorbed at room temperature (Figure 3-46).

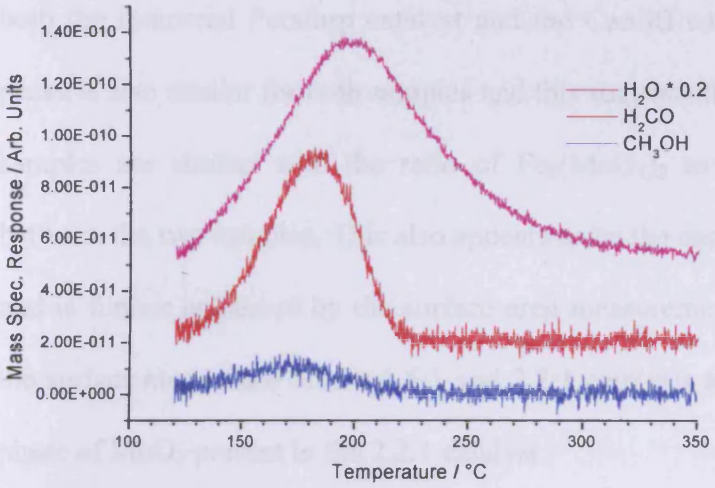


**Figure 3-53 - TPD of Mo:Fe 1.5:1 saturated with methanol at 115 °C.**

### 3.3.8 Characterisation

An essential part of any fundamental catalysis study is characterising the materials tested and linking this to reactivity observed. The ideal way to do this is to study the catalyst *in-situ* so that the structure of the catalyst under reaction conditions is known. However, this is often more complicated, if not impossible for given techniques, so the work presented here concentrates on the materials pre and post reactor.

#### 3.3.8.1 XRD

The diffractogram patterns for the single oxide species of α-$MoO_3$, and α-$Fe_2O_3$, α-$Fe_2(MoO_4)_3$ (Figure 3-54) follow the patterns given in the literature[25-27]. The samples of the Cardiff 2.2:1 Mo:Fe and the Perstorp KH 26 catalyst both show a mixture of the α-$MoO_3$ phase and α-$Fe_2(MoO_4)_3$. The most obvious signal of the presence of $MoO_3$ within these catalysts is the peak at around 12 ° 2Θ (7.01 Å), corresponding to the 020 lattice plane, while the α-$Fe_2(MoO_4)_3$ is best identified by a series of peaks at 19.5, 20.5, 21.8 and 23.0 ° 2Θ (4.56, 4.34, 4.08 and 3.87 Å), corresponding to the -204, -313, -214 and -114 lattice planes. The ratio between the $Fe_2(MoO_4)_3$ peaks and those associated with $MoO_3$, is approximately the same for

both the industrial Perstorp catalyst and the Cardiff catalyst. The broadening of the peaks is also similar for both samples and this suggests that the crystallite sizes in both samples are similar with the ratio of $Fe_2(MoO_4)_3$ to $MoO_3$ also closely matched between the two samples. This also appears to be the case for the Mo:Fe 1.5:1 sample, and is further enhanced by the surface area measurements (Table 3-2), which shows the surface area of the Mo:Fe 1.5:1 and 2.2:1 catalysts to be similar, despite the extra phase of $MoO_3$ present in the 2.2:1 catalyst.

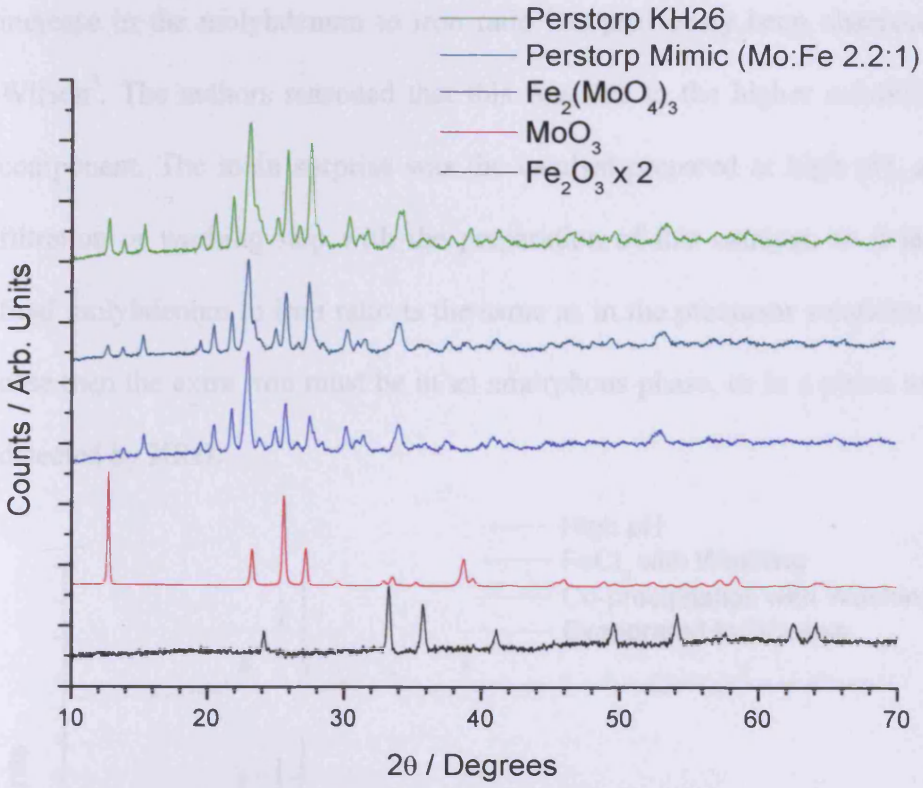


**Figure 3-54 - X-Ray diffractograms for pre reactor catalysts.**

A comparison of the 2.2:1 Mo:Fe catalysts prepared by different methods (Figure 3-55) shows the same phases of α-$Fe_2(MoO_4)_3$ and α-$MoO_3$ in all the catalysts. The presence of $MoO_3$ is more difficult to see however than in the previous XRD diagram (Figure 3-54), as a problem developed with the XRD part way through the course of research. This problem has lead to a decrease in sensitivity below ~15 ° 2Θ, and affects the spectra on preparation methods, except for that of the catalyst

evaporated to dryness. The presence of $MoO_3$ can also be seen, however, by the high example peaks at 25.7, 27.3 and 39.2 ° 2Θ (3.47, 3.26 and 2.30 Å corresponding to the lattice planes 040, 021 and 060 for $MoO_3$) in ratio to the $Fe_2(MoO_4)_3$ peaks at 19.5, 20.5, 21.8 and 23.0 ° 2Θ. From the size of these peaks, especially those at 39.2 ° compared to 21.8 °, it is possible to see that there is a greater spectral intensity of $MoO_3$ in the alternative preparations compared to that evaporated to dryness. This may be expected for the catalysts prepared using filtration and washing steps as an increase in the molybdenum to iron ratio has previously been observed by Hill and Wilson[3]. The authors reasoned that this was due to the higher solubility of the iron component. The main surprise was the catalyst prepared at high pH, as there is no filtration or washing step with the preparation of this catalyst, so it is assumed the final molybdenum to iron ratio is the same as in the precursor solutions. If this is the case then the extra iron must be in an amorphous phase, or in a phase too small to be detected by XRD.

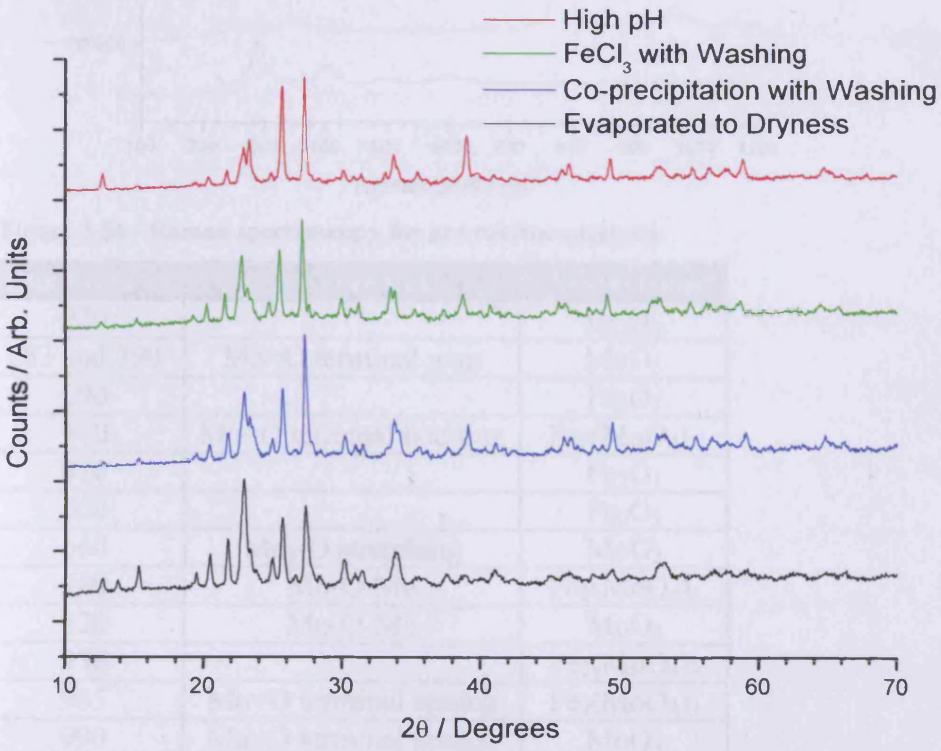


**Figure 3-55 - X-Ray diffractograms for pre reactor catalysts with nominal Mo:Fe 2.2:1.**

### 3.3.8.2 Raman Spectroscopy

When the Raman spectra are taken of the pre reactor catalysts (Figure 3-56) the major bands observed are M-O-M and M=Os stretches. Using the assignments from Hill and Wilson[3] and Palacios Alcolado[28], the major bands are determined as follows, molybdenum trioxide are 990, 820, 660, 280 $cm^{-1}$, iron oxide 600, 410, 290, 220, and $Fe_2(MoO_4)_3$ 965, 930, 780, 350 $cm^{-1}$. The bands at 990 and 965 $cm^{-1}$ for $MoO_3$ and $Fe_2(MoO_4)_3$ are Mo=O terminal vibrational stretches, while the bands at 810 and 780 $cm^{-1}$ are Mo-O-Mo vibrations. A summary of the major bands is given below (Table 3-4).

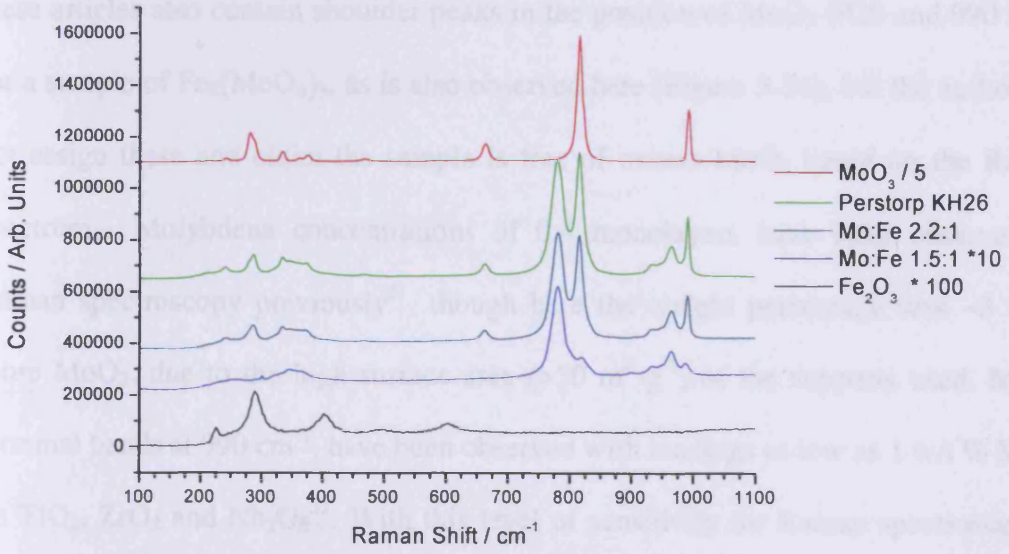


**Figure 3-56 - Raman spectroscopy for pre reactor catalysts.**

| Band ($cm^{-1}$) | Assignment | Association |
|---|---|---|
| 220 | | $Fe_2O_3$ |
| 283 and 290 | Mo=O terminal wag | $MoO_3$ |
| 290 | | $Fe_2O_3$ |
| 350 | Mo=O terminal bending | $Fe_2(MoO_4)_3$ |
| 410 | | $Fe_2O_3$ |
| 600 | | $Fe_2O_3$ |
| 660 | $Mo_3$-O stretching | $MoO_3$ |
| 780 | Mo-O-Mo | $Fe_2(MoO_4)_3$ |
| 820 | Mo-O-Mo | $MoO_3$ |
| 930 | | $Fe_2(MoO_4)_3$ |
| 965 | Mo=O terminal stretch | $Fe_2(MoO_4)_3$ |
| 990 | Mo=O terminal stretch | $MoO_3$ |

**Table 3-4 - Assignment of Raman Spectroscopy bands.**

The Raman spectroscopy helps to reinforce the evidence from the XRD that the 2.2:1 catalyst has both the $Fe_2(MoO_4)_3$ and $MoO_3$ phases present as Mo=O and Mo-O-Mo vibrations associated with both of these are observed. More surprisingly, these bands are observed, not just in the 2.2:1 catalyst, but also in the 1.5:1 Mo:Fe catalyst (characterised to be single phase α-$Fe_2(MoO_4)_3$ by XRD). This suggests there is some $MoO_3$, or at least Mo in an octahedral coordination (as in $MoO_3$, unlike $Fe_2(MoO_4)_3$ where Mo exists in a tetrahedral coordination) which is too small to be detected by XRD. This may be a monolayer of $MoO_3$, on the surface of the metal oxide, a model that has been previously described[29,30]. The spectrum presented in these articles also contain shoulder peaks in the position of $MoO_3$ (820 and 990 $cm^{-1}$) for a sample of $Fe_2(MoO_4)_3$, as is also observed here (Figure 3-56), but the authors do not assign these and claim the sample is free of excess $MoO_3$ based on the Raman spectrum. Molybdena concentrations of 0.4 monolayers have been observed by Raman spectroscopy previously[31], though here the weight percentage was ~3 % or more $MoO_3$, due to the high surface area (>50 $m^2$ $g^{-1}$) of the supports used. Mo=O terminal bands at 990 $cm^{-1}$, have been observed with loadings as low as 1 w/t % $MoO_3$ on $TiO_2$, $ZrO_2$ and $Nb_2O_5$[32]. With this level of sensitivity for Raman spectroscopy it seems there may be an enrichment of molybdenum at the surface, however with a ratio made exactly the same as the stoichiometric, only a small excess of molybdenum in the preparation may cause this to be seen, so this theme is returned to further in Chapter 5 where catalysts with a lower molybdenum to iron ratio are prepared.

The Raman spectrum for the Perstorp catalyst shows a different ratio of $MoO_3$ to $Fe_2(MoO_4)_3$ compared to that of the 2.2:1 Mo:Fe catalyst. This is seen by the higher 990 $cm^{-1}$ band ($MoO_3$) compared to that at 965 $cm^{-1}$ ($Fe_2(MoO_4)_3$) for the Perstorp

catalyst, whereas these bands present themselves in the opposite order for the 2.2:1 Mo:Fe (Low pH preparation) catalyst.

The Raman spectra from the catalyst prepared by different methods (Figure 3-57), reinforce the data observed by XRD (Figure 3-55) by showing mixture of $Fe_2(MoO_4)_3$ and $MoO_3$. There is again an increase in $MoO_3$ band intensities compared to $Fe_2(MoO_4)_3$, observed by the increase in the band at 810 $cm^{-1}$ (Mo-O-Mo vibrations in $MoO_3$) compared to that at 780 $cm^{-1}$ (Mo-O-Mo vibrations in $Fe_2(MoO_4)_3$). This shows an increase in $MoO_3$ in comparison to $Fe_2(MoO_4)_3$ for the catalysts prepared by alternative methods. This fits well with the reactor data (Section 3.3.6), which shows a reduction in CO from these catalysts at high temperatures, shown to occur because of the slower rate of CO oxidation on $MoO_3$ compared to $Fe_2(MoO_4)_3$ (Section 3.3.2).

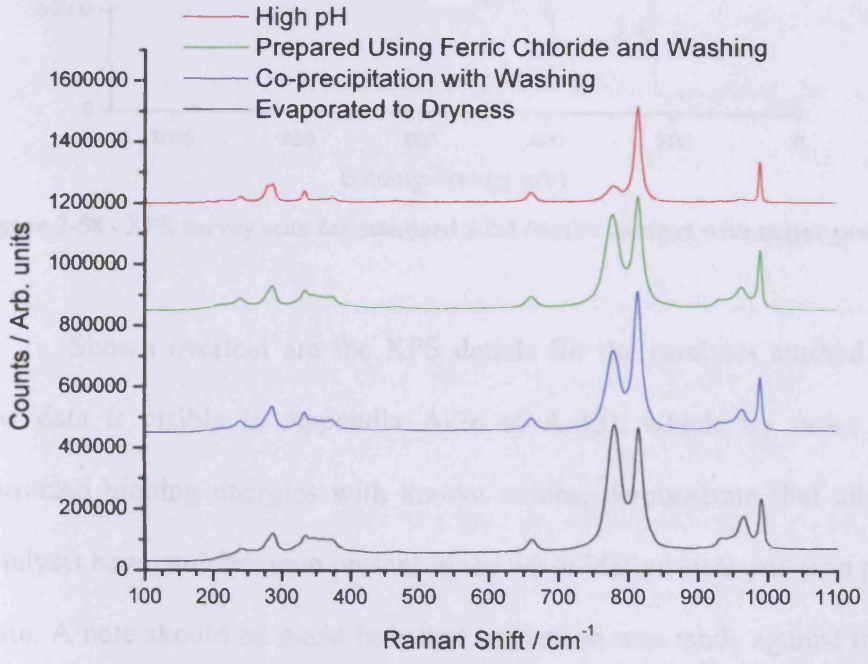


**Figure 3-57 - Raman spectra for pre reactor catalysts with Mo:Fe 2.2:1, prepared by different methods.**

### 3.3.8.3 XPS

Shown below (Figure 3-58) is an XPS wide survey scan for the 2.2:1 Mo:Fe standard catalyst with the major peaks labelled. These wide scans are taken to give an

overall picture as to the surface composition and are taken with low resolution (typical step size of 0.5 eV). From the spectrum shown it can be seen that the surface region contains molybdenum, iron, oxygen and carbon. Carbon is nearly always observed with XPS, due to the technique's high surface sensitivity, and it is merely a contaminant arising from air exposure.

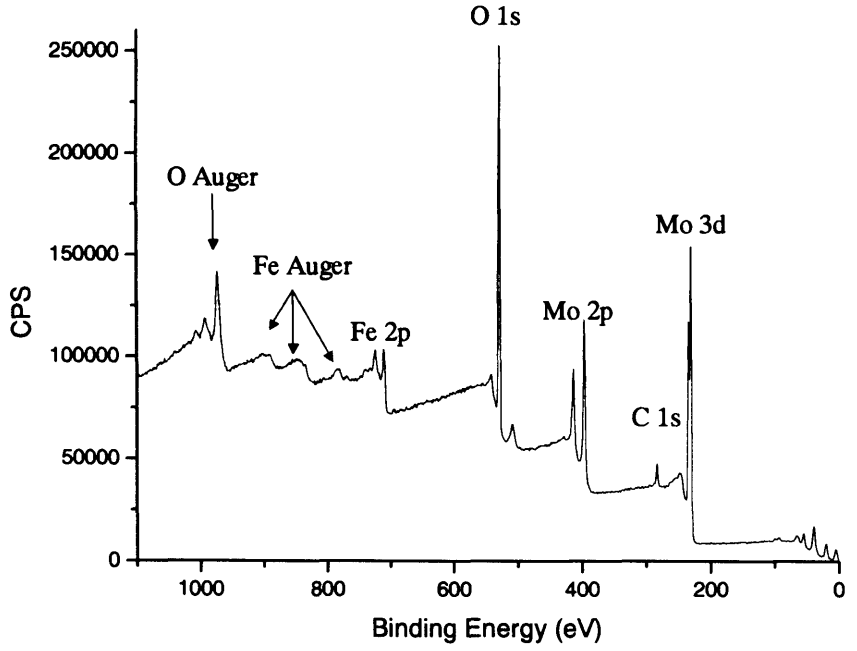


**Figure 3-58 - XPS survey scan for standard 2.2:1 Mo:Fe catalyst with major peaks labelled.**

Shown overleaf are the XPS details for the catalysts studied (Table 3-5, the raw data is visible in Appendix A-26 to A-33), which, by cross referencing the corrected binding energies with known values, demonstrate that all the pre reactor catalysts have molybdenum present in the +6 oxidation state and iron present in the +3 state. A note should be made here that correction was made against the O 1s value of 530.4 eV for all catalysts[33], as some catalyst (particularly those reduced in anaerobic conditions, Chapter 4) presented more than one carbonacous species.

| Catalyst Composition | Corrected Binding energies (eV) | | Area Under Peak | | Calculated Surface Mo Cation Fraction | Bulk Mo Cation Fraction |
|---|---|---|---|---|---|---|
| | Mo $3d^{5/2}$ | Fe $2p^{3/2}$ | Mo 3d | Fe 2p | | |
| $Fe_2O_3$ (Synthesised) | - | 711.4 | 0 | 45158 | 0 | 0 |
| Mo:Fe 1.5:1 | 232.4 | 711.7 | 11038 | 5992 | 0.62 | 0.6 |
| Perstorp KH 26 | 232.4 | 711.4 | 12308 | 4486 | 0.71 | 0.69 |
| Mo:Fe 2.2:1 (Standard Preparation) | 232.4 | 711.5 | 24135 | 9863 | 0.69 | 0.69 |
| Mo:Fe 2.2:1 (High pH) | 232.5 | 711.4 | 13429 | 2138 | 0.85 | 0.69 |
| Mo:Fe 2.2:1 (Filtered and Washed) | 231.8 | 711.7 | 13445 | 3890 | 0.76 | 0.69 |
| Mo:Fe 2.2:1 (Prepared using $FeCl_3$) | 232.3 | 711.3 | 12813 | 3109 | 0.79 | 0.69 |
| $MoO_3$ | 232.5 | - | 26796 | 0 | 1 | 1 |

**Table 3-5 - XPS results for fresh catalysts.**

Catalysts prepared by evaporation to dryness, along with the industrial Perstorp catalyst, present surface ratios of molybdenum to iron that are close to those predicted for the bulk of the catalyst. We may have predicted to see a higher molybdenum content on the surface of the Mo:Fe 1.5:1 catalyst as Raman spectroscopy observed some bands associated with octahedral Mo (present in $MoO_3$), and the prediction from this of a $MoO_3$ monolayer. These data do not exclude this possibility, as XPS is sensitive to the surface region, and not just the surface layer. There is an exponential decrease in signal observed with the layers below the surface due to the small inelastic mean free path of the photoelectrons produced. A previous XPS study on iron molybdates showed a sample (made with a bulk ratio of Mo/Fe 1.6 ± 0.1) had an excess of molybdenum over that expected, with a surface value of 1.95 Mo/Fe[34]. The ratio recorded by XPS of Mo/Fe was reduced to 1.35 with argon sputtering. This means that a molybdenum monolayer cannot be discounted from the XPS data presented here. Termination of the iron molybdate preferentially along

certain faces (e.g. 010), may lead to exposure of molybdenum without iron due to the layer structure of the atoms presented within the $Fe_2(MoO_4)_3$ structure (Chapter 1).

The catalysts with a higher ratio than those predicted are those prepared by other methods. Again this may be no surprise for the catalysts involving a filtering and washing step, where the iron ratio may be lowered due to loss of that remaining in solution or being washed off. The high pH preparation again presents a high molybdenum ratio, suggesting that the amorphous/small extra iron structure predicted from XRD (Figure 3-55) is buried within the sample, leaving a high molybdenum signal to be observed.

The catalyst prepared using $FeCl_3$ was also studied for Cl by XPS spectra (Appendix A-32), with none observed, showing that this either remained in solution during the precipitation or was removed from the surface region by the washing steps following filtration.

### 3.3.8.4 STEM and EELS

Studying the catalyst particles of $Fe_2(MoO_4)_3$ by electron microscope provides some useful images and details on the structure of the particles. The most easily visible of these are voids (Figure 3-59). In the bright field image these present themselves as lighter areas and in the dark field image (where the contrast is more favourable) as darker areas. These voids are holes contained within the catalyst particle, so while they also have a surface area, this is not useful for catalysis, as gas would have to pass through the solid to reach these areas.

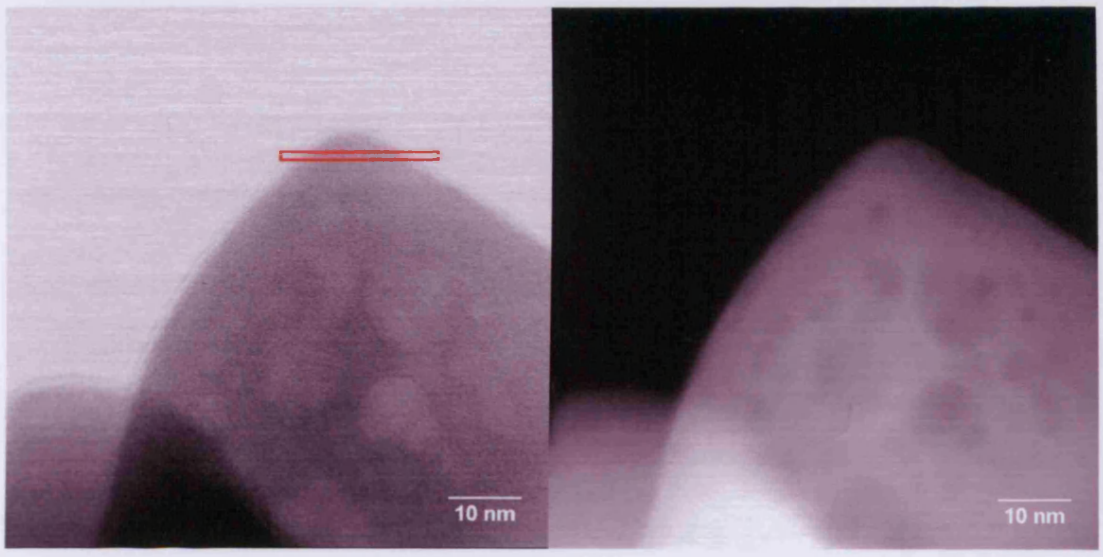


**Figure 3-59 - Images of Mo:Fe 1.5:1, before taking spectral image a) Bright field b) HAADF.**

EELS data was gained in a line profile (shown in Figure 3-59) to study the relative concentration of the elements present. After this further images were taken, and these showed a contamination of carbon of approximately 3-5 nm (Figure 3-60). As explained in the experimental chapter this is a common problem with STEM measurements when volatile organics are present. The most likely organic in this case is the ethanol used to clean the tweezers for the handling on the grid onto which the sample was placed. The presence of an increasing carbon contamination layer made interpretation of the EELS data more complicated as the peak edges of Mo and C are close in energy at ~300 eV. This made finding the edge of the particle and the carbon contamination layer complicated. To remove the carbon and allow for more quantifiable EELS data, the sample was subjected to heat treatement *in-situ* to desorb the contaminating species.

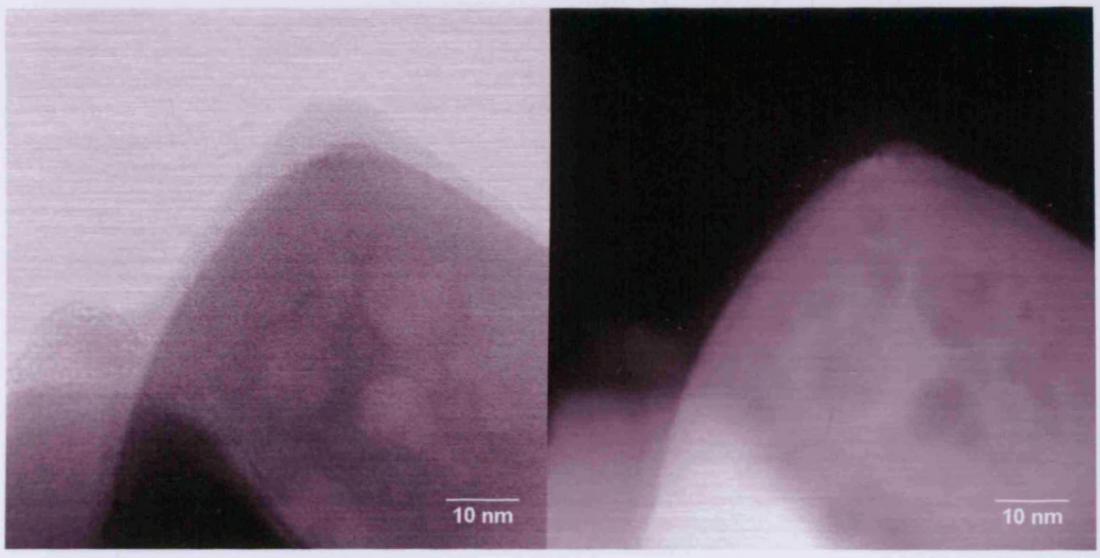


**Figure 3-60 - Images of Mo:Fe 1.5:1, after taking spectral image a) Bright field and b) HAADF.**

Following this cleaning procedure a further suitable region was found to scan (Figure 3-61). Again some voids are visible in the $Fe_2(MoO_4)_3$ particle, which is approximately 40 x 40 nm. EEL spectra were taken in a line profile across the catalyst in the area marked in red. These can then be converted into relative amounts of the elements present (Figure 3-62). While the absolute values of these may not be correct (note in the middle of the particle the measured Mo:Fe ratio is 1:3, whereas to satisfy the stoichiometry this should be 3:2), this should not take away from the usefulness of the data. Clearly visible at both ends of the line spectra are increases in the molybdenum content, with a decrease in iron. The data shown here is for one line profile only, but a further vertical line profile on this particle and on other particles showed similar results.

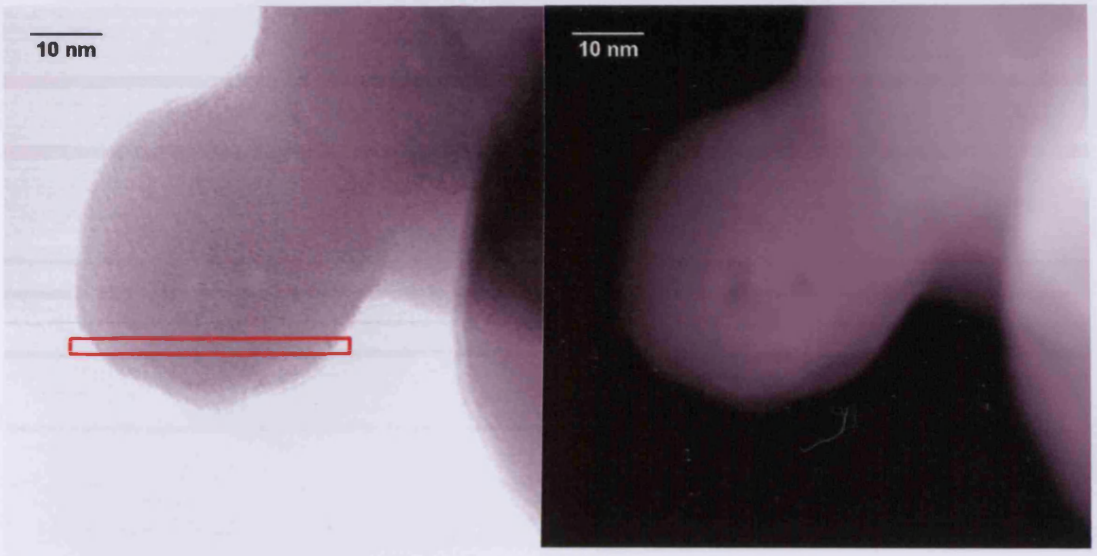


**Figure 3-61 - Images of a Mo:Fe 1.5:1 particle a) Bright Field, b) HAADF.**

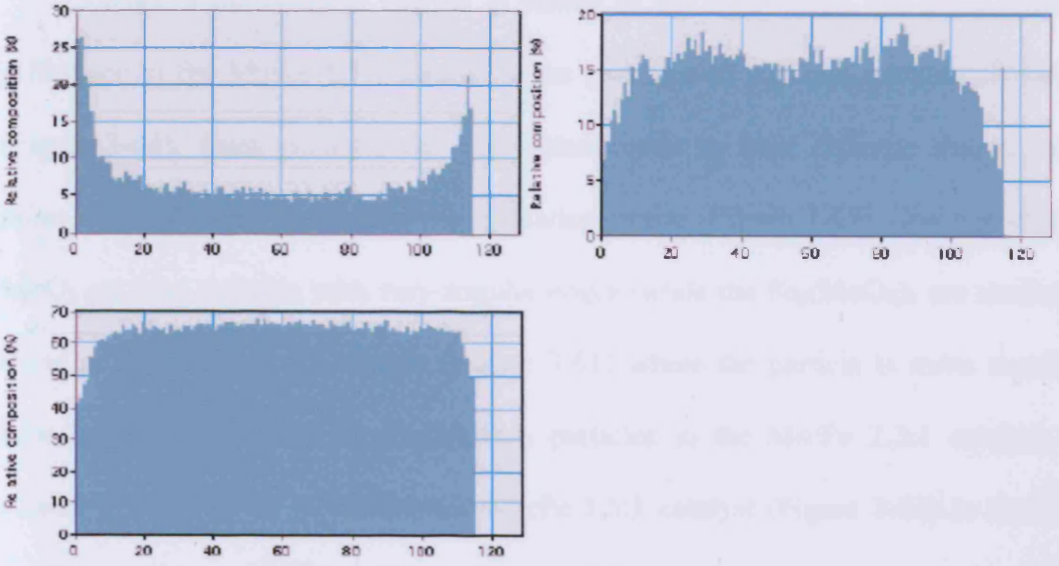

**Figure 3-62 - Relative composition of elements as measured by EELS a) Molybdenum, b) Iron and c) Oxygen.**

Some damage was caused by the electron beam itself as evidenced by microscope images (Figure 3-63). The damage presents itself as a line along the scan direction within the particle and is caused by hole drilling. In oxide particles, this is usually due to ionisation, where oxygen atoms are released from their bonds, group together as bubbles, and then burst to the surface[35].

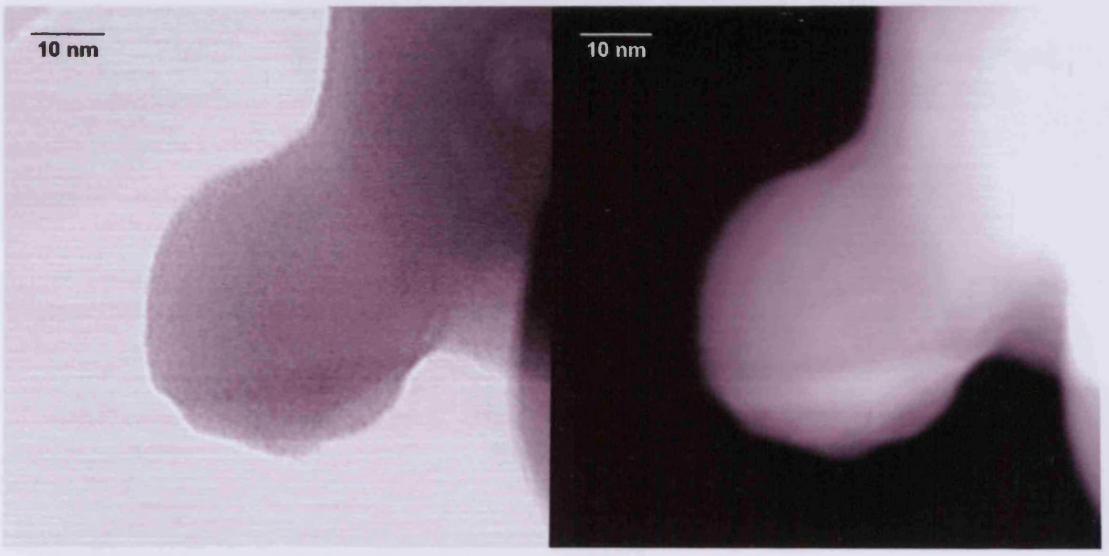


**Figure 3-63 - Images of a Mo:Fe 1.5:1 particle after EELS a) Bright Field, b) HAADF, showing the line where previous EELS data was obtained.**

When a Mo:Fe 2.2:1 sample is placed in the microscope, the most obvious difference to the Mo:Fe 1.5:1 sample is the presence of separate particles of $MoO_3$ (Figure 3-64). These particles are easily identifiable by their different shapes, as is more obviously seen in a lower magnification image (Figure 3-65). The particles of $MoO_3$ are long and thin with very angular edges, while the $Fe_2(MoO_4)_3$ are similar to those in the Mo:Fe 1.5:1 sample (Figure 3-61) where the particle is more rounded. Line profile EELS data for $Fe_2(MoO_4)_3$ particles in the Mo:Fe 2.2:1 catalyst are similar to those in the stoichiometric Mo:Fe 1.5:1 catalyst (Figure 3-62) in that they too show an increase in Mo in the surface region.

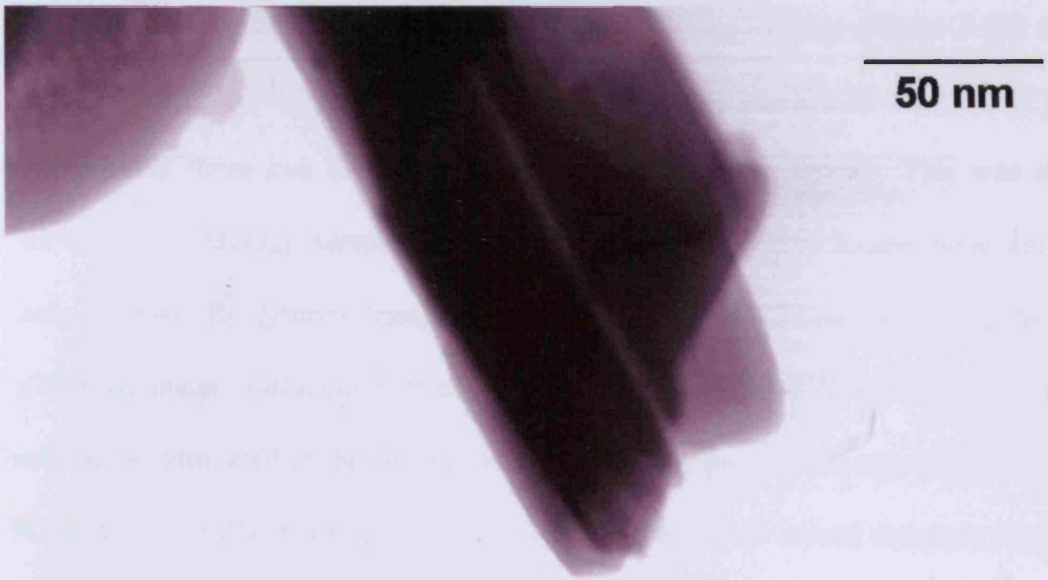


**Figure 3-64 - Bright field image of a $MoO_3$ particle within a Mo:Fe 2.2:1 catalyst.**

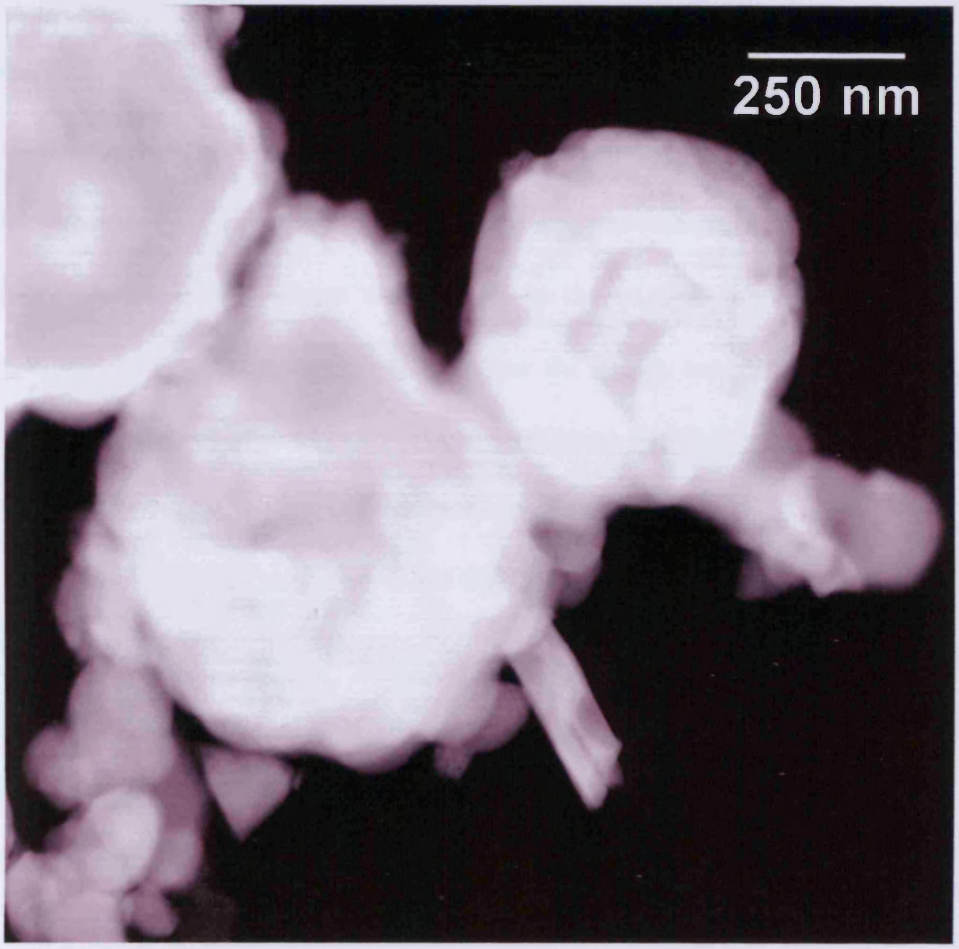


**Figure 3-65 - Low magnification HAADF imagine of Mo:Fe 2.2:1**

High resolution images were taken of both an $Fe_2(MoO_4)_3$ (Figure 3-66) and $MoO_3$ particle (Figure 3-67)), with lattice planes clearly visible. In the case of the $MoO_3$ particle these can be seen going to the edge of the sample. This was also observed in $Fe_2(MoO_4)_3$ samples, but the lattice planes in these images were not so clearly defined. By Fourier transform filtering the lattice planes shown in the α-$Fe_2(MoO_4)_3$ image, distances between planes of 9.5 and 15.4 Å can be calculated. These can be compared to the distance within the lattice parameters of a = 15.693 Å, b = 9.235 Å, c = 18.218 Å and β = 125.21 ° for the monoclinic crystal structure (shown in Chapter 1)[36], showing the planes image most likely correspond with the a and b distances.

Fourier transform fitting of the $MoO_3$ image shows planes primarily in one direction, with a distance between planes of 14.1 Å. The lattice parameters of the orthorhombic α-$MoO_3$ structure (shown in Chapter 3) are a = 3.962 Å, b = 13.858 Å and c = 3.607 Å[37], so the measured value corresponds with the 010 face. The lattice planes shown in this image are parallel to the surface presented meaning the face presented here will be the 010 face. When the highly magnified image (Figure 3-67) of $MoO_3$ is shown in lower magnification (Figure 3-64) it can be seen that the crystal is long and angular, with a high proportion of the 010 face showing.

The data provided from these STEM experiments is very interesting because it has previously been suggested that iron molybdates have a monolayer of $MoO_3$ at the surface[29], but here a molybdenum enrichment is directly observed by a spectroscopic method with nanoscale resolution. This fits with other data shown in this thesis, which also shows molybdenum enrichment through Raman, XPS and reactor studies.

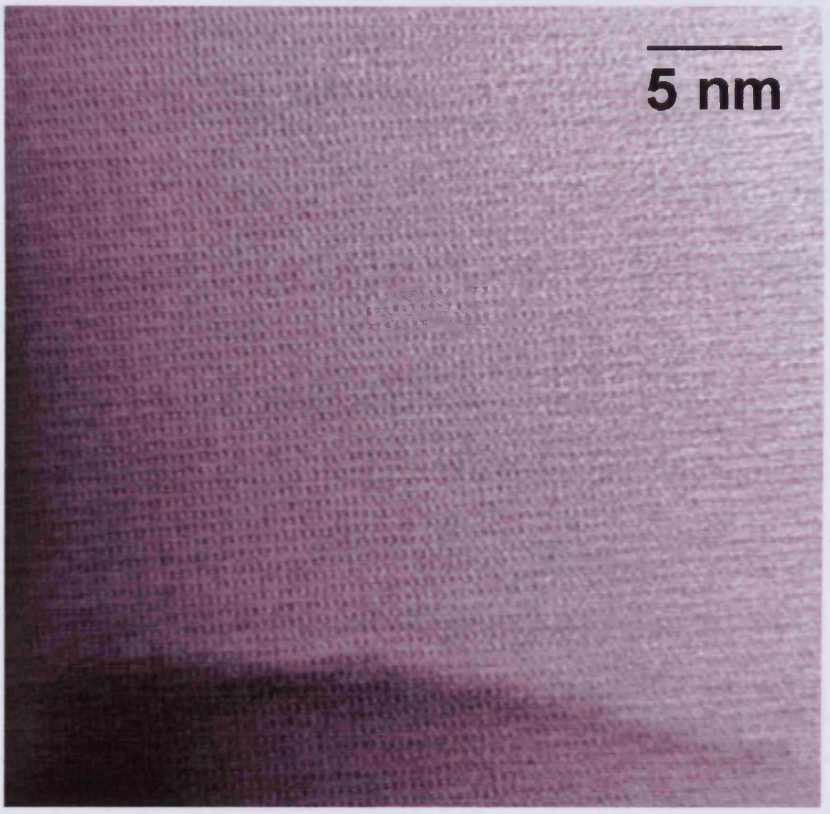


**Figure 3-66 - High Magnification bright field image of $Fe_2(MoO_4)_3$ particle.**

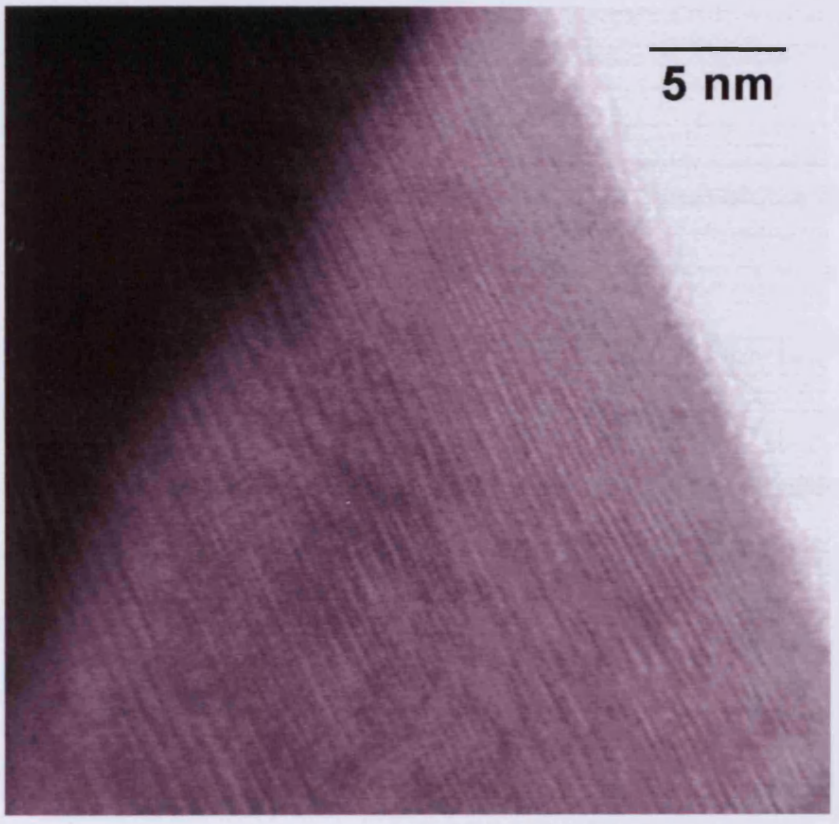


**Figure 3-67 - High Magnification bright field image $MoO_3$ particle.**

## 3.4 Conclusions

It has been demonstrated that the single metal oxide of $Fe_2O_3$ is selective purely for $CO_2$ and $H_2$, *via* a formate intermediate, $MoO_3$, $Fe_2(MoO_4)_3$ and $Fe_2(MoO_4)_3.1.4MoO_3$ are selective primarily to formaldehyde and water *via* a methoxy intermediate.

The performance of single phase $Fe_2(MoO_4)_3$ (Mo:Fe 1.5:1) is worse than that of the mixed phase $Fe_2(MoO_4)_3.1.4MoO_3$ (Mo:Fe 2.2:1) with a higher production of CO and $CO_2$. CO and $H_2$ oxidation were both shown to proceed at a higher activity on $Fe_2(MoO_4)_3$ than on $MoO_3$, due to the greater strength of Mo-O bonds within $MoO_3$.

It was also established that the preparation of a Mo:Fe 2.2:1 catalyst by evaporating to dryness leads to catalytic performance that is very similar to that shown by the industrial Perstorp KH 26 catalyst. A catalyst made using the ferric chloride and washing and drying steps (the same as used to produce the industrial catalyst) yielded a catalyst with lower activity due to a lower surface area.

The work in the early part of this chapter established that the temperature programmed pulsed flow experimental method used was suitable and compared well to continuous flow conditions, and isothermal pulsed conditions. The slight increase in conversion noted with the continuous flow conditions was ascribed to a constant methanol concentration in the gas flow leading to lower valency molybdenum sites, which are more active. Activity and selectivity of the catalyst were similar and while there was a slight drop in formaldehyde yield for the periods tested in isothermal conditions.

Variation of the catalyst loading has established that formaldehyde is produced as the primary product from methanol oxidation, while the production of CO and $CO_2$ are produced in further consecutive reactions.

Study of water lagging suggests that hydroxyl recombination is a slow step in the reaction process. Use of deuterated methanol, increased the lifetime of methoxy intermediates on the surface, and increased of the formation of dimtheyl ether, which as a coupling reaction, does not involve a O-D bond breaking process in the rate limiting step, unlike formation of formaldehyde.

Characterisation of the catalysts showed the single oxides to be present as α-$Fe_2O_3$ and α-$MoO_3$, while a Mo:Fe 1.5:1 formed the stoichiometric α-$Fe_2(MoO_4)_3$, and a catalyst made with Mo:Fe 2.2:1 had phases of both α-$Fe_2(MoO_4)_3$ and α-$MoO_3$ present. Raman analysis of the samples showed similar results, but also showed the presence of bands associated with both $Fe_2(MoO_4)_3$ and $MoO_3$ in the Mo:Fe 1.5:1 catalyst. XPS studies showed no obvious molybdenum enrichment, but this was clearly demonstrated with STEM/EELS experiments. TPD data also shows all molybdenum containing catalysts to contain $MoO_3$ at the surface as only formaldehyde and water are observed.

Iron molybdates have been prepared by different methods, all showing similar selectivity, while activity was based mainly on surface area. If a washing step was used in the catalyst, then the level of iron present seemed to decrease, while preparation at high pH left a surface with high molybdenum content and a small amorphous phase of excess iron.

## 3.5 References

(1) Liberti, G.; Pernicone, N.; Soattini, S. *Journal of Catalysis* **1972**, *27*, 52.
(2) Soares, A. P. V.; Portela, M. F.; Kiennemann, A. *Catalysis Reviews - Science and Engineering* **2004**, *47*, 125.
(3) Hill, C. G., Jr.; Wilson, J. H., III. *Journal of Molecular Catalysis* **1990**, *63*, 65.
(4) Trifiro, F. *Catalysis Today* **1998**, *41*, 21.
(5) Machiels, C. J.; Chowdhry, U.; Harrison, W. T. A.; Sleight, A. W. *ACS Symposium Series* **1985**, *279*, 103.
(6) Villa, P. L.; Szabo, A.; Trifiro, F.; Carbucicchio, M. *Journal of Catalysis* **1977**, *47*, 122.

(7) Soares, A. P. V.; Portela, M. F.; Kiennemann, A.; Millet, J. M. M. *Reaction Kinetics and Catalysis Letters* **2002**, *75*, 13.
(8) Chellappa, A. S.; Viswanath, D. S. *Industrial & Engineering Chemistry Research* **1995**, *34*, 1933.
(9) Maiti, G. C.; Malessa, R.; Baerns, M. *Thermochimica Acta* **1984**, *80*, 11.
(10) Jacques, S. D. M.; Leynaud, O.; Strusevich, D.; Beale, A. M.; Sankar, G.; Martin, C. M.; Barnes, P. *Angewandte Chemie, International Edition* **2006**, *45*, 445.
(11) Al-Shihry, S. S.; Halawy, S. A. *Journal of Molecular Catalysis A: Chemical* **1996**, *113*, 479.
(12) Otsuka, K.; Wang, Y.; Yamanaka, I.; Morikawa, A.; Sinev, M. Y. *Studies in Surface Science and Catalysis* **1994**, *81*, 503.
(13) Arnoldy, P.; De Jonge, J. C. M.; Moulijn, J. A. *Journal of Physical Chemistry* **1985**, *89*, 4517.
(14) Tkachenko, E. V.; Gur'ev, A. V.; Mikhailov, B. V. *Izvestiya Akademii Nauk SSSR, Metally* **1976**, 26.
(15) Ressler, T.; Wienold, J.; Jentoft, R. E.; Girgsdies, F. *European Journal of Inorganic Chemistry* **2003**, 301.
(16) Guidot, J.; Germain, J. E. *Reaction Kinetics and Catalysis Letters* **1980**, *15*, 389.
(17) Smith, R. L.; Rohrer, G. S. *Journal of Catalysis* **1998**, *173*, 219.
(18) Ressler, T.; Wienold, J.; Jentoft, R. E.; Neisius, T. *Journal of Catalysis* **2002**, *210*, 67.
(19) Machiels, C. J.; Sleight, A. W. *Journal of Catalysis* **1982**, *76*, 238.
(20) Chung, J. S.; Miranda, R.; Bennett, C. O. *Journal of Catalysis* **1988**, *114*, 398.
(21) Glisenti, A.; Favero, G.; Granozzi, G. *Journal of the Chemical Society, Faraday Transactions* **1998**, *94*, 173.
(22) Chowdhry, U.; Ferretti, A.; Firment, L. E.; Machiels, C. J.; Ohuchi, F.; Sleight, A. W.; Staley, R. H. *Applications of Surface Science* **1984**, *19*, 360.
(23) Stark, J. G.; Wallace, H. G. *Chemistry Data Book*, 2nd ed.; John Murray Ltd, **1982**.
(24) Ressler, T.; Timpe, O.; Neisius, T.; Find, J.; Mestl, G.; Dieterle, M.; Schlogl, R. *Journal of Catalysis* **2000**, *191*, 75.
(25) JCPDS Card Number 35-659.
(26) JCPDS Card Number 33-664.
(27) JCPDS Card Number 31-642.
(28) Alcolado, M. L. P. PhD, University of Cardiff, **2000**.
(29) Burcham, L. J.; Briand, L. E.; Wachs, I. E. *Langmuir* **2001**, *17*, 6175.
(30) Briand, L. E.; Hirt, A. M.; Wachs, I. E. *Journal of Catalysis* **2001**, *202*, 268.
(31) del Arco, M.; Carrazan, S. R. G.; Martin, C.; Martin, I.; Rives, V.; Malet, P. *Journal of Materials Chemistry* **1993**, *3*, 1313.
(32) Hu, H.; Wachs, I. E. *Journal of Physical Chemistry* **1995**, *99*, 10911.
(33) Briggs, D.; Seah, M. P. *Practical Surface Analysis*, 2nd ed.; John Wiley and Sons, **1993**; Vol. 1.
(34) Nguyen Van, T.; Tittarelli, P.; Villa, P. L. *Chem. Uses Molybdenum, Proc. Int. Conf., 3rd* **1979**, 161.
(35) Keyse, R. J.; Garratt-Reed, A. J.; Goodhew, P. J.; Lorimer, G. W. *Introduction to Scanning Transmission Electron Microscopy*; BIOS Scientific Publishers, **1998**.
(36) Rapposch, M. H.; Anderson, J. B.; Kostiner, E. *Inorganic Chemistry* **1980**, *19*, 3531.
(37) Kihlborg, L. *Arkiv foer Kemi* **1963**, *21*, 357.

# 4 Anaerobic Reaction of Methanol and Reaction with Reduced Phases

## 4.1 Introduction

As was discussed in the first chapter, the reaction of methanol to formaldehyde and water over iron molybdates is an oxidative dehydrogenation process that proceeds *via* the Mars - van Krevelen mechanism, with oxygen from the catalyst lattice used to produce the formaldehyde and water[1,2]. The role of gaseous oxygen is therefore to re-oxidise the catalyst surface after product formation has occurred. This chapter sets out to investigate the effects of not having this gaseous oxygen present on both the catalytic activity and structural effects.

The effect of reducing iron molybdates has been studied previously and a TPR profile of an iron molybdate catalyst with excess molybdena by hydrogen showed five peaks, at 580, 637, 679, 741 and 950 °C[3]. These represent transformation of $Fe_2(MoO_3)_4$ to β-$FeMoO_4$ and $Mo_4O_{11}$ (580 °C), $MoO_3$ to $MoO_2$ (673 °C), $Mo_4O_{11}$ to $MoO_2$ and most of the β-$FeMoO_4$ to $Fe_2Mo_3O_8$ and $Fe_3O_4$ (679 °C). In the fourth transformation (741 °C) β-$FeMoO_4$ was completely reduced and an Fe-Mo alloy was formed; the fifth peak (950 °C) was due to the reduction of all the metal oxide species with the products detected as $Fe_3Mo$ alloy and metallic molybdenum.

*In-situ* SEM under reaction conditions using $CH_3OH$, $CH_3OH$-$O_2$ and $H_2$ has shown that ferric molybdates are reduced by two or possibly three reaction routes simultaneously[4]. These occur *via* β-$FeMoO_4$ and α-$Fe_2O_3$ (and/or a spinel of $Fe_2MoO_4/Fe_3O_4$). The reduction was, however, limited by the presence of gaseous oxygen. The formation of β-$FeMoO_4$ was also observed by an *in-situ* Raman study using methanol as the reductant, but the possibility that α-$FeMoO_4$ was also formed could not be eliminated in this study[5]. With an aerobic exposure to methanol at 300 °C, a colour change from green-yellow to black occurred within the catalyst, with Raman scattering so weak in comparison to the background for the reduced catalyst,

that no spectra could be taken. Subsequent reoxidation at 300 °C followed by cooling to room temperature showed a Raman spectra dominated by bands for $MoO_3$[5], suggesting the $MoO_3$ phase formed was more easily reoxidised than that of $Fe_2(MoO_4)_3$. Reduction of an iron molybdate catalyst at 350 °C leads to the formation of only β-$FeMoO_4$ with methanol and β-$FeMoO_4$ and $MoO_2$ with 1-butene in nitrogen environments[6]. It has been suggested that $FeMoO_4$ is considerably less active in methanol oxidation than $Fe_2(MoO_4)_3$[7].

The level of lattice oxygen usage by the anaerobic pulsed reduction of toluene over iron molybdate catalysts at 350 °C (Fe-Mo ratio of 1:1), was found to be much greater with ultra fine particles produced by a sol-gel method than for the larger particles produced by co-precipitation[8]. The reaction of pre reduced iron molybdate ($H_2$ at 600 °C), produced a catalyst that was active for the hydrogenation of CO, and was stable towards carburisation[9].

The oxidation of $FeMoO_4$ can occur in three ways. With an excess of $MoO_3$ present it will form the ferric molybdate phase (Equation 4-1), however if this excess $MoO_3$ is not present, oxidation will lead to the formation of $Fe_2O_3$ (Equations 4-2 and 4-3)[10-12]. Of the reactions producing $Fe_2O_3$, it was speculated that it is most likely that α-$FeMoO_4$ will lead to the production of $Fe_2(MoO_4)_3$, as $Mo^{6+}$ is in octahedral coordination in both, while β-$FeMoO_4$ will lead to the production of $MoO_3$, as the $Mo^{6+}$ is in tetrahedral coordination in both. These reactions would also lead to a build up of $Fe_2O_3$, which is observed on the outside of used industrial pellets, though the authors state that the increase in iron concentration at the surface is also due to volatilisation of molybdenum.

$$2\ FeMoO_4 + 1/2\ O_2 + MoO_3 \rightarrow Fe_2(MoO_4)_3 \qquad (4\text{-}1)$$

$$3\ FeMoO_4 + 3/2\ O_2 \rightarrow Fe_2(MoO_4)_3 + 1/2\ Fe_2O_3 \qquad (4\text{-}2)$$

$2\ FeMoO_4 + 1/2\ O_2 \rightarrow Fe_2O_3 + MoO_3$ (4-3)

Reduction of the bulk material has been reported at temperatures above 230 °C using methanol, with the subsequent reoxidation procedure only beginning at temperatures of above 270 °C[13]. Different authors found β-$FeMoO_4$ oxidation to begin at 180 °C and was complete by 310 °C, while α-$FeMoO_4$ needs higher temperatures and is not complete until 355 °C[14]. A more recent ultra-fast diffraction study showed that reduction with hydrogen occurred much more slowly (not complete after 36 minutes) than reoxidation (complete after 15 seconds) at 472 °C, where β-$FeMoO_4$ was the reduced phase formed[15].

The reduction of $MoO_3$ by methanol in the absence of oxygen at 200 °C has been shown to form a bronze $H_xMoO_3$ in the first few layers[16]. This bronze has also been observed when $MoO_3$ is placed under UHV with $10^{-8}$ Torr $H_2$ heated by a tungsten filament to generate atomic hydrogen. The formation of these bronzes occurs in an identical way on the $MoO_3$ (010) surface face for reaction of methanol and from atomic H produced by "spill-over" from supported Pt particles[17]. The $H_xMoO_3$ phase forms topotactically and is aligned along the 203 direction of the $MoO_3$ (010) face. If $MoO_3$ is heated further in $H_2$, then after incorporation of $H_2$ into the bulk to form the bronze, the bronze will be consumed to form nucleation sites for $MoO_2$ formation, before the nucleation and nuclei growth of $MoO_2$ occurs[18]. Mo bronze formation occurs during the dissociative chemisorption of the methanol, but this study was unable to eliminate the possibility of formation also occurring during hydrogen abstraction from the methoxy group[16]. Hydrogen reduction of bulk $MoO_3$ at atmospheric pressure has been shown to form a bifunctional phase of $MoO_2(H_x)_{ac}$ on the surface of $MoO_2$ between temperatures of 350 and 400 °C[19].

The level of reduction of a $MoO_3$ sample helps dictate the activity and selectivity of $MoO_3$ in its reaction with 2-butanol[20]. Where reduction is stabilised through bulk Mo sub oxide phases ($MoO_3$ with sheer planes), oxygen exchangeability is lowered, so dehydration of the 2-butanol is observed (*i.e.* oxygen is not transferred to the hydrocarbon *via* the Mars - van Krevelen mechanism). When only the surface is reduced however with the presence of $Mo^{5+}$ species, exchangeability of lattice oxygen in the surface layer is enhanced, with total oxidation to $CO_2$ and water observed.

When a thin film of $MoO_3$, supported on $Al_2O_3$ is reduced through repeated methanol TPD, a feature at ~1000 $cm^{-1}$ correlating to Mo=O loses intensity with respect to the Mo-O-Mo modes at ~800 $cm^{-1}$ [21]. This loss of terminal oxygen occurred simultaneously with the rise of a feature at ~1.8 eV in HREELS, associated with a *d-d* transition in $MoO_2$. Heating of the sample to 527 °C lead to auto oxidation of the sample and the recovery of the feature at ~1000 $cm^{-1}$. This is in contrast to other work which suggests that preferential loss of bridging oxygen occurs during the formation of oxygen vacancies by ion bombardment on the $MoO_3$ (010) surface[22]. The oxygen vacancies formed lead to the reduction of neighbouring molybdenum sites with an increase in metal d occupation and corresponding computed density of states contributions above the O 2sp region.

With $MoO_3$ it is thought that below ~327 °C, participation of O from the bulk is negligible in a redox process, whereas between ~327 and 427 °C O vacancy diffusion makes the redox mechanism possible, with partially reduced $MoO_3$ observed under reaction conditions with propene[23]. At temperatures above ~427 °C there is sufficiently fast O diffusion from the lattice combined with rapid formation and destruction of crystallographic sheer planes that considerable lattice O can be used for partial oxidation.

Isotopic exchange experiments using $C^{18}O_2$ have shown that the basal (010) face of $MoO_3$ is a more rapid oxygen exchanger at 350 °C than samples with more lateral faces (truncated (110), (120) and (130) planes)[24]. This is related to the presence of oxygen vacancies on the (010) face, which cannot be filled by oxygen coming from the bulk of the $MoO_3$ structure. With a higher temperature (500 °C) and longer running time, a continuous oxygen exchange reaction occurs, especially for the samples with more lateral faces, with two contributions to this exchange reaction being distinguishable. Firstly, there is a fast surface oxygen exchange and secondly (more prominently in the sample with (100) faces) is the migration of oxygen from the lateral towards basal faces and/or to a slow migration of oxygen atoms from the bulk structure of $MoO_3$ towards the lateral faces.

A TPR study of $MoO_3$ and $MoO_2$ showed that reduction of these samples can be greatly affected by experimental parameters such as water concentration[25]. The reduction of $MoO_3$ to Mo occurred mainly in a two step process, with $MoO_2$ the only intermediate. Hydrogen dissociation was found to be a critical step in the reduction mechanism and was catalysed by low valent Mo atoms. Reduction of $MoO_3$ to $MoO_2$ was generally catalysed, except when there were insufficient sites, when oxygen diffusion became rate limiting. Two separate catalytic rate determining steps were observed: through auto catalysis when the number of sites was still limited, or Mo-O bond breaking when excess sites were present.

$Mo_4O_{11}$ is observed from the reduction of $MoO_3$ in the presence of 5 vol % $H_2$ at 500 °C[26]. Most notably, $Mo_4O_{11}$ forms after $MoO_2$ is observed as it is not directly formed from the reduction of $MoO_3$, but is instead formed from the solid state reaction between $MoO_3$ and $MoO_2$.

Oxidation of methanol and formaldehyde over $Fe_2O_3$ at 220 °C in anaerobic and aerobic conditions showed similar pathways for both conditions[27], leading to the formation of $CO_2$, with $H_2$ in the anaerobic, and $H_2O$ in the aerobic conditions. The difference in hydrogen products observed was ascribed to further reaction of the $H_2$ in the aerobic conditions. Oxygen equivalent to at least two surface layers was removed in anaerobic conditions, when heating cycles up to 400 °C, were employed between methanol doses.

The ease of reducibility has been shown to be in the order $Fe_2O_3$>$Fe_2(MoO_4)_3$>$MoO_3$, leading to the suggestion that the mobility of the oxygen ions within the oxides follows the same order with the highest mobility in $Fe_2O_3$ and lowest in $MoO_3$[28].

To investigate further the reactivity of iron molybdates in anaerobic conditions, a number of pulses of methanol were passed over the catalyst surface at different temperatures. The reactivity of the catalyst for the first pulse is compared to that seen in aerobic conditions. From the data acquired in anaerobic conditions it was possible to calculate the oxygen removed from the sample. The structural and catalytic changes in the catalyst with this oxygen loss are also investigated.

The single oxides of $MoO_3$ and $Fe_2O_3$ are briefly investigated with temperature programmed experiments to monitor changes in activity and product selectivity with no gaseous oxygen present. These were compared to the results obtained for the 2.2:1 Mo:Fe catalyst, which contained phases of both $Fe_2(MoO_4)_3$ and $MoO_3$.

If the iron molybdate is to lose large amounts of oxygen from the lattice, then different structures will be formed. To gain an understanding of this, commercially sourced $MoO_2$ and $FeMoO_4$ were studied for their reactivity towards methanol

oxidation. The catalytic and structural effects of oxidation on these compounds were also investigated.

## 4.2 Experimental

The majority of the work in this chapter concerns the Mo:Fe 2.2:1 catalyst, which is subjected to reduction in different ways, and was prepared by the standard preparation described in the experimental chapter (Section 2.2.2). This catalyst is compared with the Mo:Fe 1.5:1 catalyst and the commercially sourced $MoO_3$ and $Fe_2O_3$. The reductions were carried out with helium as the flow gas. The TPPFR experiments were conducted with a flow rate of 30 ml $min^{-1}$, 1 μl injections of methanol every 2 minutes and a ramp rate of 8 °C $min^{-1}$, while the IPR were conducted with the same flow and repeat rate, but with no temperature ramp. One exception to this was an extended reduction of the Mo:Fe 2.2:1 material, which was carried out at 350 °C, and used 3 μl methanol injections, with a repeat rate of every two minutes.

The TPD experiments were performed according to the same procedure laid out in the experimental section (Section 2.3.2).

The reduced phases of $MoO_2$ (Alfa Aesar, 99.95 %) and $FeMoO_4$ (Aldrich) were heated to 400 °C in a He flow before an initially TPD. When the TPD was complete, the gas flow was changed to the 10 % $O_2$/He mix over the bypass, before TPPFR took place. For these first TPPFR (following standard procedures, Section 2.3.2), the catalysts were not preheated in the $O_2$/He mix as this would have lead to the oxidation of the catalysts. Subsequent TPPFR did include the preheating treatment as described in the experimental chapter (Section 2.3.2).

### 4.2.1 Calculation of Oxygen Removal

The level of oxygen removal from the catalyst was calculated from the yield of each product. The formation of oxidised products (e.g. $CO_2$) requires the use of lattice oxygen, while formation of other products requires only the oxygen within the methanol molecule (e.g. CO). The removal of oxygen was calculated by using the number in brackets as the number of O atoms required to form one molecule of product: $H_2$ (0), $H_2O$ (1), CO (0), $H_2CO$ (0), $CO_2$ (1), and $CH_3OCH_3$ (-1). As can be seen, for the purpose of calculations it was assumed the O from methanol stayed with the carbon of the molecule. By multiplying the amount of product formed by the amount of oxygen to form it, and totalling these results, the total oxygen removal could be obtained. This was converted into a percentage of the total oxygen within the catalyst by assuming all the iron formed $Fe_2(MoO_4)_3$, and in the case of the Mo:Fe 2.2:1 the excess formed $MoO_3$. (From the characterisation data in Chapter 3, this seems a good assumption). Monolayers of O were calculated by assuming each monolayer contained $10^{19}$ $m^{-2}$ oxygen atoms.

An example calculation for reduction at 330 °C is given below:

Methanol in each injection = 1 μl = $2.5 \times 10^{-5}$ mol

$CO_2$ formed = Σ [($CO_2$ selectivity x methanol conversion)/10000 x $2.5 \times 10^{-5}$ mol for each injection] = $2.2 \times 10^{-4}$ mol

Water formed = Σ [(18 amu integral – contribution from other compounds) x calibration factor] = $1.34 \times 10^{-3}$ mol

Dimethyl ether formation = 0 mol

Therefore total O usage = $2.2 \times 10^{-4}$ mol + $1.34 \times 10^{-3}$ mol – 0 mol = $1.56 \times 10^{-3}$ mol

Catalyst composition = $Fe_2(MoO_4)_3.1.4MoO_3$ therefore O = 32.7 w/t %, with 0.5 g catalyst loaded

O within sample = (32.7/100) x 0.5 g = 0.16 g = 1.0 x $10^{-2}$ mol

O lost = (1.56 x $10^{-3}$ mol/1.0 x $10^{-2}$ mol) x 100 = 15.2 %

Surface area = 6.7 $m^2$ $g^{-1}$, with assumed 1 x $10^{19}$ surface sites $m^{-2}$

Sites = 6.7 $m^2$ $g^{-1}$ x 1 x $10^{19}$ surface sites $m^{-2}$ x 0.5 g = 3.35 x $10^{19}$ sites = 5.6 x $10^{-5}$ mol

O removed = (1.56 x $10^{-3}$ mol / 5.6 x $10^{-5}$ mol) = 28.0 ML equivalent

## 4.3 Results and Discussion

### 4.3.1 Anaerobic TPPFR

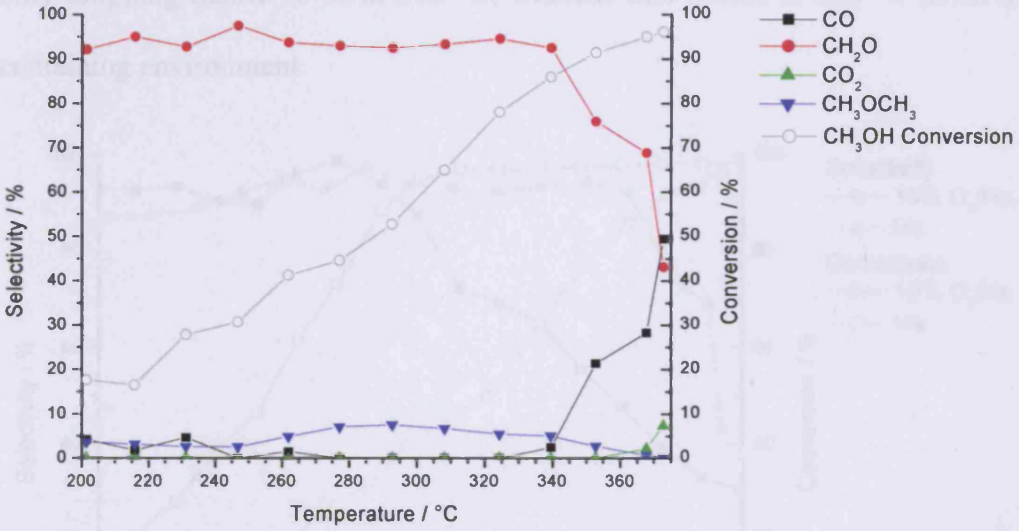


**Figure 4-1 - Selectivity and conversion for methanol oxidation over a 2.2:1 Mo:Fe catalyst in anaerobic TPPFR conditions.**

The temperature programmed pulsed flow reaction data for the Mo:Fe 2.2:1 catalyst in He alone (Figure 4-1, Appendix A-34) shows a catalyst which is highly selective (>90 %) to formaldehyde until 340 °C, where it drops rapidly to around 40 % by 380 °C. The main non-selective product that forms is CO, with production rising from zero at 320 °C, to 50 % by 380 °C. Little $CO_2$ is observed, with none observed until 360 °C, with less than 10 % seen, even by 380 °C. More dimethyl ether is

observed in these conditions than in aerobic conditions, with selectivity dropping from around 5 % at 200 °C to 3 % by 250 °C. This is followed by a further rise back to around 8 % by 290 °C, before declining back to zero by 380 °C.

Comparison of the reactor data in helium and helium/oxygen (Chapter 3) conditions shows that in helium alone the catalyst presents a much reduced activity (Figure 4-2 and Table 4-1). In the aerobic conditions 50 and 90 % conversions are reached at 210 and 260 °C, while in anaerobic conditions these are reduced to 280 and 340 °C respectively. It is also very noticeable that the catalyst in anaerobic conditions is able to produce formaldehyde with higher selectivity at more elevated temperatures, only dropping below 90 % at 340 °C, whereas this occurs at 250 °C in an oxygen-containing environment.

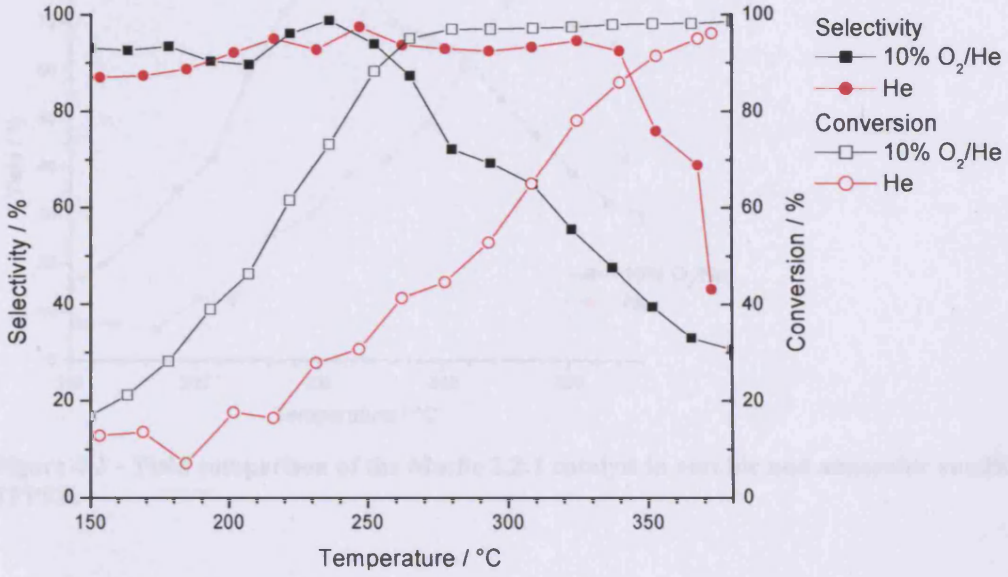


**Figure 4-2 – Methanol conversion and formaldehyde selectivity comparison of the Mo:Fe 2.2:1 catalyst in aerobic and anaerobic conditions for TPPFR.**

A comparative yield plot (Figure 4-3) shows that the difference in peak yield for these two conditions is not very large, with around 85 % for the aerobic conditions and 80 % for the anaerobic. The major difference comes in the corresponding peak

temperature, which is around 250 °C for the aerobic conditions and 340 °C for the anaerobic.

The decrease in activity of the catalyst in anaerobic conditions is most likely caused by a decrease in available surface oxygen, as the surface oxygen utilised in the oxidation can be replaced from the gas phase in the aerobic temperature programmed experiment. The increase in formaldehyde selectivity can be linked to the high oxygen demand of the non-selective products of CO and $CO_2$. Once partially reduced, it is likely the methoxy surface species has a longer residence time, as removal of oxygen becomes more difficult and this would explain the greater presence of the minor coupling product of dimethyl ether.

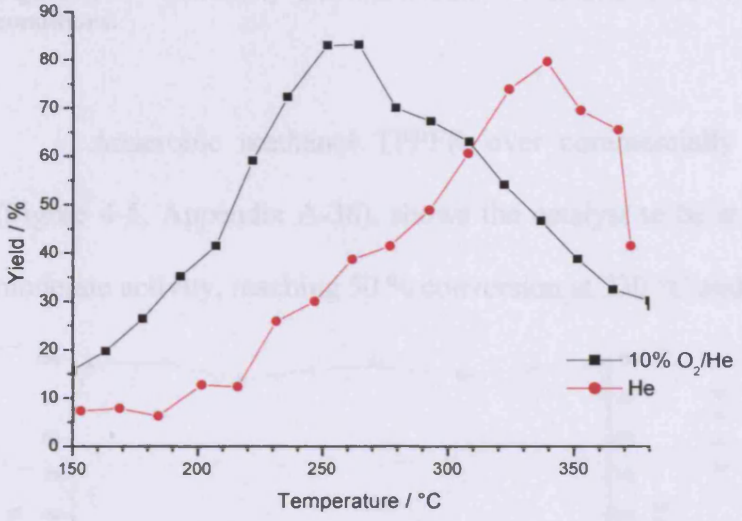


**Figure 4-3 - Yield comparison of the Mo:Fe 2.2:1 catalyst in aerobic and anaerobic conditions for TPPFR.**

An anaerobic TPPFR for $MoO_3$ (Figure 4-4, Appendix A-35), shows high formaldehyde selectivity at low temperatures, rising from around 85 % at 250 °C to 93 % at 295 °C, before dropping to near zero by 380 °C. The initial product to replace the formaldehyde is CO, which begins to be formed at 300 °C, rising to over 70 % of the products by 365 °C, before dropping back to around 60 % by 380 °C. Production of $CO_2$ is observed beginning at 340 °C, reaching nearly 40 % by 380 °C. Dimethyl ether

production is high at low conversions, with nearly 15 % selectivity at 250 °C, before dropping steadily to less than one percent by 360 °C. The activity of the catalyst is very low, reaching 50 and 90 % conversion at 330 and 375 °C respectively.

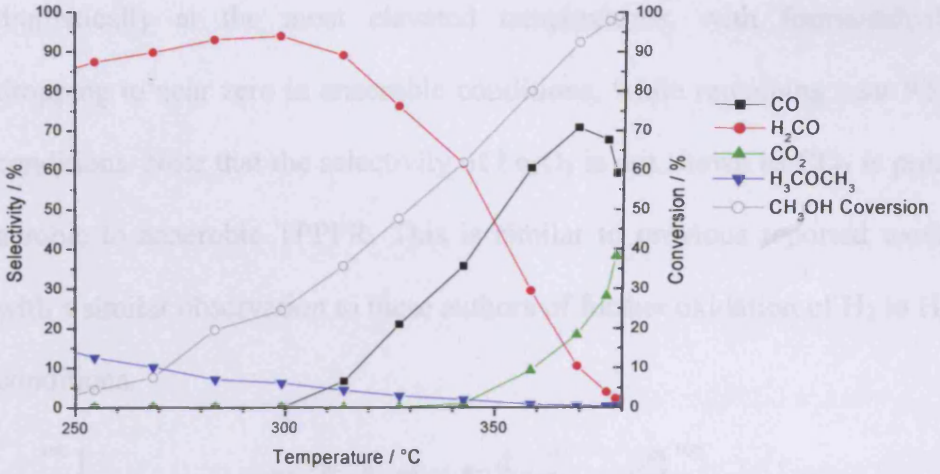


**Figure 4-4 - Selectivity and conversion for methanol oxidation over $MoO_3$ in anaerobic conditions.**

Anaerobic methanol TPPFR over commercially available (Aldrich) $Fe_2O_3$ (Figure 4-5, Appendix A-36), shows the catalyst to be selective to only $CO_2$, with a moderate activity, reaching 50 % conversion at 330 °C and 90 % at 360 °C.

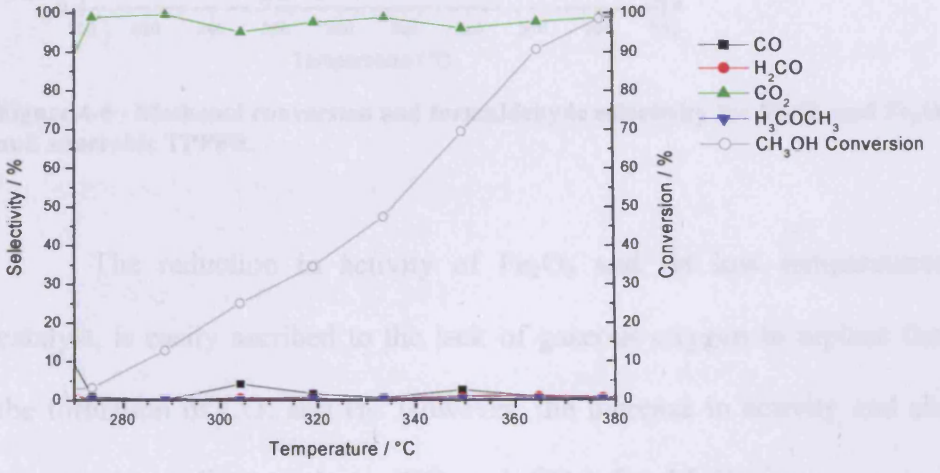


**Figure 4-5 - Selectivity and conversion for methanol oxidation over $Fe_2O_3$ (Aldrich) in anaerobic conditions.**

A comparison of the activities of both single metal oxides under anaerobic conditions with their performance in aerobic conditions (Chapter 3) shows that

activity for both is greatly reduced at lower temperatures (Figure 4-6). While at higher temperatures this remains the case for $Fe_2O_3$, the $MoO_3$ sample becomes more active at temperatures of 360 °C and above. The selectivity of the $MoO_3$ sample also changes dramatically at the most elevated temperatures, with formaldehyde selectivity dropping to near zero in anaerobic conditions, while remaining near 90 % in aerobic conditions. Note that the selectivity of $Fe_2O_3$ is not shown as $CO_2$ is produced in both aerobic to anaerobic TPPFR. This is similar to previous reported work on $Fe_2O_3$[27], with a similar observation to these authors of further oxidation of $H_2$ to $H_2O$ in aerobic conditions.

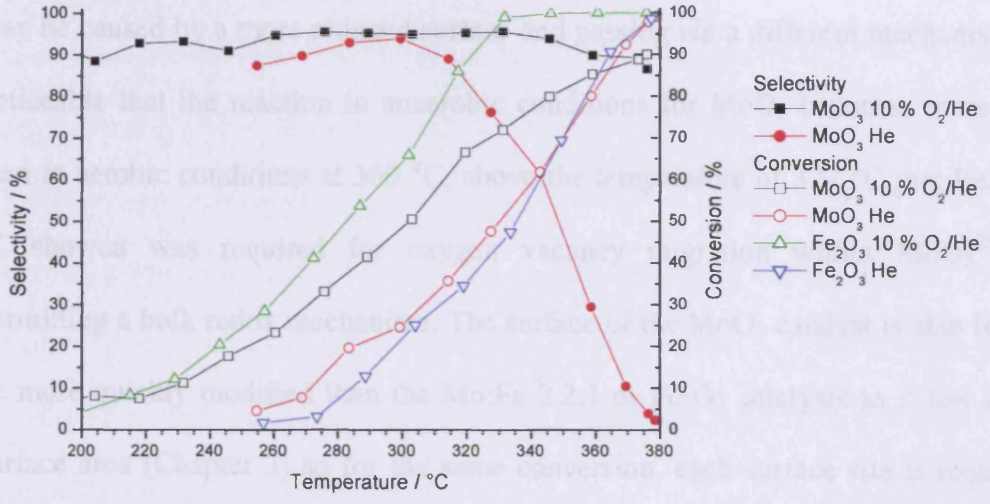


**Figure 4-6 - Methanol conversion and formaldehyde selectivity for $MoO_3$ and $Fe_2O_3$ in aerobic and anaerobic TPPFR.**

The reduction in activity of $Fe_2O_3$ and (at low temperatures) the $MoO_3$ catalyst, is easily ascribed to the lack of gaseous oxygen to replace that used within the formation of $CO_2$ and $H_2$. However, the increase in activity and change to more oxygen demanding products (CO and $CO_2$) for $MoO_3$ is more complicated. The change is most likely due to the formation of Mo surface sites reduced from the +6 oxidation state. Reduced molybdenum surface sites have previously been shown to be more active in hydrogen and 2-butanol oxidation, due to better absorption, and may be

working in a similar way here[20,25]. The idea is further enhanced when compared to catalytic data for $MoO_2$ (Section 4.4.1), which shows CO as a high temperature product with a direct pathway, not as a product of secondary oxidation of formaldehyde. This data is somewhat complicated by the oxidation of the material during the course of the reaction, so it is not possible to tell if $CO_2$ is a high temperature product off $MoO_2$. TPD suggests $CO_2$ is not a primary product (Figure 4-25), but it is possible that CO, like $H_2$ and $CH_3OH$ is easier to oxidise on this reduced molybdenum surface and so produces $CO_2$. It must also be remembered that with each injection the surface is becoming more reduced and the production of $CO_2$ may be caused by a more reduced surface and passing *via* a different mechanism. It is noticeable that the reaction in anaerobic conditions for $MoO_3$ becomes more active than in aerobic conditions at 360 °C, above the temperature of 327 °C that Ressler *et al.* showed was required for oxygen vacancy migration within $MoO_3$[23], thus permitting a bulk redox mechanism. The surface of the $MoO_3$ catalyst is also likely to be more quickly modified than the Mo:Fe 2.2:1 or $Fe_2O_3$ catalysts as it has a lower surface area (Chapter 3) so for the same conversion, each surface site is required to oxidise more methanol molecules; this will lead to a quicker surface reduction if oxygen migration through the bulk is slow.

### 4.3.2 Reduction profile at 200 °C

When the mixed phase catalyst is subjected to pulses of methanol in anaerobic conditions at 200 °C (Appendix A-37) the first pulse produces formaldehyde with a selectivity of near 100 %, with methanol conversion at around 30 %. The methanol conversion rapidly decreases and after 5 µl of methanol have been passed over the surface, the catalyst shows no activity to methanol conversion, with little observed, even with the second 1 µl injection. As the activity of the catalyst drops over these 5

pulses, the selectivity of formaldehyde drops from near 100 % to around 60 %, while selectivity to the other products of CO, $CO_2$ and dimethyl ether increases. While the selectivity decreases the yield of the products also decreases due to the lowering methanol conversion.

### 4.3.3 Reduction profile at 250 °C

The profile for anaerobic methanol oxidation at 250 °C (Figure 4-7, Appendix A-38) shows the activity of the catalyst drops quickly, with conversion dropping from nearly 75 % for the first injection to around 20 % after the fifth pulse. The methanol conversion continues to drop further reaching around 10 % after 60 µl of methanol have been passed over the surface. The selectivity of the catalyst to formaldehyde drops from 85 % in the first pulse to around 45 % after 15 injections. The drop in formaldehyde selectivity is mirrored by the rise in CO production, from 5 % in the first injection to around 40 % after 15 pulses. Dimethyl ether selectivity rises from around 3 % to around 8 % over the first five injections. A small amount of $CO_2$ is produced initially (around 5 % selectivity), but this drops away so that after the fourth injection, no more $CO_2$ is produced.

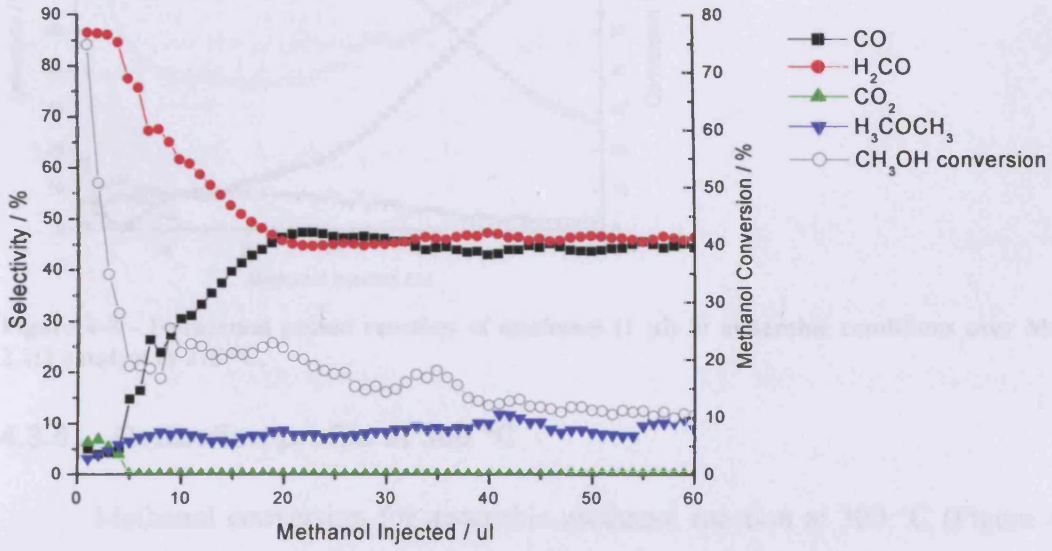


**Figure 4-7 - Isothermal pulsed reaction of methanol (1 µl) in anaerobic conditions over Mo:Fe 2.2:1 catalyst at 250 °C.**

### 4.3.4 Reduction profile at 275 °C

Methanol conversion at 275 °C starts high at around 90 % (Figure 4-8, Appendix A-39) before dropping to around 40 % after 7 pulses. The conversion remains approximately constant at 40 % until after 30 pulses it begins to rise to over 65 % by the 60$^{th}$ pulse. The selectivity to formaldehyde starts high at over 80 % and remains approximately stable until conversion begins to rise after the 30$^{th}$ pulse, when the selectivity drops to below 30 % by the 60$^{th}$ pulse. Selectivity to CO is around 17 % on the first pulse, which drops over the next 5 pulses to near zero, before slowly rising throughout the rest of the reaction, reaching over 70 % when the 60$^{th}$ pulse is made. $CO_2$ selectivity starts at around 7 %, rising to around 10 % for the following three pulses before dropping so that by the 13$^{th}$ pulse is made there is no $CO_2$ being produced. The minor product of DME starts with low (~1 %) selectivity, before passing through a maximum of 10 % after 15 pulses, before slowly diminishing so that by the 60$^{th}$ pulse selectivity is 2 %.

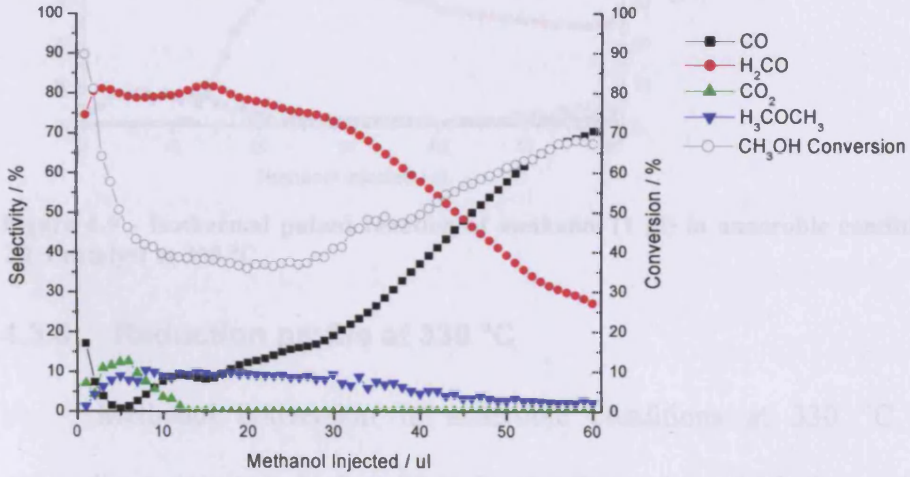


**Figure 4-8 - Isothermal pulsed reaction of methanol (1 µl) in anaerobic conditions over Mo:Fe 2.2:1 catalyst at 275 °C.**

### 4.3.5 Reduction profile at 300 °C

Methanol conversion for anaerobic methanol reaction at 300 °C (Figure 4-9, Appendix A-40) starts high at nearly 90 %, before dropping and going through a

minimum of 36 %. The methanol conversion then rises again to around 75 % after 40 pulses, and continues to be high for further injections. The selectivity to formaldehyde begins high at over 90 %, before dropping severely when the conversion begins to rise again and then throughout the course of the experiment to 36 % after 30 pulses and to 25 % after 60 pulses. The selectivity to dimethyl ether starts at below 2 %, rising to 8 % after four pulses, stabilising for a further 8 pulses, before dropping back to around 2 % after 25 pulses. No CO is produced in the first 10 pulses, after which production rises so that after 40 pulses selectivity to CO is around 70 %. Little $CO_2$ is produced at all, with production beginning after 50 pulses and selectivity never reaching higher than 5 %.

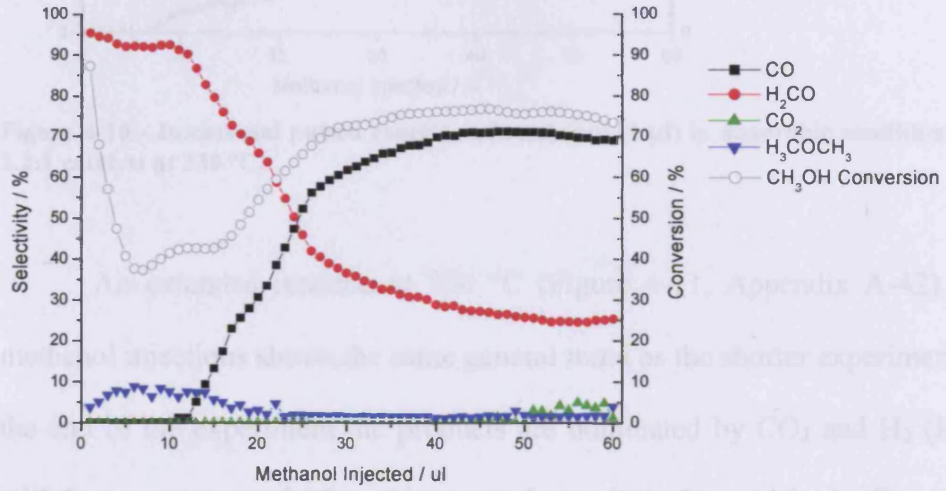


**Figure 4-9 - Isothermal pulsed reaction of methanol (1 µl) in anaerobic conditions over Mo:Fe 2.2:1 catalyst at 300 °C.**

### 4.3.6 Reduction profile at 330 °C

Methanol conversion in anaerobic conditions at 330 °C (Figure 4-10, Appendix A-41) starts high at 90 % for the first pulse, which rises quickly to around 95 % where it is maintained for all the further pulses. The selectivity to formaldehyde starts moderately, at around 57 %, before rising to 75 % after 3 pulses, before dropping quickly to 40 % after 7 pulses, and then more slowly to 25 % after 60 pulses. The selectivity of CO begins low at around 40 %, dropping to below 20 % after 3

pulses, before rising to a maximum of over 60 % after 7 pulses, and then back to around 55 % after 60 pulses. The selectivity to $CO_2$, is initially zero, with production beginning only after 7 pulses of methanol. The production of $CO_2$ rises slowly so that selectivity is around 35 % after 60 pulses of methanol.

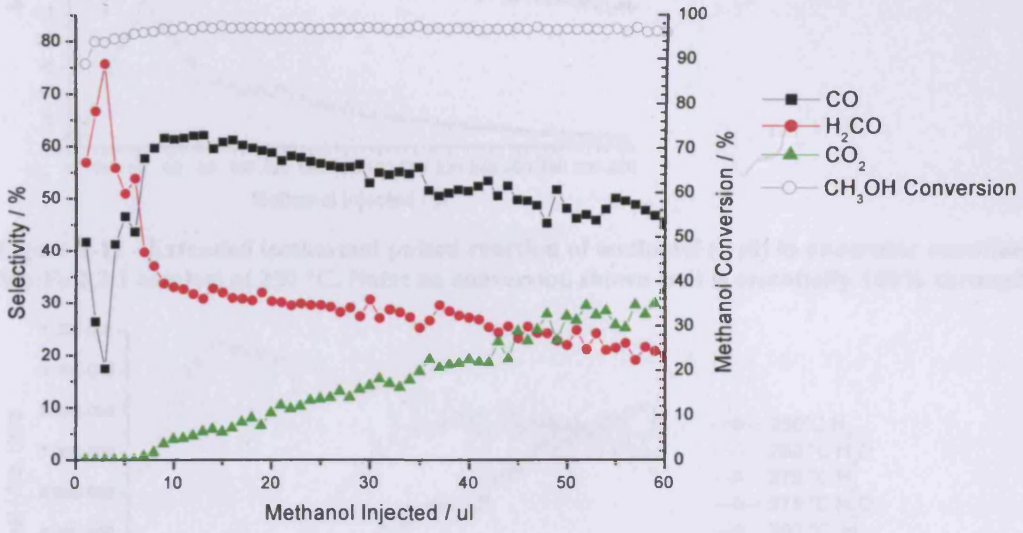


**Figure 4-10 - Isothermal pulsed reaction of methanol (1 µl) in anaerobic conditions over Mo:Fe 2.2:1 catalyst at 330 °C.**

An extended reaction at 350 °C (Figure 4-11, Appendix A-42) with larger methanol injections shows the same general trend as the shorter experiment, except by the end of the experiment the products are dominated by $CO_2$ and $H_2$ (Figure 4-12) with lesser amounts of CO and water and very little formaldehyde. The fact that $CO_2$ and $H_2O$ are still being produced indicates that catalyst reduction is still occurring even after this long exposure to methanol. The water product diminishes during the course of the reaction (Figure 4-12), while hydrogen yield increases.

The shift to production of CO and $H_2$ at the end of the reduction at 330 °C and extended reduction at 350 °C, indicate a shift from oxidative dehydrogenation to dehydrogenation and the presence of the water gas shift reaction producing $CO_2$.

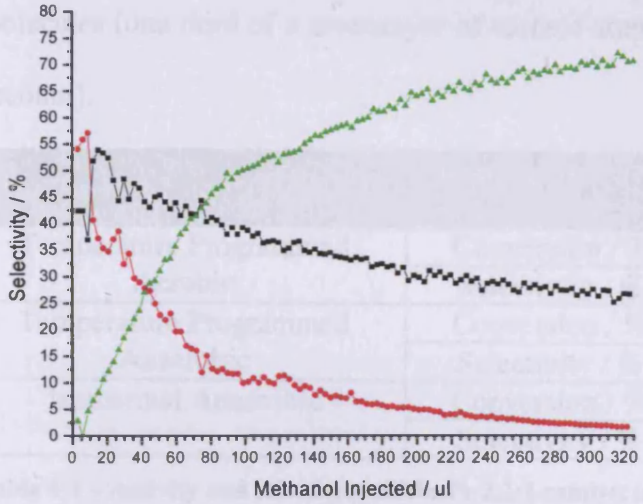


**Figure 4-11 - Extended isothermal pulsed reaction of methanol (1 µl) in anaerobic conditions over Mo:Fe 2.2:1 catalyst at 350 °C. Note: no conversion shown as it is essentially 100% throughout.**

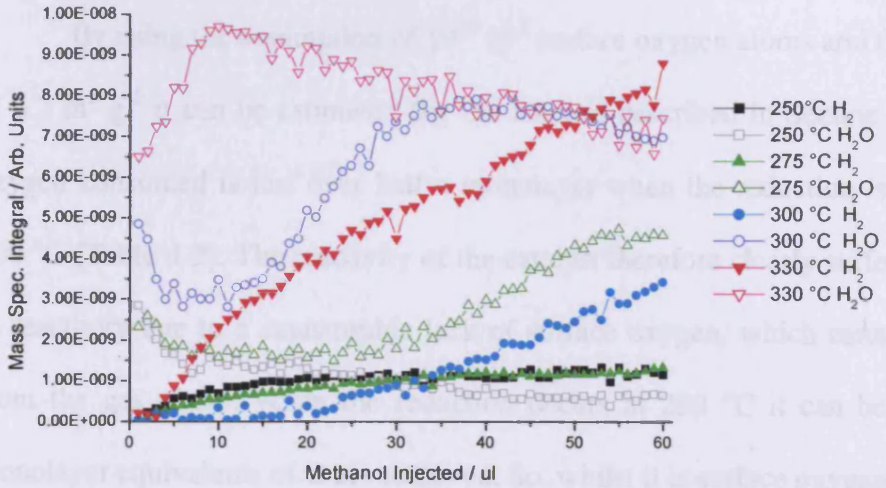


**Figure 4-12 – Evolution of hydrogen and water throughout the course of the anaerobic methanol reactions over Mo:Fe 2.2:1 catalyst.**

When the activity and selectivity of the first pulses in anaerobic conditions are compared to those in aerobic conditions (Table 4-1), a lowering of activity, with an increase in selectivity is observed. The changes observed are relatively small and are likely caused by a loss of O at the surface, which is not replaced during the pulse duration. The difference compares well to what would be expected as small injections (0.1 µl) of methanol have shown that the surface of the Mo:Fe 2.2:1 catalyst (0.5 g loading) is capable of adsorbing 0.73 µl methanol, which is approximately $1.1 \times 10^{19}$

molecules (one third of a monolayer of surface atoms, when surface area is taken into account).

| | Temperature / °C | 200 | 250 | 275 | 300 | 330 |
|---|---|---|---|---|---|---|
| Temperature Programmed Aerobic | Conversion / % | 40 | 88 | 97 | 97 | 98 |
| | Selectivity / % | 96 | 90 | 71 | 66 | 50 |
| Temperature Programmed Anaerobic | Conversion / % | 17 | 32 | 45 | 58 | 81 |
| | Selectivity / % | 70 | 90 | 82 | 82 | 85 |
| Isothermal Anaerobic | Conversion / % | 27 | 75 | 90 | 95 | 89 |
| | Selectivity / % | 96 | 84 | 83 | 87 | 57 |

**Table 4-1 – Activity and selectivity of Mo:Fe 2.2:1 catalyst in different conditions. The isothermal anaerobic data refers to the first pulse in these conditions.**

By using the assumption of $10^{19}$ $m^{-2}$ surface oxygen atoms and the surface area of 6.7 $m^2$ $g^{-1}$ it can be estimated (by the method described in Section 4.2.1) that the oxygen consumed is just over half a monolayer when the reduction is carried out at 200 °C (Table 4-2). The reactivity of the catalyst therefore clearly suffers a large drop in reactivity due to a catastrophic lack of surface oxygen, which cannot be replaced from the gas phase. When the reduction occurs at 250 °C it can be seen that 4.6 monolayer equivalents of O are removed. So, whilst it is surface oxygen that is used in the mechanism[2,29], bulk oxygen diffuses to the surface and becomes active at a significant rate above 250 °C. While diffusion of bulk oxygen maintains the activity of the catalyst, the selectivity diminishes, which is likely to be due to a partial reduction of the surface, showing the importance of high oxidation states of the surface metals to maintain selective products. The rise in CO production in anaerobic conditions is similar to that observed with the reduction of $MoO_3$ (Figure 4-4), although in that case the experiment is of a temperature programmed nature and does not produce CO until temperatures in excess of 300 °C. High oxidation states of the metals are probably required due to the heterolytic nature of methanol dissociation, which requires acid-base catalysis at the acidic proton of the methanol molecule, which is removed and

reduces the surface oxide to hydroxide. This, in turn, requires electron donation to the Mo-methoxy complex, effectively reducing the Mo from the +6 to the +5 oxidation state (though the electron transfer may include the methoxy species to which it is bonded, which may therefore be partly ionic). This could be written as follows:

$CH_3OH + Mo^{6+}O^{2-} \rightarrow Mo\text{-}OCH_3^{5+} + OH^-$ (4-4).

| Temperature of Reduction / °C | Methanol Used as Reductant / µl | O Removed from the Sample / % | Monolayer Equivalent of O |
|---|---|---|---|
| 200 | 60 | 0.3 | 0.6 |
| 250 | 60 | 2.5 | 4.6 |
| 275 | 60 | 6.7 | 12.3 |
| 300 | 60 | 12.4 | 22.8 |
| 330 | 60 | 15.2 | 28.0 |
| 350 | 321 | 49.1 | 90.2 |

**Table 4-2 - Oxygen removed by the reduction of Mo:Fe 2.2:1.**

### 4.3.7 Comparison with $Fe_2(MoO_4)_3$

As was seen in the previous chapter, the unreacted Mo:Fe 2.2:1 catalyst contains phases of both $Fe_2(MoO_4)_3$ and $MoO_3$, while the catalyst of composition Mo:Fe 1.5:1 appears as single phase $Fe_2(MoO_4)_3$. It therefore seems sensible that a comparison should be made between the two catalysts in anaerobic conditions, to see what effect (if any) the extra phase of $MoO_3$ provides.

The conversion/selectivity plot for the Mo:Fe 1.5:1 catalyst at 250 °C (Figure 4-13, Appendix A-43), shows the catalyst to have high initial activity (~80 % conversion), which declines rapidly over the course of 6 pulses to around 20 %. From here a much steadier decline is observed so that after 30 µl have passed over the surface, conversion is effectively zero. Initially the catalyst has a selectivity to formaldehyde and $CO_2$, (~55 and 45 % respectively), but these drop rapidly with values after six pulses of ~20 and 0 %. These are replaced by CO, which becomes the predominant product. The formation of dimethyl ether rises from zero initially to around 5 % throughout the course of the reaction.

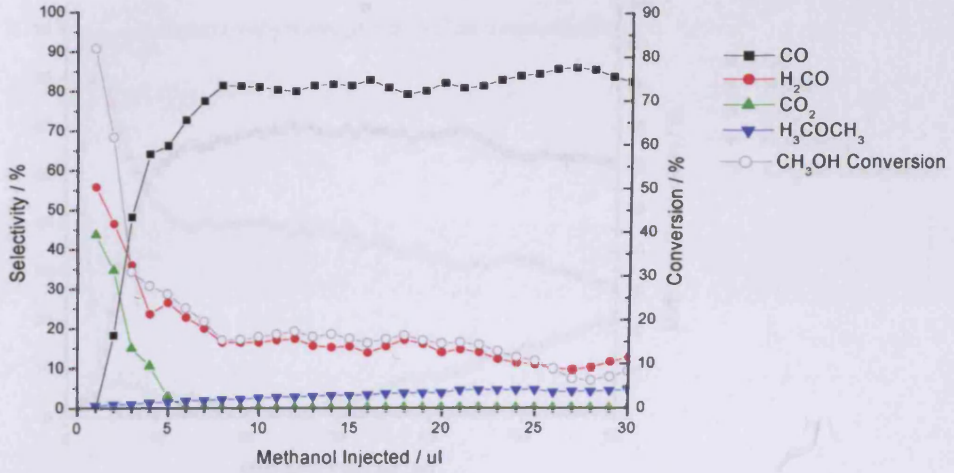


**Figure 4-13 - Isothermal pulsed reaction of methanol (1 µl) in anaerobic conditions over Mo:Fe 1.5:1 catalyst at 250 °C.**

Reduction of the Mo:Fe 1.5:1 catalyst at 330 °C (Figure 4-14, Appendix A-44) shows the catalyst now to be much more active. The first pulse shows a conversion of around 80 %, but this rises so to around 95 % for the second pulse, a level of conversion which is then maintained for subsequent injections. The formaldehyde production of the catalyst starts at a low level (~35 % selectivity), rising over the first four pulse to 75 %, before declining again over the next 7 pulses to a value of ~40 %. The catalyst then suffers only a minimal drop in formaldehyde selectivity (~10 %) so that by the end of the reaction a selectivity of 30 % is observed. $CO_2$ selectivity drops from an initial high value (~65 %) to less than 10 %, within 4 pulses. Minimal $CO_2$ production is then observed until around 30 µl of methanol have passed across the surface, when production begins to rise at a steady rate, so that by the end of the reaction ~20 % selectivity is observed. No CO is initially observed, rising only after the third pulse to around 50 % by the $10^{th}$ pulse. This level is then approximately maintained throughout the rest of the reaction.

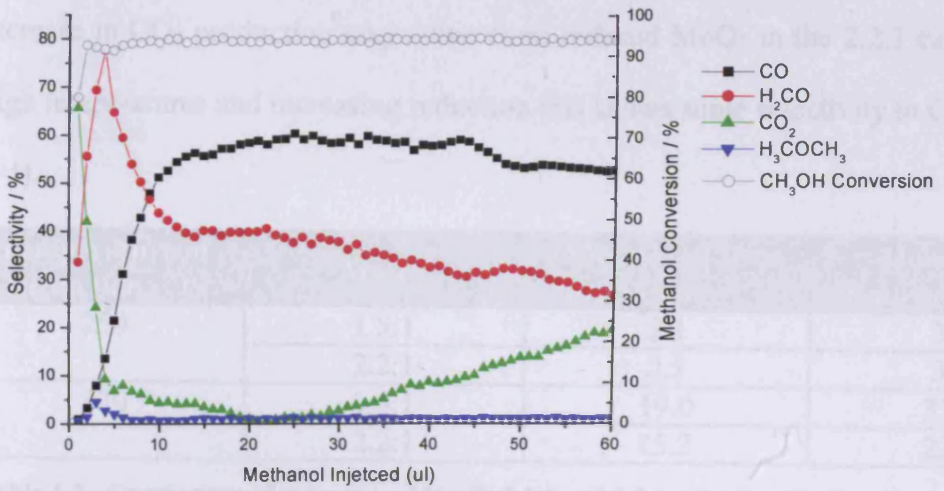


**Figure 4-14 - Isothermal pulsed reaction of methanol (1 µl) in anaerobic conditions over Mo:Fe 1.5:1 catalyst at 330 °C.**

The level of reduction that can occur on the Mo:Fe 1.5:1 catalyst is comparable to that observed with the Mo:Fe 2.2:1 catalyst at both higher and lower temperatures (Table 4-3). These data indicate that it is the mobility of the oxygen atoms through the $Fe_2(MoO_4)_3$, that leads to the reduction. This is consistent with literature data which showed the ease of O migration through $Fe_2(MoO_4)_3$ to be higher than that through $MoO_3$[28], with the former more easily reduced with $H_2$ and $NH_3$[30]. For reduction at 250 °C the product selectivity is initially enhanced towards $CO_2$ on the 1.5:1 Mo:Fe catalyst, as was also observed in aerobic conditions (Chapter 3). After the first five to ten pulses however, the reaction profiles become very similar, with a slightly higher production CO for the 1.5:1 Mo:Fe catalyst. As the fresh 1.5:1 catalyst is single phase $Fe_2(MoO_4)_3$ (Chapter 3) it must be a phase formed from the reduction of this (at least at the surface) that leads to the production of CO. The increased oxygen required for the extra production of $CO_2$ from the 1.5:1 catalyst in the first 4 pulses at 330 °C, will lead to a greater reduction of the catalyst. This may explain the lower $CO_2$ selectivity observed from this catalyst (compared to the 2.2:1 Mo:Fe), after greater than 20 µl of methanol have passed over the surface. Alternatively this

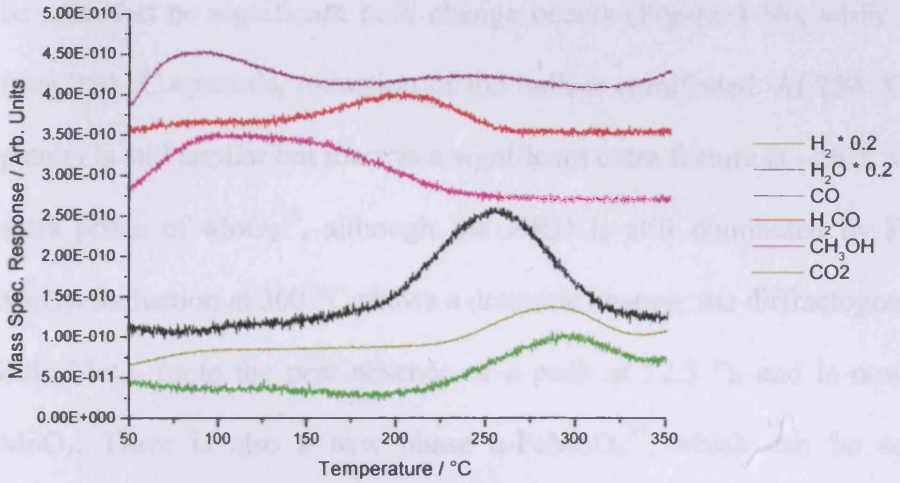


**Figure 4-15 - TPD of Mo:Fe catalyst reduced with 60 µl methanol at 330 °C, then saturated with methanol at room temperature.**

These TPD data suggest that while the sole product intermediate on the fresh surface is methoxy species, on the reduced catalyst a combination of species, including methoxys and formates are present. The methoxy species, yielding only formaldehyde are also observed on fresh $MoO_3$, whereas formate species, yielding $CO_2$ and $H_2$ are seen on $Fe_2O_3$[31,32]. The production of CO after reduction again may arise from two sources. Firstly it may be formed from a reduced phase (Section 4.3.9), and indeed, work with $MoO_2$ shows CO production (Section 4.4.1), though at lower temperature, or due to a lower molybdenum to iron ratio being formed at the surface, as this too can lead to CO production, with the temperature of production being dependant on the composition (Chapter 5). It should be noted that the $CO_2$ and $H_2$ production occur at the same temperature as they did for $Fe_2O_3$ (Chapter 3), so it appears an iron oxide species is present at the surface.

### 4.3.9 X-Ray Diffraction

As we saw in the last chapter the x-ray diffractogram of the pre reactor 2.2:1 Mo:Fe catalyst, contains phases of both molybdena[33] and ferric molybdate[34], as reported elsewhere[35], and presents these phases only. Upon reduction at 200 °C it can

be seen that no significant bulk change occurs (Figure 4-16), while at temperatures from 250 °C upwards, reduction of the bulk is manifested. At 250 °C the diffraction pattern is still similar but there is a significant extra feature at ~26 °. This indicates an extra phase of $MoO_2$[36], although the XRD is still dominated by $Fe_2(MoO_4)_3$ and $MoO_3$. Reduction at 300 °C shows a dramatic change, the diffractogram now showing little $MoO_3$ (note the near absence of a peak at 12.5 °), and is now dominated by $MoO_2$. There is also a new phase α-$FeMoO_4$[37], which can be seen along with $Mo_4O_{11}$[38]. When the reduction occurs at 330 °C, $MoO_2$, $Mo_4O_{11}$ and α-$FeMoO_4$ are the main phases observed, though also with some remaining molybdena and ferric molybdate. With extended reduction at 350 °C, $MoO_3$ and $Fe_2(MoO_4)_3$ phases are no longer observed, instead the XRD is dominated by $MoO_2$, with α-$FeMoO_4$ and $Mo_4O_{11}$ also being present.

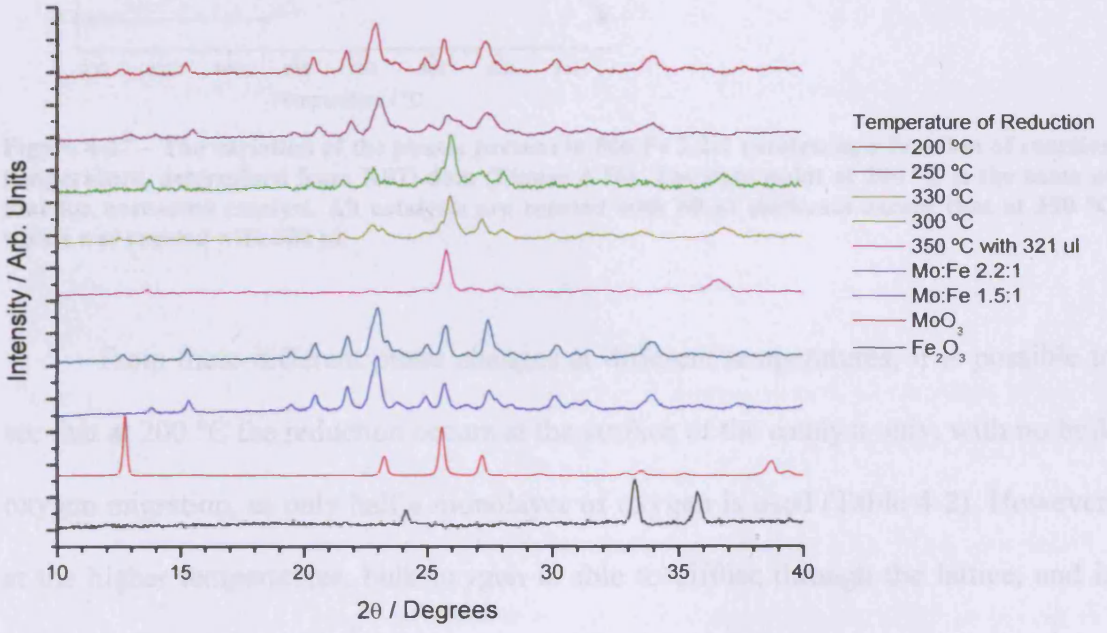


**Figure 4-16 - XRD of Mo:Fe 2.2:1 reduced with 60 µl methanol at different temperatures compared to various pre reactor catalysts.**

When the changes are summarised (Figure 4-17), the major reduction in the presence of ferric molybdate and molybdena is clearly visible, beginning at 250 °C. At

this stage, it appears that only $MoO_2$ is produced. $Mo_4O_{11}$ appears at 300 °C, together with ferrous molybdate, coincident with the apparent loss of $MoO_3$. It would therefore appear that $Mo_4O_{11}$ is not a precursor in the formation of $MoO_2$ from $MoO_3$, and $FeMoO_4$ forms during the major loss of $Fe_2(MoO_4)_3$ at 300 °C. To satisfy the stoichiometry this transformation must result in the ejection of Mo from the lattice. It is therefore appears that $Mo_4O_{11}$ occurs from the solid state reaction of $MoO_3$ and $MoO_2$[26].

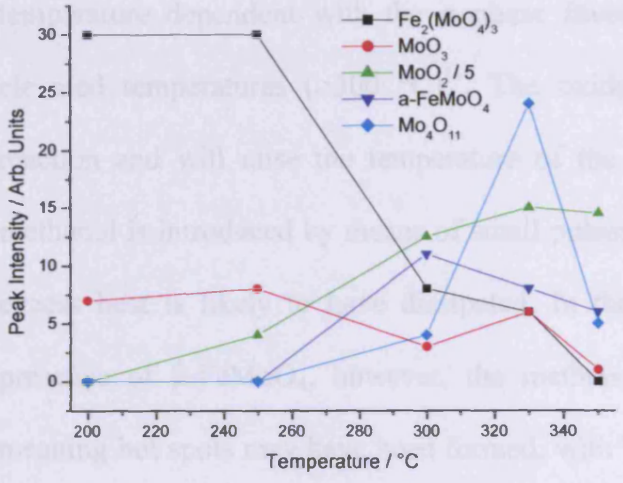


**Figure 4-17 – The variation of the phases present in Mo:Fe 2.2:1 catalyst as a function of reaction temperature, determined from XRD data (Figure 4-16). The data point at 200 °C is the same as that for unreacted catalyst. All catalysts are reacted with 60 µl methanol except that at 350 °C which was reacted with 321 µl.**

From these different phase changes at different temperatures, it is possible to see that at 200 °C the reduction occurs at the surface of the catalyst only, with no bulk oxygen migration, as only half a monolayer of oxygen is used (Table 4-2). However, at the higher temperatures, bulk oxygen is able to diffuse through the lattice, and is also removed. An important point to be noted is that at all the temperatures at or above 250 °C the catalyst is still reducing, even when the experiment is terminated, so even more oxygen is removable. The reduction of the catalysts also leads to a colour change (Figure 4-18); the fresh mixed phase catalyst is light green in colour, whereas after reduction the catalysts are black. The only catalyst which does not to become

black in colour was that reduced at 200 °C, which changed to dark green/grey. By studying the catalyst reduced with 321 µl of methanol at 350 °C, it can be seen that the catalyst can be reduced to such an extent that the initial phases of $Fe_2(MoO_4)_3$ and $MoO_3$ are now minor components, however, even after this change the catalyst is still being reduced further, so the phases noted may not be the final reduction products. The formation of α-$FeMoO_4$, instead of the β form observed in other reductions is surprising[3-6,11]. The phase of $FeMoO_4$ formed on reduction of $Fe_2(MoO_4)_3$, is temperature dependent with the α phase favoured at lower temperature and β at elevated temperatures (>300 °C)[14]. The oxidation of methanol is an exothermic reaction and will raise the temperature of the catalyst, but since in this work the methanol is introduced by means of small pulses with time of 2 minutes between, the excess heat is likely to have dissipated. In the previous studies that observed the presence of β-$FeMoO_4$, however, the methanol was introduced continuously[3-6,11], meaning hot spots may have been formed, with higher temperatures at the surface, so β-$FeMoO_4$ could be formed.

**Figure 4-18 - Mo:Fe 2.2:1 catalyst pre reduction, after reduction with 60 µl methanol at 250 °C and 330 °C.**

From the product distribution (Table 4-2), the oxygen loss from the catalyst can be calculated and it can be seen that this varies considerably depending on the temperature of reduction. Even if the catalyst were completely reduced to $FeMoO_4$ and $MoO_2$ (Equation 4-5), then the oxygen loss would be 21 %, but in the case of the Mo:Fe 2.2:1 catalyst held at 350 °C, we are able to remove ~49 % of the oxygen,

assuming no re-oxidation reactions occur (that is bimolecular reactions of methanol producing dimethyl ether and $H_2$).

$$Fe_2(MoO_4)_3.1.4MoO_3 \rightarrow 2\ FeMoO_4 + 2.4\ MoO_2 + 3.4\ O \qquad (4\text{-}5)$$

It is therefore presumed that the catalyst is further reduced to phases that are either amorphous or comprise too small crystallites to be detected by XRD, or the catalyst is becoming to some extent reoxidised once it is exposed to air prior to recording the XRD spectra.

### 4.3.10 X-Ray Photoelectron Spectroscopy

Analysis of the XPS spectra (Figure 4-19 and Figure 4-20) gives a surface molybdenum to iron ratio of 2.2:1, indicating a level of molybdenum in the surface region equal to that expected by the bulk stoichiometric composition (2.2:1). The effect of temperature broadly follows the trend observed with XRD (Section 4.3.9), *i.e.* that reduced states appear at high temperatures. However, it must be remembered that before XPS measurements were taken the samples were exposed to air, meaning it is most likely that re-oxidation of the topmost layer (at least) takes place. Before reduction the catalysts can be seen to contain $Mo^{6+}$ and $Fe^{3+}$ cations only, but after the higher temperature reductions (at 300 °C and above), $Fe^{2+}$ can clearly be seen in the iron spectra (peak at ~709.5 eV binding energy), presumably due to the formation of $FeMoO_4$ (as seen by XRD, Section 4.3.9). At this stage there is evidence of only a very small amount of reduced molybdenum (~229.4 eV binding energy). The reduced iron peak may also be present, to a very small extent, after reduction at 250 °C, as evidenced by the increase in a low binding energy shoulder. After extended reduction at 350 °C there is a more dramatic change in the XPS spectra, with evidence of carbide formation, with the C 1s spectra showing a peak at ~282 eV (Figure 4-21). The Mo peaks now show a broad, low binding energy component at ~229-231 eV,

indicating the presence of 4+ and 5+ oxidation states after this extended reduction. The formation of these species is presumably linked to the formation of $MoO_2$ and $Mo_4O_{11}$ as observed by XRD (Section 4.3.9). The Mo 3d spectrum of the reduced species (shown as an insert in Figure 4-19) was isolated by subtracting the scaled Mo 3d spectra of the fresh Mo:Fe 2.2:1 catalyst (containing pure $Mo^{6+}$) from the spectra obtained after reduction. The peaks are fitted with maxima for $Mo^{4+}$ and $Mo^{5+}$ peaks at 229.2 and 230.5 eV respectively, and give a 4+:5+:6+ ratio of 0.14:0.12:0.74 at the surface.

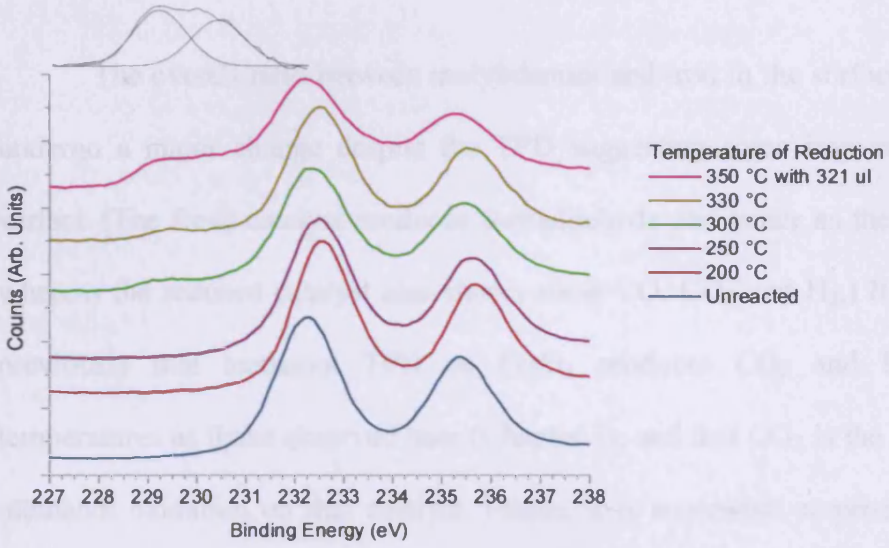


**Figure 4-19 - X-Ray Photoelectron Spectra for the Mo 3d peaks for Mo:Fe 2.2:1 catalyst after reduction with 60 µl methanol at different temperatures, with an insert to show the fitting of $Mo^{5+}$ and $Mo^{4+}$ after removal of $Mo^{6+}$ from the reduction at 350 °C with 321 µl of methanol.**

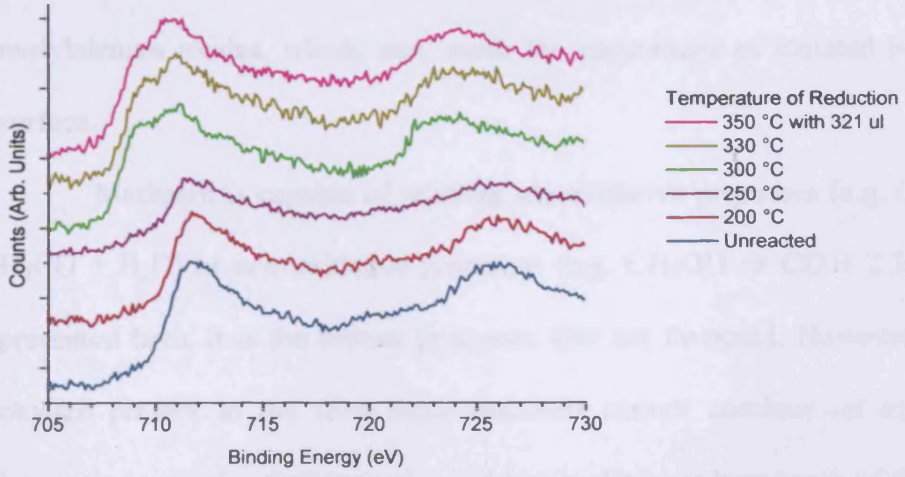


**Figure 4-20 - X-Ray Photoelectron Spectra for the Fe 2p peaks for Mo:Fe 2.2:1 catalyst after reduction with 60 µl methanol at different temperatures.**

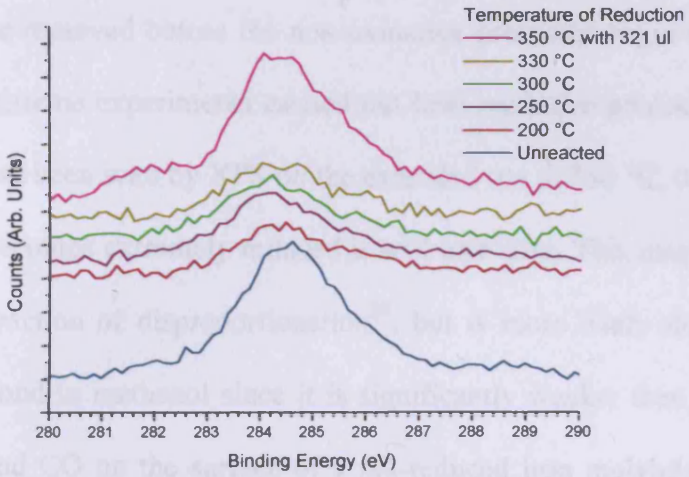


**Figure 4-21 - X-Ray Photoelectron Spectra for the C 1s peak for Mo:Fe 2.2:1 catalyst after reduction with 60 µl methanol at different tempertaures.**

The overall ratio between molybdenum and iron in the surface layers does not undergo a major change despite the TPD suggesting some iron enrichment of the surface (The fresh catalyst produces formaldehyde and water as the major products, whereas the reduced catalyst also shows some CO, $CO_2$ and $H_2$.) It has been shown previously that methanol TPD on $Fe_2O_3$ produces $CO_2$ and $H_2$ at the same temperatures as those observed here (Chapter 3), and that $CO_2$ is the major product of methanol oxidation on that catalyst. Hence, it is somewhat surprising that the ratio does not change, but this may be due to compensatory changes in the relative amounts of iron molybdates (ferric decreasing with reduction, while ferrous increases) and molybdenum oxides, which, may mask the appearance of isolated iron oxide at the surface.

Methanol is capable of reacting *via* oxidative processes (e.g. $CH_3OH + O_s \rightarrow H_2CO + H_2O$) or non-oxidative processes (e.g. $CH_3OH \rightarrow CO + 2\ H_2$). In the work presented here, it is the former processes that are favoured. However, as there is no oxygen present in the flow these reactions cannot continue *ad infinitum*, and an interesting point for further work would be to discover how much of the oxygen could

be removed before the non-oxidative processes begin to dominate. Even in the most extreme experiments carried out here oxidative products were still being formed. As has been seen by XPS on the extended run at 350 °C, it is likely that when the surface becomes extremely reduced it will carbidise. This may occur through the Boudouard reaction of disproportionation[39], but is more likely due to the cleavage of the C-O bond in methanol since it is significantly weaker than in CO and the reaction of $H_2$ and CO on the surface of a pre-reduced iron molybdate showed no sign of surface carbon build up[9].

The decrease of formaldehyde selectivity with reduction is mainly due to the formation of CO and this may arise from the over oxidation of formaldehyde (Chapter 3) or from reaction on reduced Mo species. The formation of CO appears to correlate with the reduction of $Mo^{6+} \rightarrow Mo^{4+}$ (*i.e.* $MoO_2$), seen in post reactor XRD, although the maxima in CO desorption for TPD is higher from the reduced catalysts than from the surface of $MoO_2$.

An interesting point to observe is the drop and subsequent rise in activity, when the reduction is carried out at 275 and 300 °C (Figure 4-8 and Figure 4-9). When this is compared with the XRD data (Figure 4-17), it appears that this occurs with the formation of $FeMoO_4$, presumably by the reaction:

$$Fe_2(MoO_4)_3 \rightarrow 2\ FeMoO_4 + MoO_3 + O \qquad (4\text{-}6)$$

$FeMoO_4$ has previously been found to be less catalytically active than $Fe_2(MoO_4)_3$, so this would be consistent with the decrease in activity[7]. The subsequent increase in activity can be seen to coincide with an increase in CO activity. CO formation is also seen with reduced Mo species (Figure 4-25), and it has previously been suggested that these can be more active[20,25]. Hence it appears that following the

initial reduction of $Fe_2(MoO_4)_3$, that reduction of $MoO_3$ can occur, with reduced molybdenum atoms (in the surface region at least) becoming more active.

The increase in selectivity of the catalyst towards $CO_2$ formation is in contrast to what might be expected as the catalyst is reduced. The reason for this is likely to be the increase in the iron available at the surface, as it is known that $Fe_2O_3$ directs methanol towards combustion products. This increase in iron at the surface may be due to either reduced iron passing through the catalyst bulk to the surface, or may be due to the loss of molybdenum from the surface, which is known to occur over a period of months under industrial oxidising conditions[2,10]. Note that molybdenum must be removed from the lattice in forming the ferrous molybdate observed by XRD, as ferrous molybdate has a higher iron ratio (1:1 Mo:Fe) than ferric molybdate (1.5:1), at least in the bulk. When the catalyst that was reduced at 330 °C was reoxidised it reformed the bulk phases of $Fe_2(MoO_4)_3$ and $MoO_3$, while the surface ratios in XPS were again unchanged. TPD data from the reoxidised catalyst showed methanol, formaldehyde and water as the major products in the same profile as pre-reduction.

It is likely that the major surface intermediate is the surface methoxy (decomposing at 170 °C in TPD), which dominates the surface of molybdena and the fully oxidised molybdate catalyst over the full temperature range of reaction. While CO is a secondary product of formaldehyde oxidation on the fully oxidised surfaces, with reduced molybdenum there is also a primary pathway. This means CO is not observed in methanol TPD of the fresh catalyst but is observed off a reduced catalyst. CO can undergo a secondary reaction to produce $CO_2$, but extensive reduction results in the appearance of iron oxide like phases in the catalyst, which favour over oxidation of methanol to a surface formate species, which in turn decomposes to $CO_2$ and $H_2$.

## 4.4 Action of the Reduced Phases

### 4.4.1 $MoO_2$

#### 4.4.1.1 Temperature Programmed Pulsed Flow Reaction

Methanol TPPFR for $MoO_2$ without first heating in oxygen is interesting as it shows a decrease in the formaldehyde selectivity before a further increase (Figure 4-22). The catalyst shows moderate activity, reaching 50 % conversion at 235 °C and 90 % by 290 °C. Formaldehyde selectivity starts high at over 90 %, dropping steadily to around 20 % by 320 °C, before subsequently rising back to 65 % by 380 °C. CO production starts at 180 °C, rising to 65 % at 320 °C, dropping back to around 32 % by 380 °C. $CO_2$ production begins at 270 °C, rising to 10 % at 320 °C, before returning back to zero by 370 °C. The production of dimethyl ether, starts high at ~15 %, dropping to around 5 % by 220 °C, and further still to below 1 % by 270 °C.

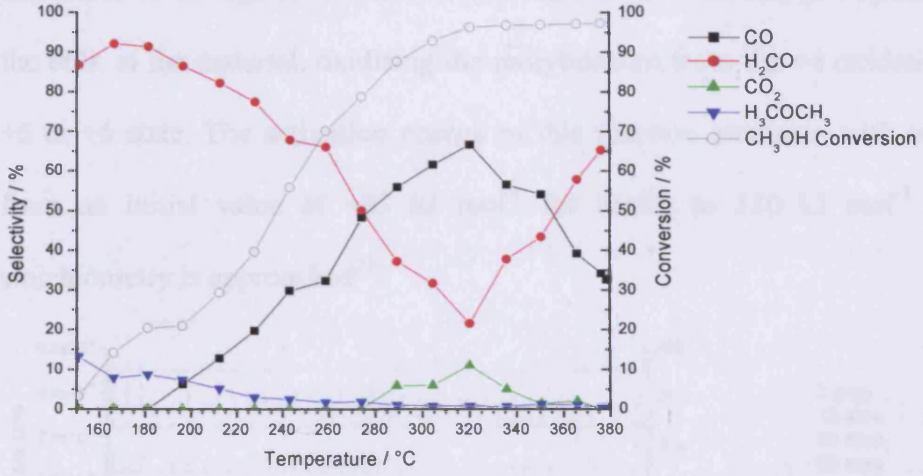


**Figure 4-22 - Selectivity and conversion for methanol oxidation over $MoO_2$, first run.**

This complicated TPPFR profile with a decrease and subsequent increase in formaldehyde selectivity, can only be fully understood by examining the raw data (Figure 4-23). While all the raw data is shown in this figure, the most important trace

to study is that corresponding to 32 amu, representing oxygen in the flow and injected methanol. When creating this figure constants were added to the traces for clarity of the figure, so the response at zero time corresponds to a zero mass spectrometer response, except for oxygen, which recorded 1 x $10^{-8}$ arb. units. Over the first 40 minutes of the experiment, the flow of oxygen is unperturbed and is constant, while the peaks observed are those corresponding to 32 amu for methanol injections. At 42 minutes (230 °C), the 32 amu begins to change, in that when an injection of methanol is made there is a negative peak. This is due to the methanol signal becoming smaller as more methanol is converted, oxygen displacement from the gas flow, and uptake to replace that used in the surface of the catalyst during the oxidation of the methanol. At around 44 minutes (250 °C) there is a further change as the 32 amu trace begins to decrease. The reason for this decrease is the uptake of oxygen into the catalyst. This oxygen is not just replacing that used in the surface reaction as the uptake can be calculated to be significantly more than this. Instead the oxygen uptake is oxidising the bulk of the material, oxidising the molybdenum from the +4 oxidation state to the +5 or +6 state. The activation energy of this reaction increases with oxygen uptake, from an initial value of ~95 kJ $mol^{-1}$ for $MoO_2$ to 180 kJ $mol^{-1}$ as the $MoO_3$ stoichiometry is approached[23].

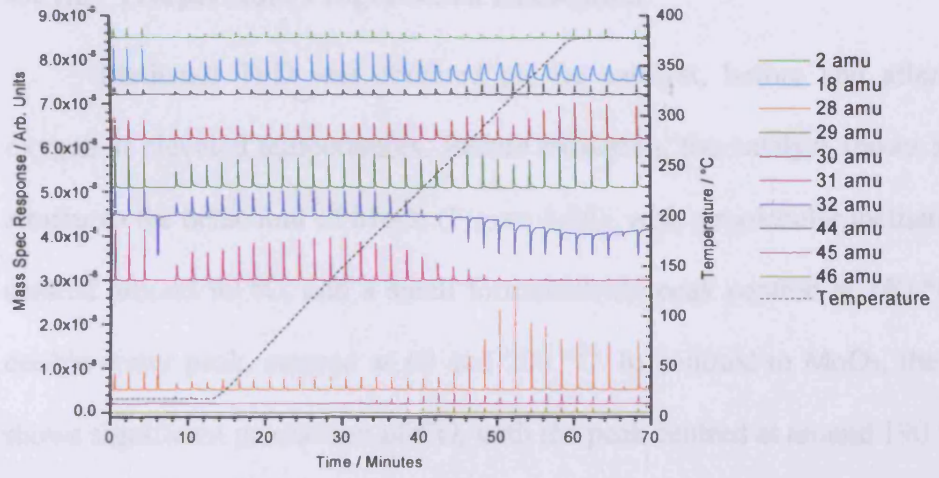


**Figure 4-23 – Raw data for methanol oxidation over $MoO_2$, first run.**

A second run of the $MoO_2$ catalyst was performed to see if the pattern of oxygen uptake was repeated and to investigate the material formed after oxidation (Figure 4-24, Appendix A-45). The material showed similar conversion, reaching 50 % at 230 °C, and 90 % at 290 °C. Formaldehyde selectivity follows a pattern observed on other catalysts, starting high (>95 %) until 280 °C, when it drops more rapidly to 72 % by 315 °C and then more steadily to 55 % by 380 °C. CO production begins at around 260 °C, and rises to 25 % by 315 °C, and to 36 % by 380 °C. Dimethyl ether production is around 5 % until 300 °C, when it begins to drop, reaching less than 1 % by 380 °C.

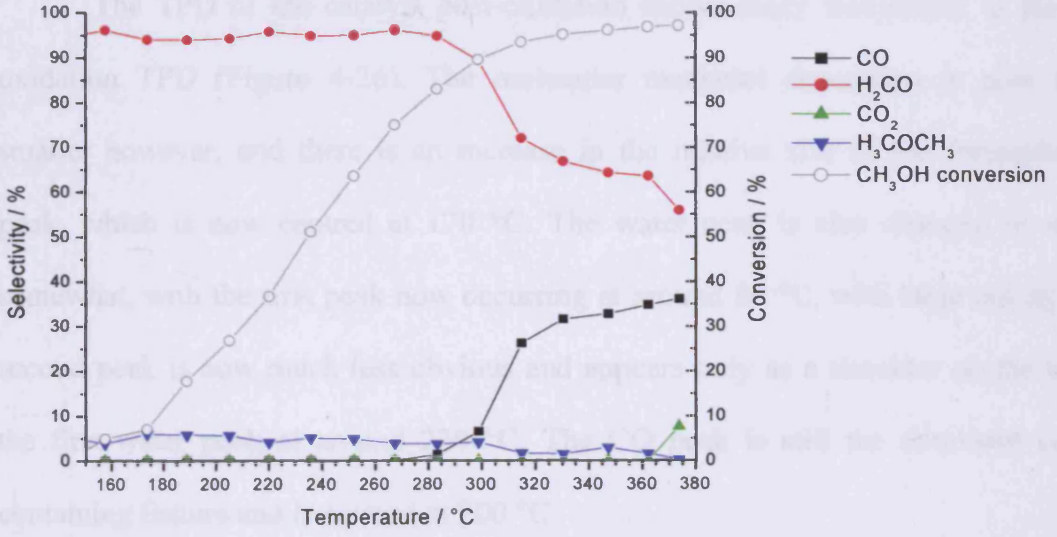


**Figure 4-24 - Selectivity and conversion for methanol oxidation over $MoO_2$, second run.**

### 4.4.1.2 Temperature Programmed Desorption

Methanol TPD was obtained on the catalyst, before and after exposure to oxygen at elevated temperatures. Before oxidation, the catalyst shows some features similar to the behaviour of $MoO_3$ (Figure 4-25), with a molecular methanol desorption centred around 90 °C, and a small formaldehyde peak centred at 160 °C. There is a double water peak, centred at 60 and 200 °C. In contrast to $MoO_3$, the catalyst also shows significant production of CO, with the peak centred at around 190 °C.

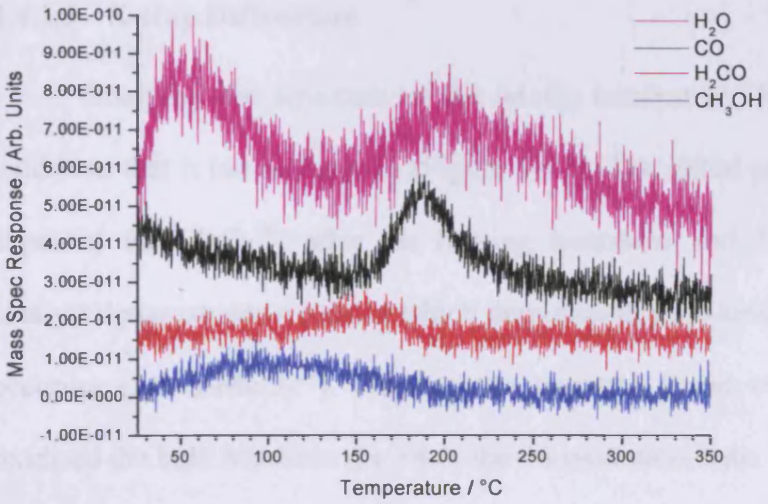


**Figure 4-25 - TPD of $MoO_2$ (before oxidation) saturated with methanol at room temperature.**

The TPD of the catalyst post-oxidation shows many similarities to the pre-oxidation TPD (Figure 4-26). The molecular methanol desorption is now much smaller however, and there is an increase in the relative size of the formaldehyde peak, which is now centred at 170 °C. The water peak is also changed in shape, somewhat, with the first peak now occurring at around 80 °C, with large tailing. The second peak is now much less obvious and appears only as a shoulder on the tail of the first water peak at around 220 °C. The CO peak is still the dominant carbon containing feature and is centred at 200 °C.

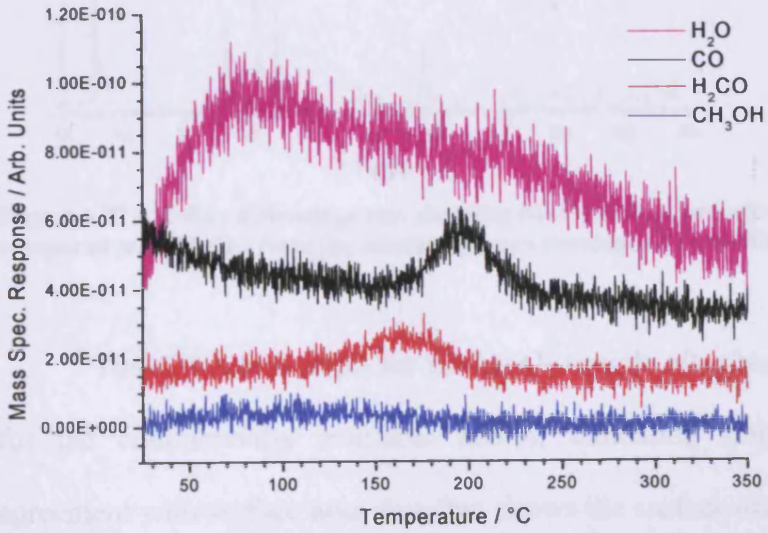


**Figure 4-26 - TPD of $MoO_2$ (after oxidation) saturated with methanol at room temperature.**

### 4.4.1.3 X-Ray Diffraction

Studying the structure of the $MoO_2$ catalyst by XRD further illustrates the oxidation that it has undergone (Figure 4-27). The initial pattern shown in black is as expected for $MoO_2$[36]; after the heating treatment and TPDs described above the catalyst demonstrates a pattern which demonstrates the new structure the material now occupies (*i.e.* α-$MoO_3$[33]). Heating the material in an oxygen flow has therefore oxidised the bulk Mo from the +4 to the +6 oxidation state. The structure of $MoO_2$ is a distorted rutile structure, with the central molybdenum having four oxygen atoms organised in a tetrahedron around it. This changes to an octahedral arrangement with six O atoms during the phase transformation. The post-heating diffractogram differs from that of fresh $MoO_3$ (BDH), in that the oxidised $MoO_2$ presents weaker 0k0 planes, suggesting a crystal with less 010 faces exposed.

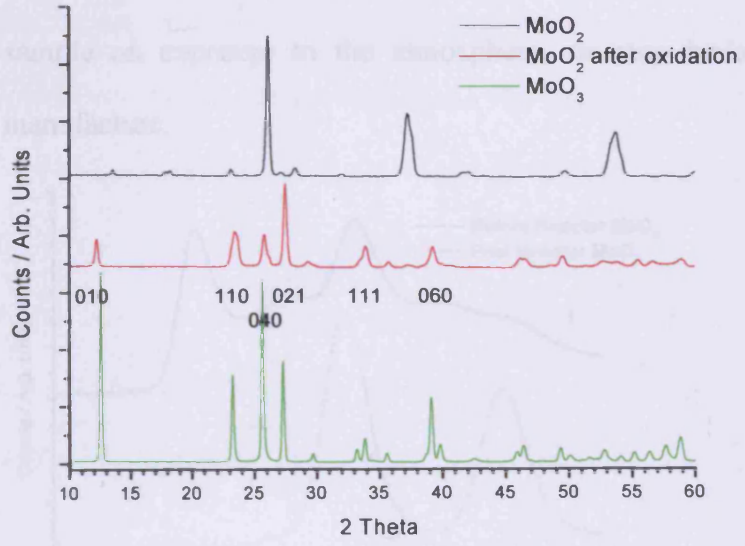


**Figure 4-27 – X-Ray diffractograms showing $MoO_2$ before and after TPPFR of methanol compared with $MoO_3$. Note the labelled planes correspond to α-$MoO_3$.**

The diffraction peaks for the $MoO_2$ sample after heating are broader than those for the commercially available $MoO_3$, indicating smaller particles. This is in agreement with surface area data that shows the surface area of the commercial $MoO_3$

to be 1.0 $m^2 g^{-1}$, much smaller than the 3.5 $m^2 g^{-1}$ recorded for the oxidised $MoO_2$, and 3.6 $m^2 g^{-1}$, recorded for the fresh sample. This surface area does represent an increase in surface area per molybdenum atom though, as a weight increase of ~12.5 % would be expected when oxidising $MoO_2$ to $MoO_3$.

#### 4.4.1.4 X-Ray Photoelectron Spectroscopy

Before reaction the $MoO_2$ sample can be seen to contain mainly $Mo^{4+}$ (~229.5 eV) in the surface region (Figure 4-28), but lesser amounts of $Mo^{+5}$ and $Mo^{6+}$ can also be fitted. Post-reactor (*i.e.* after two methanol TPPFR in 10 % $O_2$/He) the surface now contains molybdenum only in the +6 oxidation state (~232 eV). This is consistent with bulk studies (Figure 4-27), which show a transformation of the sample from $MoO_2$ to $MoO_3$. The $MoO_2$ samples shows a small of +6 and +5 oxidation state molybdenum in the pre reactor sample, presumably due to oxidation of the outermost layer of the sample on exposure to the atmosphere, or may be an artifact of the method of manufacture.

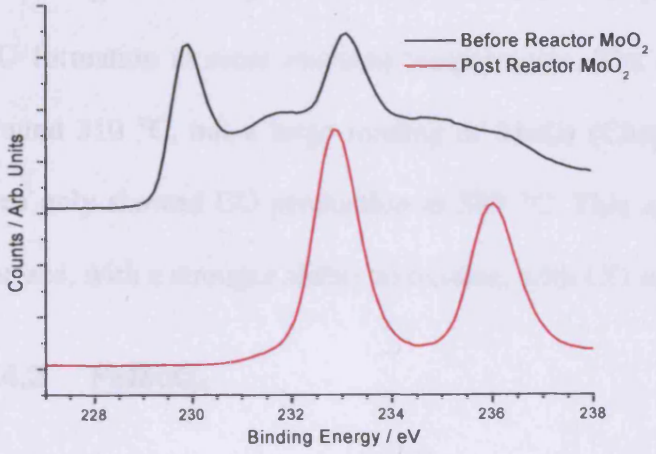


**Figure 4-28 - X-Ray photoelectron spectra of Mo 3d peaks showing $MoO_2$ before and after TPPFR of methanol.**

From the data here it seems evident that $MoO_2$ provides pathways to both formaldehyde and CO production. Unlike $MoO_3$ however, both of these are direct

pathways from different surface sites, as evidenced by the production of both products in TPD (Figure 4-25).

It appears that heating in oxygen leads to not only the surface becoming oxidised (Figure 4-28) but also a phase change as the bulk also became oxidised (Figure 4-27). While the XRD shows $MoO_3$ as the major crystal phase within the oxidised sample, it is likely that it still contains crystallographic shear planes (forming structures of a $Mo_{18}O_{52}$ type), as only at oxidation above ~400 °C are these removed[23]. These shear planes have been shown to be poor for oxygen transfer, but were only observed by *in-situ* XAFS, while *in-situ* XRD showed a transformation only from $MoO_2$ to $MoO_3$. The production of CO by TPD, even after oxidation (Figure 4-26) also suggests that the sample may not have been fully oxidised and that some defects remained at the surface, although this is not seen in the XPS measurements. However, $Mo^{4+}$ would likely not be observed even if present as even a full $Mo_{18}O_{52}$ structure would have the Mo in the average oxidation state of +5.78. The post oxidation catalyst shows high selectivity to formaldehyde in TPPFR (Figure 4-24), but does show some CO formation at more elevated temperatures. The production of CO here begins at around 310 °C, but a large loading of $MoO_3$ (Chapter 3), with similar total surface area only showed CO production at 380 °C. This again suggests some defects at the surface, with a stronger ability to oxidise, with CO and $H_2O$ being formed.

### 4.4.2 $FeMoO_4$

#### 4.4.2.1 Temperature Programmed Pulsed Flow Reaction

Methanol TPPFR over the $FeMoO_4$ catalyst when first heated in $O_2$ shows a moderate activity, reaching 50 % conversion at 270 °C, and 90 % at 340 °C (Figure 4-29, Appendix A-46). The catalyst shows good formaldehyde selectivity at over 90

% until around 310 °C, when a steady decline to 40 % by 380 °C begins. CO and $CO_2$ production begin at around 270 and 330°C, climbing to 35 and 20 % respectively by 380 °C. Dimethyl ether selectivity is high (~8 %) at low conversions dropping to ~4 % by 250 °C, and then near zero by 350 °C.

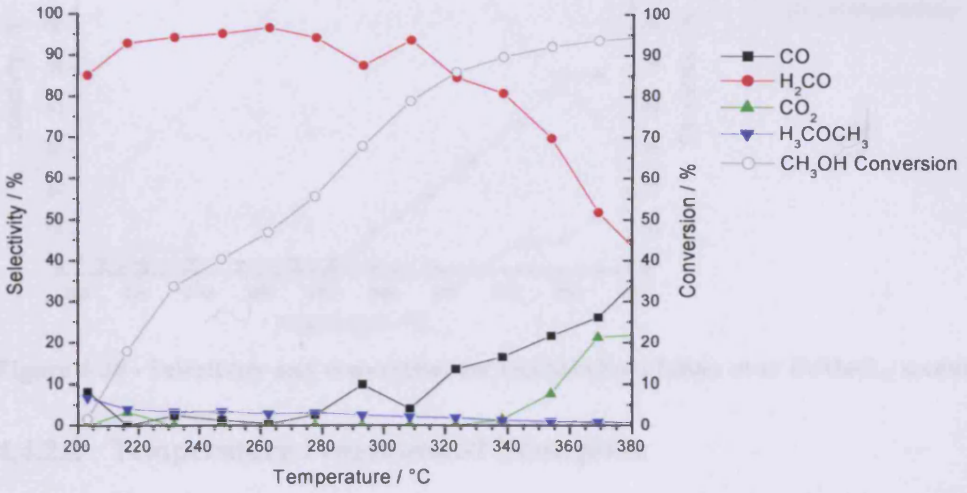


**Figure 4-29 - Selectivity and conversion for methanol oxidation over $FeMoO_4$, first run.**

While $O_2$ uptake was not seen in the first methanol TPPFR over $FeMoO_4$ in the same way that it was for $MoO_2$ (Figure 4-23), a repeat run was made to see if there was a difference in catalytic properties. It would be expected that $FeMoO_4$ would take up much less $O_2$ than $MoO_2$ anyway. The relative weight changes expected would be 3.7 % and 12.5 % for $FeMoO_4$ and $MoO_2$ respectively, if after oxidation the cations were $Mo^{6+}$ and $Fe^{3+}$.

The repeat TPPFR shows the catalyst to be more active, now reaching 50 and 90 % conversions at 250 and 315 °C, decreases of 20 and 15 °C respectively (Figure 4-30, Appendix A-47). Again the catalyst is highly selective (>95 %) to formaldehyde at low conversions, decreasing only at 285 °C, to 35 % by 375 °C. CO production begins at 280 °C and is much larger than previously observed, reaching nearly 50 % by 360 °C. $CO_2$ production is lower than before oxidation, beginning at 330 °C and

never reaching more than 15 %. Dimethyl ether production is lower, peaking at around 4 % at 280 °C.

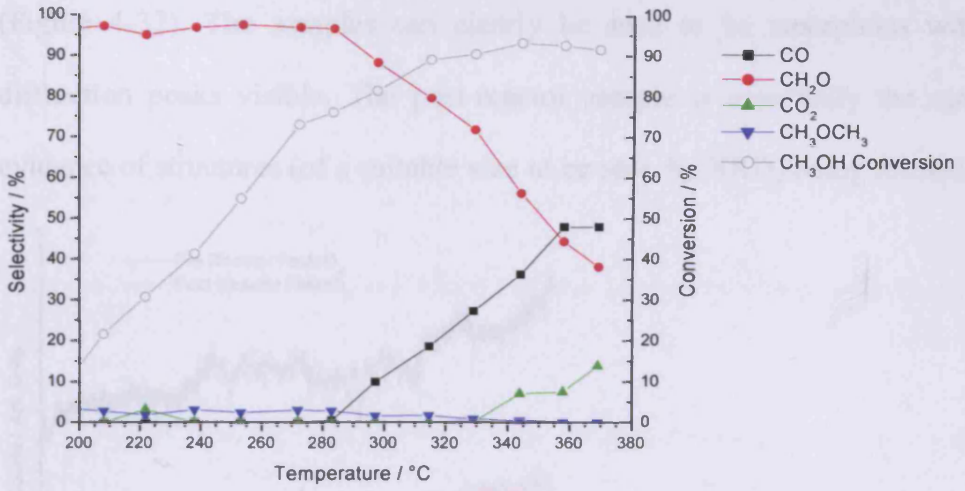


**Figure 4-30 - Selectivity and conversion for methanol oxidation over $FeMoO_4$, second run.**

### 4.4.2.2 Temperature Programmed Desorption

TPD was performed both before and after oxidation; however, only the pre-oxidation is shown here (Figure 4-31), as both were essentially the same. In the TPD it can be seen that there is a broad methanol desorption centred at around 80 °C. The major product observed is formaldehyde with a peak at 200 °C. The water desorption shows a peak at around 70 °C, with a rising background occurring after 200 °C. The CO desorption trace is also shown and indicates that no CO is produced.

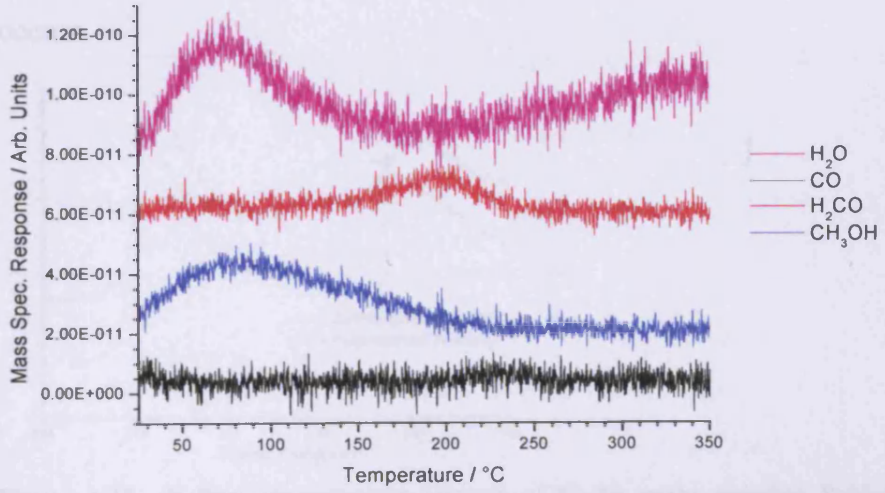


**Figure 4-31 - TPD of $FeMoO_4$ (before oxidation) saturated with methanol at room temperature.**

### 4.4.2.3 X-Ray Diffraction

XRD measurements were taken pre- and post-reactor for the $FeMoO_4$ sample (Figure 4-32). The samples can clearly be seen to be amorphous with no major diffraction peaks visible. The post-reactor sample is essentially the same, with no evidence of structures (of a suitable size to be seen by XRD) being formed.

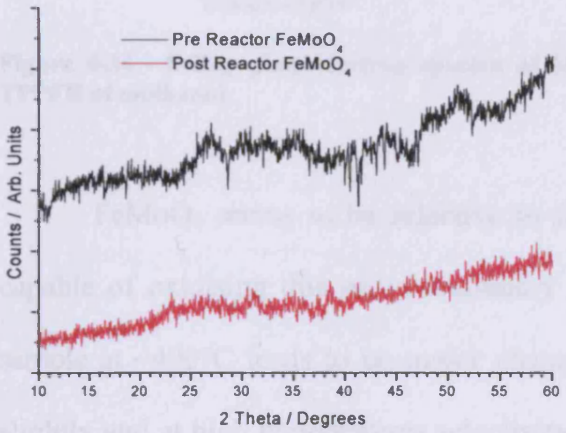


**Figure 4-32 - X-Ray diffractogram showing $FeMoO_4$ before TPPFR of methanol.**

### 4.4.2.4 X-Ray Photoelectron Spectroscopy

The catalyst has Fe in +3 and Mo in +6 oxidation states both before and after reaction (Figure 4-33 and Figure 4-34). This is somewhat of a surprise as $FeMoO_4$ should have Fe in the +2 oxidation state. The sample was supplied as $FeMoO_4$, so it is assumed that the surface is oxidised in storage and exposure to air while preparation occurs.

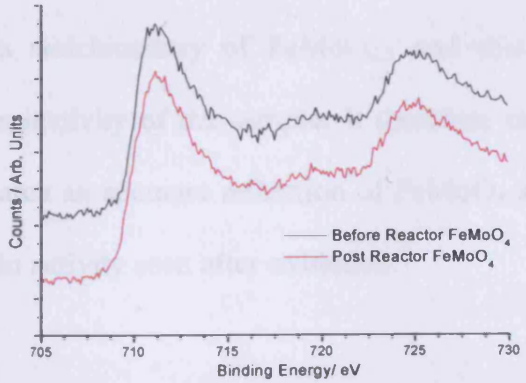


**Figure 4-33 - X-Ray photoelectron spectra of Fe 2p peaks showing $FeMoO_4$ before and after TPPFR of methanol.**

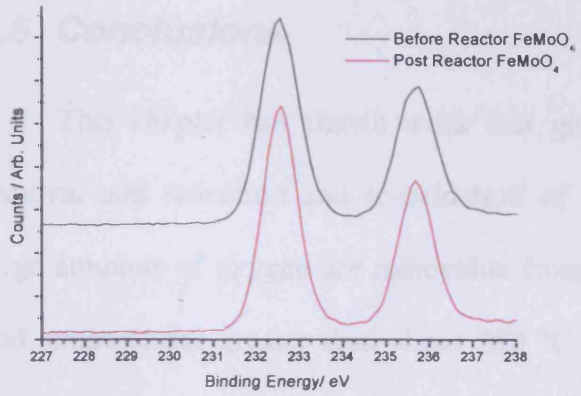


**Figure 4-34 - X-Ray photoelectron spectra of Mo 3d peaks showing $FeMoO_4$ before and after TPPFR of methanol.**

$FeMoO_4$ seems to be selective to formaldehyde as a primary product and is capable of oxidising this on in secondary reactions to CO and $CO_2$. Oxidizing this sample at ~400°C leads to no major changes in the catalyst. Activity was increased slightly and at high temperatures selectivity was lower to $CO_2$ and higher to CO. The surface area of the catalyst however remained unchanged at 14.0 $m^2 g^{-1}$.

The sample of $FeMoO_4$ tested was amorphous, so any structural effects of α-$FeMoO_4$ or β-$FeMoO_4$, cannot be considered. It is possible to see from the XRD data though that oxidation of the $FeMoO_4$ sample does not lead to the formation of $Fe_2(MoO_4)_3$ with the ejection of Fe (to form $Fe_2O_3$), or at least not in crystals of suitable size to be detected.

It appears that at least in the surface region the $FeMoO_4$ is already oxidised to a stoichiometry of $FeMoO_{4.5}$ and this will have an effect on the reactivity and selectivity of the sample. It therefore cannot be claimed that the products seen here area an accurate reflection of $FeMoO_4$ at the surface, despite the slight improvement in activity seen after oxidation.

## 4.5 Conclusions

This chapter has shown work that gives insight into the process of oxygen removal and reduction and re-oxidation of iron molybdate catalysts, showing that large amounts of oxygen are removable from the lattice in the presence of methanol and temperatures greater than about 250 °C. Above this temperature lattice oxygen becomes easily available, and is used in selective and non-selective oxidation processes. The reaction is highly efficient, with 100 % conversion over the Mo:Fe 2.2:1 catalyst throughout the reaction at 330 °C, even though the oxygen is delivered to the surface from deep within the catalyst particle. When significant amounts of lattice oxygen are removed the bulk phases convert from $Fe_2(MoO_4)_3$ and $MoO_3$, to $MoO_2$, $Mo_4O_{11}$, and α-$FeMoO_4$. This results in a reduced production of formaldehyde, with an increase in production of CO and $CO_2$. Such data help to re-emphasise the need for high oxygen levels at the end of an industrial bed, otherwise deleterious changes will occur within the catalyst, resulting in lower formaldehyde yields.

Reduction of the single oxide phases of $MoO_3$ and $Fe_2O_3$ showed both to still be active to methanol oxidation, with $Fe_2O_3$ producing the same products of $CO_2$ and $H_2$. The $MoO_3$ sample produced formaldehyde and water at low temperatures, but as temperature and level of reduction increased, changed to produce primarily CO and $H_2O$. The change in activity and selectivity associated with this was ascribed to the formation of reduced molybdenum surface species changing the reaction pathway.

$MoO_2$ shows itself to have direct oxidation pathways to both formaldehyde and CO. The activity of the catalyst, pre- and post-oxidation were very similar. Oxidation of the catalyst at ~380 °C leads to the change in the bulk of the sample from $MoO_2$ to $MoO_3$. After oxidation, and with $Mo^{6+}$ only in the surface region, TPPFR showed the catalyst to be more selective to formaldehyde.

The $FeMoO_4$ sample showed itself to be mainly selective towards formaldehyde and water, with only secondary oxidation, leading to the production of both CO and $CO_2$. The sample supplied however was oxidised, at least in the surface region.

## 4.6 References


(1) Mars, P.; van Krevelen, D. W. *Chemical Engineering Science* **1954**, *3*, 41.
(2) Pernicone, N. *Actas do Encontro Nacional de Catalise Basica e Aplicada (Industrial e Ambiental), 3rd, Lisbon,* **1995**, 195.
(3) Zhang, H.; Shen, J.; Ge, X. *Journal of Solid State Chemistry* **1995**, *117*, 127.
(4) Gai, P. L.; Labun, P. A. *Journal of Catalysis* **1985**, *94*, 79.
(5) Wilson, J. H., III; Hill, C. G., Jr.; Dumesic, J. A. *Journal of Molecular Catalysis* **1990**, *61*, 333.
(6) Carbucicchio, M.; Trifiro, F.; Villa, P. L. *Journal de Physique, Colloque* **1976**, 253.
(7) Soares, A. P. V.; Portela, M. F.; Kiennemann, A. *Catalysis Reviews - Science and Engineering* **2004**, *47*, 125.
(8) Kuang, W.; Fan, Y.; Chen, Y. *Langmuir* **2000**, *16*, 1440.
(9) Maiti, G. C.; Malessa, R.; Baerns, M. *Thermochimica Acta* **1984**, *80*, 11.
(10) Andersson, A.; Hernelind, M.; Augustsson, O. *Catalysis Today* **2006**, *112*, 40.
(11) Pernicone, N. *Catalysis Today* **1991**, *11*, 85.
(12) Petrini, G.; Garbassi, F.; Petrera, M.; Pernicone, N. *Chem. Uses Molybdenum, Proc. Int. Conf., 4th* **1982**, 437.
(13) Carbucicchio, M.; Trifiro, F. *Journal of Catalysis* **1976**, *45*, 77.
(14) Burriesci, N.; Gennaro, A.; Petrera, M. *Reaction Kinetics and Catalysis Letters* **1980**, *15*, 171.
(15) Jacques, S. D. M.; Leynaud, O.; Strusevich, D.; Beale, A. M.; Sankar, G.; Martin, C. M.; Barnes, P. *Angewandte Chemie, International Edition* **2006**, *45*, 445.
(16) Guidot, J.; Germain, J. E. *Reaction Kinetics and Catalysis Letters* **1980**, *15*, 389.
(17) Smith, R. L.; Rohrer, G. S. *Journal of Catalysis* **1998**, *173*, 219.
(18) Ressler, T.; Wienold, J.; Jentoft, R. E. *Solid State Ionics* **2001**, *141-142*, 243.
(19) Al-Kandari, H.; Al-Khorafi, F.; Belatel, H.; Katrib, A. *Catalysis Communications* **2004**, *5*, 225.
(20) Bertinchamps, F.; Gaigneaux, E. M. *Catalysis Today* **2004**, *91-92*, 105.
(21) Street, S. C.; Goodman, D. W. *Journal of Vacuum Science & Technology, A: Vacuum, Surfaces, and Films* **1997**, *15*, 1717.
(22) Tokarz-Sobieraj, R.; Hermann, K.; Witko, M.; Blume, A.; Mestl, G.; Schlogl, R. *Surface Science* **2001**, *489*, 107.
(23) Ressler, T.; Wienold, J.; Jentoft, R. E.; Neisius, T. *Journal of Catalysis* **2002**, *210*, 67.
(24) Guerrero-Ruiz, A.; Rodriguez-Ramos, I.; Ferreira-Aparicio, P.; Abon, M.; Volta, J. C. *Catalysis Today* **1996**, *32*, 223.
(25) Arnoldy, P.; De Jonge, J. C. M.; Moulijn, J. A. *Journal of Physical Chemistry* **1985**, *89*, 4517.
(26) Ressler, T.; Jentoft, R. E.; Wienold, J.; Guenter, M. M.; Timpe, O. *Journal of Physical Chemistry B* **2000**, *104*, 6360.

(27) Novakova, J.; Jiru, P.; Zavadil, V. *Journal of Catalysis* **1971**, *21*, 143.
(28) Kuang, W.; Fan, Y.; Chen, Y. *Langmuir* **2000**, *16*, 5205.
(29) Jiru, P.; Novakova, J. *Collection of Czechoslovak Chemical Communications* **1963**, *28*, 1.
(30) Trifiro, F.; DeVecchi, V.; Pasquon, I. *Journal of Catalysis* **1969**, *15*, 8.
(31) Bowker, M.; Holroyd, R.; Elliott, A.; Morrall, P.; Alouche, A.; Entwistle, C.; Toerncrona, A. *Catalysis Letters* **2002**, *83*, 165.
(32) Glisenti, A.; Favero, G.; Granozzi, G. *Journal of the Chemical Society, Faraday Transactions* **1998**, *94*, 173.
(33) JCPDS Card Number 35-609.
(34) JCPDS Card Number 31-642.
(35) Hill, C. G., Jr.; Wilson, J. H., III. *Journal of Molecular Catalysis* **1990**, *63*, 65.
(36) JCPDS Card Number 32-671.
(37) JCPDS Card Number 22-1115.
(38) JCDPS Card Number 13-142.
(39) Boudouard, O. *Comptes Rendus Hebdomadaires des Seances de l'Academie des Sciences* **1899**, *128*, 98.

# 5 Variation of the Cation Ratio

## 5.1 Introduction

As was stated in chapter 1, the main industrial catalysts contain a molybdenum to iron ratio above 1.5:1 so that they contain phases of both $Fe_2(MoO_4)_3$ and $MoO_3$. Accordingly these ratios have been the subject of most research within the literature, whilst data for ratios of Mo:Fe 1.5:1 are rarely reported.

It has been shown that the maximum selectivity and activity for iron molybdate catalysts occurs when the ratio of Mo:Fe is in the range 1.6-1.9, with the explanation that higher ratios of Mo, left the active phase of ferric molybdate covered by low activity $MoO_3$[1].

XPS studies of the surfaces of iron molybdates have shown that there is an increase in the Mo:Fe ratio at the surface, with increasing calcination temperature[2]. When these increased ratios are compared with data on the catalytic activity of these catalysts, the conclusion was made that the active phase of the catalysts was a solution of $MoO_3$ in $Fe_2(MoO_4)_3$. An alternative XPS study of iron molybdate catalysts with varying iron-molybdenum ratio suggested that the catalysts exist as core structures[3], with catalysts below the stoichiometric ratio for $Fe_2(MoO_4)_3$, presenting an $Fe_2O_3$ rich surface, whilst those above this ratio presented a surface with $MoO_3$ covering the bulk $Fe_2(MoO_4)_3$. The catalyst with the stoichiometric composition showed the best catalytic performance.

Preparation of previous catalysts with $MoO_3$ on the surface of $Fe_2O_3$, showed concentrations of <6 $nm^{-2}$ (*ca.* 70 % coverage) $MoO_3$ are supported as a monolayer, above this concentration accumulation of the molybdenum oxide on the monolayer or the aggregation of oxide was observed[4]. The catalysts showed that with molybdenum present, selectivity towards formaldehyde was achieved for methanol oxidation. A linear increase in methanol oxidation TOF was observed with increasing molybdenum

oxide on the surface (up to 6 $nm^{-2}$), which was reasoned to show the production of formaldehyde coming from adjacent molybdenum sites (one for methanol adsorption, and one for hydrogen abstraction from the methoxy). The structure of the monolayer was seen to be similar to that of $Fe_2(MoO_4)_3$, with similar methanol conversion and formaldehyde selectivity observed.

Molybdena supported on $Fe_2O_3$ catalysts have also been created by heating $MoO_3$ with $Fe_2O_3$[5]. In this case, the dispersion capacity was calculated as 0.8 $mmol/100m^2$ (5.0 $nm^{-2}$) for calcination at 420 °C. Calcination to 500 °C lead to the reaction of $MoO_3$ with the bulk $Fe_2O_3$ to form $Fe_2(MoO_4)_3$. The $Fe_2(MoO_4)_3$ formed remained at the surface, effectively encapsulating the $Fe_2O_3$ inside.

## 5.2 Experimental

Catalysts with varying bulk ratios of molybdenum to iron were created in the using the same method of precipitation, followed by evaporation to dryness as mentioned in chapter 2. One difference that was observed was that addition of the iron nitrate initially lead to the precipitation of a canary yellow precipitate, but with ratios lower than 1.5:1 Mo:Fe, this precipitate dissolved, before a dark brown gel was formed in the bottom of the crucible while the water was evaporated. The gel was then dried and calcined following the same procedure as previously used.

In addition to catalysts with varying bulk ratios, catalysts with molybdenum dosed onto the surface of iron oxide were also created. In calculating the loading to add, it was assumed that a surface of $Fe_2O_3$ contains $10^{19}$ surface sites $m^{-2}$, with a total of 5/12 of these being metal cations as it was thought a $Fe_2(MoO_4)_3$ layer may form. This corresponds reasonably well with the value previously reported for $MoO_3$ spreading on $Fe_2O_3$, which showed 70 % coverage at 6 $nm^2$ (*i.e.* complete coverage would correspond to 3.58 x $10^{18}$ surface cations $m^{-2}$)[4]. The catalysts were made by the

incipient wetness method of impregnation onto a synthesised $Fe_2O_3$ with a surface area of 11.8 $m^2$ $g^{-1}$. Ammonium heptamolybdate was made into an aqueous solution and added to iron oxide until the pores of the support were full. The material was then dried overnight at 120 °C. Calcination of the material was carried *in-situ* in 10 % $O_2$/He gas flow after loading to the reactor at 400 °C for 30 minutes. Catalysts were made with nominally 24, 60, 240 and 720 % ML (0.28, 0.70, 2.8 and 8.5 w/t %) $MoO_3$. Another catalyst was made with iron added to the surface of $MoO_3$ by the same method, using iron (III) nitrate as the source of iron. This was made to have a coverage of 2.4 ML (0.13 w/t %) $Fe_2O_3$.

A further catalyst was created with a calculated coverage of 2.4 ML $MoO_3$ onto the surface of the Mo:Fe 0.2:1 catalyst to compare the performance of a low Mo:Fe catalyst with added surface layers of molybdenum.

## *5.3 Results and Discussion*

### 5.3.1 Bulk Catalysts

#### 5.3.1.1 Reaction Profiles

The reaction profile for $Fe_2O_3$, Mo:Fe 1.5 and 2.2:1, as well as $MoO_3$, were reported in chapter 3, so the reader is guided back to this section to view the conversion selectivity plots for these catalysts.

The reaction profile for methanol over the 0.02:1 Mo:Fe catalyst (Figure 5-1, Appendix A-48) shows the catalyst with moderate formaldehyde selectivity (~50 %) at low temperatures (~180 °C) and conversions (~15 %). This drops rapidly to below 10 % by 230 °C, where conversion has reached ~65 %, and is zero by 300 °C. CO selectivity starts at around 40 % rising to between 65 – 70 %, between 210 and 260

°C. When the temperature is raised further CO selectivity drops steadily to 25 % by ~310 °C, and zero by 370 °C. $CO_2$ production begins at around 200 °C, and rises steadily to around 40 % by 270 °C and on to near 100 % by 370 °C. Little dimethyl ether is produced, with selectivity around 3 % at 180 °C, dropping below 1 % by 220 °C.

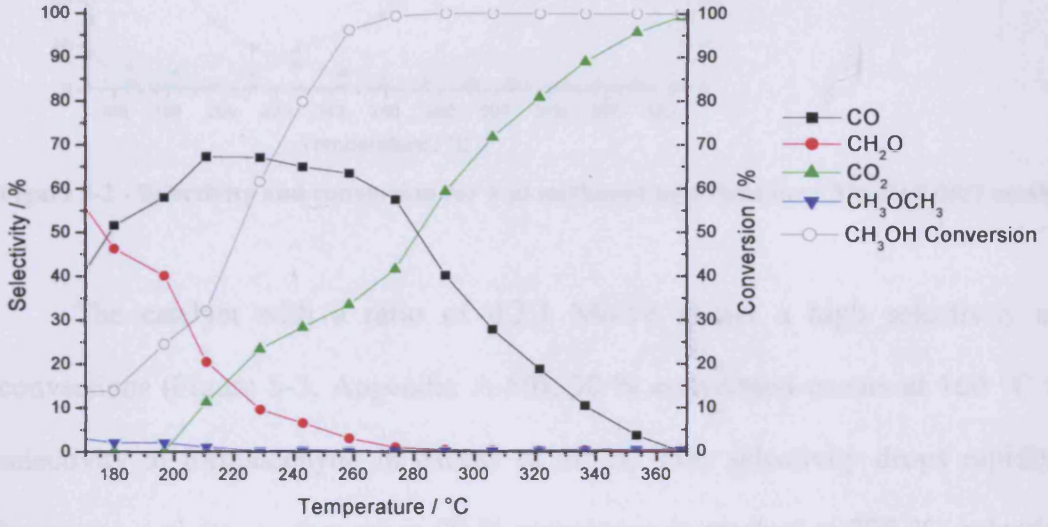


**Figure 5-1 - Selectivity and conversion for 1 µl methanol injections over Mo:Fe 0.02:1 catalyst.**

The catalyst with a ratio of 0.05:1 Mo:Fe shows a high activity (Figure 5-2, Appendix A-49), reaching 50 % conversion at ~180 °C and greater than 90 % by 210 °C. Formaldehyde selectivity drops rapidly from around 75 % at 150 °C to around 15 % by 200 °C and below 5 % by 230 °C. The drop in formaldehyde selectivity occurs as it is replaced by CO selectivity, which rises from ~15 % at 150 °C to ~85 % by 195 °C. CO selectivity then remains above 80 % until 260 °C where it drops steadily to around 10 % by 370 °C. Production of $CO_2$ starts at around 200 °C, rising to near 90 % by 370 °C.

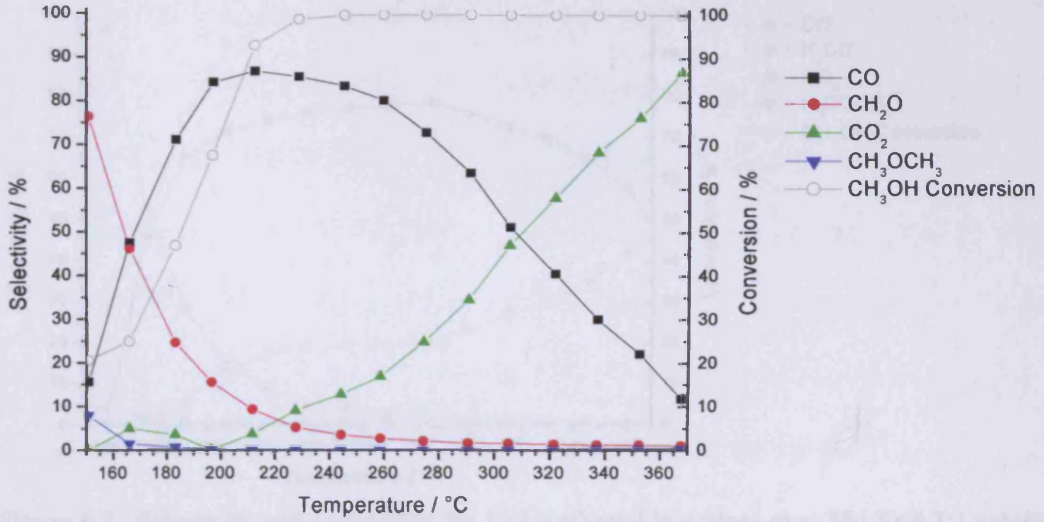


**Figure 5-2 - Selectivity and conversion for 1 µl methanol injections over Mo:Fe 0.05:1 catalyst.**

The catalyst with a ratio of 0.2:1 Mo:Fe shows a high selectivity at low conversions (Figure 5-3, Appendix A-50), 30 % conversion occurs at 160 °C with a selectivity to formaldehyde in excess of 90 %. This selectivity drops rapidly with increasing activity, so that when 90 % conversion is reached at 205 °C, selectivity is less than 15 %. This decrease in formaldehyde selectivity is matched by an increase in selectivity to CO which rises to around 65 % at 205 °C, before climbing further to around 75 % at 285 °C. $CO_2$ production rises from nothing at 175 °C to around 20 % by 220 °C, where it remains approximately constant, before rising after 280 °C to peak at over 55 % at 375 °C. The minor product of dimethyl ether shows a similar path, beginning at around 6 % selectivity at 150 °C, dropping to below 1 % by 210 °C.

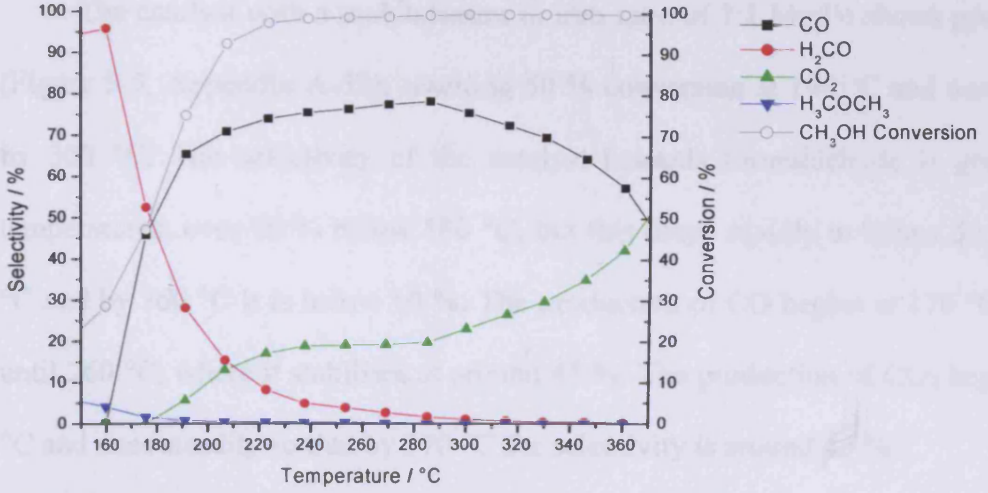


**Figure 5-3 - Selectivity and conversion for 1 µl methanol injections over Mo:Fe 0.2:1 catalyst.**

The catalyst with 0.5:1 Mo:Fe ratio follows a similar profile to that of the 0.2:1 catalyst (Figure 5-4, Appendix A-51), with high formaldehyde selectivity at low conversions, in excess of 90 %, with 15 % conversion at 160 °C. This drops to around 30 % selectivity at 90 % conversion, with a continuing decline to effectively zero by 370 °C. CO rises from less than 5 % at 160 °C to over 50 % by 210 °C, eventually rising to around 70 % at 300 °C. The selectivity of $CO_2$ rises from near zero to around 20 % by 220 °C where it remains approximately constant until 300 °C when a slow increase to above 30 % by 370 °C is observed. Dimethyl ether begins low at less than 3 % and drops further so that by 260 °C it has a selectivity of less than 1 %.

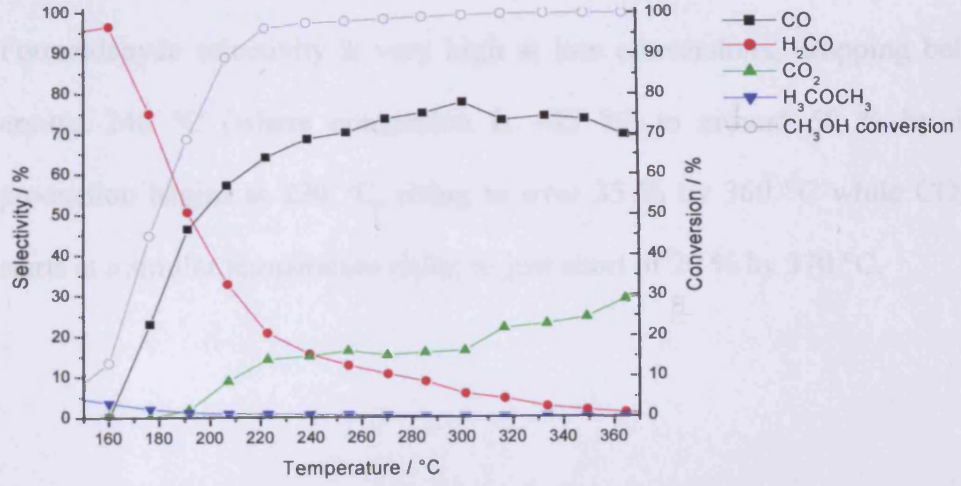


**Figure 5-4 - Selectivity and conversion for 1 µl methanol injections over Mo:Fe 0.5:1 catalyst.**

The catalyst with a molybdenum to iron ratio of 1:1 Mo:Fe shows good activity (Figure 5-5, Appendix A-52), reaching 50 % conversion at 190 °C and nearly 100 % by 300 °C. The selectivity of the catalyst towards formaldehyde is good at low temperatures, over 90 % below 180 °C, but this drops rapidly to below 50 % by 240 °C and by 360 °C it is below 10 %. The production of CO begins at 170 °C and rises until 260 °C, where it stabilises at around 45 %. The production of $CO_2$ begins at 220 °C and rises steadily so that by 370 °C the selectivity is around 45 %.

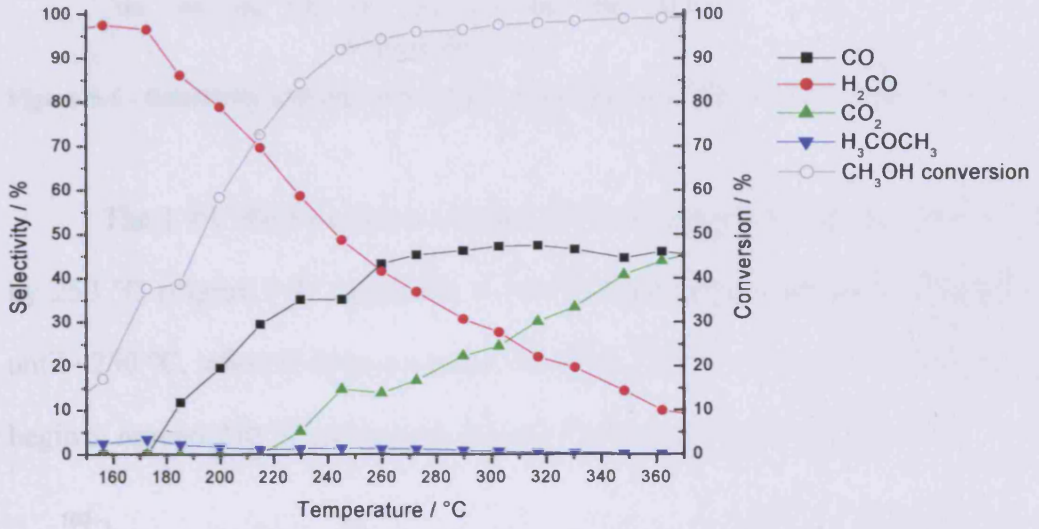


**Figure 5-5 - Selectivity and conversion for 1 µl methanol injections over Mo:Fe 1:1 catalyst.**

The reaction profile for the 1.6:1 Mo:Fe catalyst shows a good activity (Figure 5-6, Appendix A-53), reaching 50 % conversion at 200 °C and 90 % at around 260 °C. Formaldehyde selectivity is very high at low conversions, dropping below 90 % at around 240 °C (where conversion is ~85 %) to around 50 % by 370 °C. CO production begins at 230 °C, rising to over 35 % by 360 °C while $CO_2$ production starts at a similar temperature rising to just short of 20 % by 370 °C.

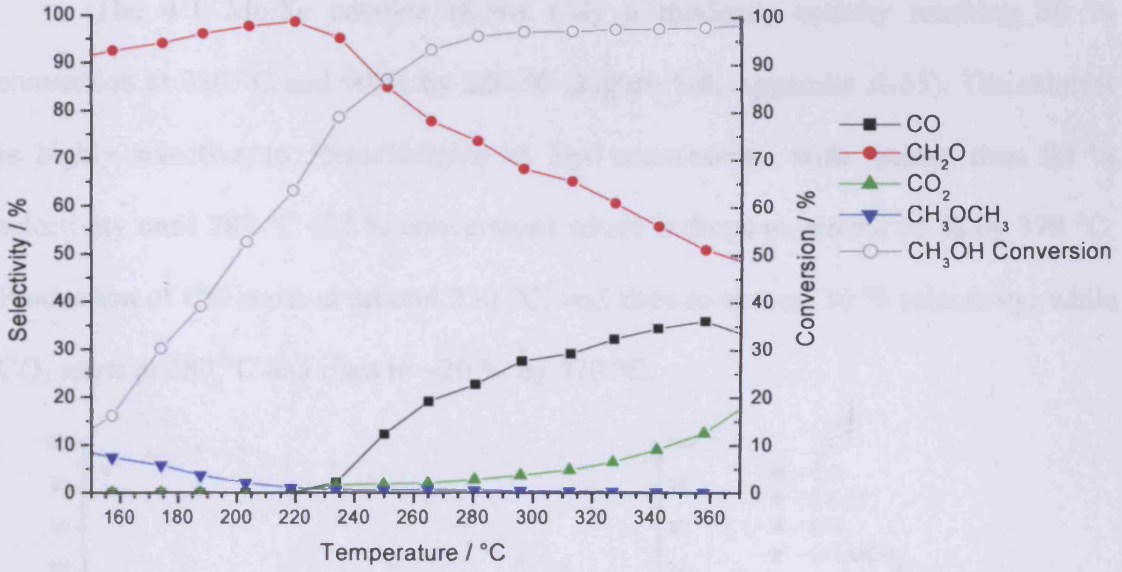


**Figure 5-6 - Selectivity and conversion for 1 µl methanol injections over Mo:Fe 1.6:1 catalyst.**

The 1.9:1 Mo:Fe catalyst reaches 50 % conversion at around 200 °C and 90 % by 250 °C (Figure 5-7, Appendix A-54). Formaldehyde selectivity is high (>90 %) until ~250 °C, where it drops to below 40 % by 370 °C. CO and $CO_2$ productions both begin at around 230 °C and reach ~50 and 15 % respectively at 370 °C.

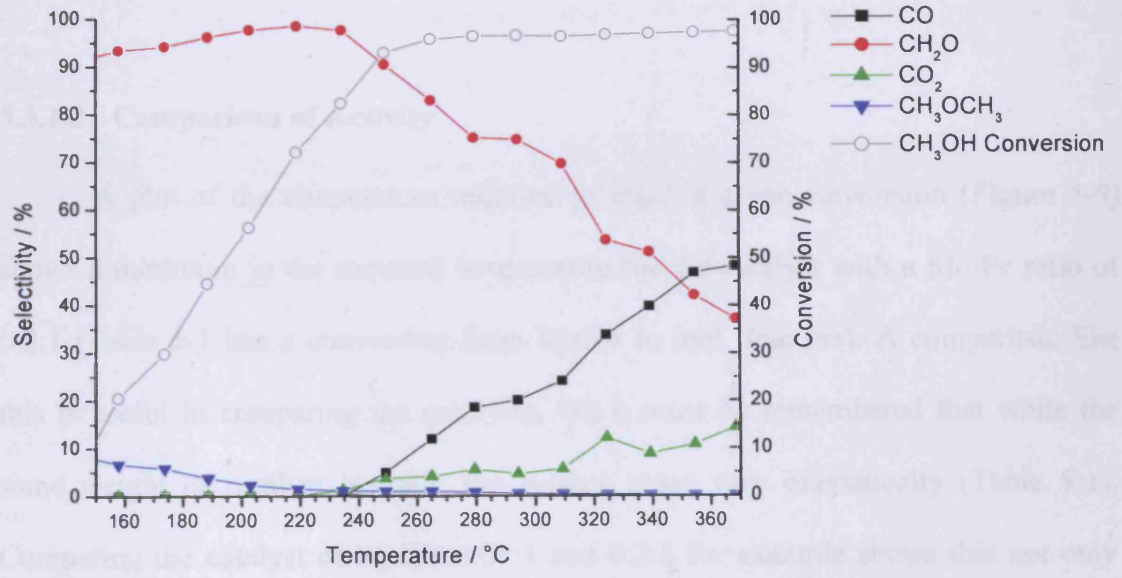


**Figure 5-7 - Selectivity and conversion for 1 µl methanol injections over Mo:Fe 1.9:1 catalyst.**

The 4:1 Mo:Fe catalyst shows only a moderate activity reaching 50 % conversion at 230 °C and 90 % by 280 °C (Figure 5-8, Appendix A-55). The catalyst is highly selective to formaldehyde at low conversions, with greater than 90 % selectivity until 280 °C (92 % conversion) where it drops to around 55 % by 370 °C. Production of CO starts at around 230 °C, and rises to around 30 % selectivity, while $CO_2$ starts at 280 °C and rises to ~20 % by 370 °C.

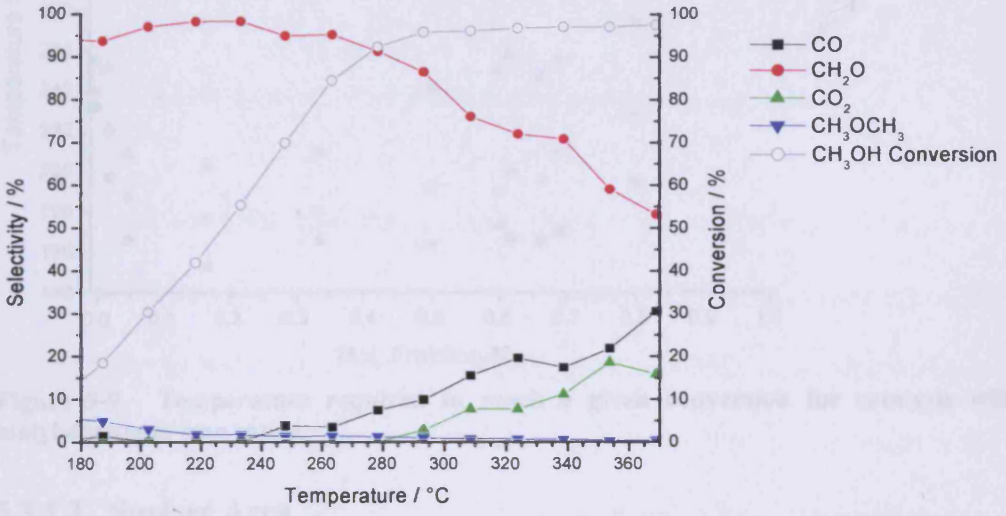


**Figure 5-8 - Selectivity and conversion for 1 µl methanol injections over Mo:Fe 4:1 catalyst.**

### 5.3.1.2 Comparison of Activity

A plot of the temperature required to reach a given conversion (Figure 5-9) shows a minimum in the required temperature for the catalyst with a Mo:Fe ratio of 0.2:1 (Table 5-1 has a conversion from Mo:Fe to mol. fraction). A comparison like this is useful in comparing the catalysts, but it must be remembered that while the same weight of catalyst is used, the surface areas vary dramatically (Table 5-1). Comparing the catalyst of Mo:Fe 0.05:1 and 0.2:1 for example shows that not only does the 0.2:1 catalyst convert more methanol at lower temperatures, but it also has a lower surface area than the 0.05:1 catalyst, thereby showing a much greater conversion per unit area. $Fe_2O_3$ can also be observed to be less reactive per unit area

than the catalysts containing 1.5-2.2:1 Mo:Fe as all reach 90 % methanol conversion at around 255 °C, but the molybdenum containing catalysts have a surface area approximately 2½ times smaller.

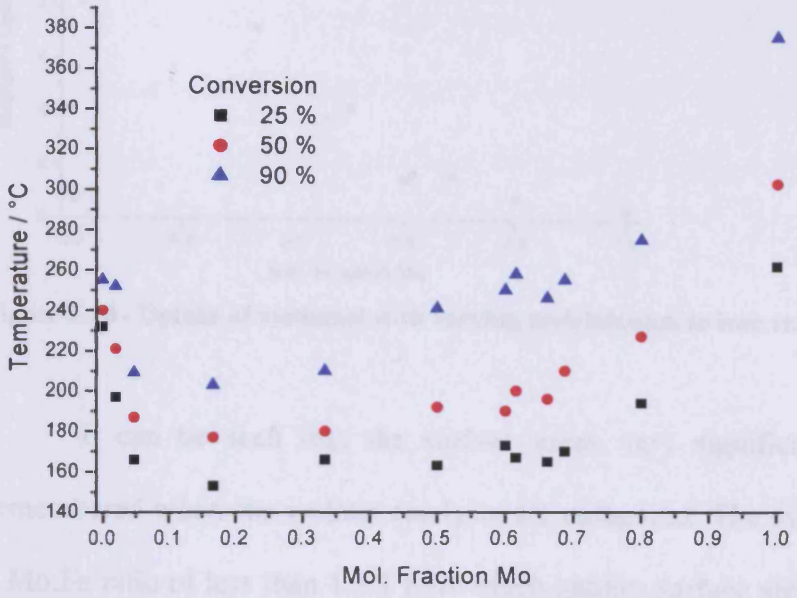


**Figure 5-9 - Temperature required to reach a given conversion for catalysts with varying molybdenum to iron ratios.**

### 5.3.1.3 Surface Area

The surface areas and uptake of methanol for the catalysts were measured and are shown in Table 5-1 and Figure 5-10.

| Catalyst | Mol. Fraction Mo. | Surface Area ($m^2 g^{-1}$) | Methanol uptake ($\mu l\ g^{-1}$) |
|---|---|---|---|
| $Fe_2O_3$ (bottle) | 0 | 2.1 | 0.70 |
| $Fe_2O_3$ (synthesised) | 0 | 16.8 | 4.22 |
| Mo:Fe 0.02:1 | 0.0196 | 34.0 | 8.2 |
| Mo:Fe 0.05:1 | 0.0476 | 65.6 | 14.7 |
| Mo:Fe 0.2:1 | 0.167 | 55.4 | 10.4 |
| Mo:Fe 0.5:1 | 0.333 | 38.7 | 7.2 |
| Mo:Fe 1:1 | 0.5 | 16.3 | 4.2 |
| Mo:Fe 1.5:1 | 0.6 | 6.5 | 1.46 |
| Mo:Fe1.6:1 | 0.615 | 6.4 | 1.72 |
| Mo:Fe1.9:1 | 0.655 | 4.3 | - |
| Mo:Fe:2.2:1 | 0.688 | 6.7 | 1.64 |
| Mo:Fe 4:1 | 0.8 | 3.6 | 0.78 |
| $MoO_3$ (bottle) | 1 | 1.0 | 0.36 |

**Table 5-1 - Measured surface area of catalysts.**

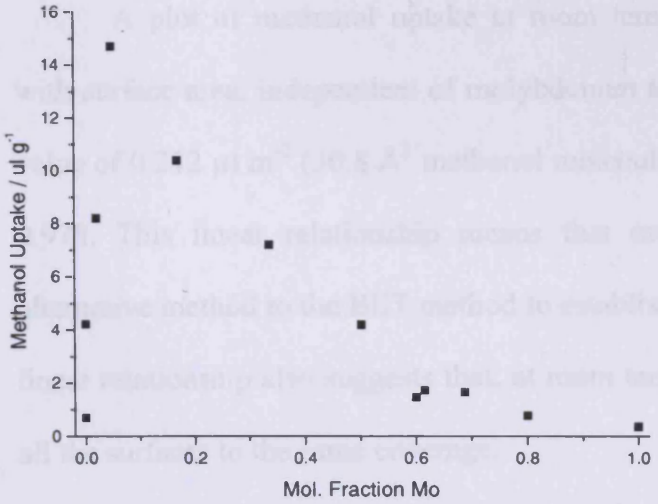


**Figure 5-10 - Uptake of methanol with varying molybdenum to iron ratios**

It can be seen that the surface areas vary significantly and this must be remembered when the various catalysts are compared. The synthesised catalysts with a Mo:Fe ratio of less than 1.5:1 have much greater surface areas, this is most likely to be due to different mechanism of formation, as with the higher ratio catalysts the addition of the ferric nitrate solution to the acidified ammonium molybdate solution lead to direct coprecipitation before evaporation to dryness, whereas, in contrast, the lower ratio catalysts formed as a gel during the evaporation to dryness stage.

The results presented here show that addition of molybdenum leads to catalysts with lower surface areas (Table 5-1 and Figure 5-10), except for catalysts where there is a very high iron content ($Fe_2O_3$, Mo:Fe 0.02:1 and Mo:Fe 0.05:1) where the areas are reduced. There is little difference in surface area between the catalysts that present a small excess of $MoO_3$ (Mo:Fe 1.6, 1.9, 2.2:1) over stoichiometric $Fe_2(MoO_4)_3$. The addition of further molybdenum (Mo:Fe 4:1 and $MoO_3$) to this leads to a decrease in surface area. This is in contrast to two previous works, where an excess of $MoO_3$ was found to add to the surface area[6,7]. The excess of molybdena was found to always form with precipitation preparations, while the oxidation rate per unit area was the same, despite the $MoO_3$ excess.

A plot of methanol uptake at room temperature shows a linear relationship with surface area, independent of molybdenum to iron ratio (Figure 5-11). An uptake value of 0.212 μl $m^{-2}$ (30.8 $Å^2$ methanol $molecule^{-1}$) was recorded with an $R^2$ value of 0.978. This linear relationship means that methanol uptake can be used as an alternative method to the BET method to establish the surface area of the catalyst. The linear relationship also suggests that, at room temperature, methanol is adsorbed onto all the surfaces to the same coverage.

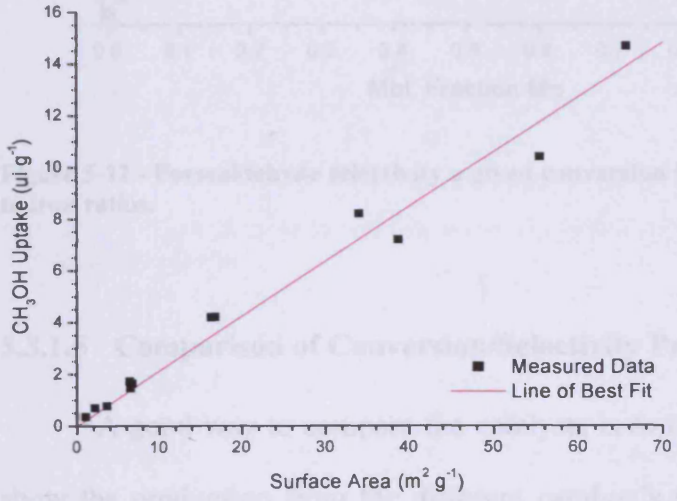


**Figure 5-11 – Methanol uptake at room temperature measured against surface area.**

### 5.3.1.4 Comparison of Selectivity

A plot of formaldehyde selectivity at a given conversion (Figure 5-12) shows that at 25 % conversion, all catalysts except those with very low molybdenum content (≤ 0.05:1 Mo:Fe) show good formaldehyde selectivity (~90 %). Raising conversion to 50 % shows that the drop off in performance now occurs for catalysts with a Mo:Fe ratio lower than 1.5:1 Mo:Fe (0.6 mol. fraction Mo *i.e.* less than that required for $Fe_2(MoO_4)_3$). At 90 % conversion, even this catalyst shows diminished selectivity, with only catalysts having a Mo:Fe ratio 1.9:1 or above showing greater than 90 % formaldehyde selectivity.

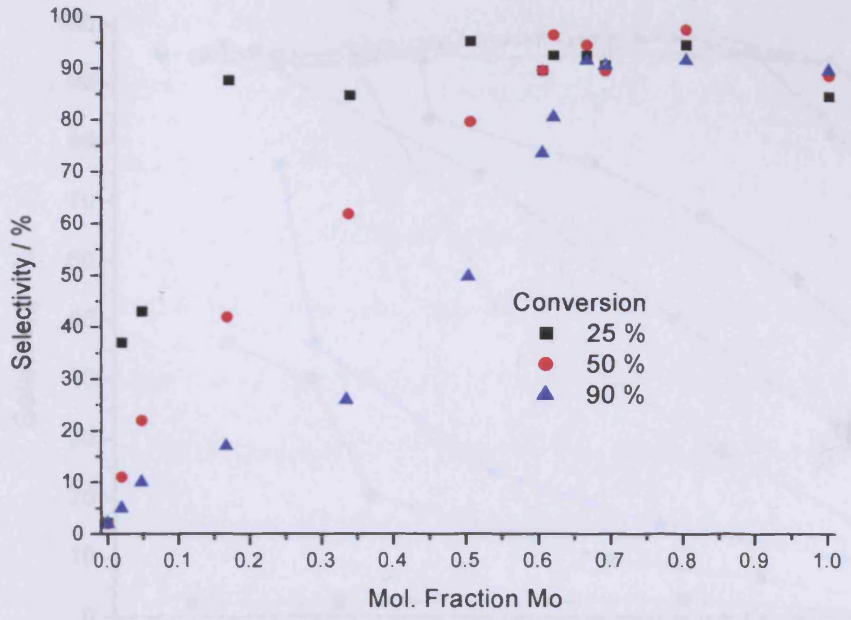


**Figure 5-12 - Formaldehyde selectivity a given conversion for catalysts with varying molybdenum to iron ratios.**

### 5.3.1.5 Comparison of Conversion/Selectivity Profiles

A good way to compare the catalysts is to use a conversion selectivity plot to show the production from the different catalyst's surfaces. One problem with these plots is that a difference in reaction temperature is not displayed, so while a point for 50 % conversion on the 0.2:1 catalyst may occur at 180 °C, on $MoO_3$, this point occurs at nearly 300 °C. Such profiles are commonly used in the catalyst literature. Using these type of plots for different loadings of 2.2:1 Mo:Fe in chapter 3 established that there was only a limited difference despite the difference in temperature required to gain the same conversion.

Looking at the plot for formaldehyde production (Figure 5-13) shows that all the catalysts containing molybdenum show some formaldehyde selectivity at low conversions, with only the 0.02:1 and 0.05 Mo:Fe catalysts never showing more than 90 % selectivity (the maximum for these catalyst being ~50 and 80 % selectivity at ~10 % conversion respectively).

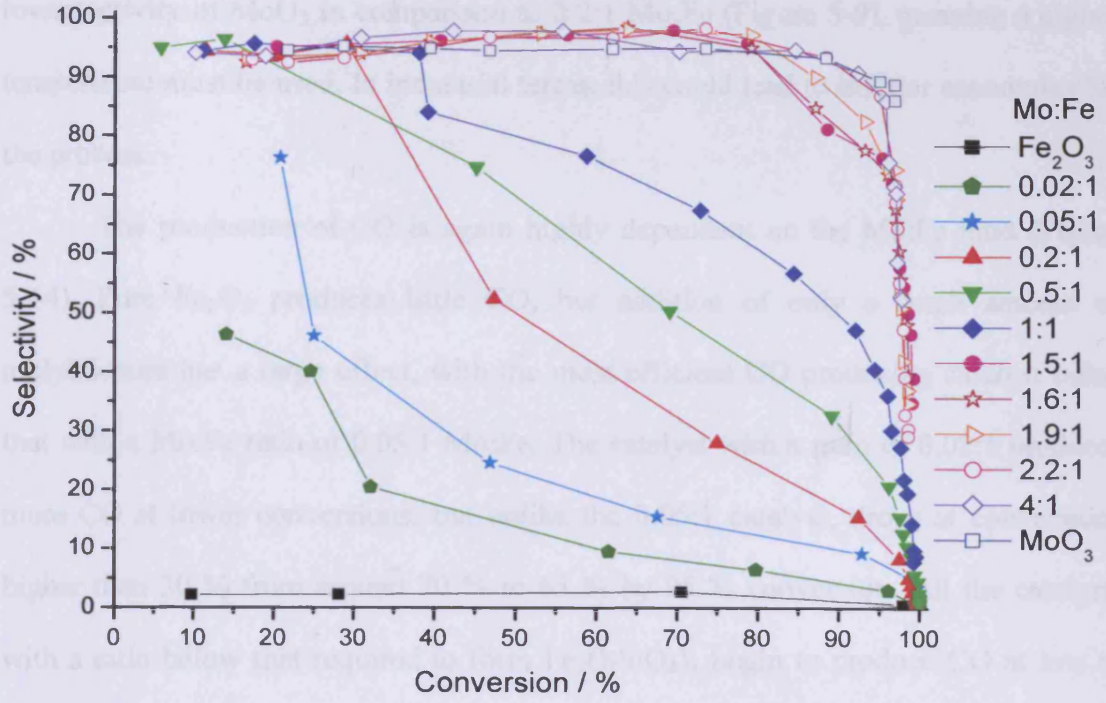


**Figure 5-13 - Selectivity to formaldehyde vs. methanol conversion for different ratios of molybdenum to iron.**

The greatest yield of a product is indicated by the data in the top right corner of the graph. It can therefore be seen that increasing the level of molybdenum, all the way to $MoO_3$ leads to optimised catalyst performance. There is an increase in catalyst performance when moving from a catalyst of stoichiometric $Fe_2(MoO_4)_3$ to those with an excess of $MoO_3$ (*i.e.* >1.6:1 Mo:Fe), though there is little difference between the ratios of 1.5 and 1.6:1 Mo:Fe. This contrasts with a recent paper by Kim *et al.* who showed there was little difference between a catalyst contain a Mo:Fe ratio of 3.0:1 and 1.5:1[8]. However in this work the conversions used were only moderate (~70 %) and at this conversion, work presented in this thesis, shows little difference is also observable. The difference in performance is instead most appreciable at the high conversions (>90 %) that are used in the industrial process. It can be seen that the catalyst with an industrial-like composition (2.2:1 Mo:Fe) is also a little less selective to formaldehyde at high conversions than $MoO_3$. However, one must remember the

lower activity of $MoO_3$ in comparison to 2.2:1 Mo:Fe (Figure 5-9), meaning a higher temperature must be used. In industrial terms, this could lead to inferior economics for the process.

The production of CO is again highly dependent on the Mo:Fe ratio (Figure 5-14). Pure $Fe_2O_3$ produces little CO, but addition of only a small amount of molybdenum has a large effect, with the most efficient CO producing catalyst being that with a Mo:Fe ratio of 0.05:1 Mo:Fe. The catalyst with a ratio of 0.02:1 produces more CO at lower conversions, but unlike the 0.05:1 catalyst, drops at conversions higher than 30 % from around 70 % to 65 % by 95 % conversion. All the catalysts with a ratio below that required to form $Fe_2(MoO_4)_3$ begin to produce CO at low to medium conversions, reaching at least 30 % CO selectivity by 80 % conversion. CO production occurs even on the high Mo:Fe catalysts, with a rapid increase above 80 % conversion for $Fe_2(MoO_4)_3$ and closer to 90 % for those with an excess of $MoO_3$.

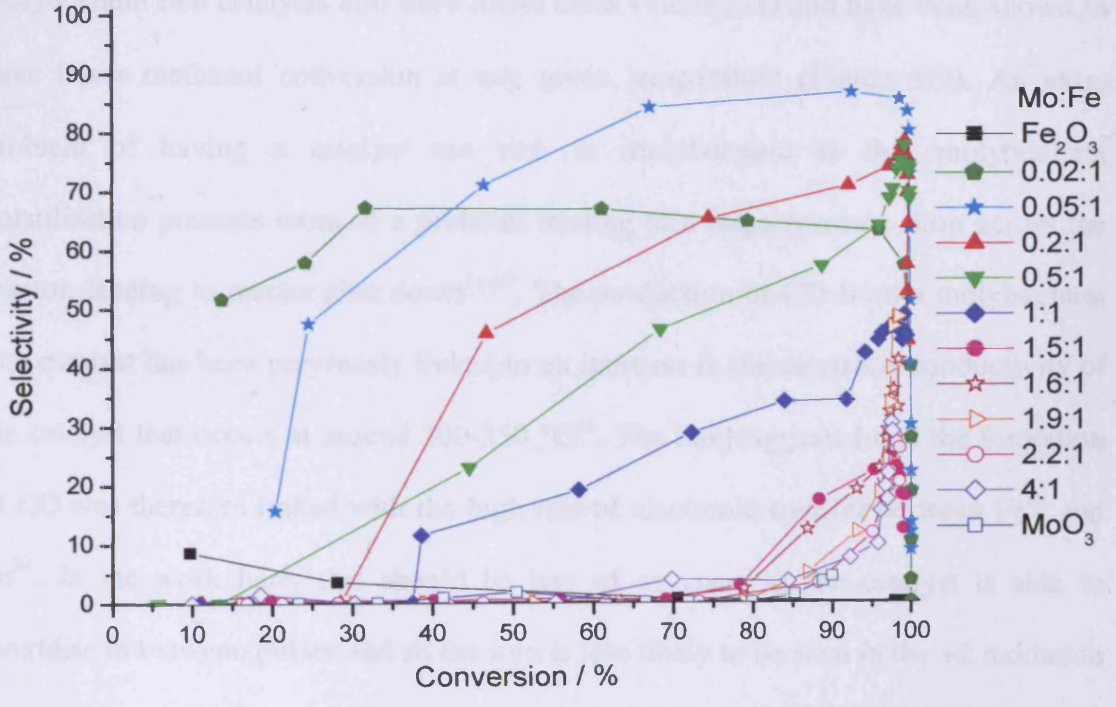


**Figure 5-14 - Selectivity to CO vs. methanol conversion for different ratios of molybdenum to iron.**

The production of CO is the major reason for lost selectivity within the industrial process and, it can be seen to be the reason for the drop in formaldehyde selectivity for the high Mo:Fe catalysts. The production of CO at temperatures above 300 °C has been reported directly from methanol, but the study claims that this formation is condition dependent[9]. In this work the production of CO was earlier assigned (Chapter 3) to secondary oxidation of formaldehyde on catalysts of 1.5:1 Mo:Fe and above. This secondary oxidation process seems to be somewhat inhibited by the presence of excess $MoO_3$, meaning that the more $MoO_3$, the less CO is produced. It has previously been reported that one reason for the excess molybdenum is to dope the $Fe_2(MoO_4)_3$ to reach an Mo/Fe ratio higher than 1.5 in the active phase[10]. This may be the case but continuing to increase the molybdenum beyond a slight excess (Mo:Fe 1.6:1) still shows improvement in catalytic performance. A balance must be reached between excess molybdena and ferric molybdate as heavily molybdenum rich catalysts also have lower areas (Table 5-1) and have been shown to have lower methanol conversion at any given temperature (Figure 5-9). An extra problem of having a catalyst too rich in molybdenum is that molybdenum volatilisation presents more of a problem leading to a large pressure drop across the reactor, leading to reactor shut down[11-13]. The production of CO from a molybdenum rich catalyst has been previously linked to an increase in the electrical conductivity of the catalyst that occurs at around 300-350 °C[14]. The link suggested that the formation of CO was therefore linked with the high rate of electronic transfer between $Fe^{2+}$ and $Fe^{3+}$. In the work here, this should be less of an issue as the catalyst is able to reoxidise in between pulses and so the iron is less likely to be seen in the +2 oxidation state. In chapter 3 it was also shown that the formation of CO in molybdenum rich

catalysts comes from the secondary oxidation of formaldehyde, rather than directly from methanol.

The large production of CO from the low ratio catalysts (Mo:Fe ≤0.05:1) can be ascribed to formation of a direct pathway to CO on these catalysts (evidence is described in Section 5.3.1.6 for this). This is contrast to the more molybdenum rich catalysts where CO is only formed from the secondary reaction of methanol.

For the $Fe_2O_3$ catalyst it can be seen that $CO_2$ is the major product formed at all conversions (Figure 5-15), while on all other catalysts it is only a minor product until very high (>95 %) conversions. The 0.02:1 Mo:Fe catalyst begins to produce $CO_2$ at around 30 % conversion, reaching around 30 % selectivity by 95 % conversion before a more rapid rise to near 100 %. The early production of $CO_2$ can be linked to the easy production of surface formate groups and the appearance of $CO_2$ and $H_2$ within TPD spectra (Section 5.3.1.6). Catalysts with a ratio of 1.5:1 or greater of Mo:Fe, do not produce any $CO_2$ until greater than 95 % conversion, while the other catalysts below this ratio start to evolve it at around 70-80 % conversion, typically reaching around 15 % selectivity by 95 % conversion. The production of $CO_2$ off all catalysts at high conversion can be attributed to the higher temperatures used here allowing access to the thermodynamically most stable compound of $CO_2$. In the case of $Fe_2O_3$ the $CO_2$ is a primary product, going *via* the formate intermediate (Chapter 3), while that from the catalysts with a higher molybdenum ratio (Mo:Fe ≥0.5:1) is secondary oxidation produced by the linear pathway (Chapter 3):

$$CH_3OH \rightarrow CH_2O \rightarrow CO \rightarrow CO_2 \qquad (5\text{-}1)$$

For catalysts with a low molybdenum ratio (Mo:Fe <0.5:1), the $CO_2$ produced is a combination of direct $CO_2$, *via* formate groups on an $Fe_2O_3$ like surface and secondary oxidation of CO and formaldehyde (Section 5.3.1.6).

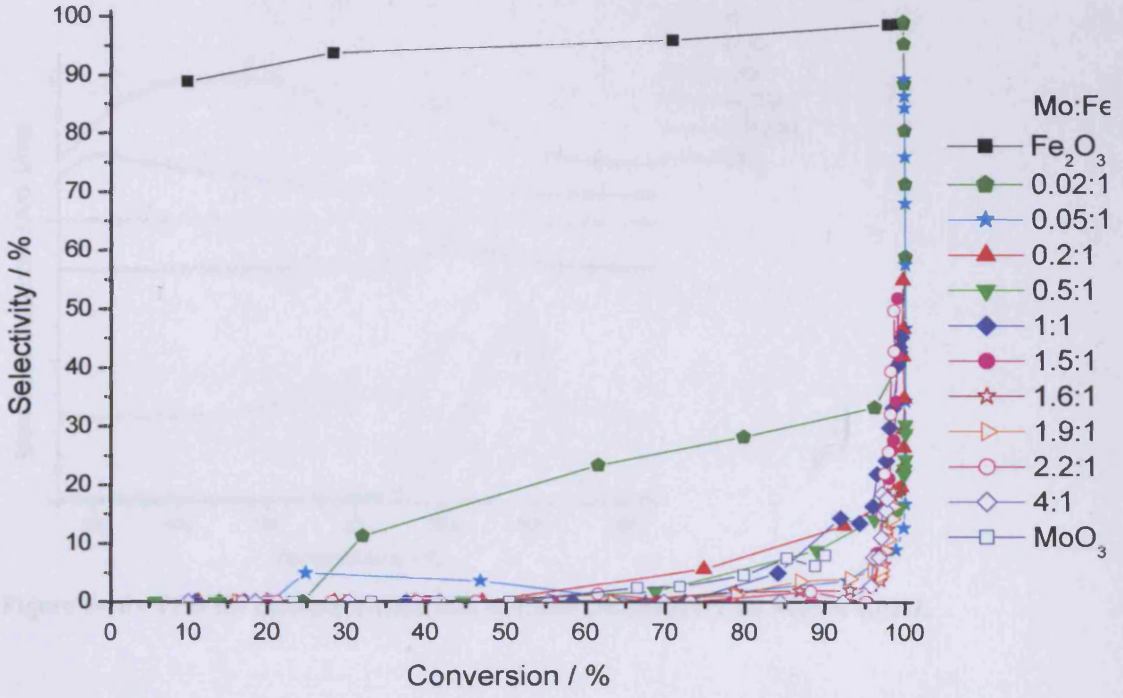


**Figure 5-15 - Selectivity to $CO_2$ vs. methanol conversion for different ratios of molybdenum to iron.**

### 5.3.1.6 Temperature Programmed Desorption

The methanol TPD for $Fe_2O_3$, Mo:Fe 1.5, 2.2:1, and $MoO_3$ were reported in chapter 3, so the reader is guided back to this section to view the temperature programmed desorption plots for these catalysts.

The TPD profile for the 0.02:1 Mo:Fe catalyst shows a small methanol desorption centred at around 60 °C, with no formaldehyde observed (Figure 5-16). A small CO desorption is observed centred at 260 °C, while the major carbon product observed is $CO_2$, centred at 285 °C. The water desorption shows a triple peak, with the first a very broad shoulder at ~70 °C, before the major peak at 145 °C. The second peak has not returned to the base line when the third, smaller water peak occurs near coincident with the CO peak at 260 °C. There is a double peak in the hydrogen production with the first, smaller peak centred at 185 °C, and the second at 275 °C, which occurs nearly coincidently with the $CO_2$.

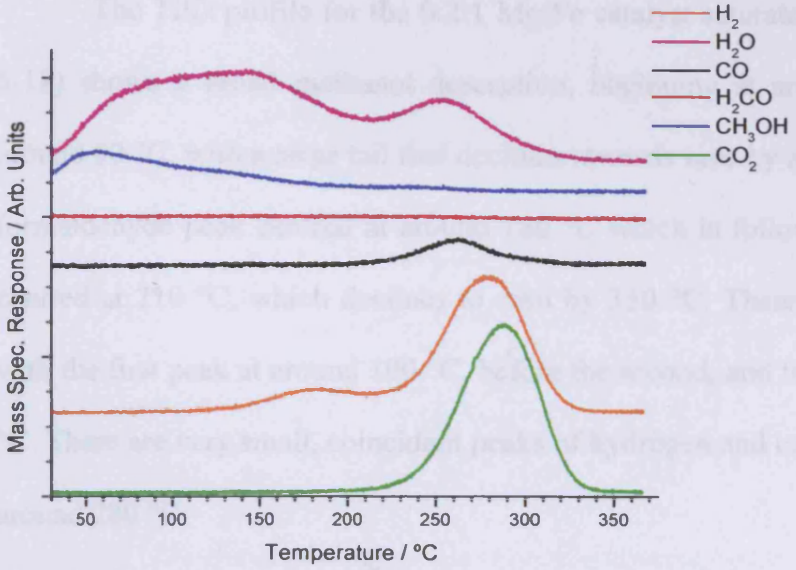


**Figure 5-16 - TPD for methanol adsorbed at room temperature on Mo:Fe 0.02:1.**

TPD from the 0.05:1 Mo:Fe catalyst shows a broad methanol desorption centred ~80 °C, with a shoulder feature at ~160 °C (Figure 5-17). A small formaldehyde desorption is centred at ~185 °C, while a large broad CO desorption has a maximum at 265 °C. Much more CO is observed compared with the Mo:Fe 0.02:1 catalyst. Water desorption shows a broad feature centred at around 100 °C, before two further peaks centred at 170 and 260 °C respectively. Large hydrogen and carbon dioxide desorptions are seen near coincident at 290 and 300 °C respectively.

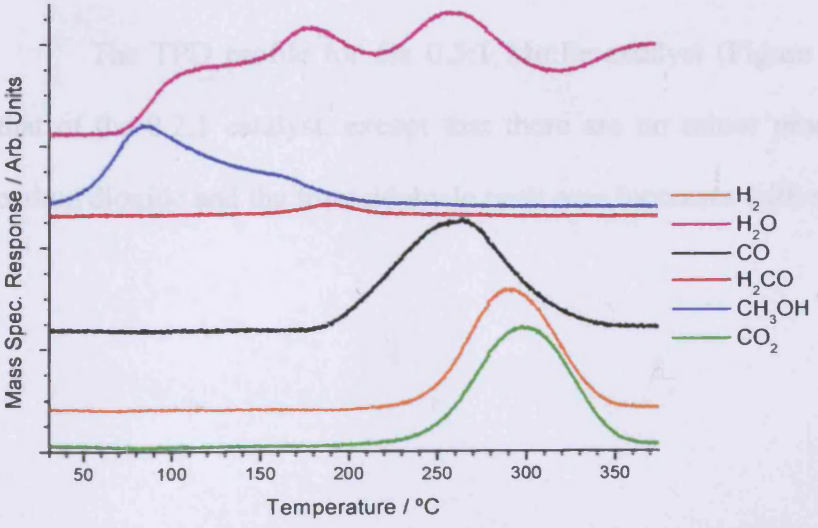


**Figure 5-17 - TPD for methanol adsorbed at room temperature on Mo:Fe 0.05:1.**

The TPD profile for the 0.2:1 Mo:Fe catalyst saturated with methanol (Figure 5-18) shows a broad methanol desorption, beginning at around 50 °C, peaking at around 80 °C, with a large tail that declines towards zero by around 210 °C. There is a formaldehyde peak centred at around 180 °C which is followed by a large CO peak centred at 210 °C, which declines to zero by 350 °C. There is a double water peak, with the first peak at around 100 °C, before the second, and larger peak centred at 265 °C. There are very small, coincident peaks of hydrogen and carbon dioxide, peaking at around 280 °C.

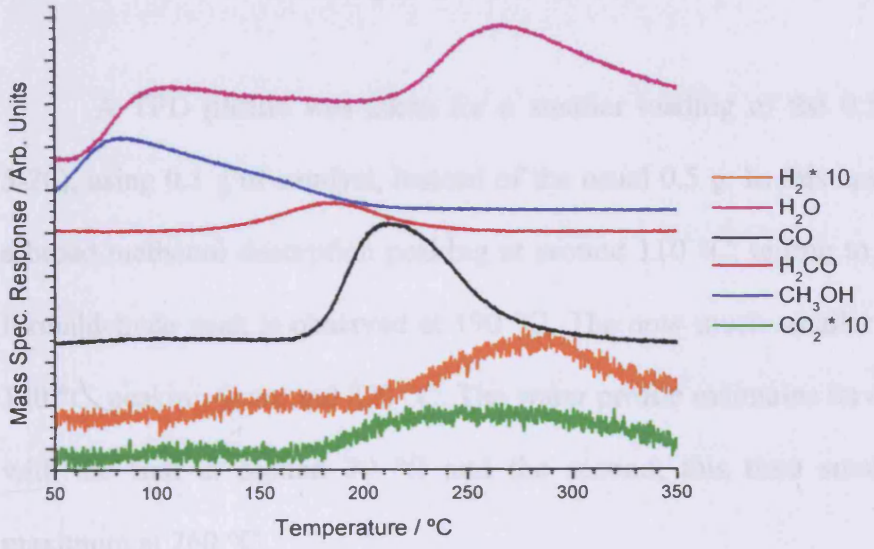


**Figure 5-18 - TPD for methanol adsorbed at room temperature on Mo:Fe 0.2:1.**

The TPD profile for the 0.5:1 Mo:Fe catalyst (Figure 5-19) looks similar to that of the 0.2:1 catalyst, except that there are no minor products of hydrogen and carbon dioxide and the formaldehyde peak area increases with respect to that of CO.

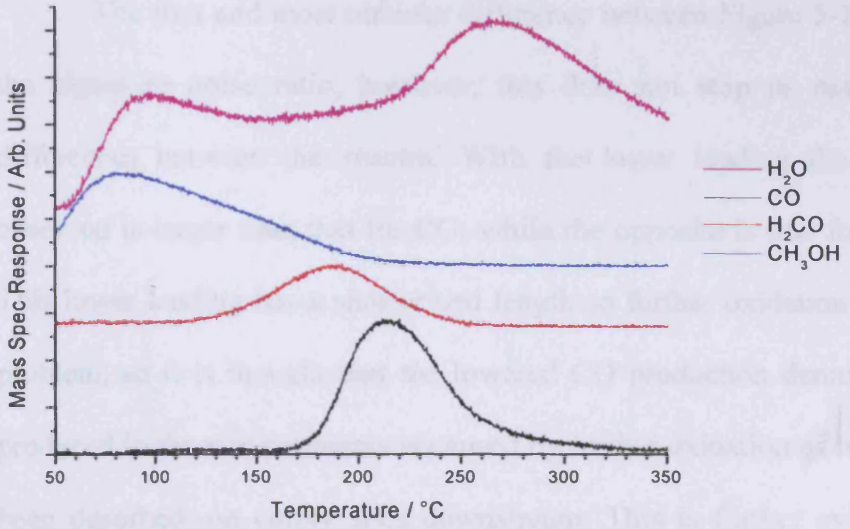


**Figure 5-19 - TPD for methanol adsorbed at room temperature on 0.5 g Mo:Fe 0.5:1.**

A TPD profile was taken for a smaller loading of the 0.5:1 catalyst (Figure 5-20), using 0.1 g of catalyst, instead of the usual 0.5 g. In this case the profile shows a broad methanol desorption peaking at around 110 °C, tailing to zero by 220 °C. A formaldehyde peak is observed at 190 °C. The now much smaller CO peak begins at 180 °C, peaking at around 220 °C. The water profile maintains its double peak profile, with the first at around 70 °C and the second, this time smaller peak having a maximum at 260 °C.

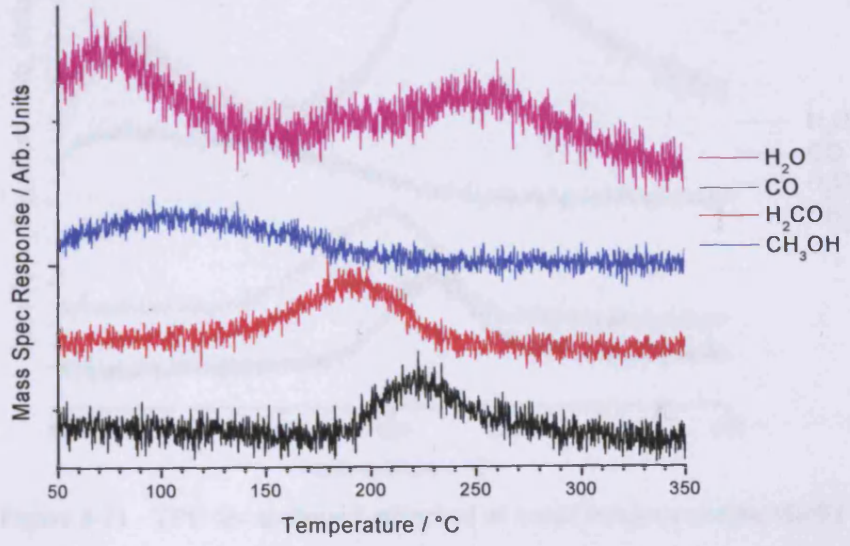


**Figure 5-20 - TPD for methanol adsorbed at room temperature on 0.1 g Mo:Fe 0.5:1.**

The first and most obvious difference between Figure 5-19 and Figure 5-20 is the signal to noise ratio, however, this does not stop us noting some important differences between the spectra. With the lower loading the formaldehyde peak observed is larger than that for CO, while the opposite is true for the higher loading. This lower loading has a shorter bed length so further oxidation is less likely to be a problem, so it is thought that the lowered CO production demonstrates that the CO produced in these experiments is caused by further oxidation of formaldehyde that has been desorbed, on empty sites downstream. This is further evidenced by the ratio difference of the water peaks. In the smaller loading of catalyst the second water peak is smaller than the first, (unlike in the larger loading), this suggests further oxidative dehydrogenation of the formaldehyde.

TPD from the 1:1 Mo:Fe catalyst shows a broad methanol desorption, roughly centred around 80 °C and essentially complete by 230 °C. Formaldehyde and CO desorptions are centred at around 200 and 220 °C respectively. Two peaks in water desorption are seen at 80 °C, and a second, larger peak at 235 °C.

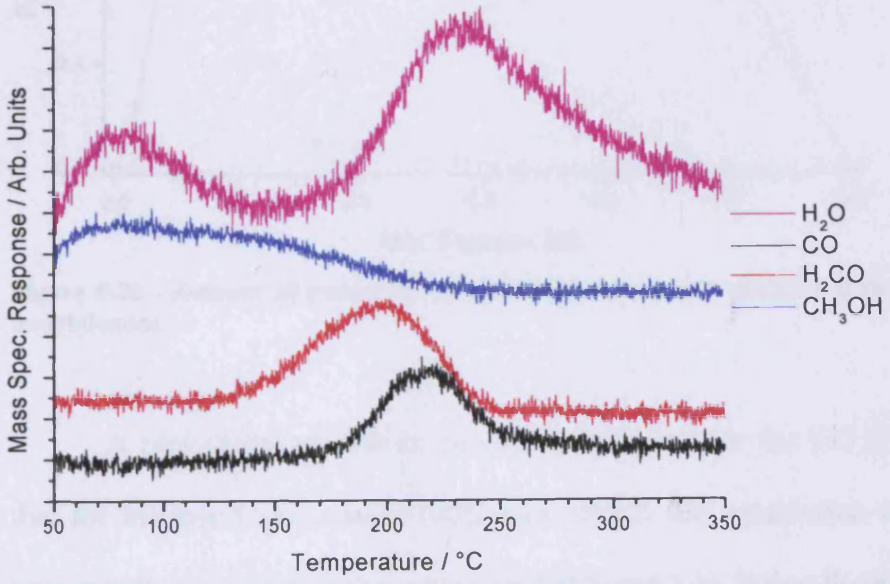


**Figure 5-21 - TPD for methanol adsorbed at room temperature on Mo:Fe 1:1.**

TPD spectra for the catalysts of 1.6:1 Mo:Fe and above are not shown as they are essentially the same as that recorded for Mo:Fe 2.2:1 and reported in chapter 3.

A comparison plot of the areas under the desorption profiles shows $CO_2$ to be the major product at low Mo:Fe ratios (Table 5-2 shows the conversion from Mo:Fe ratio to mole fraction molybdenum), formaldehyde at high levels and CO in between these (Figure 5-22). $CO_2$ is the only product observed off the surface of pure $Fe_2O_3$, with a decrease as molybdenum is added, to less than 50 % of the product by a ratio of Mo:Fe 0.05:1 and to zero by Mo:Fe ~0.3:1. The stoichiometric sample of $Fe_2(MoO_4)_3$ (Mo:Fe 1.5:1) shows only formaldehyde as a carbon product, and with a decreasing amount of this phase present, the amount of formaldehyde formed decreases.

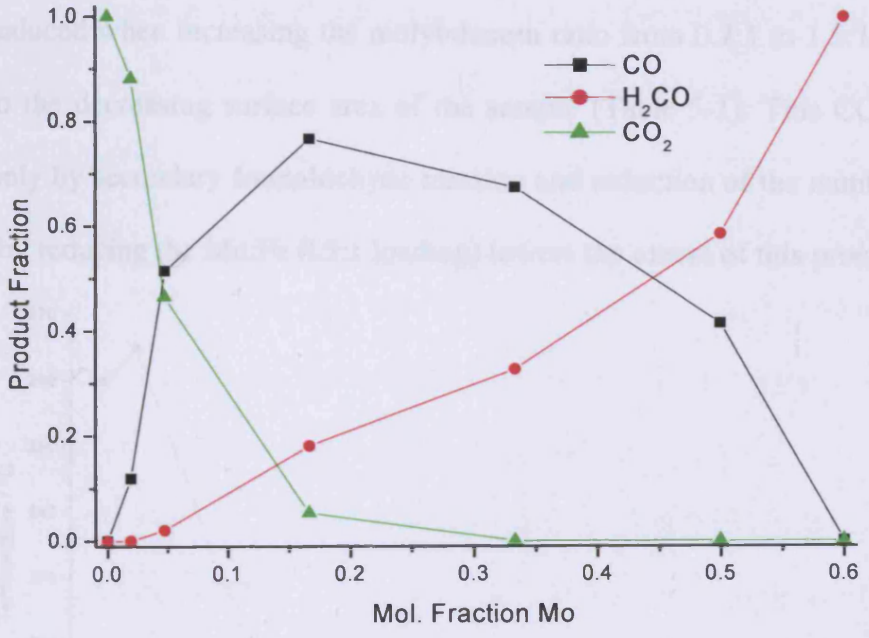


**Figure 5-22 - Amount of carbon based products formed off catalysts with varying mol fraction molybdenum.**

A plot of the maximum desorption temperature for CO (Figure 5-23) shows that for the low Mo:Fe ratios (0.02 and 0.05:1) CO production occurs *via* a higher energy pathway than for other ratios (0.2, 0.5 and 1:1). Using the Redhead equation to gain the activation energy shows ~15 kJ $mol^{-1}$ more energy is required for the low

molybdenum content (Table 5-2). The high temperature CO (produced from the Mo:Fe 0.02 and 0.05:1 catalysts) appears to be a primary product, while the work adjusting bed length shows the lower energy CO, from higher ratio catalysts (Mo:Fe 0.2, 0.5 and 1:1) is a secondary product from formaldehyde oxidation. The difference in the maximum desorption temperature between formaldehyde and secondary production of CO, from Mo:Fe 0.2, 0.5 and 1:1 (shown in Figures 5-18 to 21), can be reasoned to be due to a slightly higher activation energy for the second reaction involving further dehydrogenation. The secondary nature of the reaction is evidenced by the decrease in CO production when the smaller loading of the Mo:Fe 0.5:1 catalyst was used (Figure 5-20). It can therefore be reasoned that CO production is reduced when increasing the molybdenum ratio from 0.2:1 to 1.5:1 (Figure 5-22) due to the decreasing surface area of the sample (Table 5-1). This CO is then produced only by secondary formaldehyde reaction and reduction of the number of surface sites (by reducing the Mo:Fe 0.5:1 loading) lowers the extent of this process.

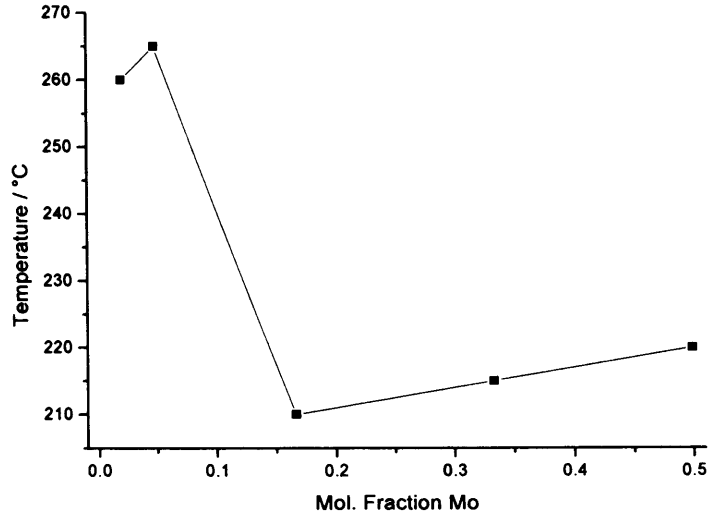


**Figure 5-23 - Temperature of maximum CO desorption.**

| Catalyst | Mol. Fraction Mo | Product Formed | Peak Temperature / °C | Energy (kJ $mol^{-1}$) |
|---|---|---|---|---|
| $Fe_2O_3$ | 0 | $CO_2$ | 300 | 155 |
| Mo:Fe 0.02:1 | 0.0196 | CO | 260 | 144 |
| Mo:Fe 0.02:1 | 0.0196 | $CO_2$ | 285 | 151 |
| Mo:Fe 0.05:1 | 0.0476 | $H_2CO$ | 185 | 123 |
| Mo:Fe 0.05:1 | 0.0476 | CO | 265 | 146 |
| Mo:Fe 0.05:1 | 0.0476 | $CO_2$ | 300 | 155 |
| Mo:Fe 0.2:1 | 0.1667 | $H_2CO$ | 180 | 122 |
| Mo:Fe 0.2:1 | 0.1667 | CO | 210 | 130 |
| Mo:Fe 0.2:1 | 0.1667 | $CO_2$ | 270 | 147 |
| Mo:Fe 0.5:1 | 0.33 | $H_2CO$ | 185 | 123 |
| Mo:Fe 0.5:1 | 0.33 | CO | 215 | 132 |
| Mo:Fe 1:1 | 0.5 | $H_2CO$ | 200 | 128 |
| Mo:Fe 1:1 | 0.5 | CO | 220 | 133 |

**Table 5-2 - Activation energy to formation of products.**

The formation of the products can be correlated with the surfaces they are formed on. The $Fe_2O_3$ surface produces $CO_2$ with an activation energy of approximately 155 kJ $mol^{-1}$, while the formaldehyde production can be ascribed to the $Fe_2(MoO_4)_3$ phase, with an activation energy of 123 kJ $mol^{-1}$. At lower molybdenum content CO formation occurs, from both primary and secondary processes, with maximum CO production occurring from the 0.2:1 Mo:Fe catalyst, which also presents the most amorphous XRD (Figure 5-26).

On $Fe_2O_3$ alone, the adsorbed methanol will form formate species[15], but this appears to be impeded by the presence of molybdenum in the surface region and instead oxidative dehydrogenation to CO and $H_2O$ becomes dominant. In chapter 3 the surface group on an $Fe_2O_3$ surface was shown to be a stable formate species bound in a bidentate manner using two neighbouring sites (Figure 5-24). Addition of molybdenum effects the surface structure, with the distances between cations (in the $Fe_2(MoO_4)_3$ structure the shortest distance is 3.6 Å), being greater than the iron to iron distances (in the $Fe_2O_3$ structure the Fe-Fe distance is ~3.0 Å) and this increased distance would create too much strain, so the bidentate formate species does not form.

The average cation distance is greater in the $Fe_2(MoO_4)_3$ structure as there is a greater concentration of oxygen.

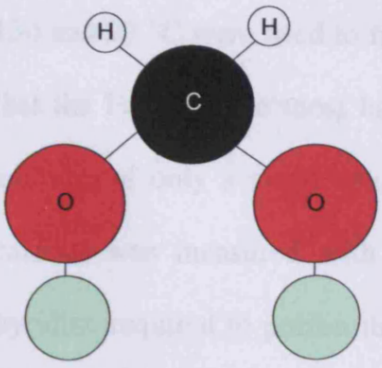


**Figure 5-24 - Schematic of an adsorbed formate group.**

When the methanol is adsorbed onto a molybdenum surface site, a methoxy group is formed (Figure 5-25)[16]. When this is neighboured by another molybdenum site oxidative dehydrogenation of the methoxy can occur to yield formaldehyde, as is seen with the more molybdenum rich catalysts. When the molybdenum site is isolated (and surrounded by iron sites), then the methoxy group is stabilised and provides a primary pathway to dehydrogenation to yield CO. This is seen primarily on the Mo:Fe 0.02 and 0.05:1 catalysts. The production of CO has previously been observed in reactor studies for a physical mixture of $Fe_2(MoO_4)_3$ and $Fe_2O_3$, presumably as there was some migration of Mo onto the surface of the $Fe_2O_3$[17], thus modifying the properties towards CO production.

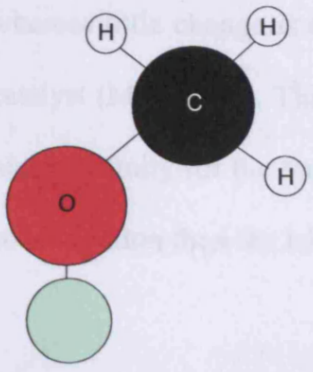


**Figure 5-25 - Schematic of an adsorbed methoxy.**

The production of $CO_2$ and CO show a good correlation with basic and acidic sites on the catalysts respectively[18]. Irreversible adsorption of acetic acid and $CO_2$ at 130 and 20 °C were used to find the basicity of iron molybdates, with the observation that the $Fe_2O_3$ is the most basic compound with this basicity decreasing rapidly on addition of only a small amount of molybdenum (2-5 atom %). The acidity of the catalyst was measured with irreversible ammonia adsorption and the amount of pyridine required to poison the isomerisation reaction of 1-butene. $Fe_2O_3$, is scarcely acidic, which rises to a maximum for about 30-40 atom % Mo, before decreasing back to a low level for pure $MoO_3$. The base sites of $Fe_2O_3$ seem to promote the reaction of methanol to $CO_2$ and $H_2$ with the removal of both the acidic hydrogen and one methyl hydrogen with the formation of the bidentate formate. The presence of a high number of acid sites promotes the secondary oxidation of formaldehyde and leads to a high production of CO. This work can be compared with that of Tatibouët who showed that in molybdate catalysts the presence of both weak acid and base sites in close proximity were required for formaldehyde formation[19]. If base sites were too strong then the adsorbed species could be oxidised to formate groups which lead to the formation of carbon oxides (CO and $CO_2$).

A noticeable change in surface reactivity is observed with the addition of only a small amount of molybdenum to a mainly iron oxide catalyst (Mo:Fe 0.02:1), whereas little change is observed when iron is added to a mainly molybdenum oxide catalyst (Mo:Fe 4:1). This would suggest that in these preparations that the iron has a higher affinity for the bulk with a surface that has a considerably higher molybdenum concentration than the bulk.

### 5.3.1.7 X-Ray Diffraction

The catalysts were composed of three phases, namely, $MoO_3$, $Fe_2(MoO_4)_3$ and $Fe_2O_3$, with up to two phases being present in each sample and the ratio between the phases being dependent on the ion ratio, Figures 5-26 and 5-27.

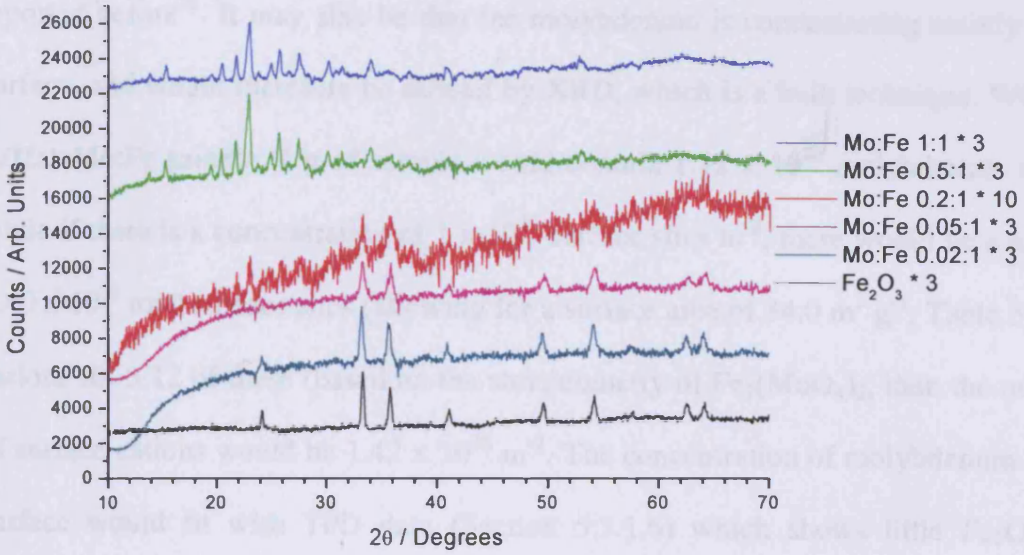


**Figure 5-26 - XRD spectra from the catalysts with Mo:Fe ratio below required for $Fe_2(MoO_4)_3$.**

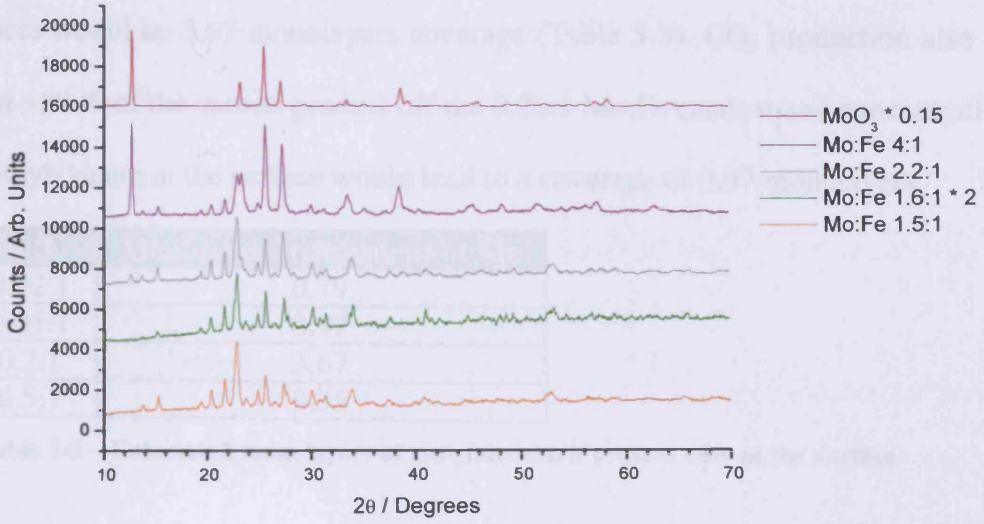


**Figure 5-27 - XRD spectra from the catalysts with Mo:Fe ratio of that required for $Fe_2(MoO_4)_3$ and above.**

The catalysts with ratios of 0.05:1 Mo:Fe and below show only $Fe_2O_3$ in the XRD spectra. There must be a molybdenum containing phase within these catalysts, and presumably this is $Fe_2(MoO_4)_3$, as these are seen within the other low ratio

catalysts. If the crystallites of this are too small or are amorphous, then they would not be detected by XRD. The concentration of the species is obviously considerably less than that of $Fe_2O_3$, due to the concentration of the metal atoms. The inability to see a molybdenum phase by XRD with small molybdenum concentrations have been reported before[20]. It may also be that the molybdenum is concentrating mainly at the surface, and would therefore be missed by XRD, which is a bulk technique. With the 0.02:1 Mo:Fe sample, 1 g of sample would contain $1.12 \times 10^{20}$ molybdenum atoms, while if there is a concentration of $1 \times 10^{19}$ surface sites $m^{-2}$, there would be a total of $3.40 \times 10^{20}$ total surface sites (allowing for a surface area of 34.0 $m^2$ $g^{-1}$, Table 5-1). If cations fill 5/12 of these (based on the stoichiometry of $Fe_2(MoO_4)_3$, then the number of surface cations would be $1.42 \times 10^{20}$ $m^{-2}$. The concentration of molybdenum at the surface would fit with TPD data (Section 5.3.1.6) which shows little $Fe_2O_3$-like behaviour from the 0.2:1 Mo:Fe catalyst; if all the molybdenum was at the surface there would be 3.67 monolayers coverage (Table 5-3). $CO_2$ production also accounts for ~50 % of the carbon product off the 0.05:1 Mo:Fe catalyst and concentration of the molybdenum at the surface would lead to a coverage of 0.97 monolayers.

| Mo:Fe | Monolayers equivalent of Mo |
|---|---|
| 0.02:1 | 0.79 |
| 0.05:1 | 0.97 |
| 0.2:1 | 3.67 |
| 0.5:1 | 9.35 |

**Table 5-3 – Calculated monolayers of molybdenum if present only at the surface.**

Work previously has used turn over frequencies of methanol oxidation on iron-molybdates and molybdena to argue that the surface of iron molybdates is covered with a monolayer of $MoO_3$[21,22]. While the data in these articles relates to stoichiometric molybdates, it may be imagined that even at much lower molybdenum content, that this high surface affinity still exists, and evidence of this is presented

later in this chapter (Section 5.3.2.2). As explained above, this high concentration of molybdenum atoms in the surface region would also help to explain the large affect on desorption products of the addition of a small amount of molybdenum to iron oxide (Section 5.3.1.6).

The catalyst with a ratio of Mo:Fe 0.2:1 is more amorphous than the other samples, with a spectrum with a large noise to signal ratio recorded. The phase of $Fe_2O_3$ is still visible, with the $Fe_2(MoO_4)_3$ now also present, as evidenced by peaks at ~21 and 23 °. In the catalyst with a ratio of 0.5:1 Mo:Fe the main phase observed is $Fe_2(MoO_4)_3$, with only a small amount of $Fe_2O_3$ seen by two small peaks at ~33.5 and 36 °. In the 1, 1.5 and 1.6:1 Mo:Fe catalysts only monoclinic $Fe_2(MoO_4)_3$ is observed, in the case of the 1:1 catalyst the stoichiometry dictates there must be an extra iron phase (presumably $Fe_2O_3$) which, since it cannot be detected in the XRD, is either amorphous or is in a highly dispersed form. The 1.6:1 Mo:Fe catalyst must also present an extra molybdenum phase, presumably this is $MoO_3$. The case of this catalyst is confused further as this spectrum was taken after a problem with the diffractometer which lead to a lowering of sensitivity below ~15 °, which affects the ability to see the most characteristic peak of $MoO_3$ at ~12 °. The higher ratio catalysts present a mixture of $Fe_2(MoO_4)_3$ and $MoO_3$ phases.

XRD spectra were also collected of the post reactor samples for Mo:Fe 0.05, 0.2, 1.5 and 2.2:1, these however showed no changes from the spectra of the fresh catalysts.

### 5.3.1.8 Raman spectroscopy

Assignment of Raman bands was tabulated in chapter 3, and the reader is guided to here for reference to assignments that follow.

Raman spectra of the low Mo:Fe catalysts (Figure 5-28) shows that the catalysts with the ratio of 0.05:1 Mo:Fe and below present essentially the same Raman spectrum as $Fe_2O_3$. When the 0.2:1 Mo:Fe catalyst is examined then the most obvious band is that at ~780 $cm^{-1}$, which was shown in chapter 3 to correspond with Mo-O-Mo vibrations in $Fe_2(MoO_4)_3$[23]. This peak also presents a shoulder feature at around 820 $cm^{-1}$, which was assigned to be a Mo-O-Mo vibration. Also visible are bands at 965 and 990 $cm^{-1}$ which are associated with terminal Mo=O bonds in $Fe_2(MoO_4)_3$ and $MoO_3$ respectively. With a ratio as low as this, it would be expected that no bands associated with $MoO_3$ would have been observed, as no evidence of this phase is seen in XRD. This band is most likely seen due to a high concentration of molybdenum in the surface region, which fits with reactor data (Section 5.3.1.6) and the XRD data (Section 5.3.1.7). The spectrum also still shows bands associated with $Fe_2O_3$, most notably that at around 290 $cm^{-1}$, and also one at ~400 $cm^{-1}$.

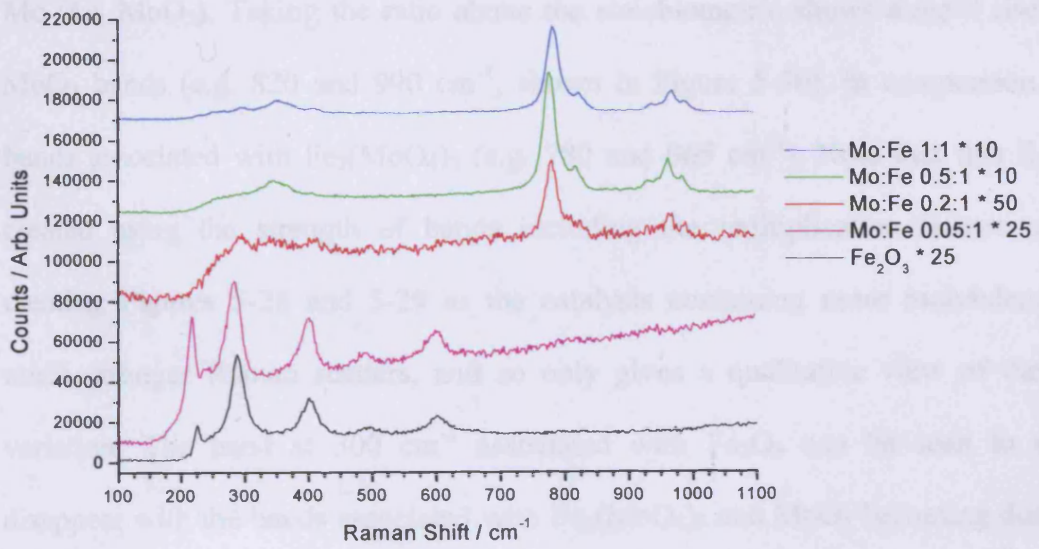


**Figure 5-28 - Raman spectroscopy for pre reactor catalysts with Mo:Fe ratio below required for $Fe_2(MoO_4)_3$.**

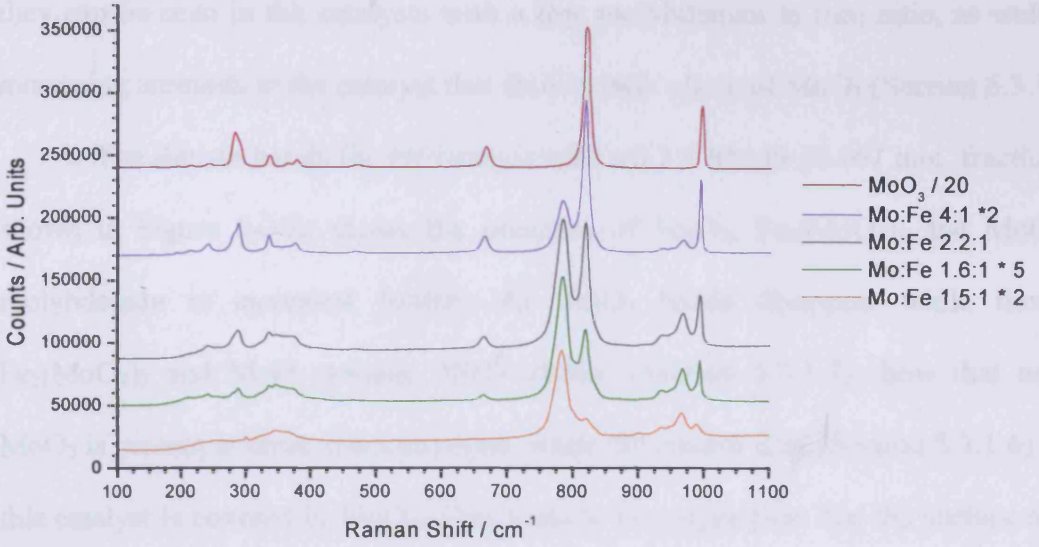


**Figure 5-29 - Raman spectroscopy for pre reactor catalysts with Mo:Fe ratio of that required for $Fe_2(MoO_4)_3$ and above.**

When the molybdenum ratio is raised further (Mo:Fe 0.5:1) all the bands presented are the same as those in stoichiometric $Fe_2(MoO_4)_3$ (where molybdenum is in a tetrahedral arrangement), and also include the bands associated with octahedral Mo (*i.e.* $MoO_3$). Taking the ratio above the stoichiometric shows a rapid rise in the $MoO_3$ bands (e.g. 820 and 990 $cm^{-1}$, shown in Figure 5-30), in comparison to the bands associated with $Fe_2(MoO_4)_3$ (e.g. 780 and 965 $cm^{-1}$). Note that this figure is created using the strength of bands including the multiplication factors used in creating Figures 5-28 and 5-29 as the catalysts containing more molybdenum are much stronger Raman scatters, and so only gives a qualitative view of the phase variation. The band at 300 $cm^{-1}$ associated with $Fe_2O_3$ can be seen to quickly disappear with the bands associated with $Fe_2(MoO_4)_3$ and $MoO_3$ becoming dominant. The two bands of $Fe_2(MoO_4)_3$ (780 and 965 $cm^{-1}$) show the same pattern, rising in presence, passing through a maximum, before declining away as $MoO_3$ takes over. The presence of the $MoO_3$ bands (820 and 990 $cm^{-1}$) follow the same pattern in that

they can be seen in the catalysts with a low molybdenum to iron ratio, as well as in increasing amounts in the catalyst that show a bulk phase of $MoO_3$ (Section 5.3.1.7).

The Raman bands for the catalyst with a 0.2:1 Mo:Fe (0.167 mol. fraction Mo, shown in Figure 5-30), shows the presence of $Fe_2O_3$, $Fe_2(MoO_4)_3$ and $MoO_3$. As molybdenum is increased further, the $Fe_2O_3$ bands disappear while those for $Fe_2(MoO_4)_3$ and $MoO_3$ remain. XRD studies (Section 5.3.1.7) show that no bulk $MoO_3$ is present at these concentrations, while the reactor data (Section 5.3.1.6) shows this catalyst is covered in $MoO_3$. This leads to the suggestion that the surface of both the $Fe_2O_3$ and $Fe_2(MoO_4)_3$ phases are covered in a molybdena monolayer.

Hill and Wilson suggest that comparison of the ($Fe_2(MoO_4)_3$) bands at 780 and 965 bands with those ($MoO_3$) at 820 and 990 $cm^{-1}$ can be used to give an estimation of the $Fe_2(MoO_4)_3$ to $MoO_3$ ratio in catalysts with a Mo:Fe greater than 1.5:1[23]. The value obtained by this method was not reported but was claimed that it could be used to obtain an estimate only and accurate measurements of molybdenum/iron ratios cannot be made.

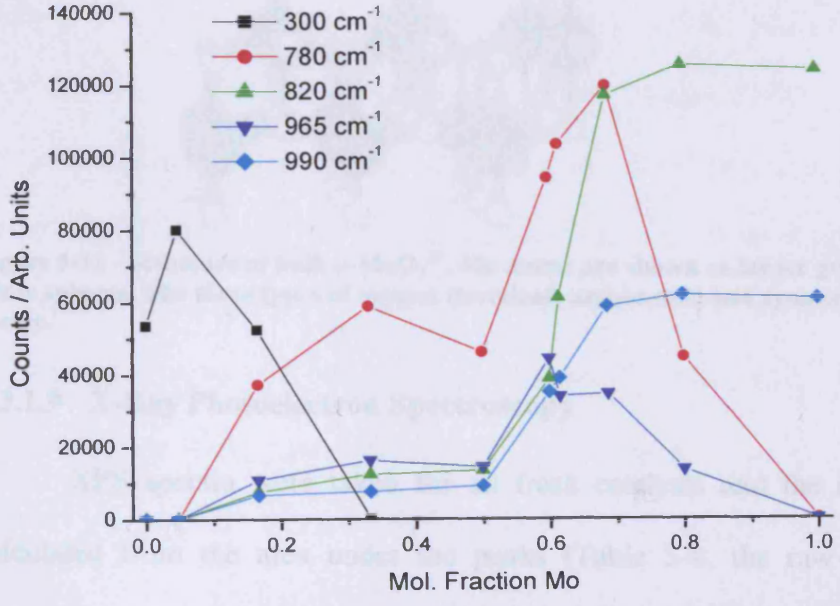


**Figure 5-30 - Graph of strength of bands seen in Raman Spectroscopy.**

The presence of an extra $MoO_3$ band is observed at ~660 $cm^{-1}$ for sample of Mo:Fe 1.6:1 and higher; this can be attributed to triply coordinated oxygen ($Mo_3$-O) stretching mode, shown in the structure of $MoO_3$ (Figure 5-31)[24]. This fits with XRD data which shows the presence of both $Fe_2(MoO_4)_3$ and $MoO_3$ phases. In the lower ratio samples (Mo:Fe 1.5:1 and below), Mo-O-Mo and Mo=O terminal vibrations (820 and 990 $cm^{-1}$) are observed, while that for $Mo_3$-O stretch (660 $cm^{-1}$) is not seen. This bond is associated with the symmetrical bridging oxygen (Figure 5-31) that connects the layers of atoms within the sheet like structure of $MoO_3$. It appears then that the $MoO_3$ seen is in a single layer, and when combined with the reactor data (Section 5.3.1.6), this layer must be at the surface of the sample and guides the methanol reaction towards selective products.

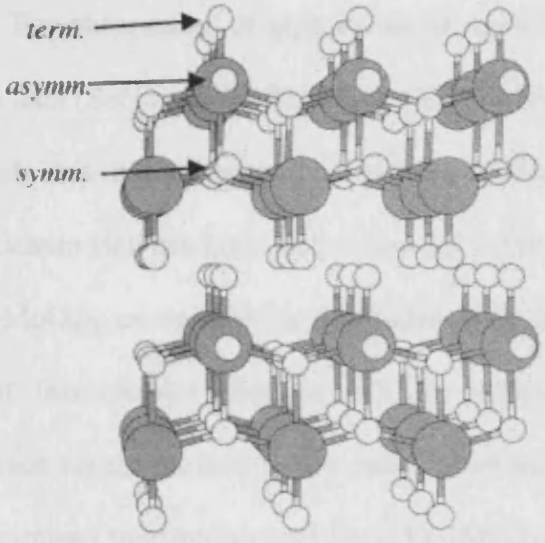


**Figure 5-31 - Structure of bulk α-$MoO_3$[25]. Mo atoms are shown as larger grey spheres, O atoms as white spheres. The three types of oxygen (terminal, asymmetric and symmetrical bridging) are shown.**

### 5.3.1.9 X-Ray Photoelectron Spectroscopy

XPS spectra were taken for all fresh catalysts and the ratio of Mo:Fe was calculated from the area under the peaks (Table 5-4, the raw data are shown in Appendix A-26, A-27, A-29, A-33 and A-56 to A-63). The calculated surface ratios suggest that the bulk ratio is similar to that observed at that at the surface for the high

ratio catalysts. However, in the low ratio catalysts there appears to be some enrichment, and we would expect the difference to be more easily observed at these ratios as an added monolayer of molybdenum to a sample that already contains a considerable amount will make less difference to the signal than a surface monolayer when the sample contains little or no bulk molybdenum. These calculations are made by taking the ratio of the metal peak areas after adjustment for the sensitivity of the elements (as calculated for the metallic species). These ratios are most likely an underestimate of the molybdenum content as cations make up only 25 % of the atoms within a $MoO_3$ structure, whereas in $Fe_2O_3$, iron cations make up 40 % of the structure. This higher number of cations in $Fe_2O_3$ would give a higher signal and could distort the values reported by the simple calculation method used.

The observation of high levels of surface molybdena is in agreement with the Raman data (Section 5.3.1.8), which shows a layer of molybdena at the surface of the catalysts. It is also in agreement with the STEM/EELs data (Chapter 3) for the more molybdenum rich catalysts of 1.5 and 2.2:1 Mo:Fe which suggested that the particles of $Fe_2(MoO_4)_3$ are enriched in molybdenum at the surface. It is also linked to the TPD data of this chapter (Section 5.3.1.6) which suggests that molybdenum has a preference for the surface in low ratio catalysts, where addition of Mo to $Fe_2O_3$ has a greater impact than addition of Fe to $Fe_2(MoO_4)_3$ product distribution. The reason this is more obviously seen in the low ratio catalysts is that the molybdenum signal should be very small if the bulk and surface ratios are the same, so a change is more easily observed. It is likely that molybdenum surface enrichment is also the case for the higher ratio catalysts, as evidenced by STEM/EELs and TPD data (Chapter 3).

| Catalyst Composition | Corrected Binding energies (eV) Mo 3d$^{5/2}$ | Fe 2p$^{3/2}$ | Area Under Peak Mo 3d | Fe 2p | Calculated Surface mol. fraction Mo | Bulk mol. fraction Mo |
|---|---|---|---|---|---|---|
| $Fe_2O_3$ (Synthesised) | - | 711.4 | 0 | 45158 | 0 | 0 |
| Mo:Fe 0.02:1 | 232.8 | 711.4 | 1778 | 16140 | 0.09 | 0.02 |
| Mo:Fe 0.05:1 | 232.8 | 711.2 | 2315 | 14316 | 0.13 | 0.05 |
| Mo:Fe 0.2:1 | 232.8 | 711 | 8393 | 30166 | 0.16 | 0.17 |
| Mo:Fe 0.5:1 | 232.6 | 711 | 4093 | 13223 | 0.22 | 0.33 |
| Mo:Fe 1:1 | 232.7 | 711.4 | 9537 | 8367 | 0.50 | 0.50 |
| Mo:Fe 1.5:1 | 232.4 | 711.7 | 11038 | 5992 | 0.62 | 0.60 |
| Mo:Fe 1.6:1 | 232.2 | 711.5 | 23301 | 12163 | 0.63 | 0.62 |
| Mo:Fe 1.9:1 | 232.4 | 711.4 | 13448 | 4722 | 0.71 | 0.66 |
| Mo:Fe 2.2:1 | 232.4 | 711.5 | 24135 | 9863 | 0.69 | 0.69 |
| Mo:Fe 4:1 | 232.7 | 711.2 | 55009 | 20601 | 0.70 | 0.8 |
| $MoO_3$ | 232.5 | - | 26796 | 0 | 1 | 1 |

**Table 5-4 - XPS results for fresh catalysts.**

The XPS data shows the catalysts with molybdenum in the +6 state and iron in the +3. In a previous study this was observed with the pure oxides, but in the mixed oxides the binding energies are lowered, with the claim that this indicates the presence of $Mo^{5+}$ and $Fe^{2+}$ [20]. These samples were referenced to C 1s, as opposed to O 1s in this work meaning the presence of different carbon species on the surface may lead to the lowering of both the molybdenum and iron signals.

The most recent review of iron molybdate catalysis by Soares *et al.* gave evidence that the active phase in the selective oxidation is the $Fe_2(MoO_4)_3$, although a molybdenum excess is present for replacing volatilised molybdenum, for use in reoxidation and to dope the $Fe_2(MoO_4)_3$ to ensure a high molybdenum ratio[10,26]. The work in this chapter does not deal with the first two of these points, but does show that an excess of molybdenum gives a better catalytic performance. $MoO_3$ is said to be less active per unit area (by up to an order of magnitude[10]). This is demonstrated by the Mo:Fe 4:1 catalyst reaching 90 % conversion at ~270 °C (Figure 5-8), while, with 2 g

of $MoO_3$ (a similar total surface area, shown in Chapter 3), this conversion level is not reached until ~310 °C. The $MoO_3$ can therefore be said to be highly selective, however, the active catalytic phase seems to be $Fe_2(MoO_4)_3$, which has an excess of $MoO_3$ in the surface region.

## 5.3.2 Monolayer Catalysts

### 5.3.2.1 Reaction Profiles

TPPFR of $Fe_2O_3$ was carried out previously (Chapter 3) showing selectivity purely towards $CO_2$. The sample used in this area of work was from a separate production batch and had a surface area of 11.8 $m^2 g^{-1}$. This $Fe_2O_3$ sample shows the same high selectivity to $CO_2$ that was observed with previous samples (Chapter 3) and shows itself to have moderate activity, 50 % conversion being reached at around 240 °C.

Addition of just 24 % of a ML $MoO_3$ onto the surface of $Fe_2O_3$ has a dramatic impact on the reaction profile (Figure 5-32, Appendix A-64). The catalyst shows improved activity, reaching 50 % conversion at around 220 °C, and 90 % at 275 °C. Formaldehyde selectivity is high at low conversions, which is replaced initially by CO production. At the highest conversions (>80 %), $CO_2$ production begins which rises to 80 % by 370 °C.

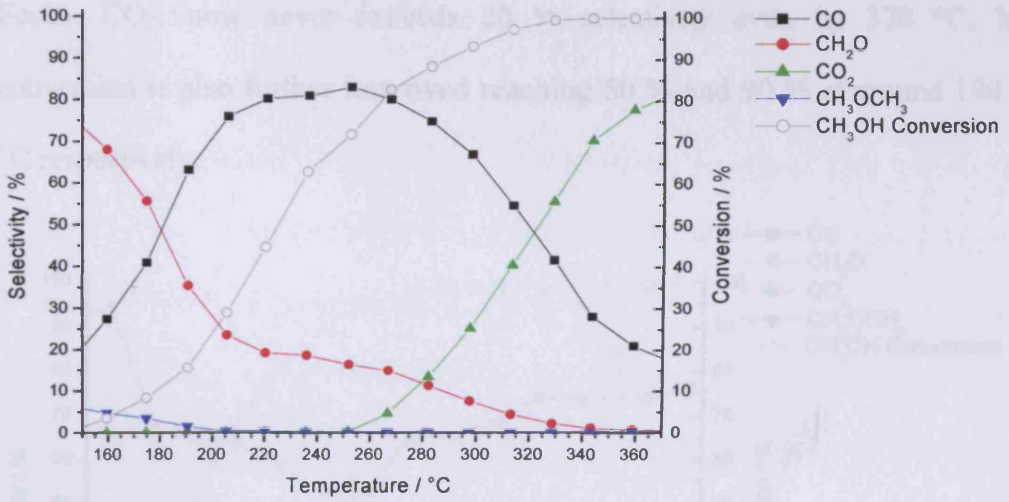


**Figure 5-32 - Selectivity and conversion for methanol oxidation over 24 % ML $MoO_3$ on $Fe_2O_3$.**

Another catalyst with 60 % ML $MoO_3$ (Figure 5-33, Appendix A-65) shows improvement to the formaldehyde formation and a reduction in the $CO_2$ formed. $CO_2$ production begins at around 200 °C, and now reaches no more than 50 % even by 370 °C. The activity of the catalyst shows a big increase reaching 50 % methanol conversion at 190 °C and 90 % by 250 °C.

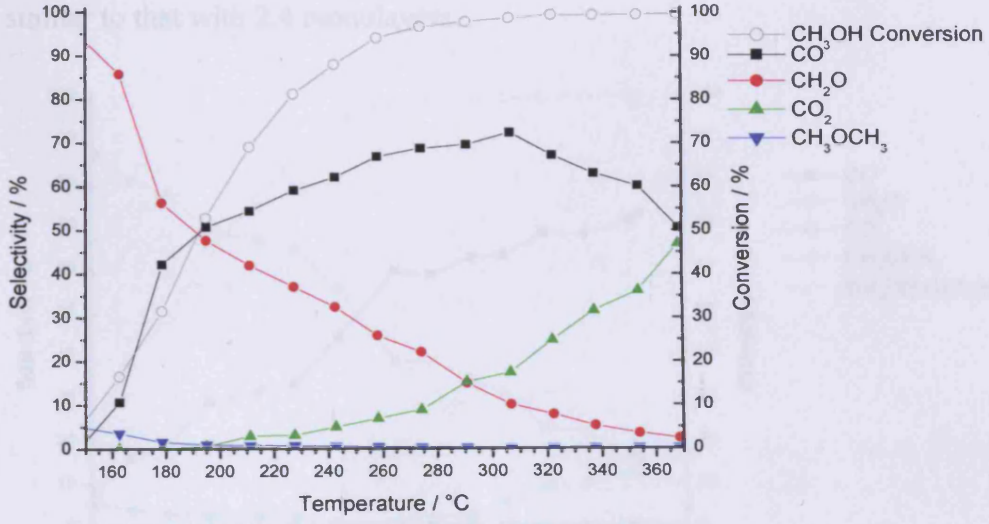


**Figure 5-33 - Selectivity and conversion for methanol oxidation over 60 % ML $MoO_3$ on $Fe_2O_3$.**

When 2.4 ML $MoO_3$ is added to the $Fe_2O_3$, the reaction profile is improved further (Figure 5-34, Appendix A-66), to the extent that the preferred product of

$Fe_2O_3$, $CO_2$, now never exceeds 20 % selectivity even by 370 °C. Methanol conversion is also further improved reaching 50 % and 90 % at around 190 and 230 °C respectively.

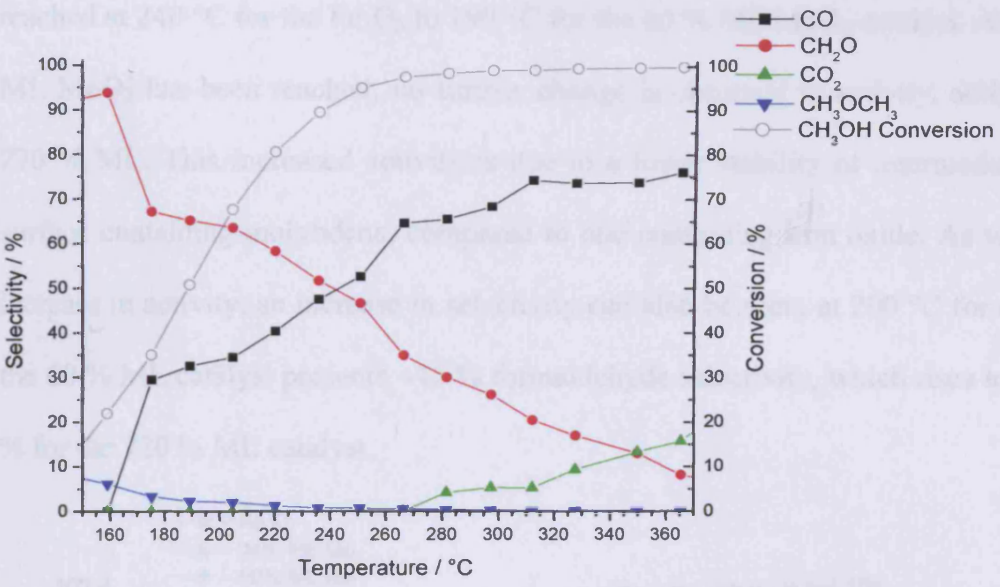


**Figure 5-34 - Selectivity and conversion for methanol oxidation over 240 % ML $MoO_3$ on $Fe_2O_3$.**

A catalyst with 7.2 monolayers of $MoO_3$ (Figure 5-35, Appendix A-67), is similar to that with 2.4 monolayers.

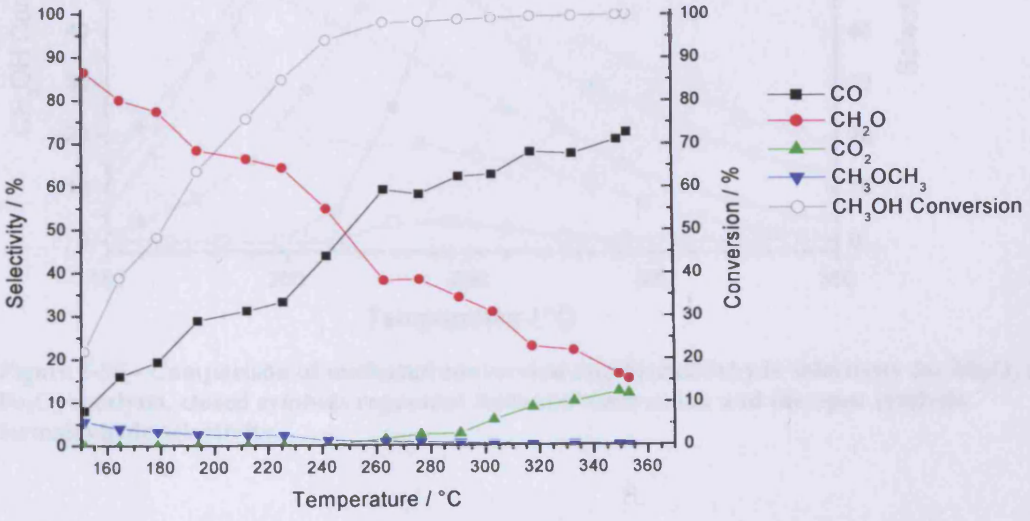


**Figure 5-35 - Selectivity and conversion for methanol oxidation over 720 % ML Mo on $Fe_2O_3$.**

A comparison plot for the monolayer catalysts can be made in terms of methanol conversion and formaldehyde selectivity (Figure 5-36). With the addition of $MoO_3$ to the surface, it can be seen that activity increases with 50 % conversion reached at 240 °C for the $Fe_2O_3$ to 190 °C for the 60 % ML $MoO_3$ catalyst. After 60 % ML $MoO_3$ has been reached, no further change is observed in activity, adding up to 720 % ML. This increased activity is due to a lower stability of intermediates on a surface containing molybdena, compared to one containing iron oxide. As well as an increase in activity, an increase in selectivity can also be seen, at 200 °C for example, the 60 % ML catalyst presents ~45 % formaldehyde selectivity, which rises to over 70 % for the 720 % ML catalyst.

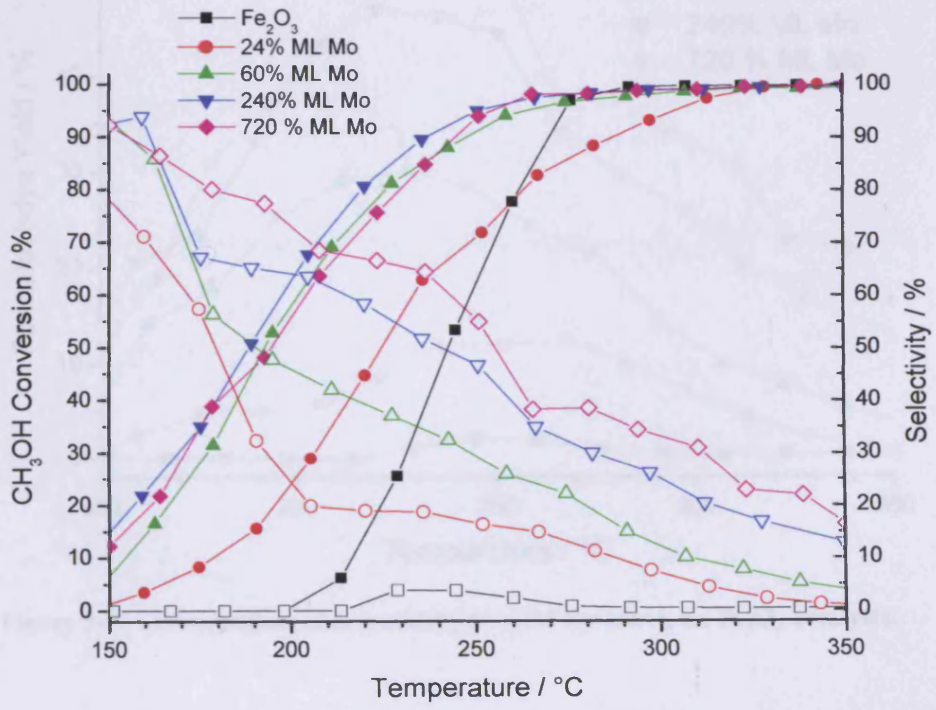


**Figure 5-36 - Comparison of methanol conversion and formaldehyde selectivity for $MoO_3$ on $Fe_2O_3$ catalysts, closed symbols represent methanol conversion and the open symbols formaldehyde selectivity.**

The selectivity and conversion can be combined to a yield *vs.* temperature plot (Figure 5-37). From this it can be seen the yield improves with added molybdenum, and the peak in yield occurs at lower temperatures. The maximum in yield is

improved noticeably with addition up to 240 % ML, with a small increased when taking the level to 720 % ML $MoO_3$. When the TPD data is studied (Section 5.3.2.2), it can be seen that there are two reasons for the loss of selectivity to formaldehyde being direct CO production from isolated molybdenum sites and secondary oxidation of formaldehyde. This is further backed by data from low bulk Mo:Fe catalysts (Section 5.3.1.6), which show primary CO coming from molybdenum sites neighboured by iron sites, whereas formaldehyde is formed from neighbouring molybdenum sites, which can then undergo secondary oxidation.

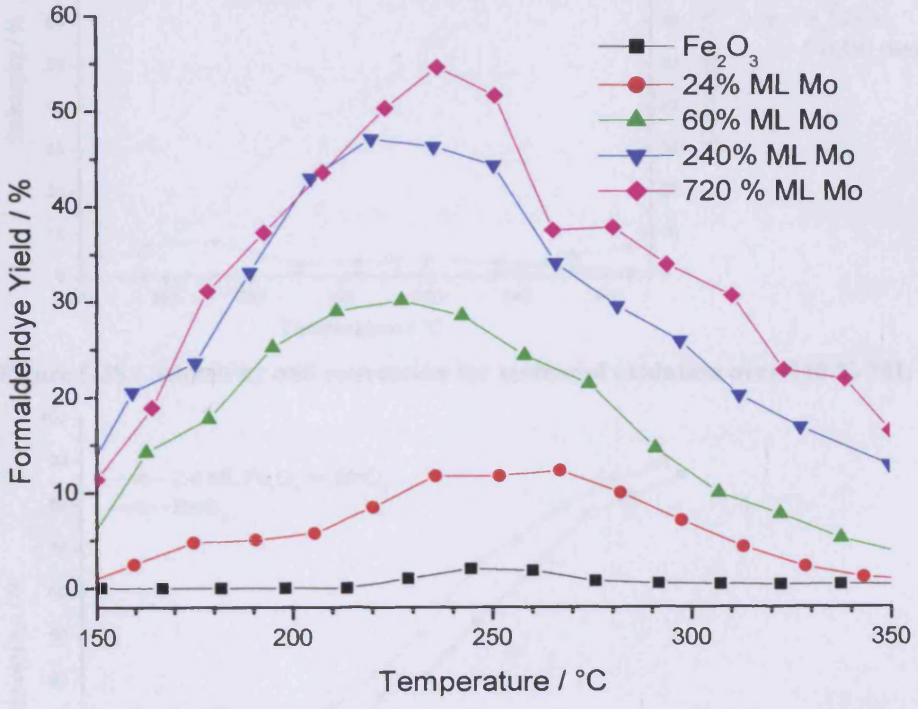


**Figure 5-37 - Comparison of formaldehyde yield for $MoO_3$ on $Fe_2O_3$ catalysts.**

The 2.4 monolayers of $Fe_2O_3$ on $MoO_3$ catalyst shows itself to be highly selective towards formaldehyde (>90 %) throughout the temperature range tested (Figure 5-38, Appendix A-68). The catalyst shows dimethyl ether selectivity (~8 % at 270 °C) at low temperatures, with a small $CO_2$ production beginning at around 340 °C, which never reaches above 5 %. The high selectivity of the catalyst is very similar

to that of unmodified $MoO_3$ (Chapter 3). Like $MoO_3$, the catalyst also shows poor activity, reaching 50 % conversion at around 315 °C and never reaches more than 85 % conversion, even by 370 °C. Comparing this conversion to that of $MoO_3$, shows that the catalyst containing the iron oxide monolayer may be lower in activity than the pure $MoO_3$ (Figure 5-39), with 50 % conversion here occurring at around 300 °C, but this difference is most likely error from the measurements.

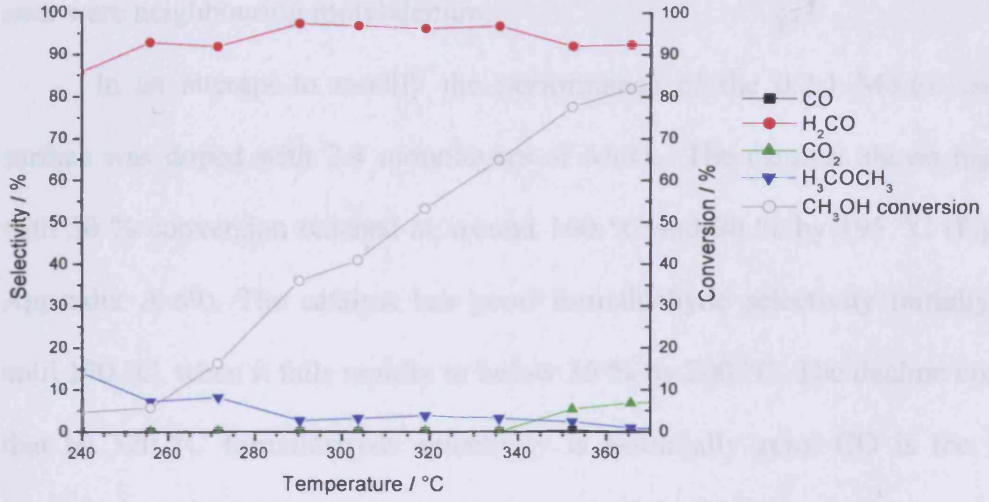


**Figure 5-38 - Selectivity and conversion for methanol oxidation over 240 % ML $Fe_2O_3$ on $MoO_3$.**

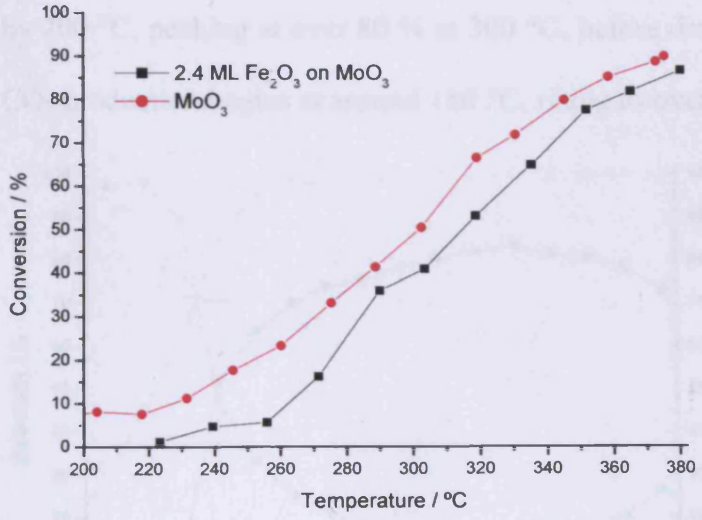


**Figure 5-39 - Comparison of methanol conversion over $MoO_3$, with and with and 2.4 monolayers of added $Fe_2O_3$.**

It can be seen that the addition of iron oxide monolayers affects the performance of $MoO_3$, far less than the addition of $MoO_3$ to $Fe_2O_3$. With the addition

of $MoO_3$ to $Fe_2O_3$ the activity of the catalyst is increased markedly and the product distribution is moved away from the formation of $CO_2$ (as occurs on pure $Fe_2O_3$) to formaldehyde (high Mo surfaces) and CO (from isolated Mo surface sites). With $Fe_2O_3$ added to $MoO_3$ however, the catalyst retains similar activity and selectivity towards formaldehyde. This suggests that the iron is no longer at the surface, as the selectivity would otherwise be guided to $CO_2$, with a pure $Fe_2O_3$ layer or CO, if iron sites were neighbouring molybdenum.

In an attempt to modify the performance of the 0.2:1 Mo:Fe catalyst, the surface was doped with 2.4 monolayers of $MoO_3$. The catalyst shows high activity with 50 % conversion reached at around 160 °C and 90 % by 195 °C (Figure 5-40, Appendix A-69). The catalyst has good formaldehyde selectivity initially (>90 %) until 170 °C, when it falls rapidly to below 35 % by 200 °C. The decline continues so that by 370 °C formaldehyde selectivity is essentially zero. CO is the main loss product, with production beginning at around 170 °C, rising rapidly to around 65 % by 200 °C, peaking at over 80 % at 300 °C, before dropping back to 75 % by 370 °C. $CO_2$ production begins at around 180 °C, rising to over 25 % by 370 °C.

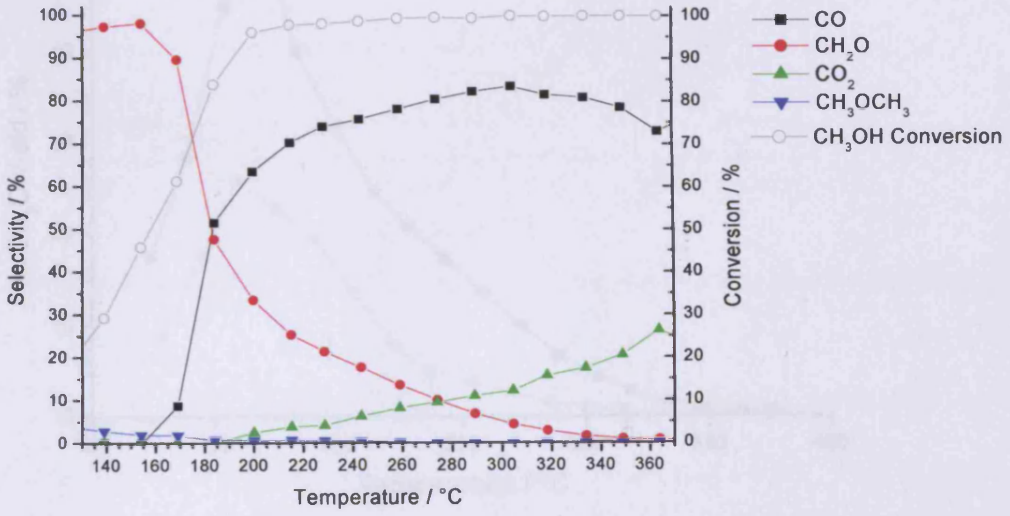


**Figure 5-40 - Selectivity and conversion for methanol oxidation over 240 % ML $MoO_3$ on Mo:Fe 0.2:1.**

A comparison of the formaldehyde yield from the Mo:Fe 0.2:1 catalyst with and without the added 2.4 $MoO_3$ monolayers shows an improvement due to higher activity with the added monolayer (Figure 5-41). Without the added monolayer a maximum yield of just over 25 % is reached at 160 °C, while with the monolayer the yield reaches over 55 % at 170 °C. This improvement in formaldehyde yield again demonstrates the highly selective nature of surface molybdenum oxide. The added molybdenum oxide presumably adds to the surface Mo that is already present in the Mo:Fe 0.2:1 catalyst covering some iron based sites helping to destabilise the intermediates and guide the reaction towards formaldehyde. The high surface area of this catalyst (Table 5-1) also makes it much more active than either the industrial catalyst or the mimic, both with Mo:Fe ratios of 2.2:1. While the catalyst with the $MoO_3$ monolayer here produces over 55 % formaldehyde yield at 170 °C, the mimic catalyst produced by copreciptation, followed by evaporation to dryness only produces around 25 % formaldehyde yield at this temperature.

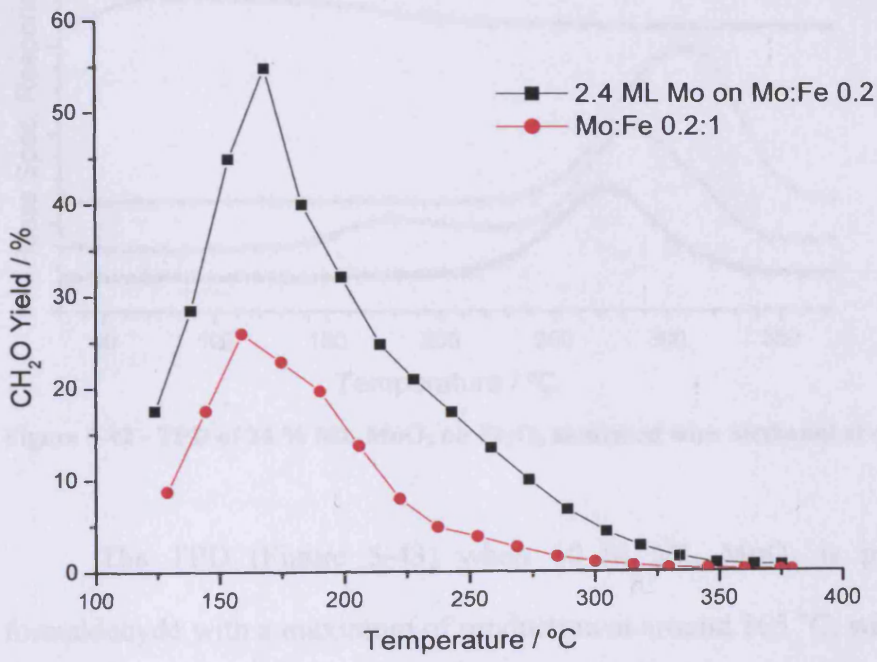


**Figure 5-41 - Formaldehyde yield comparison for Mo:Fe 0.2:1 catalyst, with and without and added 2.5 monolayers of $MoO_3$.**

### 5.3.2.2 Temperature Programmed Desorption

The TPD profile of $Fe_2O_3$ was shown in chapter 3 and showed the catalyst to be selective to $H_2$ and $CO_2$, with maximum desorption temperatures of 290 and 300 °C.

The TPD profile of the 24 % ML $MoO_3$ catalyst shows carbon products of CO and $CO_2$ with peak desorptions of 270 and 310 °C respectively (Figure 5-42). There is a double peak in the water desorption with the first being very broad and peaking at around 160 °C, with the second peak occurring at 270 °C, coincident with the CO. There is also a double peak in the hydrogen production as well, with the first, smaller peak occurring at 180 °C, and the second peak occurring at 290 °C.

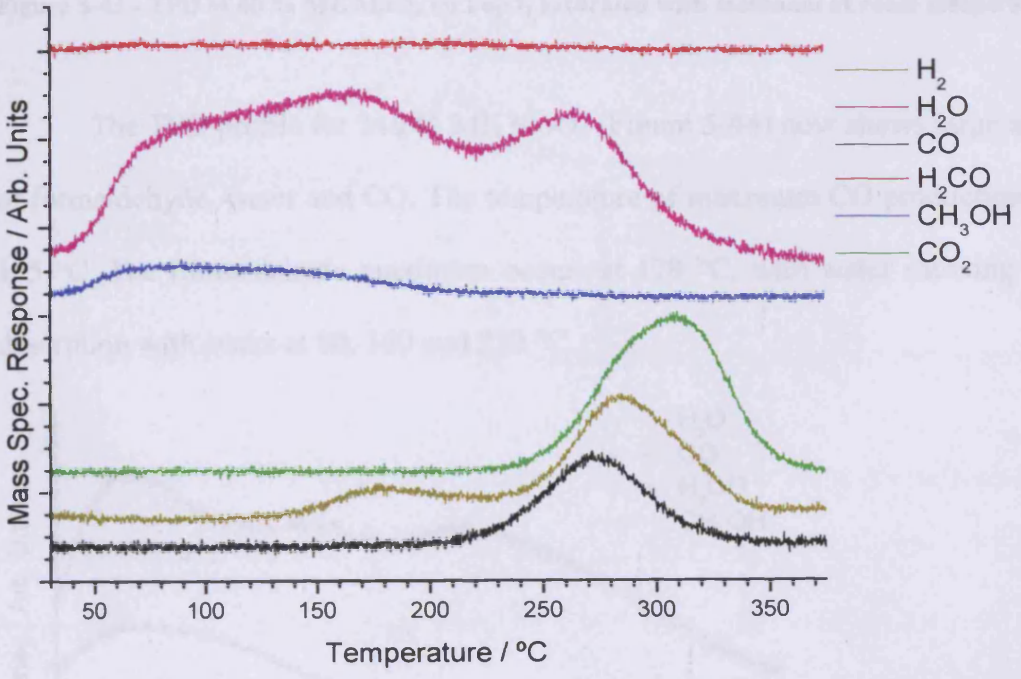


**Figure 5-42 - TPD of 24 % ML $MoO_3$ on $Fe_2O_3$ saturated with methanol at room temperature.**

The TPD (Figure 5-43) when 60 % ML $MoO_3$ is present now shows formaldehyde with a maximum of production at around 165 °C, with a great reduction in the $CO_2$ and $H_2$ formation though the maxima still occur at the same temperature. The desorption of CO shows a maximum at 205 °C.

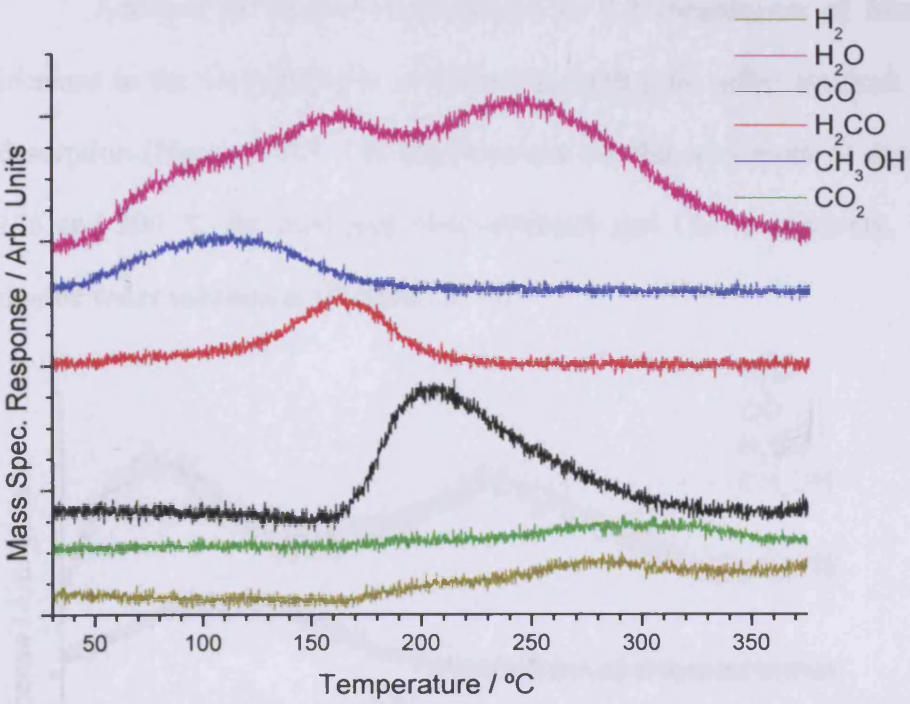


**Figure 5-43 - TPD of 60 % ML $MoO_3$ on $Fe_2O_3$ saturated with methanol at room temperature.**

The TPD profile for 240 % ML $MoO_3$ (Figure 5-44) now shows large amounts of formaldehyde, water and CO. The temperature of maximum CO production is now 195 °C. The formaldehyde maximum occurs at 170 °C, with water showing a triple desorption with peaks at 80, 160 and 220 °C.

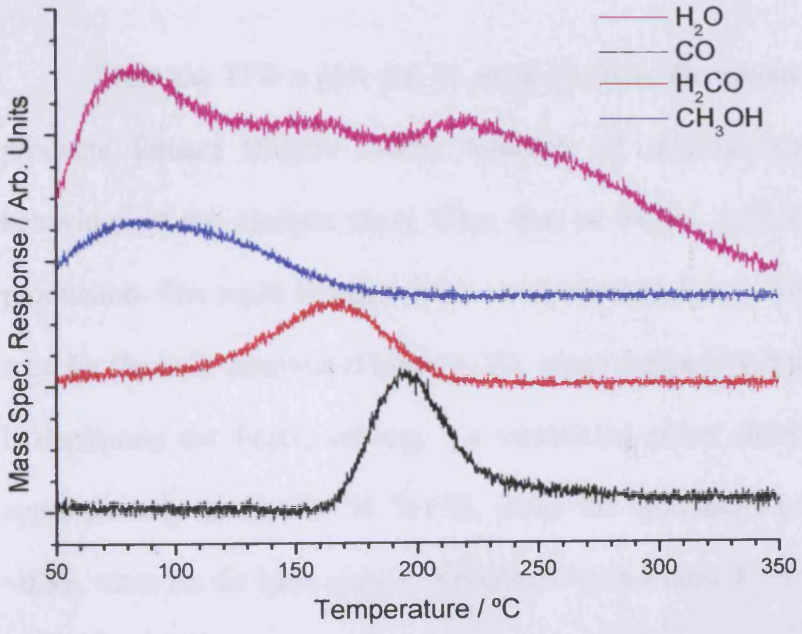


**Figure 5-44 - TPD of 240 % ML $MoO_3$ on $Fe_2O_3$ saturated with methanol at room temperature.**

Addition of further molybdenum to 7.2 monolayers of $MoO_3$, leads to an increase in the formaldehyde to CO ratio, with little effect on peak temperatures of desorption (Figure 5-45). The temperatures for the maximum of desorption are 120, 175 and 200 °C for methanol, formaldehyde and CO respectively, while there is a double water maxima at 80 and 220 °C.

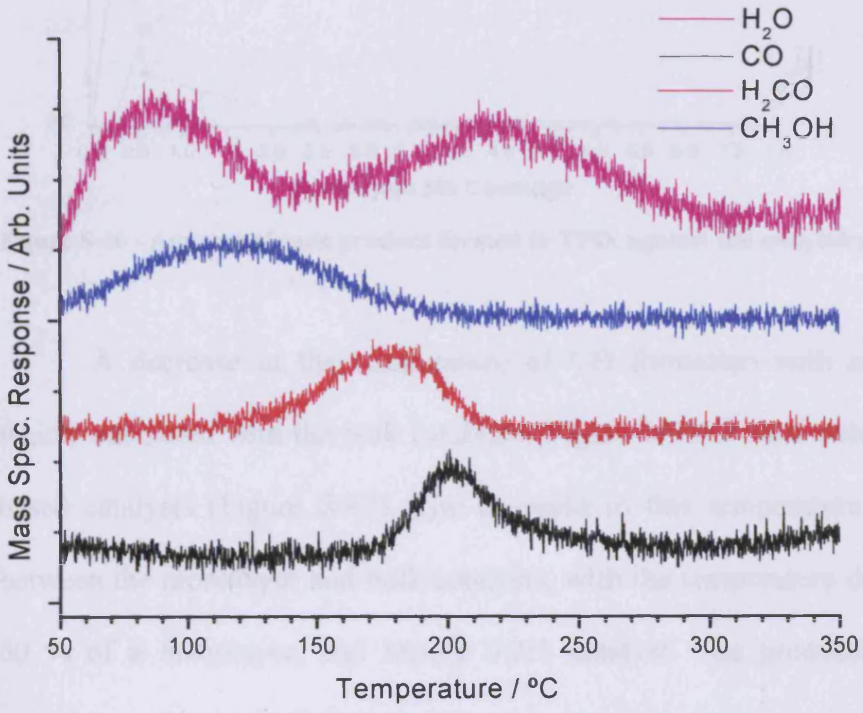


**Figure 5-45 - TPD of 720 % ML Mo on $Fe_2O_3$ saturated with methanol at room temperature.**

From the TPD a plot can be made to show the amount of the different carbon products formed (Figure 5-46). Addition of molybdenum quickly changes the behaviour of the catalyst away from that of $Fe_2O_3$, with a rapid drop in the $CO_2$ production. The rapid change of the catalyst away from $CO_2$ to CO is similar to that seen for the bulk catalysts (Figure 5-22), again suggesting that the added molybdenum is disrupting the $Fe_2O_3$ surface. An interesting point observe is that distribution is approximately 50 % CO, 50 % $CO_2$ when the monolayer coverage is approximately ~0.35, while on the bulk sample this occurs with a ratio 0.2:1 Mo:Fe.

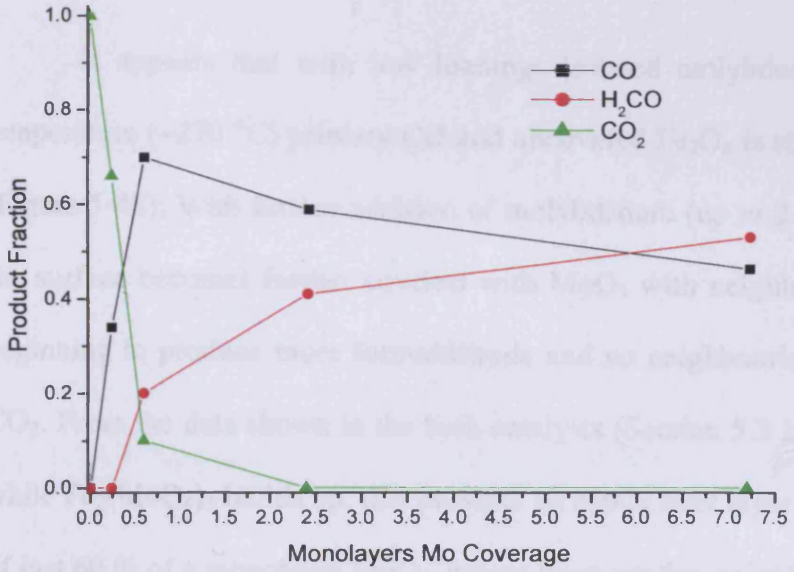


**Figure 5-46 - Amount of each product formed in TPD, against the molybdenum coverage.**

A decrease in the temperature of CO formation with added molybdenum, which was noted with the bulk catalysts (Figure 5-23) is also noted in the monolayer based catalysts (Figure 5-47). The decrease in this temperature also matches well between the monolayer and bulk catalysts, with the temperature down to 210 °C with 60 % of a monolayer, and Mo:Fe 0.2:1 catalyst. The production of CO in TPD experiments seems well linked with an extra water desorption of water at ~160 °C, showing dehydrogenation of the adsorbed species occurring more easily on these surfaces.

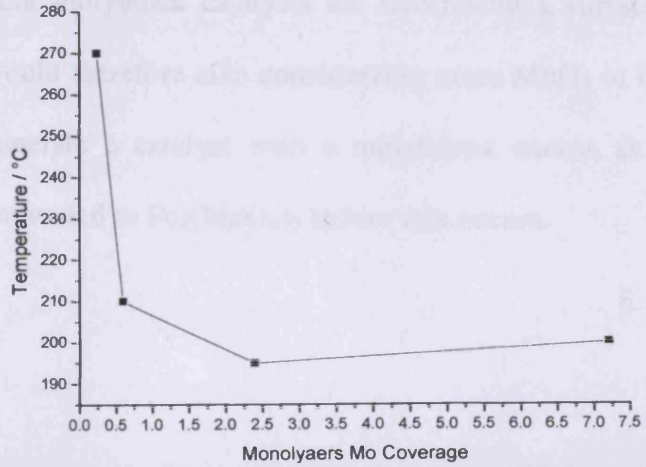


**Figure 5-47 - The temperature of maximum CO desorption for catalysts with different monolayer coverages of $MoO_3$ on $Fe_2O_3$.**

It appears that with low loadings isolated molybdenum sites produce high temperature (~270 °C) primary CO and uncovered $Fe_2O_3$ is shown by $CO_2$ production (Figure 5-48). With further addition of molybdenum (up to 2.4 monolayers coverage) the surface becomes further covered with $MoO_3$ with neighbouring molybdena pairs beginning to produce more formaldehyde and no neighbouring iron pairs to produce $CO_2$. From the data shown in the bulk catalysts (Section 5.3.1), it is important to note while $Fe_2(MoO_4)_3$ builds up, this presents an $MoO_3$ over layer at the surface. Addition of just 60 % of a monolayer $MoO_3$, means there are few neighbouring iron pairs left to form the surface formate group (Figure 5-24), with $CO_2$ selectivity of ~10 % observed by TPD (Figure 5-46). Once the monolayer is complete layers of $Fe_2(MoO_4)_3$ are formed below the surface (Figure 5-48), with little difference observed in reactor (Figure 5-36) and TPD (Figure 5-46) data. This theory is enhanced when the XPS data is studied (Section 5.3.2.5), which shows only a minimal increase in surface molybdenum for the catalyst prepared with 240 ML of $MoO_3$ to that prepared with 720 ML.

The layer like growth, with high molybdenum surface concentration is complimented by studies on bulk catalysts, which suggested that most stoichiometric bulk molybdate catalysts are covered in a surface monolayer of molybdena[21,22]. It would therefore take considerably more $MoO_3$ to be added to the surface of $Fe_2O_3$ to generate a catalyst with a molybdena excess as the bulk of the $Fe_2O_3$ would be converted to $Fe_2(MoO_4)_3$ before this occurs.

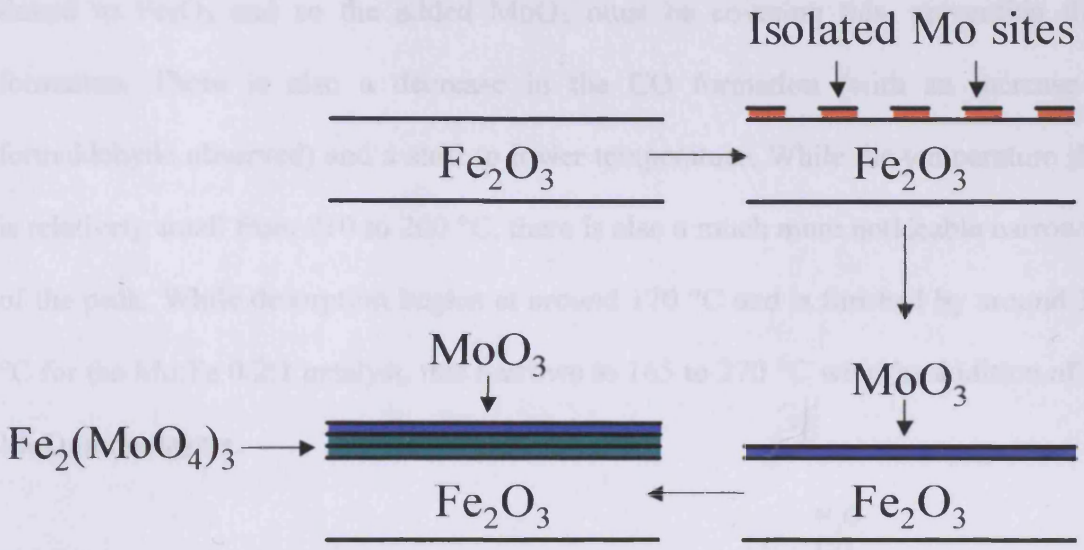


**Figure 5-48 - Build up $Fe_2(MoO_4)_3$ with addition of $MoO_3$ monolayers to $Fe_2O_3$. Note that $Fe_2(MoO_4)_3$ presents octahedral Mo (i.e. $MoO_3$) in a surface over layer.**

The temperature of the CO production from the catalyst made of 60 % of a monolayer and over (Figure 5-47), suggests that this is from secondary oxidation of formaldehyde. This was seen to be the case for the 0.5:1 Mo:Fe catalyst when different loadings were used (Section 5.3.1.6). The 60 % monolayer catalyst also produces some CO by a direct pathway from isolated molybdenum sites, as evidenced by the tailing of the CO peak to 300 °C (Figure 5-43), while the CO desorption essentially complete on the 2.4 monolayers catalyst by 240 °C (Figure 5-44).

TPD for 0.2:1 Mo:Fe catalyst with an added 2.4 monolayers of $MoO_3$ shows a broad methanol desorption centred at around 80 °C, with formaldehyde and CO desorptions centred at 175 and 200 °C (Figure 5-49). There is a double peak in water production, with the smaller peak at around 85 °C, and the much broader and larger second peak at 245 °C. Comparing this TPD to the catalyst without the added monolayer (Figure 5-18) a few differences can be observed. Firstly, with the added monolayer, no $CO_2$ or $H_2$ are produced, while very small amounts of these are produced at high temperature without the additional surface $MoO_3$. These products are

linked to $Fe_2O_3$ and so the added $MoO_3$ must be covering this, preventing their formation. There is also a decrease in the CO formation (with an increase in formaldehyde observed) and a shift to lower temperature. While the temperature shift is relatively small from 210 to 200 °C, there is also a much more noticeable narrowing of the peak. While desorption begins at around 170 °C and is finished by around 310 °C for the Mo:Fe 0.2:1 catalyst, this narrows to 165 to 270 °C with the addition of the $MoO_3$ monolayers.

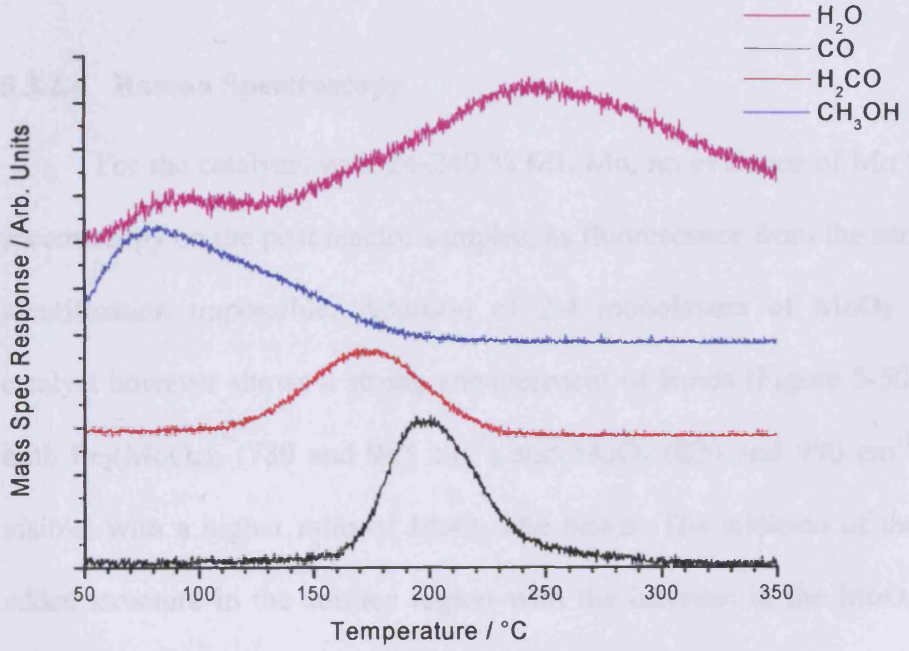


**Figure 5-49 - TPD of 240 % ML Mo on Mo:Fe 0.2:1 saturated with methanol at room temperature.**

Again these data shows the ability of molybdenum to selectively oxidise methanol to formaldehyde, this time supported on a high area material. A major problem with these monolayer catalyst is that on both iron oxide and a low molybdenum to iron ratio catalyst is the high surface area and so formaldehyde is lost by secondary oxidation. In reactor experiments the CO is formed directly off isolated molybdenum sites on the catalyst surface and from the secondary oxidation of

formaldehyde, while on higher ratio catalysts, CO is formed only as a secondary oxidation product.

#### 5.3.2.3 Characterisation

With only a small amount of a substance to the support surface, characterisation becomes much more difficult. XRD diffraction was taken of the catalysts, but due to the bulk nature of the technique, the spectra resembled the support with no evidence for the added monolayers.

#### 5.3.2.4 Raman Spectroscopy

For the catalysts with 24-240 % ML Mo, no evidence of Mo found by Raman spectroscopy on the post reactor samples, as fluorescence from the samples made peak identification impossible. Addition of 2.4 monolayers of $MoO_3$ to Mo:Fe 0.2:1 catalyst however shows a strong enhancement of bands (Figure 5-50). The bands for both $Fe_2(MoO_4)_3$ (780 and 965 $cm^{-1}$) and $MoO_3$ (820 and 990 $cm^{-1}$) are both more visible, with a higher ratio of $MoO_3$ like bands. The addition of the monolayer has added structure in the surface region with the increase in the $MoO_3$ the bands. The increase in surface molybdenum can be linked to the improvement in catalytic performance (Figure 5-41) reaffirming the thought that it is surface molybdenum that is important for the selective oxidation of methanol to formaldehyde[6].

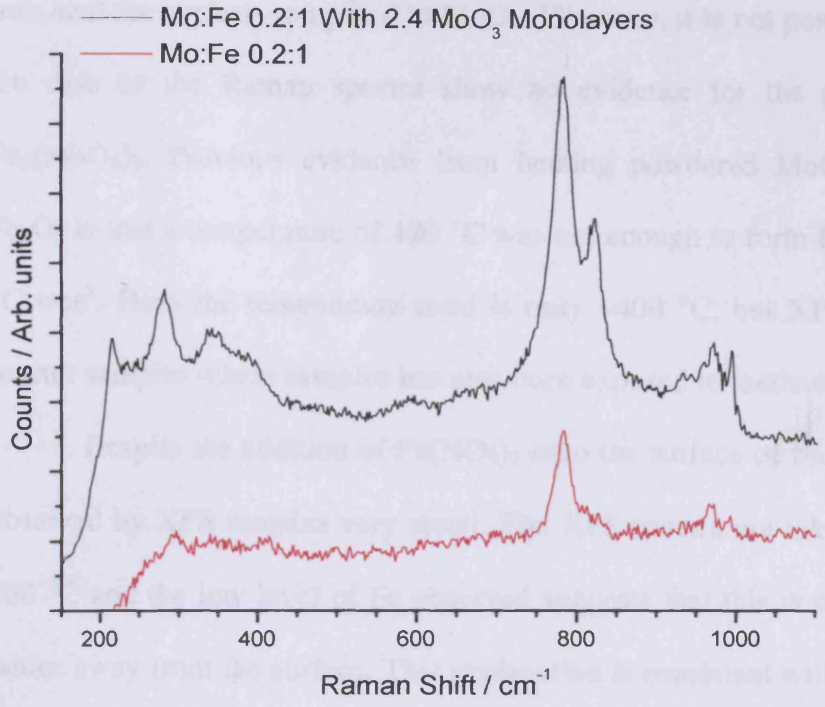


**Figure 5-50 - Raman Spectra for Fe:Mo 1:0.2 catalyst, and the same catalyst with an added monolayer of $MoO_3$.**

### 5.3.2.5 X-Ray Photoelectron Spectroscopy

Studying the surface composition of the post reactor catalysts (subjected to heat treatment to 400 °C) shows a more significant change with the addition of 2.4 monolayers of $MoO_3$ to $Fe_2O_3$, rather than 2.4 $Fe_2O_3$ monolayesr on $MoO_3$ (Table 5-5, raw data are shown in Appendix A-26, A-58 and A-70 to A-75).

The addition of molybdenum to the surface of iron oxide shows that the iron remains in the +3 oxidation state, while the added molybdenum is in the +6 state. The addition of increasing molybdenum levels increases the Mo 3d signal observed in comparison to that of Fe 2p. Again it must be noted that the surface coverage is an underestimate of the Mo:Fe ratio in the surface layer for the reason described earlier (Section 5.3.1.9). The very small increase from 2.4 monolayers coverage to 7.2 monolayers coverage suggests that the oxide is building up on itself, or the excess molybdenum is going subsurface during calcination. It may be that with a larger molybdenum coverage that $Fe_2(MoO_4)_3$ begins to form, and this obviously needs more

iron near the surface compared to $MoO_3$. However, it is not possible to know if this is the case as the Raman spectra show no evidence for the presence of $MoO_3$ or $Fe_2(MoO_4)_3$. Previous evidence from heating powdered $MoO_3$ finely mixed with $Fe_2O_3$ is that a temperature of 420 °C was not enough to form $Fe_2(MoO_4)_3$, while 500 °C was[5]. Here the temperature used is only ~400 °C, but XPS were taken on post reactor samples where samples has also been exposed to methanol.

Despite the addition of $Fe(NO_3)_2$ onto the surface of $MoO_3$, the signal of iron observed by XPS remains very small. The XPS spectra are taken after calcination to 400 °C and the low level of Fe observed suggests that this is moving into the $MoO_3$ lattice away from the surface. This explanation is consistent with the observed reactor results that show $MoO_3$ behaving similarly with and without the added iron.

| Catalyst Composition | Corrected Binding energies (eV) | | Area Under Peak | | Calculated Surface Cation Fraction Mo |
|---|---|---|---|---|---|
| | Mo $3d^{5/2}$ | Fe $2p^{3/2}$ | Mo 3d | Fe 2p | |
| $Fe_2O_3$ (Synthesised) | - | 711.4 | 0 | 45158 | 0 |
| 24 % ML | 232.8 | 711.3 | 1790 | 14131 | 0.10 |
| 60 % ML | 232.8 | 711.1 | 2358 | 11402 | 0.16 |
| 240 % ML | 232.8 | 711.2 | 2871 | 9816 | 0.21 |
| 720 % ML | 233 | 711.2 | 3847 | 11932 | 0.22 |
| Mo:Fe 0.2:1 | 232.8 | 711.0 | 8393 | 30166 | 0.16 |
| Mo:Fe 0.2:1 with 2.4 ML Mo | 232.8 | 711.4 | 4923 | 10904 | 0.29 |
| 240 % ML Fe on $MoO_3$ | 232.4 | 711.9 | 15188 | 420 | 0.97 |

**Table 5-5 - XPS data for post reactor monolayer based catalysts.**

## 5.4 Conclusions

From the data collected within this work it seems that the most important aspect to formaldehyde production is the presence of surface molybdenum. The highest yielding catalysts present a bulk ratio of Mo:Fe 2.2:1 or higher with lower ratios producing more CO. Production of $CO_2$ and $H_2$ is observed with good efficiency off an $Fe_2O_3$ surface *via* a formate intermediate. Addition of only small amounts of

molybdenum, either to the surface or to the bulk leads to a high levels of surface molybdenum which can produce formaldehyde, CO and $H_2O$ *via* methoxy intermediates. The energy to the production of CO is linked to molybdenum surface concentration, with the lowest concentrations of surface molybdenum, the energy barrier to CO production is ~155 kJ $mol^{-1}$, while this drops to ~123 kJ $mol^{-1}$ above a critical value. The high energy CO is from isolated molybdenum sites where the adsorbed methoxy is stabilised by the neighbouring iron sites, before undergoing direct dehydrogenation to CO. The low energy CO is produced from the over oxidation of formaldehyde.

While it is surface molybdenum that is crucial to determining the selectivity of the catalyst, it has also been demonstrated that the catalyst surfaces tend to be enriched in molybdenum. This is evidenced by Raman spectroscopy, where bands (Mo-O-Mo vibrations and Mo=O terminal vibrations) associated with $MoO_3$ (or at least octahedral Mo-O) along with those for $Fe_2(MoO_4)_3$ (tetrahedral molybdenum) are observed even for catalysts with a Mo:Fe of 0.2:1. A higher than expected surface ratio of Mo:Fe was also seen in these low catalysts by XPS and TPD data showed that a ratio of 0.05:1 Mo:Fe produced less than 50 % $CO_2$ (a sign of $Fe_2O_3$). If all the molybdenum was concentrated at the surface for this catalysts it would create a coverage of 0.97 ML. For higher ratio catalysts (1.5 and 2.2:1 Mo:Fe), an enrichment of particles of $Fe_2(MoO_4)_3$ with Mo in the surface region was shown by STEM/EELs (Chapter 3).

When $MoO_3$ is supported on the surface of $Fe_2O_3$ it raises both the activity of methanol conversion and the selectivity towards formaldehyde of the material. Above ~60 % of a monolayer $MoO_3$, the activity does not change further although some further improvements in selectivity are noted. Even once the monolayer is complete

the catalyst still produces CO by the secondary oxidation of the formaldehyde formed due to the high surface area. In contrast, the addition of $Fe_2O_3$ to $MoO_3$ causes minimal change in catalytic performance, with characterisation data suggesting the Fe goes subsurface.

Addition of $MoO_3$ monolayers to the surface of a high surface area, low bulk ratio Mo:Fe catalyst lead to further improvement in catalytic performance that gave a catalyst with considerably better formaldehyde yield at low temperatures than the current industrial catalyst. This was primarily due to higher activity. However, as higher conversions were approached the catalyst still produced large amounts of CO, as the formaldehyde produced underwent secondary oxidation.

## 5.5 References

(1) Popov, B. I.; Skomorokhova, N. G. *Reaction Kinetics and Catalysis Letters* **1981**, *18*, 107.
(2) Popov, B. I.; Pashis, A. V.; Shkuratova, L. N. *Reaction Kinetics and Catalysis Letters* **1986**, *30*, 129.
(3) Okamoto, Y.; Morikawa, F.; Oh-Hiraki, K.; Imanaka, T.; Teranishi, S. *Journal of the Chemical Society, Chemical Communications* **1981**, 1018.
(4) Yamada, H.; Niwa, M.; Murakami, Y. *Applied Catalysis, A: General* **1993**, *96*, 113.
(5) Xu, F.; Hu, Y.; Dong, L.; Chen, Y. *Chinese Science Bulletin* **2000**, *45*, 214.
(6) van Nguyen , T.; Tittarelli, P.; Villa, P. L. *Chem. Uses Molybdenum, Proc. Int. Conf., 3rd* **1979**, 161.
(7) Soares, A. P. V.; Farinha Portela, M.; Kiennemann, A.; Hilaire, L.; Millet, J. M. M. *Applied Catalysis, A: General* **2001**, *206*, 221.
(8) Kim, T. H.; Ramachandra, B.; Choi, J. S.; Saidutta, M. B.; Choo, K. Y.; Song, S. D.; Rhee, Y. W. *Catalysis Letters* **2004**, *98*, 161.
(9) Soares, A. P. V.; Portela, M. F.; Kiennemann, A. *Studies in Surface Science and Catalysis* **2001**, *133*, 489.
(10) Trifiro, F.; Carbucicchio, M.; Villa, P. L. *Hyperfine Interactions* **1997**, *111*, 17.
(11) Andersson, A.; Hernelind, M.; Augustsson, O. *Catalysis Today* **2006**, *112*, 40.
(12) Popov, B. I.; Bibin, V. N.; Boreskov, G. K. *Kinetika i Kataliz* **1976**, *17*, 371.
(13) Pernicone, N. *Catalysis Today* **1991**, *11*, 85.
(14) Trifiro, F.; Notarbartolo, S.; Pasquon, I. *Journal of Catalysis* **1971**, *22*, 324.
(15) Glisenti, A.; Favero, G.; Granozzi, G. *Journal of the Chemical Society, Faraday Transactions* **1998**, *94*, 173.
(16) Groff, R. P. *Journal of Catalysis* **1984**, *86*, 215.

(17) Habersberger, K.; Jiru, P. *Collection of Czechoslovak Chemical Communications* **1972**, *37*, 535.
(18) Ai, M. *Journal of Catalysis* **1978**, *52*, 16.
(19) Tatibouet, J. M. *Applied Catalysis, A: General* **1997**, *148*, 213.
(20) Al-Shihry, S. S.; Halawy, S. A. *Journal of Molecular Catalysis A: Chemical* **1996**, *113*, 479.
(21) Briand, L. E.; Hirt, A. M.; Wachs, I. E. *Journal of Catalysis* **2001**, *202*, 268.
(22) Burcham, L. J.; Briand, L. E.; Wachs, I. E. *Langmuir* **2001**, *17*, 6175.
(23) Hill, C. G., Jr.; Wilson, J. H., III. *Journal of Molecular Catalysis* **1990**, *63*, 65.
(24) Ramans, G.; Gabrusenoks, J.; Lusis, A.; Patmalnieks, A. *Journal of Non-Crystalline Solids* **1987**, *90*, 637.
(25) Remediakis, I. N.; Kaxaris, E.; Chen, M.; Friend, C. M. *Journal of Chemical Physics* **2003**, *118*, 6046.
(26) Soares, A. P. V.; Portela, M. F.; Kiennemann, A. *Catalysis Reviews - Science and Engineering* **2004**, *47*, 125.

# 6 Conclusions and Future Work

## 6.1 Conclusions

The aim of this thesis was to establish the role of the different phases of $Fe_2(MoO_4)_3$ and $MoO_3$ for the selective oxidation of methanol to formaldehyde. It has been established that the most important factor in the production of formaldehyde is a high surface concentration of molybdenum in the 6+ oxidation state. If the surface presented is $Fe_2O_3$, then the catalyst is non-selective producing only $CO_2$ and $H_2$, while at molybdenum ratios below that required to form $Fe_2(MoO_4)_3$, CO becomes a major product. At very low molybdenum concentrations (Mo:Fe $\leq$0.05:1), isolated molybdenum sites are found at the surface and these lead to a high energy (maximum TPD desorption of ~260 °C), direct pathway to CO. At higher ratios, the surface is covered with molybdenum and guides the reaction to the primary product of formaldehyde with CO observed as a secondary oxidation product in reactor studies (off all catalysts) and TPD in catalysts with a high surface area (*i.e.* those with a ratio Mo:Fe <1.5:1). To achieve the best selectivities (>90 %) to formaldehyde with high conversions (>90 %), a ratio of 2.2:1 Mo:Fe or higher is required. This is required to ensure all the surface of $Fe_2(MoO_4)_3$ is covered with $MoO_3$, and so help to prevent secondary oxidation of the formaldehyde to CO.

The surface of iron molybdates have been shown to have a higher level of molybdenum than the bulk concentration. In the case of low Mo:Fe ratio catalysts this was observed with Raman spectroscopy, TPD and XPS. In catalysts with a higher ratio (*i.e.* Mo:Fe 1.5 and 2.2:1) an increase in molybdenum concentration was seen in the surface layers of $Fe_2(MoO_4)_3$ particles by STEM/EELS. The bulk of iron molybdates, with a ratio below that required for the stoichiometric $Fe_2(MoO_4)_3$ consists of the phases of $\alpha$-$Fe_2O_3$ and $\alpha$-$Fe_2(MoO_4)_3$ although the excess iron is highly dispersed and not seen with XRD in a Mo:Fe ratio of 1:1. When the ratio is raised

above that required for stoichiometry then an extra phase of $MoO_3$ is observed, although the extra $\alpha$-$MoO_3$ phase was not seen with a ratio of Mo:Fe 1.6:1, presumably again due to high dispersion, or due to the small added content.

A method for producing a catalyst with similar properties to the industrial Perstorp KH 26 catalyst by coprecipitating iron nitrate and ammonium heptamolybdate before evaporating the solid to dryness so that the ratio of molybdenum to iron remained as required has been achieved. The current industrial catalyst is prepared by coprecipitation of iron chloride and ammonium heptamolybdate with washing and filtering of the precipitate. The catalyst performed similarly in both pulsed and continuous flow conditions, so the conditions of pulsed flow (where pulse shape can be studied) were utilised for the rest of the experimentation.

The reaction normally proceeds *via* a Mars-van Krevelen mechanism[1] with the role of gaseous oxygen to replace the bulk oxygen used within the oxidation process. If the gaseous oxygen is removed then the bulk can become reduced as diffusion of lattice oxygen occurs to the surface, which can be used to produce oxidised products. If this happens and the molybdenum oxidation state is lowered below +6, then formaldehyde selectivity drops considerably, with direct production of CO and secondary production of $CO_2$ observed.

The surface reduction of Mo:Fe 2.2:1 by methanol has been shown to be possible at temperatures as low as 200 °C. If the temperature of reduction is raised to $\geq$250 °C oxygen is supplied from the bulk lattice of the particle (through diffusion to the surface) and can be used in both selective and non-selective oxidation processes. At 330 °C, the Mo:Fe 2.2:1 catalyst continues to convert 100 % of the methanol throughout the reaction tested with oxygen continuing to be delivered from deep

within the catalyst particle when the reaction is terminated. With heavy reduction the phases of $Fe_2(MoO_4)_3$ and $MoO_3$ are converted to α-$FeMoO_4$, $MoO_2$ and $Mo_4O_{11}$.

While production of CO and $CO_2$ can happen directly off low Mo:Fe catalysts (from isolated molybdenum and iron oxide sites respectively) or those presenting molybdenum in an oxidation state below +6, it has been established that sequential reaction ($CH_3OH \rightarrow CH_2O \rightarrow CO \rightarrow CO_2$) also happens on a fully oxidised catalyst with molybdenum at the surface by variation of the catalyst load, and varying the size of methanol injection. $Fe_2(MoO_4)_3$ was shown to be much more active in both $H_2$ and CO oxidation than $MoO_3$, pressumably due to the greater Mo-O bond strength in $MoO_3$ and/or the difference in distance between the cations.

Catalysts of $MoO_3$ monolayers supported on $Fe_2O_3$ are more active than $Fe_2O_3$ alone, with the presence of surface molybdenum leading to the formation of less stable methoxy species. When present on $Fe_2O_3$ a surface formate is formed which decomposes to $CO_2$ and $H_2$. On isolated molybdenum sites methoxy groups are stabilised and lead to the direct formation of CO.

## 6.2 Future Work

The field of methanol oxidation by iron molybdate catalysts is far from exhausted in terms of future research. While the work presented here deals with the roles of the phases within the catalytic process, it does not deal with the deactivation of the catalyst. This is known to occur primarily through molybdenum volatilisation[2,3], and preventing or at least limiting this process would lead to increased catalyst lifetimes. There are two major thoughts for the reason behind deactivation, the first is that water (as in other selective oxidations over molybdate catalysts[4,5]) leads to the formation of the volatile molybdenum based compound[6,7], while the other thought is that the volatile compound is methanol based[8-11]. Clarity on the method of

molybdenum volatilisation, and conditions leading to the formation of the volatile compound, may allow for modification of the catalyst to help prevent this.

The work may also be extended further to study the effect of replacing the iron within the system. Replacement with another cation that forms an isostructural molybdate (e.g $Al_2(MoO_4)_3$, $Cr_2(MoO_4)_3$ or $\alpha$-$Bi_2(MoO_4)_3$) may continue to give a molybdenum rich surface that is selective to formaldehyde, but may lead to different structures upon reduction. In iron molybdate it is speculated that this is where the volatile molybdenum comes from, so this may be prevented. A difference in Mo-O bond strength will also occur and this may effect the secondary oxidation of formaldehyde (as is observed on iron molybdates).

An interesting point to study could be the oxidation of other alcohols on the surface of iron molybdates. If primary, secondary and tertiary alcohols were used this may help give further details on the oxidation mechanism. If surface intermediates of these alcohols have a longer residence time than methanol on the surface, it may be envisaged that greater coupling reactions (such as that to from dimethyl ether) may occur. Enhancement of these reactions could be reached by using an iron tungstate, as it is known to present longer residence times, and greater dimethyl ether, for methoxys by decreasing the rate of hydrogen abstraction and thus formaldehyde formation[12].

Surface science techniques may also prove useful in developing the system further. In this work, it has been shown how effective small amounts of $MoO_3$ on the surface of $Fe_2O_3$ can be at producing selective catalysts, therefore generating models of this system may prove useful. In the same way that molybdenum volatilisation has been observed from a $MoO_3$ single crystal with the (010) face exposed using AFM[11], it could be envisaged that this may also be the case for films of $Fe_2(MoO_4)_3$.

## 6.3 References

(1) Mars, P.; van Krevelen, D. W. *Chemical Engineering Science* **1954**, *3*, 41.
(2) Andersson, A.; Hernelind, M.; Augustsson, O. *Catalysis Today* **2006**, *112*, 40.
(3) Soares, A. P. V.; Portela, M. F.; Kiennemann, A. *Catalysis Reviews - Science and Engineering* **2004**, *47*, 125.
(4) Zhang, L.; Liu, D.; Yang, B.; Zhao, J. *Applied Catalysis, A: General* **1994**, *117*, 163.
(5) Dazhuang, L.; Lixiong, Z.; Biguang, Y.; Jiaofeng, L. *Applied Catalysis, A: General* **1993**, *105*, 185.
(6) Arnoldy, P.; De Jonge, J. C. M.; Moulijn, J. A. *Journal of Physical Chemistry* **1985**, *89*, 4517.
(7) Pernicone, N. *Catalysis Today* **1991**, *11*, 85.
(8) Popov, B. I.; Bibin, V. N.; Boreskov, G. K. *Kinetika i Kataliz* **1976**, *17*, 371.
(9) Popov, B. I.; Skomorokhova, N. G. *Reaction Kinetics and Catalysis Letters* **1981**, *18*, 101.
(10) Carbucicchio, M.; Forzatti, P.; Trifiro, F.; Tronconi, E.; Villa, P. L. *Studies in Surface Science and Catalysis* **1980**, *6*, 103.
(11) Smith, R. L.; Rohrer, G. S. *Journal of Catalysis* **1998**, *180*, 270.
(12) Harrison, W. T. A.; Chowdhry, U.; Machiels, C. J.; Sleight, A. W.; Cheetham, A. K. *Journal of Solid State Chemistry* **1985**, *60*, 101.